

Development of a synthetic small calibre vascular bypass graft

Sandip Sarkar

Vascular Research Fellow

Royal Free and University College Medical School

PhD thesis submitted to University College
London, University of London

Declaration of originality

I, Sandip Sarkar confirm that the work presented in this thesis is my own. Where information has been derived from other sources, I confirm that this has been indicated in the thesis.

My parents were the foundation.

Sudeshna was the key.

Ananya – you are the reason.

Acknowledgements

It was my good fortune to be pointed in the direction of my supervisors, Prof George Hamilton and Prof Alex Seifalian when I expressed an interest in undertaking formal research in vascular surgery. They both gave me a host of ideas, free reign to run with these, gentle nudges in the right direction, as well as motivation, inspiration and encouragement. I have grown academically as a result.

Dr Kevin Sales and Geoff Punshon became my close friends. They facilitated all my administrative needs, and made time for me even when their busy jobs provided very little. They were instrumental in my success in obtaining the Peter Samuel Grant.

I decided to study a topic I knew absolutely nothing about. This was only possible due to the guidance and expertise of Dr Henryk Salacinski, who guided me through the complex physics and chemistry required to start in this field. His premature death is a great sadness to our whole personal and scientific community.

Arnold Darbyshire was a 24 hour mine of information with respect to the polymers. He synthesised polymer preparations for me at short notice. I must have been a complete nuisance.

Mechanical concepts and the need for extreme precision in the mechanical testing were supervised by my teacher and friend, Dr Gaetano Burriesci. Thank you too for the espressos. Dr Adam Wojcik was another friend at UCL Mechanical Engineering, who used his ingenuity to make the hoop testing grips from links from a watch bracelet, and the environmental chamber from a perspex toilet brush holder!

Dr Clare Hillery was a post-doctoral co-investigator who lead me to her mentor and supervisor, Prof Steve Greenwald at QMUH, who provided me with the burst pressure testing facilities, image analysis software (which he wrote and adapted for my purposes) and guidance. He asked for nothing in return.

Dr Nima Roohpour performed and helped me to interpret thermal analysis tests. Mr Colin Hart undertook the immunostaining with me.

Finally, I must thank the trustees of the Peter Samuel Fund, who contributed £10 000 towards the animal work presented here.

Peer-reviewed publications arising from this period of research.

Publications relating directly to work presented in this thesis

- ❖ **Sarkar S**, Salacinski HJ, Hamilton G, Seifalian AM. The mechanical properties of infrainguinal bypass grafts: their role in influencing patency. *Eur J Vasc Endovasc Surg* 2006;**31**:627-36
- ❖ **Sarkar S**, Sales K, Hamilton G, Seifalian AM. Addressing thrombogenicity in vascular graft construction. *J Biomed Mater Res B* 2007;**82(1)**:100-8
- ❖ **Sarkar S**, Schmidt-Rixen T, Hamilton G, Seifalian AM. Achieving the ideal properties for vascular bypass grafts using a tissue engineered approach. *Medical Biology Engineering and Computing* 2007;**45(4)**:327-36
- ❖ **Sarkar S**, Hillery C, Seifalian AM, Hamilton G. Critical parameter of burst pressure measurement in development of bypass grafts is highly dependent on methodology used. *J Vasc Surg* 2006;**44(4)**:846-52
- ❖ **Sarkar S**, Burriesci G, Wojcik A, Aresti N, Hamilton G, Seifalian AM. Manufacture of small calibre quadruple lamina vascular bypass grafts using a novel automated extrusion-phase-inversion method and nanocomposite polymer. *J Biomech.* 2009;**42(6)**:722-30
- ❖ **Sarkar S**, Seifalian AM. Tissue engineering of blood vessels. Book chapter in *Recent Advances in Surgery 30* (Ed. Irving Taylor) – commissioned, not peer-reviewed.

Publications on work related to this thesis

- ❖ Desai M, Mirzay-Razzaz J, von Delft D, **Sarkar S**, Hamilton, G, Seifalian AM. Inhibition of neointimal formation and hyperplasia in vein grafts by external stent/sheath. *Vasc Med* 2010;**15(4)**:287-97
- ❖ Vara D, **Sarkar S**, Punshon, G, Sales KM, Hamilton G, Seifalian,AM. Endothelial cell retention on a viscoelastic nanocomposite vascular conduit is improved by exposure to shear stress preconditioning prior to physiological flow. *Artificial Organs* 2008; **32(12)**:977-81

- ❖ Kannan RY, **Sarkar S**, Mirzay-Razaz J, Seifalian, AM. Vascular tissue engineering: New Vessels. *The Biochemist* 2007;**29**:12-15 – commissioned, not peer reviewed.
- ❖ Kidane AG, Burriesci G, Cornejo P, Dooley A, **Sarkar S**, Bonhoeffer P, Edirisinghe M, Seifalian AM. Current Developments and Future Prospects for Heart Valve Replacement Therapy. *J Biomed Mater Res B* 2009; **88(1)**:290-303
- ❖ de Mel A, Punshon G, Ramesh B, **Sarkar S**, Darbyshire A, Hamilton G, Seifalian AM. In situ endothelialization potential of a biofunctionalised nanocomposite biomaterial-based small diameter bypass graft. *Biomed Mater Eng.* 2009;**19(4-5)**:317-31.

Contents.

Acknowledgements	4
Peer-reviewed publications arising from this period of research	5
Abstract	13
List of abbreviations	14
List of figures and tables	17
1. Development of a synthetic small calibre vascular bypass graft	30
1.1 Introduction	30
1.2 Historical Perspective	33
1.2.1 The birth of vascular surgery	33
1.2.2 Peripheral artery bypass	34
1.2.2.1 Polypropylene	35
1.2.2.2 Compliant materials	35
1.2.2.2.1 Silicone rubber	36
1.2.2.2.2 Polyurethane	36
1.3 Current standing	38
1.3.1 Polycarbonate-based polyurethane	38
1.3.2 Poly(carbonate-urea) urethane incorporating polyhedral oligomeric silsesquioxane nanocomposite	39
1.4 The importance of mechanical testing	39
1.5 Thesis overview	40
2. The mechanical properties of infrainguinal vascular bypass grafts: their role in influencing patency	41
2.1 Introduction	41
2.2 Basic mechanical theoretical considerations	42
2.3 Mechanical variables influencing graft success	48
2.3.1 Compliance	48
2.3.1.1 The importance of correct compliance matching	57
2.3.2 Conduit calibre	59
2.3.3 Porosity	60

2.3.4	Burst pressure	62
2.4	Properties of bypass conduits in clinical use	63
2.4.1	Autologous vein	63
2.4.2	Expanded polytetrafluoroethylene	64
2.5	Prostheses of the future	64
2.5.1	Synthetic grafts	64
2.5.2	Tissue-engineered grafts	65
3.	Addressing thrombogenicity in vascular graft construction	68
3.1	Introduction	68
3.2	The arterial surface	69
3.3	Surface modification to attenuate the coagulation cascade	74
3.4	Electrical charge	77
3.5	Surface wettability	78
3.6	Mechanical considerations	79
3.7	Endothelialisation	80
3.8	Conclusions	81
3.9	Future directions	82
4.	Achieving the ideal properties for vascular bypass grafts using a tissue-engineered approach	86
4.1	Introduction	86
4.2	The major factors for consideration	88
4.2.1	Scaffold	89
4.2.2	Cells	92
4.2.3	Mechanical properties	94
4.2.4	Blood compatibility – endothelial lining	96
4.2.4.1	Veins	97
4.2.4.2	Adipose	98
4.2.4.3	Bone marrow	98
4.2.4.4	Endothelial progenitor cells	98
4.2.5	Off the shelf availability	99
4.3	Conclusion and future directions	101
5.	Materials and methods	103

5.1	Background	103
5.1.1	Silsesquioxane	105
5.1.2	Polyurethane	106
5.1.2.1	Poly(ester)urethane	106
5.1.2.2	Poly(ether)urethane	106
5.1.2.3	Poly(carbonate-urea)urethane	106
5.2	Synthesis of PCU-POSS	112
5.3	Tensile testing of graft material	112
5.3.1	Introduction	112
5.3.2	Stress-strain behaviour	113
5.3.3	Stress-relaxation	117
5.3.4	The longitudinal sample	117
5.3.5	The testing grips	120
5.3.6	The circumferential sample	120
5.3.7	The environmental chamber	127
5.3.8	The tensillometry machine	129
5.3.8.1	Method	129
5.3.8.2	Stress-strain and tensile strength	129
5.3.8.3	Stress-relaxation	129
5.4	Compliance measurement	130
5.4.1	Introduction	130
5.4.2	Method overview	131
5.4.2.1	Fluid in the circuit	133
5.4.2.1.1	Consideration of blood's viscous flow in the circuit	135
5.4.2.2	The biomimetic pulsatile flow generator	138
5.4.2.2.1	Consideration of the biomimetic waveform	140
5.4.2.3	Accessory tubing	140
5.4.2.4	Ultrasound	140
5.4.2.5	Wall track system	141
5.5	Burst strength testing/longitudinal strain	145
6.	Extrusion-phase inversion of a small calibre compliant graft	146
6.1	Introduction	146
6.2	Techniques currently used for polymeric vascular graft	146

manufacture	
6.3	Extrusion-phase inversion 149
6.3.1	Technique 151
6.3.2	Troubleshooting 156
6.3.3	Rheological considerations 158
6.3.3.1	Inter-batch variability 158
6.3.4	Reproducibility of graft manufacture 165
6.4	PCUPOSS incorporating porosifier and surfactant 168
6.5	PCUPOSS grafts 169
6.6	The effect of coagulant temperature on porosity 170
6.7	The effect of DMAC in the coagulant 179
6.8	The mechanical and physiological implications of the graft pore structure 181
6.9	Conclusion 182
7.	Mechanical characterisation 184
7.1	Introduction 184
7.2	Tensile testing protocol 185
7.3	Testing porous samples 185
7.4	Failed tests 188
7.4.1	Noise 188
7.4.2	Initial graft placement 191
7.4.3	Slippage 192
7.5	Tensile test results 195
7.5.1	PTFE 195
7.5.2	PCUPOSS cast sheet 197
7.5.3	PCUPOSS graft 199
7.6	Addressing mechanical anisotropy 208
7.6.1	Ultimate tensile stress 208
7.6.2	Curve shape 212
7.7	Viscoelasticity 214
7.8	Conclusion 216
8.	Functional mechanical characterisation 217
8.1	Introduction 217

8.2	Compliance	218
8.2.1	Compliance of lower limb arteries	218
8.2.2	Compliance of PCUPOSS grafts	221
8.3	Burst pressure	232
8.4	Viscoelasticity	234
8.5	Longitudinal strain	236
8.6	Conclusion	240
9.	The methodology of burst pressure measurement	243
9.1	Introduction	243
9.2	Materials and methods	244
9.2.1	Burst pressure assessment	245
9.2.2	Data collection and statistical analysis	245
9.3	Results	247
9.4	Discussion	250
9.5	Conclusion	255
10	In vivo durability testing	256
10.1	Introduction	256
10.2	Biodegradation studies of the graft	257
10.2.1	Biodegradation of PCU: in vitro assessment	257
10.2.2	Biodegradation of PCU: in vivo assessment	263
10.2.3	Biodegradation of PCUPOSS: in vitro assessment	264
10.3	Which is the most suitable animal model?	265
10.4	Method	268
10.4.1	Animal model protocol	268
10.4.2	Scanning electron microscopy	269
10.4.3	Histological and Immunohistological analysis	269
10.4.4	Mechanical testing	269
10.4.5	Chemical analysis - Fourier transform infra-red spectroscopy	270
10.4.6	Thermal analysis	270
10.4.6.1	Thermal gravimetric analysis	270
10.4.6.2	Differential scanning calorimetry	271
10.4.6.3	Dynamic mechanical analysis	271

10.5	Results	272
10.5.1	Number of grafts	272
10.5.2	Gross appearance of grafts	273
10.5.3	Scanning electron microscopy	276
10.5.4	Histology	279
10.5.5	Endothelial cell characterisation	279
10.5.6	FTIR analysis	282
10.5.7	Compliance of pre and post-implantation grafts	282
10.5.8	Pre and post-implantation burst strength	283
10.5.9	Thermal gravimetric analysis	284
10.5.10	Differential scanning calorimetry	284
10.5.11	Dynamic mechanical analysis	285
10.6	Discussion	287
10.7	Conclusion	288
11.	Conclusion	290
11.1	Introduction	290
11.2	Mechanical properties	291
11.3	Thrombogenicity	292
11.4	Tissue-engineering	293
11.5	Materials	294
11.6	Graft manufacture	295
11.7	Mechanical characterisation	297
11.8	Functional mechanical characterisation	298
11.9	Burst pressure measurement	300
11.10	In vivo model	301
11.11	Further work	302

References

Abstract

Polyurethanes are an attractive class of material for bioprosthesis development due to the ability to manipulate their elasticity and strength. However, their use as long term biological implants is hampered by biodegradation. A novel polyurethane has been developed which incorporates nano-engineered polyhedral oligomeric silsesquioxane within poly(carbonate-urea) urethane to improve the biostability of the latter. Previous investigators have found this material to be cytocompatible and to have low thrombogenicity.

The medium and long term clinical results of currently available prosthetic small calibre vascular bypass grafts are poor, due to neo-intimal hyperplasia associated with their non-compliant properties.

The investigation reported here commences with the benchtop manufacture of compliant small calibre grafts using an original extrusion-phase inversion technique. The reproducibility of the technique as well as the effect on the pore structure of different coagulation conditions is demonstrated. Fundamental mechanical characterisation of the grafts produced is then presented, by way of tensillometry to demonstrate the viscous and elastic properties of the material. These are made more relevant to the clinical setting with functional mechanical characterisation of the grafts, showing graft compliance in a biomimetic flow circuit along with viscoelastic hysteresis, along with burst pressure testing. An examination of burst pressure testing methodology is also shown, in the light of the various non-standardised strategies reported in the graft-testing literature. Mechanical characterisation shows the short-term safety for use, but durability studies in the biological haemodynamic environment serve to assess longer term fatigability as well as confirming biostability. This has been reported using a stringent ovine carotid interposition model which remained patent over the full investigation period representing at least 45 million pulsatile cycles. Physico-chemical analysis; integrity of the structure, microstructure and ultrastructure; preservation of mechanical properties and immunohistological analysis were used to examine the grafts after implantation to show their healing properties and biostability.

List of abbreviations.

ADP	Adenosine diphosphate
ADPase	Adenosine diphosphatase
AT	Anterior tibial
ATM-FTIR	Attenuated total reflectance Fourier transform infra-red spectroscopy
bFGF	Basic fibroblast growth factor
CEC	Canine endothelial cell
cGMP	Cyclic 3'5'-guanosine monophosphate
CM	Compliance mismatch
CPD	Citrate/phosphate/dextrose
CT	Computed tomography
DMA	Dynamic mechanical analysis
DMAC	Dimethylacetamide
DMF	Dimethylformamide
DP	Dorsalis pedis
DSA	Digital subtraction angiography
DSC	Differential scanning calorimetry
EC	Endothelial cell
ECG	Electrocardiogram
ECM	Extracellular matrix
EDR	Elastic distension ratio
EDRF	Endothelium derived relaxing factor
EPC	Endothelial progenitor cell
ePTFE	expanded polytetrafluoroethylene
ETE	End-to-end
ETS	End-to-side
FDA	Food and drug administration
FTIR	Fourier transform infra-red spectroscopy
GPM	Gluteraldehyde preserved matrix
H&E	Haematoxylin and eosin
HUVEC	Human umbilical vein endothelial cell
IH	Intimal hyperplasia

IMT	Intima-media thickness
LDL	Low density lipoprotein
MDI	Methylene diphenyl diisocyanate
MR	Magnetic resonance
MRI	Magnetic resonance imaging
N/S	Non-significant
NO	Nitric oxide
P4HB	Poly-4-hydroxybutyrate
PCB	Printed circuit board
PCU	Poly(carbonate-urea) urethane
PCUPOSS	Poly(carbonate-urea) urethane incorporating polyhedral oligomeric silsesquioxane
PDMS	Polydimethylsiloxane
PDS	Polydioxanone
PEG	Polyethylene glycol
PEO	Polyethylene oxide
PFV	Peak flow velocity
PGA	Polyglycolic acid
PHZ	Perianastomotic hypercompliance zone
PLA	Poly lactide
POSS	Polyhedral oligomeric silsesquioxane
PT	Posterior tibial
PTFE	polytetrafluoroethylene
PVD	Peripheral vascular disease
RF	Radio frequency
RGD	Arginine-Glycine-Aspartic acid
SAGM	Sodium/adenine/glucose/mannitol
SEM	Scanning electron micrograph
SFA	Superficial femoral artery
SMC	smooth muscle cell
TE	Tissue-engineered
TF	Tissue Factor
TFPI	Tissue factor pathway inhibitor
TGA	Thermal gravimetric analysis
vEC	Vascular endothelial cell

VEGF	Vascular endothelial growth factor
VSM	Vascular smooth muscle
vWF	von Willebrand factor
WSS	Wall shear stress
YIGSR	Tyrosine-Isoleucine-Glycine-Serine-Arginine

List of figures and tables

Figures

Chapter 1

Fig 1.1 Distal bypass using PTFE has considerably worse patency than proximal bypass or autologous vein grafting.

Chapter 2

Fig 2.1. The parabolic profile of laminar flow. A purely 'Newtonian' fluid displays this flow pattern. However, blood is not a homogenous mixture of small particles, and so is not 'Newtonian' in its behaviour.

Fig 2.2. The hysteresis loop observed during repeated cycles of applying and removing a force from a vessel wall as would occur during pulsatile flow.

Fig 2.3. The consequence of a 1mm graft stenosis is much greater in a small caliber vessel than in a large calibre conduit.

Fig 2.4. Illustration of the para-anastomotic hypercompliance zone.

Fig 2.5. For an anastomosis between ePTFE and native artery, the per-anastomotic compliance is intermediate between that of its constituent vessels. Adapted from Sonada et al.

Fig 2.6. Tai's investigation of compliance in a flow circuit showed the 'anisotropy of compliance' for the external iliac artery – the distensibility is dependent on the pressure level at which the distending stress is exerted. The commercial bypass graft materials have low compliance compared to the artery, but saphenous vein also has low compliance, illustrating the importance of cellular and biochemical factors in graft success. PCU refers to poly(carbonate-urea) urethane, which is the basis for the nanocomposite.

Chapter 3

Fig 3.1. The multilayered structure of the arterial wall showing the distribution of collagen and elastin in the arterial wall resulting in anisotropy of distensibility..

Fig 3.2. The clotting cascade.

Chapter 4

Fig 4.1. The graph demonstrates the timeline for the development of a tissue engineered bypass graft using a synthetic biodegradable scaffold, which is gradually replaced by arterial matrix.

Fig 4.2. A living cellular matrix, comprising of Type I collagen & porcine smooth muscle cells, which is contracted on a central mandrel within a bioreactor.

Chapter 5

Fig 5.1. The repeating monomer of polydimethylsiloxane (PDMS). A large number of repeats (n) reduces viscosity.

Fig 5.2. Chemical structure of trans-cyclohexanediolisobutylsilsesquioxane, the POSS moiety used in PCUPOSS.

Fig 5.3. Molecular schematic to describe the segmented structure of polyurethanes. The ordered hard segments are highly polar groups with strict alignment and strength. These float in a 'sea' of soft segment, which allows considerable movement. Hence the combination can be elastic and simultaneously strong.

Fig 5.4. The formation of the urethane bond. See text for details.

Fig 5.5. A typical stress-strain curve.

Fig 5.6. The typical tensile test curve for foam structures.

Fig 5.7. The dimensions of the dogbone specimens used (not actual size).

Fig 5.8a. The longitudinal sample held in the neutral position within the nylon block grips.

- Fig 5.8b. Close-up of the grips used for longitudinal dogbone samples.
- Fig 5.9. The concept of hoop testing of tubular structures.
- Fig 5.10a. The use of links and bracelet from a stainless steel wrist-watch band to design the rig for hoop testing of circumferential samples.
- Fig 5.10b. Close-up of the hoop testing rig.
- Fig 5.11. The tensile test including environmental chamber filled with water at 37°C.
- Fig 5.12. Schematic diagram of the flow circuit used to measure dynamic compliance.
- Fig 5.13. The viscous relation to shear rate for Newtonian and Non-Newtonian fluids. The gradient of the lines correspond with viscosity, so a Newtonian fluid maintains the same viscosity for all shear rates, whereas a Non-Newtonian fluid (blood) has a low viscosity at high shear rates (high flow rates).
- Fig 5.14. Schematic diagram of the biomimetic pulsatile flow generator used in the circuit.
- Fig 5.15. Distension and pressure waveforms through the compliant grafts in the biomimetic pulsatile flow circuit used for compliance testing. The waveform data was generated from the wall-tracking duplex and Millar probe placed within the graft respectively.
- Fig 5.16. A two dimensional image of the graft can be built up by utilising a linear array of piezoelectric crystals emitting parallel waves.
- Fig 5.17. By centering the graft precisely under the ultrasound probe, distension will be in the plane of the ultrasonic wave, leading to accuracy of measurement and elimination of a noisy signal.

Chapter 6

- Fig 6.1. Electrospinning as a method of producing a porous graft from a liquid polymer.
- Fig 6.2. The ternary model of phase inversion. The polymer can exist in a solid phase, dissolved phase or any intermediate phase, depending on the amount of solvent present. A non-solvent can exchange with the solvent to control the polymer phase precisely, making the system a combined

interaction between three constituents.

Fig 6.3. The bench-top extrusion-phase inverter device.

Fig 6.4. The polymer chamber, showing the entry aperture through which the mandrel fits snugly. The polymer inlet can be seen on the right side of the perspex block.

Fig 6.5. The undersurface of the polymer chamber showing the exit aperture along with three adaptors for varying the aperture size.

Fig 6.6. The mandrel is positioned such that there is an equal gap around it in all directions. Its lower level is flush with the lower border of the exit aperture.

Fig 6.7. The mechanical arm has lowered the mandrel through the polymer chamber, in so doing coating it with the nanocomposite. The exit aperture controls the thickness of this coating which further descends into the coagulant solution, causing phase inversion.

Fig 6.8. The polymer must not be so viscous that it starts to pour past the mandrel before the polymer chamber has had a chance to fill up (above). It must also be driven down by the mandrel into the coagulant rather than slide down the mandrel (below).

Fig 6.9. Bohlin CVO Rheometer – 4° cone and plate type, with full rheological testing capabilities including temperature adjustment using a Peltier plate system.

Fig 6.10. The viscosity of the three batches of nanocomposite when measured using an up-down shear rate ramp.

Fig 6.11. The increase in viscosity seen after storage of nanocomposite (batch 1) for four months.

Fig 6.12. Exit aperture cover closed.

Fig 6.13. Exit aperture open.

Fig 6.14. The intra and inter-graft variation in wall thickness for the thin-walled grafts.

Fig 6.15. The intra and inter-graft variation in wall thickness for the thick-walled grafts.

Fig 6.16. The compliance of grafts manufactured from PCUPOSS using 5% Na(HCO₃)₂ filler and surfactant (n=6). The compliance characteristics of human external iliac artery (n=6) and PTFE graft (n=1) were measured

by Mr Michael Mikhael and Mr William Khor and have been included with kind permission for comparison.

Fig 6.17. Coagulant is deionised water at 0°C (scale bar 2mm)

Fig 6.18. Coagulant is deionised water at 10°C (scale bar 2mm)

Fig 6.19. Coagulant is deionised water at 20°C (scale bar 2mm)

Fig 6.20. Coagulant is deionised water at 30°C (scale bar 2mm)

Fig 6.21. Coagulant is deionised water at 40°C (scale bar 2mm)

Fig 6.22. Coagulant is deionised water at 50°C (scale bar 2mm)

Fig 6.23. Four-layered structure of the graft wall (scale bar 250microns)

Fig 6.24. Lumen of graft (scale bar 125 microns)

Fig 6.25. Outer skin of graft demonstrating microscopic ridges throughout the surface (scale bar 125microns)

Fig 6.26. The temperature dependence of viscosity for the three nanocomposite batches.

Fig 6.27. High resolution macro-photography in an attempt to show the specific pore structure of the graft cross section.

Chapter 7

Fig 7.1. The typical stress-strain relationship found on exerting compressive forces to a foam.

Fig 7.2. Compression of a foam structure.

Fig 7.3. The serrated appearance of the tensile test curves generated with initial samples on the Hounsfield Universal Tester.

Fig 7.4. Premature halting of tensile test – the sample had not achieved its failure point.

Fig 7.5. Typical tensile test obtained from a ring specimen when the pins were aligned at the initiation of the test such that they were both in contact with the ring, but without deforming it. This results in an extension of approximately one millimetre before significant stress is applied to the sample.

Fig 7.6. Slippage of the graft within the grip leading to a period of apparent extension with no increase in load. The initial steep gradient before the slippage may represent the graft not being placed exactly perpendicularly in the grips, hence the stress was not uniformly across the whole cross section of the sample. The placement error may also have contributed to there being residual force on the specimen before commencement of the test, as one side of the specimen could still have appeared slack to the investigator's eye.

Fig 7.7. Dramatic slippage of the PCB within the PTFE blocks leading to a sharp decrease in stress during the tensile test.

Fig 7.8. Tensile test of expanded PTFE.

Fig 7.9. Tensile test of initial cast sheet of 2% POSS nanocomposite.

Fig 7.10. Tensile test of PCU with no POSS moiety incorporated. The maximum stress achieved was in the range 20.74 - 28.17 MPa; SD 2.745; mean 25.57 MPa.

Fig 7.11. Spontaneous dimerisation of MDI stored at room temperature in its solid state. This can be avoided by storing at 0°C or in melted state at 50°C.

Fig 7.12. Tensile test of the POSS-incorporated nanocomposite, using non-dimerised MDI. Compared with initial nanocomposite sheets as well as with PCU, this resulted in a threefold increase in maximum stress to the range 58.05 – 68.68MPa; SD 3.908; mean 65.29 MPa.

Fig 7.13. Tensile test of thin and thick-walled porous grafts in the circumferential direction.

Fig 7.14. Tensile test of thin and thick-walled porous grafts in the longitudinal direction.

Fig 7.15. Typical tensile test curve for a thin-walled ring specimen.

Fig 7.16. Typical tensile test curve for a thick-walled ring specimen

Fig 7.17. Typical tensile test curve for a thin-walled dogbone specimen

Fig 7.18. Typical tensile test curve for a thick-walled dogbone specimen

Fig 7.19. The linear relation between graft specimen dimensions and

longitudinal strength.

Fig 7.20. The linear relation between graft specimen dimensions and circumferential strength.

Fig 7.21. The direct correlation between measured thickness and unit weight for longitudinal graft samples.

Fig 7.22. The direct correlation between measured thickness and unit weight for circumferential graft samples.

Fig 7.23. Tensile testing in the circumferential direction using a dogbone cutter.

Fig 7.24. Stress-relaxation of a PTFE longitudinal dogbone specimen.

Fig 7.25. Stress-relaxation of a thick-walled longitudinal dogbone specimen.

Fig 7.26. Stress-relaxation of a thin-walled longitudinal dogbone specimen.

Chapter 8

Fig 8.1. The increase in systolic pressure along the arterial vasculature resulting in increased pulse pressure in the smaller arteries. Concept for diagram taken from Nichols and O'Rourke³⁵³.

Fig 8.2. The hyper-compliant conduit achieved by using 5% Na(HCO₃)₂ porosifier and surfactant mixed in with the polymer solution before extrusion/coagulation. The coagulant used was de-ionised water at 50°C. This graft matched the compliance at low mean pressure of the explanted swine common femoral artery but failed at a mean pressure of only 140mmHg. The standard deviations shown relate to 3 readings taken at equally spaced points along the graft.

Fig 8.3. The compliance profiles of thick and thin-walled 2% POSS conduits.

Fig 8.4. Initial distension of highly compliant inner conduit until the less compliant outer sleeve is abutted results in a composite stress strain relationship which can approximate the 'J-shaped' stress-strain curve of artery.

Fig 8.5. The typical sigmoid curve generated from tensile testing of polymeric samples. Tangential points are included to demonstrate the incremental elastic modulus at different parts of the curve.

Fig 8.6. The compliance profiles of thick and thin-walled 6% POSS conduits

Fig 8.7. Increasing the hard segment results in a reduction of compliance.

Fig 8.8. Chain-disruption of the hard segment results in a maintenance of compliance.

Fig 8.9. Burst pressures and standard deviations for each graft type.

Fig 8.10. A single viscoelastic loop measured during steady pulsatile flow through a 2% POSS thin conduit.

Fig 8.11. Fifteen consecutive viscoelastic cycles during steady state pulsatile flow through a 2% POSS thin conduit. The area within each loop was similar, with the demonstrated variation being caused by lateral conduit wall movement due to the pulsatile flow.

Fig 8.12. Elastic Distension Ratios for each graft type with standard deviation.

Fig 8.13. Longitudinal strain due to pressure within the grafts: 2% POSS thin

Fig 8.14. Longitudinal strain due to pressure within the grafts: 2% POSS fat.

Fig 8.15. Longitudinal strain due to pressure within the grafts: 6% POSS thin

Fig 8.16. Longitudinal strain due to pressure within the grafts: 6% POSS fat.

Fig 8.17. Longitudinal strain due to pressure within the grafts: 2% POSS thin with increased hard segment.

Fig 8.18. Longitudinal strain due to pressure within the grafts: 2% POSS thin with hard segment chain disruption.

Chapter 9

Fig 9.1. Summary of the different burst pressure measuring techniques.

Fig 9.2. Burst pressures obtained via the different measuring techniques. Data are mean \pm SD of six experiments.

Fig 9.3. Subjecting a graft with an interconnected porous structure to intraluminal pressure of 300mmHg leads to 'sweating' of water through the wall.

Fig 9.4. The aneurysmal point is a more accurate term than burst pressure, defined as the point at which further infusion at the same rate does not result in any increase in pressure (in this case 347mmHg).

Chapter 10

Fig 10.1. The mechanism of free radical stimulated oxidative crosslinking of adjacent polycarbonate soft segments.

Fig 10.2. Free radical mediated crosslinking between polycarbonate soft

segment and the hard segment.

Fig 10.3. After initial (oxidative) free radical damage, polycarbonate soft segment degradation is caused by a combination of oxidative and hydrolytic means.

Fig 10.4. Uniform smooth lining on the lumen seen on longitudinal cleavage of the graft. The prolene suture (blue) at the anastomotic line is visible.

Fig 10.5. Close up of the smooth, uniform lumen lining of the explanted graft.

Fig 10.6. The fibrous capsule surrounding the explanted graft.

Fig 10.7. Cross section of the explanted graft, showing the florid fibrous capsule. The section has been cut near the anastomotic line, showing the native artery and the suture line.

Fig 10.8. Outer Surface SEM of the explanted graft showing no evidence of pitting, fissuring, cracking or balding. Scale bar is 125µm

Fig 10.9. Inner lumen SEM showing ultrascope ridges covered with a lattice structure. Scale bar is 125µm

Fig 10.10. Higher magnification SEM of the ultrascope ridges of the lumen lining of the explanted graft showing cell-like structures on the surface with varying degrees of flattening. Scale bar is 10µm.

Fig 10.11. H&E staining of the graft wall, showing the lumen (superior).

Fig 10.12. CD31 antibody staining showing uptake throughout the slide including the graft wall. There is a concentration of uptake at the blood contact surface on the periphery of the fibrinocellular layer which developed within the graft lumen. There is a second increased uptake in cellular tubular organisations within the pores.

Fig 10.13. The immediate graft wall luminal surface where the fibrinous layer is not present showing increased uptake of the anti-vWF immunostain.

Fig 10.14. Small tubular cellular structures within the graft pores which immunostain heavily with anti-vWF.

Fig 10.15. FTIR analysis of the pre and post-implantation grafts showing preservation of the Si-O peak at 1240 cm⁻¹ and the -NHCO- bonds at 1740 cm⁻¹.

Fig 10.16. The compliance of the post-implantation graft compared with the pre-

implantation graft. The results are shown for the graft alone and with the fibrous capsule attached.

Fig 10.17. TGA results for the pre-implantation and post-implantation grafts, showing the two distinct points of increasing weight loss as the temperature is increased – approximately 275 and 425°C. This is the same for both samples.

Fig 10.18. DSC thermograms for pre and post-implantation grafts. There was no significant difference in T_g . The test was terminated at 250°C which was before the melting point (T_m) was reached.

Fig 10.19. DMA result showing the storage modulus from the glassy phase, through the T_g into the rubbery plateau for the pre and post-implantation grafts. The increase in storage modulus after implantation is significant in the glassy phase.

Fig 10.20. DMA result showing the loss modulus from the glassy phase, through the T_g into the rubbery plateau for the pre and post-implantation grafts. The increase in loss modulus after implantation is significant in the glassy phase.

Fig 10.21. $\tan \delta$ against temperature for pre and post-implantation grafts, showing the maximum peak value, corresponding with T_g .

Tables

Chapter 2

Table 2.1. The positive correlation between graft compliance and patency when used in infrainguinal bypass

Table 2.2. Proportional change in cross sectional area (A/a) due to a 1mm reduction of internal diameter.

Table 2.3. Prolonged culture increases burst strength of seeded PGA grafts (From Niklason et al.).

Chapter 3

Table 3.1. Summary of research into heparin-bonded vascular grafts in the last two years.

Table 3.2. Summary of surface modification to enhance endothelialisation (in chronological order).

Chapter 5

Table 5.1. The composition of SAGM additive.

Table 5.2. The composition of CPD anticoagulant.

Chapter 6

Table 6.1. The effect of amount of nanocomposite injected on the uniform usable length of conduit produced.

Table 6.2. The variation of wall thickness for each graft based on image analysis at 72 equally spaced points around the circumference.

Table 6.3. The actual and mean weight of 1cm lengths of graft extruded into water coagulant at different temperatures. Lighter grafts resulted from higher temperature coagulation suggesting greater porosity at high temperature coagulation, in view of the similar graft dimensions.

Table 6.4. Effect of different coagulants on composition of the graft wall.

Chapter 7

Table 7.1. Youngs Modulus (E) and Ultimate Tensile Strength for five sections of 4mm ePTFE sourced from same graft.

Table 7.2. Results obtained from circumferential tensile testing of ring

specimens taken from thin-walled (t) and thick-walled (f) grafts.

Table 7.3. Results obtained from longitudinal tensile testing of dogbone specimens taken from thin-walled (T) and thick-walled (F) grafts. The shaded samples were technically failed tests due to graft slippage (T2) and sample failure occurring at the grip edge rather than within the test area (F1).

Chapter 8

Table 8.1. Non-invasive dynamic compliance as measured in a healthy young adult volunteer at a brachial blood pressure of 110/65 mmHg. SFA – superficial femoral artery; AT – anterior tibial artery; PT – posterior tibial artery; DP – dorsalis pedis artery.

Table 8.2. Summary of all conduits tested. The basic polyurethane consisted of a polycarbonate soft segment with hard segment containing 2 or 6% silsesquioxane. The hard segments were further modified by increasing their proportion overall (without adding more POSS) and by interrupting their three dimensional structure.

Chapter 9

Table 9.1. The significance of the differences in results between the four different methods. (N/S) = non-significant

Table 9.2. Methods used and results obtained for burst pressure testing of tubular conduits over the last ten years. A Medline search was undertaken for the key-term “burst pressure”.

Chapter 10

Table 10.1. Graft summary for each sheep, including duplex results pre and post-implantation.

Table 10.2. Burst pressure for the graft pre and post-implantation. The post-implantation burst pressure was obtained with and without the fibrous capsule.

I

Development of a synthetic small calibre vascular bypass graft

1.1 Introduction

The infrainguinal arterial bypass is one of the key vascular procedures¹, with an estimated 12810 revascularisation procedures carried out in 1993 in the United Kingdom with a lower limb critical ischaemia prevalence of 1 in 2500. More recent actual (non-estimated) figures have not been available although there is a national database of index vascular procedures (Dendrite) which relies on voluntary data submission. Approximately 50% of the membership of the Vascular Society of Great Britain and Ireland (VSGBI) does not submit numbers to the database. The success of lower limb arterial bypass is limited if a prosthetic graft is used² or the distal anastomosis crosses the knee joint (Fig 1.1).

Wherever possible, the patients own long saphenous vein is used³; however, this is not available or suitable in a significant proportion of cases⁴. Arm veins may be used with primary patency of 60%-85% at 3-5 years⁵, the difference with saphenous vein being attributable to previous venepuncture, phlebitis, oversized diameter, a propensity towards phlebitis and aneurysmal dilatation. Human umbilical vein grafts, which are commercially available have been shown to have a higher patency than prosthetic alternatives, but are prone to aneurysm formation in the long term and their use has not been widespread⁶. Cryopreserved allografts have one year patency rates of only 52%⁷ with the additional complications over autologous grafts of immunoreaction and proximal post-anastomotic stenosis. Good patency rates with the use of segments of the

deep venous system of the leg have been found⁸ with Schulman achieving 89% secondary patency at 3 years in selected patients⁹, but the surgery is difficult and prolonged due to the need for extensive dissection at both the proximal and distal anastomotic sites; also the fear of severe venous oedema as a result of venous outflow obstruction¹⁰ has meant that this approach has never been in favour with clinicians. The main prosthetic materials developed for bypass grafting are polyethylene terephthalate (Dacron) and polytetrafluoroethylene (PTFE). The former is a condensation polymer obtained from ethylene glycol and terephthalic acid. It is manufactured into a woven corrugated graft that is suitable for large vessel segment replacement where flow rates are high, such as diseased aorta replacement. In small vessel disease however, there is considerable reaction between Dacron and the native artery as well as with blood¹¹ causing a rapid build up of fibrin at the blood/graft interface, so making it appear unsuitable for infrainguinal bypass. However, the early experience of high thrombogenicity of Dacron grafts resulting in poor results infrainguinally has not been reevaluated in the light of platelet inhibitory therapy and the development of coated Dacron grafts which remove the need for pre-clotting. Devine and McCollum¹² have recently reported a multicentre randomized controlled trial with a minimum of five years follow-up where heparin-bonded Dacron showed a greater patency than PTFE for the first three years with a statistically insignificant difference thereafter. Expanded PTFE has achieved widespread use as a smaller diameter tubular graft for infrainguinal bypass. In above knee femoropopliteal revascularisation, individual groups have published data to suggest that the patency rates when using PTFE are not significantly different to that for saphenous vein^{13;14}. However, these studies lack power and a meta-analysis of the collated data showed that at every point in time, the patency was greater when autologous saphenous vein was used³.

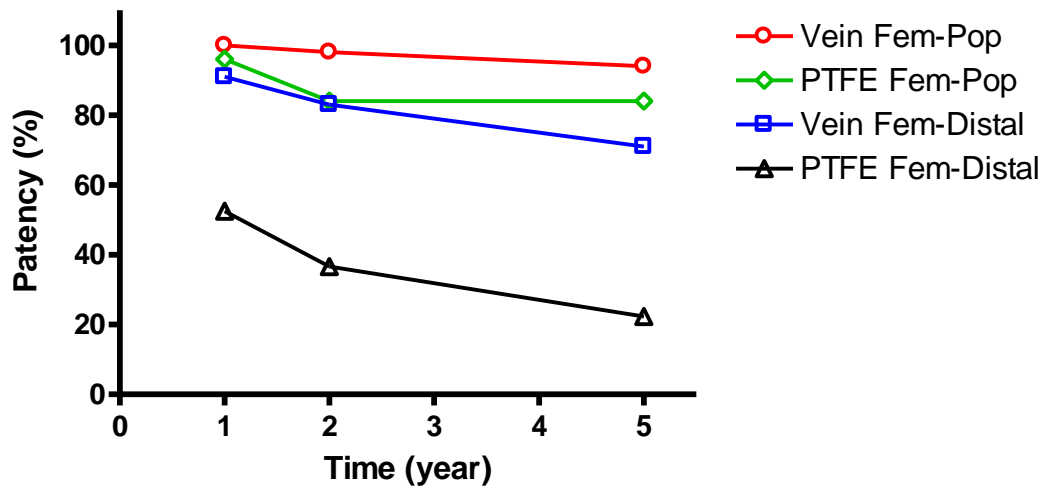


Fig 1.1 Distal bypass using PTFE has considerably worse patency than proximal bypass or autologous vein grafting^{13;15;16}.

1.2 Historical Perspective

1.2.1 The birth of vascular bypass surgery

Modern vascular surgical practice has evolved as a result of the development of angiography. This in turn was made possible by the observation of the Roentgen ray (or X-ray) by Wilhelm Konrad Roentgen in 1895 for which he was awarded the Nobel Prize. It was around this time that Alexis Carrel (another Nobel laureate) started considering the repair of vascular structures and in particular, the use of venous conduits, vascular anastomosis and aseptic technique. Soon after, x-ray visualisation of cadaveric vessels was demonstrated by Haschek and Lindenthal. Brooks used iodine-based contrast media for lower-limb arteriography in 1923 and in 1929 Reynaldos Dos Santos performed translumbar aortography. His son, John Cid Dos Santos subsequently developed endarterectomy, which he called “disobliteration of the artery”. In 1948, autologous saphenous vein was used by Kunlin¹⁷ to successfully bypass a popliteal ‘swelling’ and subsequently femoropopliteal bypass.

Since that time, no conduit has managed to better or even match the patency rates of autologous vein segments for small vessel peripheral vascular bypass in the distal limbs. This is despite a considerable research effort aimed at developing alternatives. The drive for this research is due to two factors. Firstly, autologous vein is not available for bypass in approximately a third of patients. In addition, the long term patency rates of the available alternatives are poor, causing high re-intervention rates, morbidity and low quality of life. A very short period of clinical trials of allografts was terminated due to antigenicity problems encountered, leading to dilatation and aneurysm, even after attempted attenuation with ethylene oxide; radiation; cryopreservation; protein denaturing and dessication.

Whilst angiography and anticoagulant technology was developing, attention was focusing more and more on synthetic materials as possible vascular replacement. Voorhees’ critical observation that a loose silk thread in the canine right ventricle became coated with a glistening endothelial-like surface which did not attract a thrombus covering lead to him replacing a canine

aorta with vinyon-N in 1952, after experimenting with silk handkerchiefs and nylon. He determined that the glistening layer was mainly fibrin and realised that it was necessary to encourage fibroblast infiltration and reorganisation with a porous structure to achieve endothelialisation. Vinyon-N afforded these properties as well as enough stiffness to prevent buckling of the conduits on bending and tissue incorporation. In 1954 Voorhees undertook a successful clinical trial with 17 femoropopliteal bypasses and a popliteal aneurysm bypass¹⁸.

This success achieved with vinyon-N stimulated the clinical evaluation of grafts made from a number of textiles including Nylon and Orlon in 1955. However, all of these synthetic fabrics lost tensile strength over time after implantation. In 1957 DeBakey introduced Dacron, which due to its superior post-implantation fatigue testing quickly became the gold-standard synthetic graft for aortic aneurysm repair and remains so to this day. In 1965, Dacron grafts were modified by adding a velour component to the inner and outer surfaces to provide a filamentous texture which encouraged tissue attachment and simplified the pre-clotting process. External support was added to resist kinking of grafts as they crossed joints.

However, the success of Dacron in large calibre high flow vessel replacement was not replicated when considering small diameter vessels with low flow rates. Here the relative vascular stasis combined with inherent thrombogenicity of the material caused early thrombotic occlusion and neointimal hyperplasia concentrated at the anastomotic sites contributed to long-term failure. Instead, the search shifted away from textile technology towards polymeric synthetics.

1.2.2 Peripheral artery bypass

The drive to find suitable alternatives to autologous vein for lower limb bypass was given fresh impetus by the commencement of the Korean war in 1950. Vein grafting for arterial injury salvaged thousands of limbs¹⁹ but the traumatic extent left many more victims without available vein. This was in direct contrast with the apparent indifference and delay in building on Carrel's work on venous grafts, until Kunlin revisited it two world wars later. In 1959,

polytetrafluoroethylene (PTFE) grafts were introduced by Edwards (Teflon). Aortic grafts were difficult to make from PTFE but they were successfully used by Matsumoto in 1973 for small calibre arterial replacement²⁰. Initial evaluation of clinical trials suggested PTFE to be as effective as vein for infrainguinal bypass^{21;22}. However, medium term use demonstrated neointimal hyperplasia as a mechanism for graft occlusion²³. In 1978, Kidson and Abbott made the direct association between occlusion and the lack of elasticity of PTFE and Dacron²⁴. This association appeared stronger for distal bypass involving small calibre vessels (<6mm internal diameter). Controversy exists however as to whether or not graft inelasticity results in neointimal hyperplasia. Nevertheless, alternative graft materials to PTFE for small vessel bypass have been sought, concentrating on elastic materials, with a view to compliance matching between graft and artery.

The classes of material investigated with limited success so far as potential synthetic small diameter vascular grafts include polypropylene, silicone rubber and polyurethanes.

1.2.2.1 Polypropylene

Polypropylene has the advantages of having low thrombogenicity, low inflammatory reaction and a highly crystalline, hence strong structure. However, this crystallinity means that it is non-compliant like PTFE. It is susceptible to slow oxidative degradation in vivo but as a small calibre vascular graft, has been shown to outperform PTFE in the medium term²⁵. However long term biostability is suspect, with surface cracking and serious wall weaknesses developing over several years, making polypropylene ultimately unsuitable²⁶. Therefore, this polymer has since been discounted from further investigation.

1.2.2.2 Compliant materials for peripheral artery bypass

Sottiurai has characterised intimal hyperplasia in detail and shown it to be multiple laminae of extracellular matrix (ECM) and cells – principally myofibroblasts deep to the lumen and mesenchymal type cells adjacent to the lumen²⁷. He has also shown that physical stresses on smooth muscle cells

trigger their synthesis of ECM²⁸. In vitro flow simulations and mathematical models have demonstrated that anastomotic geometry²⁹ and inelastic grafts³⁰ contribute to abnormal stresses at the heel, toe and floor of the anastomotic region – precisely the points of intimal hyperplasia. Any approach to optimise anastomotic geometry and simulate the elastic nature of the native artery will therefore reduce intimal hyperplasia, which is the principle cause of medium term occlusion in small vessel bypass. This has been the driving force behind the development of compliant materials as vascular conduits.

1.2.2.2.1 Silicone rubber

The need for high elasticity would suggest silicone as a potential graft material, as it is largely inert³¹ with low leucocyte and complement activation³². Its medical use is well established including long term implantation³³ and demonstrable in vitro biostability³⁴. Silicone elasticity is not lost after implantation and tissue incorporation³⁵. However, the hydrophobicity of pure polysiloxane makes it thrombogenic, with a high affinity for fibrinogen. Therefore graft technology exploiting the compliance characteristics of silicone have involved hydrophilic copolymer copolymerisation³⁶ or organic group attachment³⁷ to reduce thrombogenicity.

Recently, however, the issue of long term biostability has been readdressed, mainly due to a number of reports of rupture and migration of silicone breast implant material³⁸. Silicone bonds may hydrolyse and oxidise, with accumulation of silica and other breakdown products in the liver³⁹. This long term uncertainty has meant a move away from the use of silicones in biomedical devices involving prolonged implantation.

1.2.2.2.2 Polyurethane

The nylons were discovered in 1935 and soon monopolised the synthetic textile market with multiple patents ensuring exclusivity for DuPont. The search for alternative fabrics lead to the discovery of polyurethanes in 1937 by Otto Bayer⁴⁰. Initially, his product was viewed with scepticism but the concept of reacting diisocyanates with diols or diamines to form chains linked by urethane

bonds, soon attracted widespread interest due to the sheer range of physical characteristics possible. In particular they could be hard or soft; flexible or rigid. They were seen as superior to silicone for implantation purposes due to their considerable hardness. This translated to greater flex-fatigue resistance in the case of Lycra. Marketing Lycra under the tradename Biomer signalled an explosion in polyurethane development for medical device technology.

The initial polyurethanes considered utilised polyester as the amorphous macroglycol matrix in which the crystalline urethane-linked hard segment floated. However the ester bonds were shown to undergo rapid hydrolysis and degradation in vivo, making them unsuited to use within the body, even for short periods. Polyether macroglycol was more promising allowing implantation for over a week, before any signs of surface fissuring. The ether bonds were susceptible to slow oxidative degradation. They were suited to temporary implantation and biomer was clinically tested as a material for temporary ventricular assist devices, showing mechanical integrity in the short term⁴¹. The biostability of polyurethanes is considered in detail in Chapter 10.

1.3 Current Standing

Even now, there is no synthetic small calibre vascular prosthesis which has been clinically proven to improve on PTFE. The vascular surgical community is desperate for an improved graft due to the poor long term patency of PTFE grafts <6mm despite immaculate surgical technique, medical adjuncts and patient cooperation. For this reason, if autologous vessels are available, they are used whenever possible for small vessel replacement. However, suitable autologous vessels are not always available, and so PTFE is often necessary despite its poor performance. In the United States, vascular surgeons' performance is already assessed and compared by operative success rates for key procedures such as peripheral artery bypass. This is also being formally instituted in the United Kingdom via the VSGBI and informally via freedom of information requests from the national media. However as things currently stand, the success of distal bypass may have more to do with availability of good quality saphenous vein than surgical competence.

1.3.1 Polycarbonate-based polyurethane

For longstanding implantation without biodegradation, the polycarbonate macroglycol is currently considered to be much more stable than either polyester or polyether. The Chronoflex graft is made from polycarbonate macroglycol, eliminating ester and ether links⁴² and thus improving biostability. It is an elastic self sealing graft, making it potentially suitable for vascular access and small vessel bypass⁴³. Compared with its contemporary polyurethanes, it has favourable haemocompatibility⁴⁴, although its thrombogenicity can be lowered further by surface modification⁴⁵⁻⁴⁷ or endothelial cell seeding⁴⁸. Unfortunately, even polycarbonate-based polyurethane shows biodegradation and aneurysmal changes after just 10 weeks implantation in a sheep model⁴⁷. In fact, polycarbonate soft segments are susceptible to hydrolysis, as might be expected from their chemical structure. However, it is the enhanced hard segment interaction with polycarbonate which can render the overall structure resistant to degradation⁴⁹. The challenge now is to optimise this interaction to yield a non-biodegradable graft.

1.3.2 Poly(carbonate-urea) urethane incorporating polyhedral oligomeric silsesquioxane nanocomposite

The initial aim in producing this nanocomposite polymer was to improve biostability further for long term biological implant functionality. However in vitro studies have shown it to have a very favourable blood compatibility profile as well⁵⁰. This suggests the exciting prospect of a novel compliant synthetic vascular bypass prosthesis. The problems associated with graft thrombosis and neointimal hyperplasia are most prevalent in small calibre (<6mm) prostheses, leading to poor medium and long term results, so the development of these conduits from the nanocomposite would have the highest impact.

1.4 The Importance of mechanical testing

The major reasons for extensive testing of new materials at every stage of their development include:

- a. Safety.
- b. Proof of reliability.
- c. Quality control.
- d. Show adherence to accepted standards.
- e. Demonstrate improvement over established products.

Historically, the development of potential synthetic small calibre bypass prostheses has been rushed with a number of fundamental mechanical flaws being uncovered only after clinical use has started. PTFE was initially introduced clinically with a reported burst pressure of 600mmHg⁵¹. However, after human implantation, a number of early reported aneurysms of the graft wall required further reinforcement and improvements in the sintering process used.

1.5 Thesis overview

The above highlights the great importance of rigorous mechanical testing of potential grafts. To this end, a discussion of the mechanical properties which need to be considered when developing small calibre vascular prostheses follows. If mechanical properties relate to intimal hyperplasia and its role in medium and long term graft occlusion, thrombogenicity of synthetic materials cause immediate occlusion with thrombus. The blood compatibility of the polymer has been shown to be highly favourable previously⁵⁰. This unique property could not be predicted at the conceptual stages for the nanocomposite, and the mechanism is not fully understood. Nevertheless, when considering low flow states, anti-thrombogenicity is hugely desired and manipulation of materials to this aim is a large field of research. An examination of graft surface thrombogenicity as well as the methods used to improve the blood:graft interface is reviewed. The opposite philosophy is to accept the inherent thrombogenicity of synthetic materials, and look to alternatives. This view has contributed to the determined trek towards the tissue engineered vascular graft. The rapid advances in this blood vessel replacement technology have been appraised, with emphasis on the clinical viability of the tissue-engineered approach. The original work presented commences with the description of a novel process for the manufacture of porous tubular conduits from the polymer solution. Mechanical characterisation of the resultant grafts was undertaken. The mechanical properties as relevant to the physiological and surgical environments were also elucidated. These two served to describe the viscoelastic nature of the grafts as well as assessing their mechanical safety for in vivo work. The grafts were exposed to haemodynamic flow within the biological environment in a long-term ovine model and the results are reported here. The aim in carrying out these testing procedures is to show their potential for further development as vascular bypass grafts for clinical use. Industry standard test methods have been used, and where test standards are controversial, these controversies have been delineated with justification for the methodology used.

2

The mechanical properties of infrainguinal vascular bypass grafts: their role in influencing patency.

2.1 Introduction

Small diameter grafts (<6mm) are especially liable to occlusion and research into the causes of this failure and possible alternative materials with properties more akin to the original artery has been undertaken in recent times.

Between 2 and 24 months, Intimal Hyperplasia (IH) has been shown to be responsible for poor graft patency⁵². Vascular endothelial cell damage triggers the formation of IH. The postulated reasons for IH are mechanical in origin; the difference in compliance between native vessel and graft; change in direction of flow at the anastomosis; luminal diameter difference at the anastomosis; vessel wall damage⁵³ and suture technique⁵⁴. Interposing an autologous vein cuff, and in so doing, making the compliance mismatch more gradual, redistributes IH away from the most critical areas of the anastomosis, principally the heel, the toe and recipient artery floor⁵⁵, leading to some improvement in patency but keeping the overall levels of IH unchanged.

Fluid dynamics studies have revealed how endothelial damage may result from compliance mismatch. The cells are directly affected by altered stresses of blood flow through the anastomosis, known as wall shear stress (WSS). Even within the human arterial system, the shear stress varies between

different vessels⁵⁶ with superficial femoral artery mean wall shear rates of 130.3 sec⁻¹ compared with a carotid value of 333.3 sec⁻¹. In addition, in a large vessel such as the aorta, WSS and flow rate have been shown to vary according to different physiological conditions such as exercise. This is obviously not associated with IH. Experimental evidence suggests both high and low⁵⁷ shear stress as causative factors for IH. One explanation for this would be that it is the resultant flow pattern changes rather than the shear stress itself that is the cause. These include divergent flow associated with low shear stress resulting in flow separation, rarefaction and increased oscillatory shear. On the other hand, there is convergent flow associated with high shear stress which is responsible for endothelial cell injury.

The research into alternatives to ePTFE and Dacron has concentrated on new materials with viscoelasticity properties similar to native artery, principally polyurethane due to its compliance and favourable biocompatibility. This review aims to discuss the critically important roles mechanical properties such as viscoelasticity and haemodynamics play in maintaining patency of infrainguinal bypass grafts.

2.2 Basic Mechanical Theoretical Considerations

Poiseuille's law states that the head of pressure flowing in a tube (P) is directly proportional to the tube length (L), the rate of flow (Q) and the viscosity (η), and inversely proportional to the fourth power of the internal radius (r_i) of that tube.

$$P = KLQ\eta/r_i^4 \quad (1)$$

Substituting the Ohms Law analogy which states that $P=RQ$ (R=impedance) and the value of K, calculated experimentally:

$$R = 8\eta L/\pi r_i^4 \quad (2)$$

Therefore, when considering bypass conduits, the impedance to flow is drastically increased by reducing the graft calibre, thereby reducing flow rate and increasing the risk of vascular stasis and so promoting the thrombogenic

state.

However these equations hold only for pure laminar flow in a rigid pipe – every particle is moving parallel to the axis of the tube with a constant velocity. Within one lamina, all particles will have the same velocity and moreover, laminae near the centre of the tube have greater velocity than more peripheral ones – this flow profile being parabolic. (See Fig 2.1).

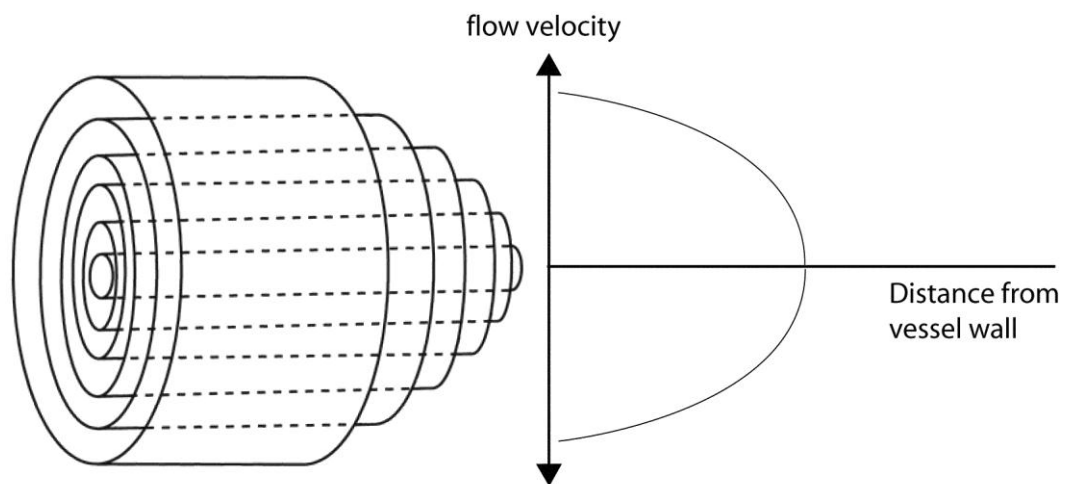


Fig 2.1. The parabolic profile of laminar flow. A purely 'Newtonian' fluid displays this flow pattern. However, blood is not a homogenous mixture of small particles, and so is not 'Newtonian' in its behaviour.

These theoretical considerations do not hold true completely in the arterial system for numerous reasons. Firstly, the artery is not a rigid pipe. In fact it is a complexly compliant structure with intrinsic and extrinsic mechanisms to vary its compliance and shape, and in so doing, contributing to the pressure for flow itself. Next, blood flow only approaches laminar flow in the largest arteries. Even in these vessels, the rate of flow is not steady and it is only in diastole and early systole that laminar flow is observed. Turbulent flow due to branching vessels is also widespread. Being a suspension of particles of various size, blood is a non-Newtonian fluid. This makes its behaviour unpredictable, especially in small diameter vessels.

Nevertheless the laminar model can be used to describe useful concepts in the investigation and description of the mechanical properties of blood vessels and flow. One such model is Wall Shear Stress (WSS).

The resistance R in Poiseuille's Formula relates to the impedance to flow of a particle in one lamina caused by the friction of the adjacent lamina. In the same way, at the most peripheral lamina there is a force exerted by the particles flowing here on the wall of the vessel itself. This action against the wall is termed WSS. Therefore when considering the vessel wall;

$$WSS = R = 8\eta L / \pi r_i^4 \quad (3)$$

The tendency for deformation of the vessel wall due to pulsatile flow of blood within it is, within physiological limits, elastic. This is to say that if the blood force is removed, the vessel will return to its previous shape. However, the force does not cause an instantaneous deformation, like when a weight is placed on a spring. The shape change, in the presence of a constant force is a gradual one and the same is true when the force is removed. This property of delay is termed viscosity. The blood vessel demonstrates a combined viscoelastic tendency.

Overall the mechanical behaviour of an artery is complex. The ideal graft for anastomosis would replicate this behaviour. In order to simplify the investigation and description of this behaviour in arteries and graft materials, the term 'compliance' is used, encompassing the changing mechanical properties depending on the haemodynamic pressure within the graft, unlike established

physical concepts such as Young's Modulus, E^{58} , which increases with increasing pressure within the compliant graft lumen⁵⁹. At a given pressure P in a vessel of diameter d and wall thickness t :

$$E = \text{stress/strain} = (Pd/2t)/(\Delta d/d) \quad (4)$$

$$\text{Rearranging this: } \Delta d/dP \text{ ie. Compliance} = d/2Et \quad (5)$$

Compliance is therefore inversely proportional to vessel wall thickness, and manufacturing a synthetic graft with a thinner wall results in greater distensibility. Conversely, patients with peripheral vascular disease have increased intima-media thickness, contributing to their rigidity⁶⁰.

The overall result of the viscosity of the arterial wall and its compliance (ie. viscoelasticity) is to convert the pulsatile ejection of the heart into a continuous flow, storing a part of the energy of propulsion in systole and restoring it to the circulation during diastole. Therefore, viscoelasticity is important in energy transfer and dissipation. All vascular tissues have greater dimensions during unloading than during loading, leading to a hysteresis loop when the pressure/diameter characteristics of the vessel are plotted on a graph (Fig. 2.2).

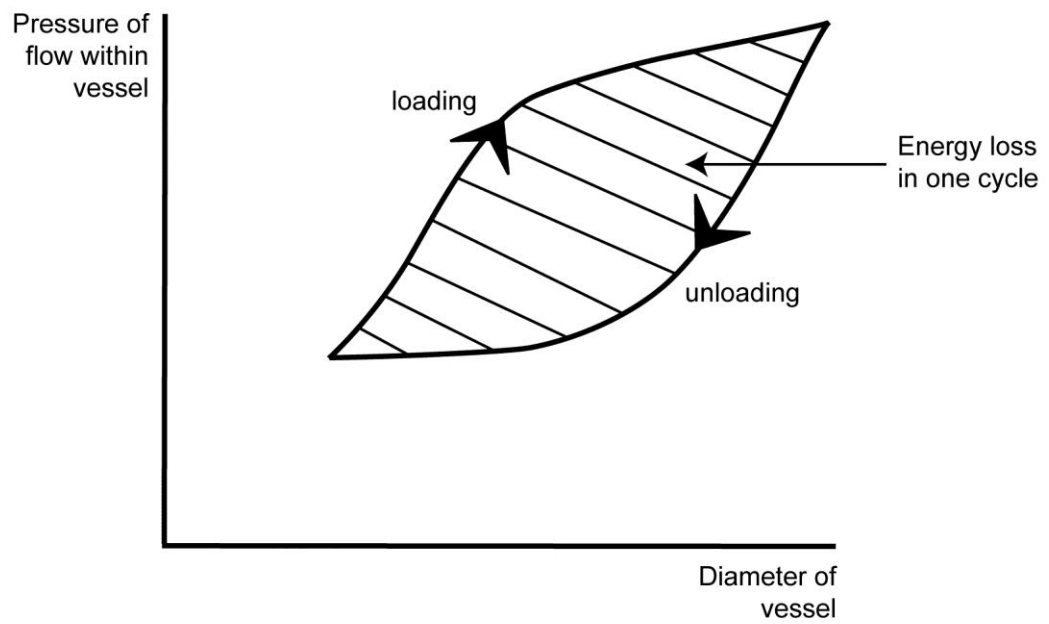


Fig 2.2. The hysteresis loop observed during repeated cycles of applying and removing a force from a vessel wall as would occur during pulsatile flow.

The area within the loop represents the loss of energy to the vessel wall and so viscosity. Very high viscosity may reduce distensibility under dynamic pressure conditions and arterial viscosity is higher in vitro than in vivo. Boutouyrie's group⁶¹ hypothesized that this was in part endothelium-dependent, the mechanism of control being via vascular smooth muscle (VSM) tone. They showed that de-endothelialization lead to a 40% rise in viscosity. However, the same department subsequently investigated the viscosity of arteries subjected to phenylephrine and sodium nitroprusside, and thereby providing a range of VSM tone⁶². They showed that there was no significant difference in viscosity with different VSM tone and found that viscosity rose with rising pulse pressure. This has been confirmed clinically with the arteries of hypertensive patients found to have greater viscosity than equivalent normotensive controls⁶³. Other investigations of the mechanical properties of arteries that have not specifically concentrated on viscosity have measured the phase delay between pulse pressure and distension(ie. the dampening effect). This method demonstrates viscosity when considering a single pulse of flow. However, in physiological pulsatile flow, the alternating storage and discharge of energy by the vessel wall leads to an intrinsic energy capacitance as well as a continuous loss of energy, which is more accurately measured from hysteresis curves.

2.3 Mechanical variables influencing graft success

2.3.1 Compliance

There is widespread reporting of compliance mismatch being primarily responsible over geometric factors³⁰ for IH and subsequent poor graft patency²⁴ (see Table 2.1).

	<i>Compliance *</i>	<i>1 Yr % Patency</i>	<i>2 Yr % Patency</i>
Host artery	5.9	-	-
Saphenous vein	4.4	88	84
Umbilical vein	3.7	83	80
Bovine heterograft	2.6	65	59
Dacron	1.9	65	42
ePTFE	1.6	60	42

*% radial change per mm Hg x10⁻². Adapted from Walden et al.⁶⁴

Table 2.1. The positive correlation between graft compliance and patency when used in infrainguinal bypass

However, rather than the compliance per se, it is in fact that the resultant haemodynamic flow changes cause increased shear stress to damage endothelial cells and reduced shear stress⁶⁵ leading to areas of relative stasis and increasing interaction between platelets and vessel wall; pooling of chemokine factors⁶⁶ promoting IH as well as increasing oscillatory forces. The aim of matching compliance is to minimise these disruptive flow characteristics.

The creation of an anastomosis itself causes a local reduction of compliance at the suture line, as shown by Ulrich and colleagues⁶⁷ on artery to artery end to end (ETE) anastomoses. A continuous suture technique causes a greater loss of compliance than interrupted sutures⁵⁴ with greater concentration of stresses at the suture line tethering it against distension in the case of the former. Clips that do not penetrate the intima also results in an anastomosis with less compliance mismatch (CM)⁶⁸.

It is postulated that the high flow at the proximal anastomosis is partly protective as it allows for the rapid dispersal of chemotactic factors released due to endothelial injury. It is the distal anastomosis where the majority of IH is seen. Here the artery is of small calibre, especially in an infragenicular bypass and even a slight thickening of the intima will cause a considerable stenosis, compared with a large calibre vessel (see fig.2.3/table2.2).

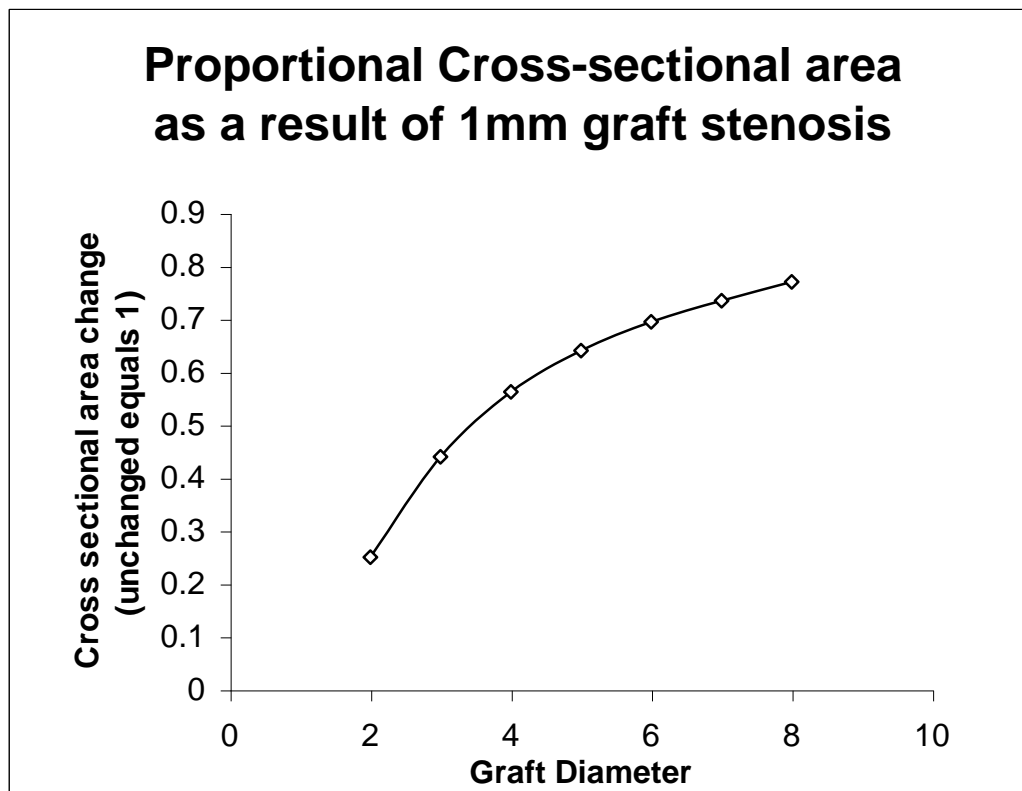


Fig 2.3. The consequence of a 1mm graft stenosis is much greater in a small caliber vessel than in a large caliber conduit.

<i>Graft diameter (mm)</i>	<i>Cross-sectional area A (mm²)</i>	<i>Cross-sectional area after 1mm stenosis a (mm²)</i>	<i>A/a</i>
2	π	$\pi/4$	0.25
3	2.25π	π	0.44
4	4π	2.25π	0.5625
5	6.25π	4π	0.64
6	9π	6.25π	0.69
7	12.25π	9π	0.73
8	16π	12.25π	0.77

Table 2.2. Proportional change in cross sectional area (A/a) due to a 1mm reduction of internal diameter.

The proportional change in cross-sectional area for a graft with diameter d and calibre reduction Δd is given by the equation:

$$1 - 2\Delta d/d + \Delta d^2/d^2 \quad (6)$$

Stenosis due to IH promotes platelet adherence, thrombus formation and resultant graft blockage by causing abnormal flow disturbances as outlined earlier.

The vortices created by the compliance mismatch is further complicated by a perianastomotic hypercompliance zone (PHZ)^{54;68;69} (see Fig.2.4). This contributes to give the overall perianastomotic region compliance properties somewhere in between those of artery and graft (see Fig. 2.5).

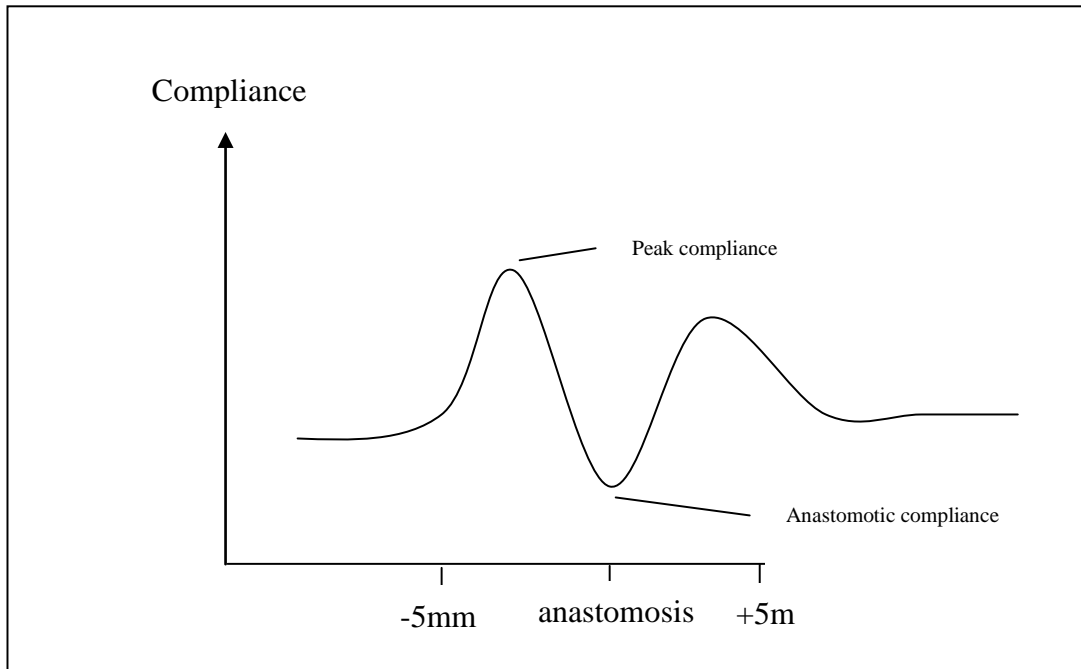


Figure 2.4. Illustration of the para-anastomotic hypercompliance zone

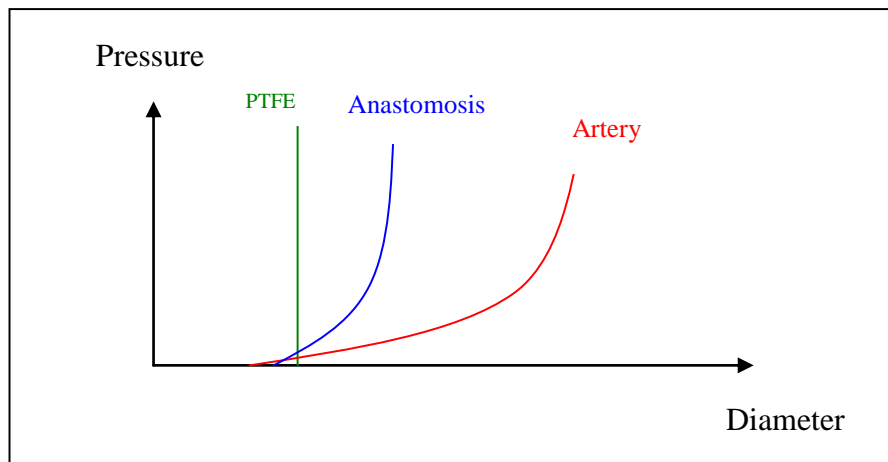


Figure 2.5. For an anastomosis between ePTFE and native artery, the per-anastomotic compliance is intermediate between that of its constituent vessels. Adapted from Sonada et al.⁷⁰

This has been confirmed experimentally by Sonada and co-workers⁷⁰. The artery's J-shaped curve of compliance shown in Figure 6 demonstrates how it does not obey Hooke's Law when subjected to pulsatile flow. It is due to highly elastic elastin fibres controlling its distension at low pressure flow and relatively inelastic collagen fibres taking over at higher pressures⁷¹. At 100mmHg only 5-6% of collagen fibres are recruited with progressive recruitment with rising pressure. Physiological influence causes recruitment of vascular smooth muscle cells in conjunction with some collagen fibres with elastin fibres bearing the remaining share of the stress⁷².

Design of alternative grafts to ePTFE has concentrated on achieving a compliant structure. This has been approached in several ways including porous 'spongy' materials⁷³ and co-axial double tubular grafts with a more compliant inner lining and a less compliant outer layer⁷⁴. As these latter grafts are distended, they become progressively less compliant as the outer sleeve properties become more prominent. Our own unit has produced and characterized porous compliant poly(carbonate)polyurethane (PCU) grafts (MyolinkTM)⁷⁵⁻⁷⁷ – see Fig 2.6.

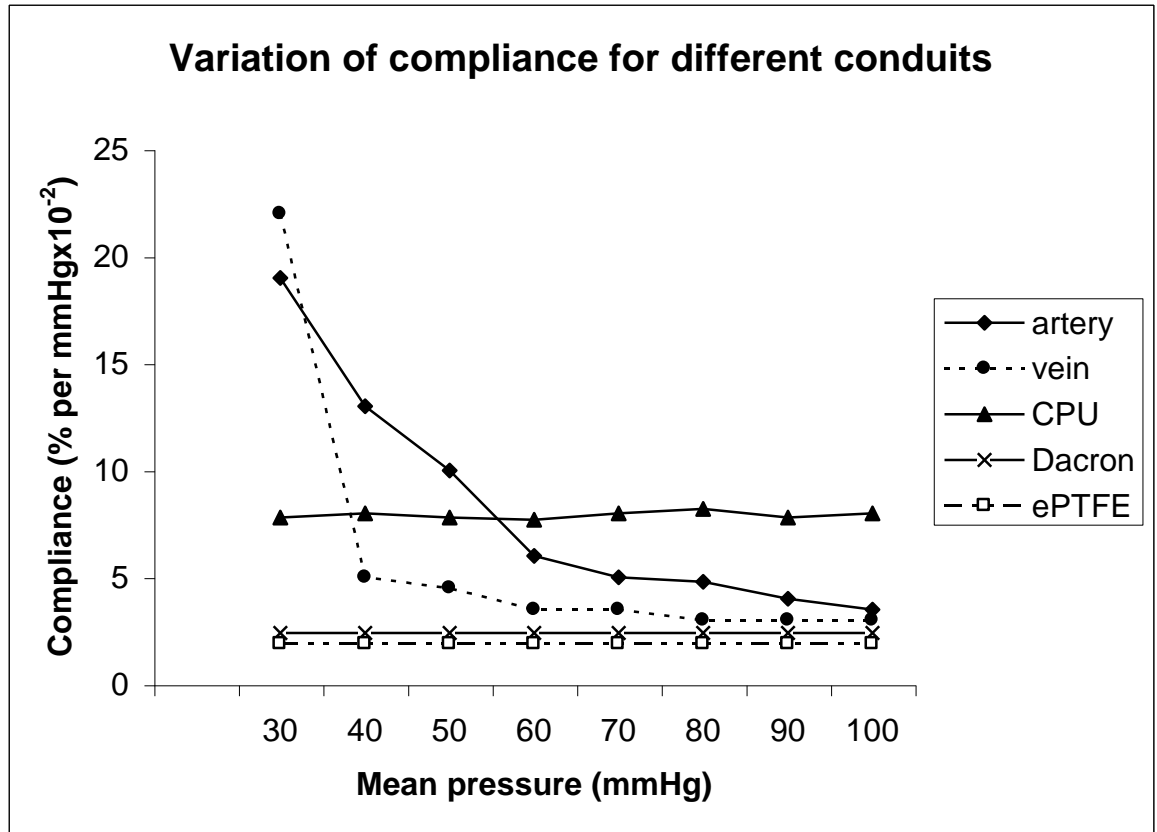


Figure 2.6. Tai's investigation of compliance in a flow circuit showed the 'anisotropy of compliance' for the external iliac artery – the distensibility is dependent on the pressure level at which the distending stress is exerted. The commercial bypass graft materials have low compliance compared to the artery, but saphenous vein also has low compliance, illustrating the importance of cellular and biochemical factors in graft success. PCU refers to poly(carbonate-urea) urethane, which is the basis for the nanocomposite.

Another aspect of interest to graft designers is the long term change in compliance of a graft after implantation. The artery has an astonishing capacity to maintain its intrinsic compliance despite abnormal chronic physiological changes such as hypertension⁷⁸. This is observed to cause wall thickening but compliance is unaffected due to intrinsic changes in the vessel wall properties⁷⁹. Interestingly, when a vein graft is used, it undergoes wall thickening which also does not lose its compliance properties⁶⁴. However, the effect of the surrounding tissues on an implanted prosthetic graft is to reduce compliance with time⁸⁰. This is especially the case in porous structures with a pore size greater than 45 μ m when considerable fibrous tissue ingrowth takes place⁸¹. MyolinkTM with its small pore size does not lose compliance after implantation in an animal model for 36 months⁸².

A variety of methods have been employed to measure conduit compliance in the research setting, although it is not routinely investigated clinically. The majority of research carried out to date has been based on the measurement of diameter changes at given pressures. Accurate (blood) pressure measurement can be obtained through use of a pressure transducer device both in-vivo and in-vitro. In the former case, this requires invasive introduction of an arterial catheter which may have significant complications such as bleeding and embolism.

The alternative in vivo and particularly in human studies is to use indirect blood pressure measurement via sphygmomanometry. This is less accurate for absolute pressures as well as temporally less precise. Peripheral pressure measurement does not completely reflect central blood pressure due to the physiological increase in pulse pressure between the central arteries and the periphery⁸³. Interestingly, the loss of compliance in calcified vessels results in the disappearance of this difference, and in the elderly patient with peripheral vascular disease, peripheral blood pressure equals its central counterpart.

Multiple modalities have been used to measure the diameter of vascular conduits. These are again invasive or non-invasive. In vitro models have the advantage of having the conduit free of surrounding tissues. However, explantation or even surgical dissection of arteries in-vivo inherently changes the compliance properties being measured⁸⁴. The most invasive techniques involve placing electrical transducers against the internal vascular wall. Electromagnetic principles are used to measure internal diameters using

Intravascular Absolute Induction Angiometry in this way⁸⁵. A pre-sized intravascular loop is introduced to line the artery wall in a circumferential direction. This loop is made up of 3 separate wires. One of these wires has a high frequency alternating current flowing through it. This causes the generation of an electromagnetic force which varies depending on the wire circumference and is transduced by the other two wires into precise internal diameter readings in real time. Exposed vessels can also be visualised closely using high speed camera technology and calibrated measurement software⁶⁹ or scanning laser beams⁸⁶ seeking out photocells on the far side of the vessel. These technologies however measure the external wall diameters. The difference between the two is roughly equal throughout and hence does not affect the resultant compliance significantly⁸⁷.

Historically, human studies have involved the use of electrical transducers intraoperatively⁸⁸ but these are individualised time intensive studies that could not be used in routine practice. More recent is the use of various ultrasound techniques, principally using wall tracking mode high frequency ultrasound⁸⁹ or radiofrequency (RF) signal based systems, which requires equipment that is now widely available. Vernhet et al⁹⁰ have evaluated the use of standard B mode ultrasound to measure compliance. This method gives lower resolution pictures and uses a simultaneous ECG trace for timing with average systolic and diastolic pressure changes. They have compared this system preoperatively against sonomicrometry postoperatively in a similar animal model. Their main difficulties were in ensuring perpendicular views of the aortas, correcting for respiratory movement and obtaining high quality artifact-free views. Long and colleagues⁹¹ used similar tissue doppler imaging on human aortas and concluded that this was an accurate simple and quick process that could easily be used in routine clinical practice to measure aortic aneurysm compliance serially to give warning of the risk of rupture. Our unit has used wall tracking duplex ultrasound to study the compliance of peripheral vessels in a range of systemic conditions. The carotid and femoral artery intima-media thickness (IMT) was higher in patients with known peripheral vascular disease (PVD) than age and gender-matched control patients⁶⁰. These thicker vessels were also less compliant than normal, increasing cardiac afterload. These results were replicated in patients with PVD and abdominal aortic aneurysms compared with patients with aneurysms alone⁹², suggesting a way

of stratifying cardiovascular risk perioperatively. Similarly, a reduction in compliance of femoral and carotid arteries associated with increased IMT was observed in women with polycystic ovary syndrome^{93;94}. Patients with scleroderma were found to have reduced carotid compliance but no apparent change in IMT⁹⁵.

MRI technology has been utilised to measure aortic diameter and calculate compliance⁹⁶ but its use with small calibre vessels has not taken off yet due to prohibitive costs and the relatively poor quality of image. However, continuous improvement in MR magnet technology means that the resolution issues will be in time resolved. In the meantime, MR images have been used as a basis for computational fluid dynamic studies in smaller vessels⁹⁷.

Digital subtraction angiography (DSA) is widely used to assess the arterial system of patients. This has also been used by Seifalian and colleagues to accurately measure compliance of arterial segments both in vitro and in vivo⁹⁸. Flow rate information can be obtained simultaneously with distension by measuring the intensity of the contrast bolus in an arterial segment or graft over time.

Validation of their technique in flow circuits has revealed high accuracy of compliance measurement. Arterial catheterisation is required in order to perform an angiogram as well as to simultaneously measure blood pressure throughout the cardiac cycle. However, this does open up the possibility of accurate, routine clinical compliance studies in patients with peripheral vascular disease at the time of angiography, using equipment that is widely available in the x-ray department.

2.3.1.1 The Importance of Correct Compliance Matching

Compliance mismatch (CM) is thought to cause IH. However the evidence for this is still equivocal. The evidence for and against CM as the cause of IH is given below.

Hirayama et al. undertook a mathematical study of impedance to flow through infrainguinal arterial bypass grafts anastomosed to normal and calcified arteries⁹⁹. Taking both wall tensions and the tethering effects of surrounding tissues into account with linear dynamical equations, they found that for an artery with high resistance, a correspondingly rigid, inelastic graft minimized

both impedance to flow and reflection coefficient. A compliant artery as in the healthy individual with no peripheral vascular disease had better flow characteristics if anastomosed with a similarly compliant graft. Perktold et al.¹⁰⁰ used Navier-Stokes equations to describe flow through an end to side (ETS) anastomosis, a Miller cuff and a Taylor patch. They showed that the vein cuffs reduced suture line hyperplasia by geometrical modification to some extent, but more importantly by a decrease in the compliance mismatch as a result of vein interposition. Stewart and Lyman⁶⁶ gave flow visualisation evidence for stagnation of flow near the distal anastomosis as a result of CM. In a numerical study using finite element simulations of ETE anastomoses, they subsequently showed that unusual concentration gradients of a model protein could build up at the anastomosis as a result of CM¹⁰¹, suggesting the possibility of pooling of chemotactic agents of IH. A mathematical model considering stress and strain at the artery wall with evolution equations to describe wall remodeling due to the deformation of the artery examined a compliance-mismatched anastomosis¹⁰² showing that such a configuration causes abnormal axial and circumferential stress on the artery leading to remodelling including wall thickening with the aim of correcting the abnormal stress. This points to IH as a possible adaptive response to try to return shear forces towards baseline. An in vitro ETS anastomosis between artery and PTFE graft shows a greater concentration of fluctuation energy at the anastomosis than the same anastomosis using Ultraflex compliant graft¹⁰³.

There are a number of in-vivo investigations offering doubt on CM as cause for IH. Wu et al's¹⁰⁴ animal model of ETE anastomoses showed no difference in IH levels between Dacron and carotid artery as graft material. However, the Dacron anastomoses were made with the carotid artery, whereas the arterial grafts were anastomosed to the femoral artery, making this a possible confounding variable. At 14 weeks, Uchida et al.¹⁰⁵ also found no statistical difference in ETE anastomoses between artery and compliant/non-compliant grafts. Okuhn et al.⁸⁵ created abrupt changes in compliance by placing bands on segments of common iliac artery. They found no significant IH at 6 months. Vein-cuffed anastomoses have been considered, due to them reducing the sudden CM⁶⁹ but Norberto et al.¹⁰⁶ encircled vein cuffs with ePTFE jackets eliminating their high compliance properties and found no difference in IH compared to unjacketed cuffs.

Ballyk et al's¹⁰⁷ theoretical model has demonstrated that a high CM does cause high anastomotic stress in ETS anastomoses, but does not do so in ETE configurations, which may explain why some groups found CM to be critical whilst others didn't.

2.3.2 Conduit Calibre

From Poiseuille's law, it can be seen that the pressure of flow for blood through a conduit is inversely proportional to the fourth power of its radius:

$$P \propto 1/r^4$$

When considering an implanted bypass graft with no side branches, a purposeful tapering of the graft would lead to a massive concentration of pressure across the graft¹⁰⁸ ($\Delta P \propto 1/\Delta r^4$). The natural tapering of the vasculature distally is workable without rises in pressure due to the extensive branching of the native vessels. Moore et al. showed in a numerical model simulation of an ETS anastomosis that graft-to-host diameter ratio was the most important of the geometric factors in determining WSS¹⁰⁹.

Treiman et al.¹¹⁰ have conducted duplex studies to show that utilising a larger diameter venous graft is associated with lower distal graft velocity. In the case of above knee femoropopliteal bypass, it has been clinically confirmed that larger diameter grafts confer better patency rates than smaller conduits^{111;112}. The same has been shown for coronary artery bypass grafts¹¹³.

Abnormally high flow velocities are associated with changes in the pattern of wall shear stress, if not an increased mean or peak wall shear rate¹¹⁴. These haemodynamic flow changes are associated with the development of IH and indeed, doppler flow studies of the distal anastomosis revealing high flow velocity predicts stenosis due to IH¹¹⁵. This is a vicious cycle as stenosis results in a further increase in flow velocity. Papanicolaou et al.¹¹⁶ have used the observation to offer a clinical guideline on graft surveillance, suggesting that low levels of vein graft stenosis with a peak systolic flow velocity (PFV) of less than 250cm/sec. on duplex scanning can safely undergo watchful waiting, whereas greater stenosis should lead to prophylactic revision of the revision of the bypass as this gives better results than if the inevitable symptoms of graft

occlusion are awaited. Papanicolaou et al.¹¹⁷ also give a mechanism by which occlusion results from a critical stenosis, by making a comparison of duplex-derived pre-stenotic and stenotic PFV. They calculate that for a typical 80% diameter stenosis, a minimum perfusing blood pressure of 144mmHg is required to maintain flow across it. They hypothesise that failure to achieve this blood pressure at all times leads to stasis of flow and resultant thrombosis. Their calculations are based on the assumption that the lowest flow velocity seen clinically on duplex scanning is equivalent to the thrombotic threshold velocity. In reality this may be an oversimplification with flow velocity being only one of the determinants of thrombotic threshold as detailed in Virchow's triad of hypercoagulability, vessel wall damage and stasis, but the hypothesised mechanism for graft failure would still stand. However, a grossly oversized distal conduit will result in a sudden decrease in flow rate with relative stasis and flow separation. The resultant low shear rate is associated with IH as discussed earlier. Polo et al.¹¹⁸ showed that higher flow rates in arteriovenous dialysis access grafts was associated with less occlusion and lower frequency of rescue intervention.

Hence the ideal diameter difference between graft and artery at the distal anastomosis is a balance to maintain the ideal flow velocity and characteristic. Longest and Kleinstreuer²⁹ used a theoretical ePTFE:ePTFE anastomosis model to calculate the ideal ETS geometric properties. By using ePTFE for both ends of the anastomosis, the potential confounding factor of compliance mismatch was avoided. They found that a 2:1 (proximal to distal) ratio was too great a difference with respect to favourable haemodynamics whereas 1.5:1 predicted less anastomotic stress.

2.3.3 Porosity

In order to construct a bypass graft that mirrors the properties of the artery it is replacing, the concept of porosity has been considered. The artery is a selective permeable structure and a microporous architecture in a prosthesis has been shown to mimic arterial function¹¹⁹.

Endothelialisation of the luminal aspect of a graft comes about directly from the artery at the anastomotic site as well as via fibrovascular infiltration of the graft material from the surrounding tissues. It is this latter that allows speedy

uniform endothelial lining of a long graft. Zhang et al.¹²⁰ showed that with physiological pulsatile flow within an animal model, full ordered endothelialisation of a small diameter prosthesis is possible within 8 weeks, providing a pore size of 30µm diameter. They also demonstrated that the external aspect pore size correlated with the rate of endothelialisation. White et al.'s⁸¹ review of pore size shows that the ideal pore size for fibrovascular infiltration is between 10 and 45µm. However, larger pores allow too much surrounding fibrous tissue invasion risking a dramatic loss of compliance⁸⁰.

Fujimoto et al.¹²¹ demonstrated that pore size was important for patency rate, but it was rather the density of pores which determined graft compliance.

In our department, Salacinski and colleagues¹²² showed that porous PCU promoted successful seeding of endothelial cells onto its surface. By isolating the effects of surrounding tissues and fibrovascular infiltration in a laboratory model, Giudiceandrea et al.¹²³ showed that after initial seeding, a porous graft allows stronger endothelial cell adherence when exposed to pulsatile flow than smooth ePTFE. They hypothesise that this may be due to the luminal surface pitted with a "honeycomb structure", as seen on scanning electron microscopy.

MacLeod and coworkers¹²⁴ investigated the percentage porosity (a function of both pore size and pore density) of collagen based prostheses. They found a proportional relationship between porosity and vascularity at one and two weeks.

ePTFE grafts which have low porosity were explanted after a mean implantation time of 523 days, from human subjects and examined by Guidoin et al.¹²⁵ They found that cellular infiltration into the grafts was poor, with mostly thin patchy fibrinous cover to the lumen.

The thrombogenicity of a graft's luminal surface is an important concept in prevention of early failure. Losi and colleagues¹²⁶ found that platelet adherence to the lumen had an inverse relationship with porosity. This was elucidated by measuring the levels of circulating platelets and subtracting monitored platelet aggregation levels. The findings were then confirmed optically. Hence it was shown that a porous material may confer anti-thrombogenic properties. The reasons for this are not clear.

Therefore in the development of a new graft, the precise measurement of its porosity is critical. This has been addressed since 1961 when Wesolowski et al.¹¹⁹ used a machine to compress the graft wall and measure the rate of flow of

water through the wall at a water pressure of 120mmHg. They found this measure to be highly reproducible.

Pore size measurement can be simply achieved from high resolution optical microscopy or scanning electron microscopy¹²¹ but this does not take account of pore density and is not a true reflection of porosity. Simple computer analysis using photo-editing software of the cross sectional structure can determine the proportion of area which is made up of pores as a percentage of the whole area¹²⁰. Further computational extrapolation and 3D reconstruction can then correct for precise pore shape¹²⁷.

Pycnometry involves subtracting the mass volume of a substance from the volume of a fluid (gas or liquid) displaced, the resulting figure giving an approximation of porosity. A pycnometer¹²⁸ utilises a cell with a known pressure of a gas inside. The porous structure is introduced into this cell and the resultant increase of gas pressure is accurately measured. Mass and volume calculations then reveal the density of the material. Gas adsorption techniques require the material under investigation to have all air removed from it by vacuum, and nitrogen or water vapour reintroduced – the amount taken up being an indicator of porosity¹²⁹.

2.3.4 Burst pressure

This relates to the pressure that the vascular conduit can be subjected to before an acute leak develops and the conduit fails. The maximum force, f , applicable to any material is represented by:

$$f = Pd/2t$$

where P represents (burst)pressure, d represents diameter and t represents wall thickness⁵⁸.

Therefore it can be seen that the burst pressure decreases with increasing diameter and with decreasing wall thickness, since f is a finite entity. It is therefore very likely that the burst pressure for a small diameter graft will far exceed the physiological range of blood pressures possible in man. For example, the burst pressure of a typical carotid artery is in the region of 5000mmHg¹³⁰ and for a saphenous vein is around 2250mmHg¹³¹. Suture line

weakness makes it far more likely that the anastomosis will fail before the conduit material. Burst pressure of porous polyurethane grafts have been found to be 1850-2050mmHg¹³², again much greater than any possible physiological blood pressure.

2.4 Properties of bypass conduits in clinical use.

2.4.1 Autologous vein.

Unlike the arterial system, veins do not physiologically have to deal with pressures greater than 75mmHg¹³³, and have a lower compliance range than arteries due to a lower collagen-elastin ratio and much less smooth muscle. Their role is to maximize capacitance rather than to contribute to pulsatile flow transmission. However a venous graft anastomosed to an artery will suddenly overdistend to its limit. This will lead to immediate de-endothelialisation¹³⁴. The sequence of events over the next 30 days is often termed 'arterialisation'¹³⁵. This involves luminal wall platelet deposition; vascular smooth muscle cell (SMC) apoptosis and necrosis; monocytic infiltration; adventitial fibroblastic activity and angiogenesis; myointimal thickening with media SMC proliferation and infiltration. Finally there is re-endothelialisation.

From three months onwards, considerable remodelling of a venous graft in-situ has been shown to occur¹³⁶. There is wall thickening with concomitant reduction in wall tension; lumen size changes proportional to the initial lumen size with lumens larger than 3.75mm in diameter actually getting smaller; and a significant increase in wall stiffness. These changes along with re-endothelialisation equip the graft for use as an arterial conduit. This is reflected in the sizeable failure rate for venous grafts in the first year compared with subsequent annual occlusion rates¹³⁷.

As a result of low elastin levels compared to an artery, the overdistension caused by arterial blood pressure gives the vein poor compliance properties, making it in effect a rigid tube. Stoker et al.¹³⁸ found lower leg saphenous vein to be more distensible than its upper leg equivalent in the venous pressure range. They could not show a histological explanation for this with similar proportions of extracellular matrix and SMCs in both areas. Davies et al.¹³⁹

found however, that compliance of a vein was inversely proportional to both circular muscle hypertrophy and focal hyperplasia. They confirmed that the thicker-walled distal saphenous vein segments show less compliance. This latter study was an in-vivo investigation with all the effects of the surrounding tissues. Also studying vein grafts ex-vivo causes changes to exactly those mechanical properties which are of interest¹⁴⁰.

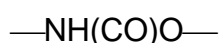
2.4.2 ePTFE

ePTFE has shown to be very stable in vivo with no reported failures due to degradation of the graft¹²⁵. It is a poorly compliant material made up of fibrils extruded into a tubular structure with moderate stiffness¹¹. Perivascular reaction reduces its compliance further to only 14% of its pre-implantation level. The gaps between the fibrils form very small pores which are so small (<0.05µm) that many studies consider it to be a non-porous material¹²¹. Because of this ePTFE grafts have very poor luminal endothelialisation in vivo¹²⁵. Higher porosity can be conferred to PTFE by constructing a graft with a larger fibril size (60µm vs. 20µm) leading to the promotion of transmural tissue growth¹⁴¹.

2.5 Prostheses of the future

2.5.1 Synthetic grafts

The search for new compliant prostheses to replace ePTFE has concentrated on polyurethane materials⁷³. The fundamental building block is a repeating sequence of urethane:



Polyurethanes are formed by the reaction of a polyol (an alcohol containing more than two reactive hydroxyl groups per molecule) with either a diisocyanate or a polymeric isocyanate. The resulting product is termed the hard segment. A soft segment is mixed with this to give the desired mechanical

and degradation properties. These include polyesters, polyethers and polycarbonates. The hard and soft segments mix incompletely to allow microphase separation within the polymer⁷³. Soft segments consisting of polyester groups are susceptible to rapid hydrolysis and hence are not suited to prolonged implantation in vivo. Polyether undergoes oxidative degradation and so is also unsuitable. Polycarbonate however, has low biodegradation when exposed to an adverse environment in vitro. In our department, the Pulse-Tec polyether based polyurethane was compared with a compliant poly(carbonate-urea) urethane (PCU) which was developed in-house - Myolink™, in a variety of solutions simulating biological extremes¹⁴² and the PCU graft was found to have far greater stability and preservation of mechanical properties. Furthermore, comparative thermomechanical analysis⁷⁷ also showed that the chemical changes evident in the case of Pulse-Tec were not present with Myolink™, with hydrolysis of the soft segment only achieved in an environment of glutathione/t-butyl peroxide/ CoCl₂. Implantation of PCU into an animal model suggested that it was appropriate for in vivo use⁸² with only minor hydrolysis of the soft segment after 3 years in situ and no change in mechanical properties.

PCU has yet to be used clinically as an infrainguinal bypass graft. Before this can occur, further research into PCU development with particular consideration of anti-thrombogenic properties and spontaneous endothelialisation in vivo is required. In addition, a host of different manufacturing processes have been identified and the most suitable one needs to be identified in terms of reproducibility and quality control. However this class of polymer is an exciting future prospect for the development of a compliant small caliber bypass graft.

2.5.2 Tissue-engineered grafts

It is realized that a biological arterial substitute incorporating the cellular layers of the native vessel could reflect the mechanical properties of the artery as well as providing its inherent antithrombogenicity. In addition, the mechanical properties of the conduit would adapt to the prevailing haemodynamics from moment to moment precisely like an artery does, and in the long-term, remodel to suit its environment. Generally speaking, such tissue engineered grafts are created with a biodegradable scaffold to provide a

template on which the cellular components can align and the overall structure can mature. Those conduits where cells are seeded to a non-degradable scaffold are termed hybrid grafts – the mechanical properties of these vessels depend on the scaffold and these will not be considered further.

Alternatively, the use of a biodegradable polymer scaffold to give temporary strength to a vessel and a template for culturing SMCs will lead to gradual replacement of the synthetic material by collagen. In contrast with hybrid grafts, permanent remodeling to suit the conditions of flow will be possible, potentially resulting in ideal mechanical properties in the long term¹⁴³.

The bioresorbable scaffolds used are based on polyglycolic acid (PGA), polydioxanone (PDS) or Polylactide (PLA)¹⁴⁴. PGA forms a porous structure but is resorbed within 8 weeks and in order to slow degradation it is often combined with an adjunct such as polyhydroxyalkanoate, poly-4-hydroxybutyrate (P4HB) or polyethylene glycol¹⁴⁵. Hoerstrup et al.¹⁴⁶ used PGA coated with PH4B to form grafts which they subsequently seeded with myofibroblasts and endothelial cells. After 21 days these tubes achieved burst strength over 300mmHg and good suture retention strength. Greisler combined PDS and PLA to achieve neo-arteries with burst pressure of 800mmHg¹⁴⁷. Niklason's group¹⁴⁸ demonstrated the consolidation of burst strength of seeded PGA grafts with prolonged culture in-vitro before implantation (see Table 2.3).

Culture time (weeks)	Burst strength (mmHg)
3	Too fragile to manipulate
5 (n=4)	570 +/- 100
8 (n=3)	2150 +/- 700

Table 2.3. Prolonged culture increases burst strength of seeded PGA grafts (From Niklason et al.¹⁴⁸).

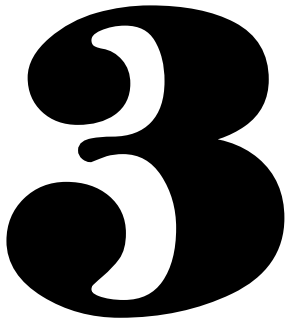
Prolonged culture was also associated with a reduction in compliance of the resultant vessels, suggesting the need for an intermediate culture time to promote a clinically viable balance between the two mechanical properties.

Natural scaffolds which can remodel as a result of haemodynamic conditions have been considered as the framework for TE materials.

However, it is possible to create TE vessels without any scaffold in place

by forming tissue around mandrels implanted subcutaneously¹⁴⁹ or intraperitoneally¹⁵⁰. This technique uses the body's own foreign body reaction to form a myofibroblast and collagen matrix which is robust enough to be implanted as a vascular prosthesis in that same body. The resultant pulsatile flow causes matrix thickening with further collagen deposition and elastic lamellae formation; myofibroblast differentiation into SMCs along with their circular alignment¹⁵⁰. However, ultimately this technology will require an invasive procedure to implant a foreign body intraperitoneally in a human, being dependent on an immune response against it. The consequences of infection would be very serious in patients with critical ischaemia especially since they are usually already at high medical risk.

Therefore it would be desirable to construct a fully tissue-engineered graft made up of autologous cells ex-vivo. L'Heureux's group¹⁵¹ achieved burst pressures of 2594±501mmHg with a tubular structure made from coaxial sheets of cultured vascular SMCs and human fibroblasts which was seeded with endothelial cells. This was as a result of a well organized collagen matrix with parallel fibres in perpendicular bundles. Elastin fibres were also seen. The overall structure was macroscopically and microscopically similar to an artery.



Addressing thrombogenicity in vascular graft construction

3.1 Introduction

Clearly the main determinants of patency of vascular bypass grafts are thrombogenic potential and level of intimal hyperplasia (IH). Of these two, the former is arguably more important as it is responsible for earlier graft occlusion. Also IH is associated with the abrupt change in distensibility between native vessel and stiff prosthesis at the anastomosis¹⁵², but this causal link appears to be less clearly demonstrated for blood compatible vascular conduits than for thrombogenic graft surfaces³⁵. It is obvious that synthetic graft development must not focus on mechanical properties in isolation, as blood/surface interactions and biological behaviour during graft healing and after incorporation are critical in the ultimate success of the implant.

As discussed in the previous chapter, the currently used grafts for vascular bypass in small calibre (<6mm), low flow states are autologous vessels or if these are not available, polytetrafluoroethylene (PTFE) prostheses. The autologous vessels used are long saphenous vein in the case of infrainguinal bypass; for coronary artery bypass the preferred alternative to saphenous vein is the internal mammary (or internal thoracic) artery. The results of bypass procedures with autologous vessels are considerably greater than when synthetic alternatives are used (Fig 1.1) and every attempt is made to utilise the former. However, in as many as one third of cases, this is not possible due to

previous use, inadequate calibre or diseased vessel.

Considerable research effort is being made to develop synthetic graft materials with a favourable blood compatibility. This is hampered by the relatively poor understanding of how surface properties relate to thrombogenic potential as well as the difficulties faced in surface modification technology.

On implantation of a vascular graft, plasma proteins immediately adsorb to the wall. They present binding sites for integrin receptors which are to be found on platelets and many cells¹⁵³. Adhesion to these as well as to the vessel wall itself may cause activation of the platelets. Surface modification to improve blood compatibility includes methods to reduce both plasma protein adsorption and platelet adhesion to the prosthesis wall. In addition, the interactions between plasma proteins and platelets that ultimately lead to platelet activation have also been targeted.

The aim here is to present what is already known about. The topic of blood/ graft surface interactions could be exhaustively presented as a textbook, incorporating anatomy, biochemistry and physiology. However, I have examined the subject from the point of view of a graft developer – showing how grafts being researched have fared when tested for thrombogenicity in vitro and in vivo as well as discussing the main controversies in vascular surface thrombogenicity, illustrating with examples of the approaches used to address these issues. There is after all no point in developing a graft from a thrombogenic material.

3.2 The Arterial surface

A theme of the mechanical considerations for potential vascular prostheses is to attempt to match the mechanical properties of the artery being bypassed. A similar philosophy holds true when considering the design of a graft from the thrombogenicity point of view. Arterial structure needs to be examined in more detail to appreciate its design features specifically geared toward enhancing blood compatibility. Much of this detail is at the biomolecular level. As a foundation we can return to the theme from the last chapter that the arterial wall is composed of a number of histologically separate layers, which allow a multitude of specialized functions, only one of which is blood compatibility (Fig

3.1). The innermost layer is a single layer of vascular endothelial cells (vEC) attached to a basement membrane. This layer is in close contact with the blood flowing through the vessel and so is intimately involved in preventing thrombosis. The vascular endothelium is non-thrombogenic. The basement membrane attaching it has moderate thrombogenicity; but it is the highly thrombogenic collagen¹⁵⁴ of the subendothelial connective tissue which rapidly instigates platelet adhesion followed by the cascade of events leading to thrombus formation (Fig 3.2). Additional subendothelial components promoting platelet adherence include fibronectin, laminin and thrombospondin. Adherence is facilitated by the presence of Von Willebrand Factor, a platelet adhesive protein synthesized by vEC. Exposure of the subendothelium to blood components also reduces the expression and activity of antithrombin III. This design is to ensure speedy coagulation in the event of serious arterial damage which in conjunction with vasospasm prevents heavy bleeding.

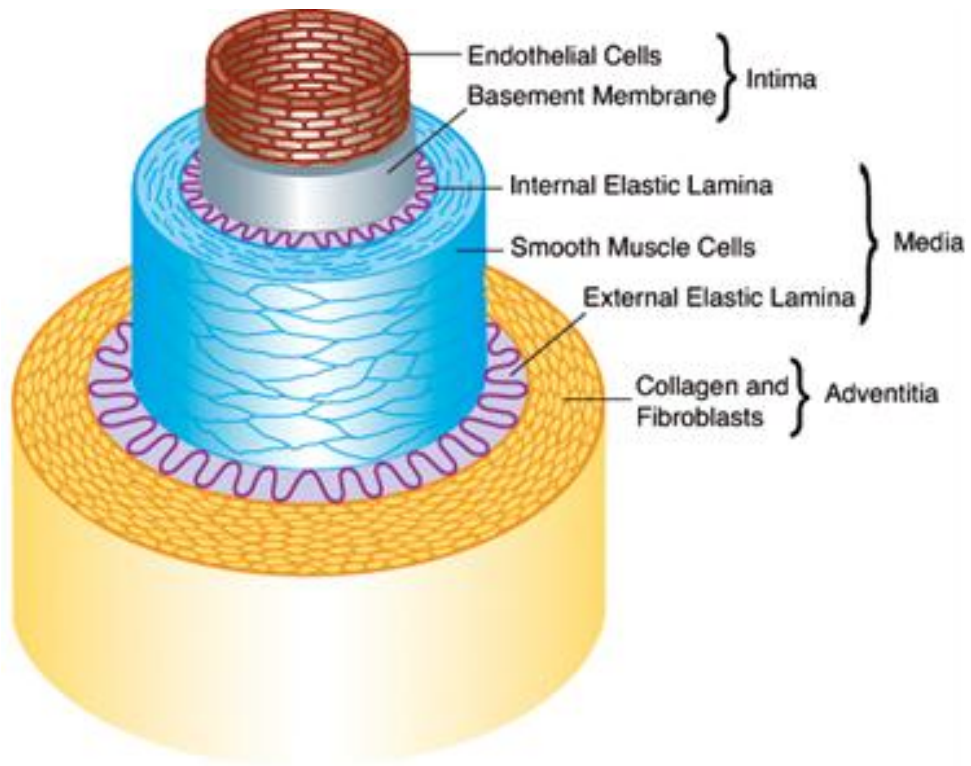


Fig 3.1.

The multilayered structure of the arterial wall

There are numerous biochemical pathways involving multiple cell surface receptors and intracellular signalling pathways by which vEC modulate plasma protein and platelet adhesion. Even with no physiological stimulus, vEC inhibit platelet aggregation. To some extent, this is prostacyclin mediated and can be reversed by application of non-steroidal anti-inflammatory drugs¹⁵⁵. The remainder of this platelet aggregation inhibition is mediated by endothelium derived relaxing factor (EDRF). Anticoagulant factors present in the vEC membrane include heparin-like glycosaminoglycans (heparans), thrombomodulin and adenosine diphosphatase (ADPase). The heparans moiety is essential for antithrombin III activity. vEC also express procoagulant Tissue Factor (TF) to exert fine control over overall thrombotic tendency. Any trigger for thrombosis such as vascular injury tilts homeostasis towards increased TF expression and downregulation of membrane anticoagulants, particularly thrombomodulin¹⁵⁶. This latter forms complexes with circulating thrombin, reducing its availability for fibrinogenesis. TF acts by binding Factor VII/VIIa causing the subsequent activation of Factors IX and X. Circulating low density lipoproteins (LDL), desmopressin¹⁵⁷ and homocysteine enhance this activity. The oxidised form of LDL further enhances platelet adhesion¹⁵⁸. To counteract TF and regulate its activation, the serine protease inhibitor Tissue Factor Pathway Inhibitor (TFPI) circulates alone or in complexes with plasma lipoproteins and acts to inhibit Factor X directly¹⁵⁹ by binding to the TF/Factor VIIa complex. Its activity is reduced by LDL. Nitric oxide (NO) which has an anti-aggregatory effect on platelets is released by vECs and by platelets themselves.

These are the principle mechanisms utilised by the vEC to regulate thrombogenicity.

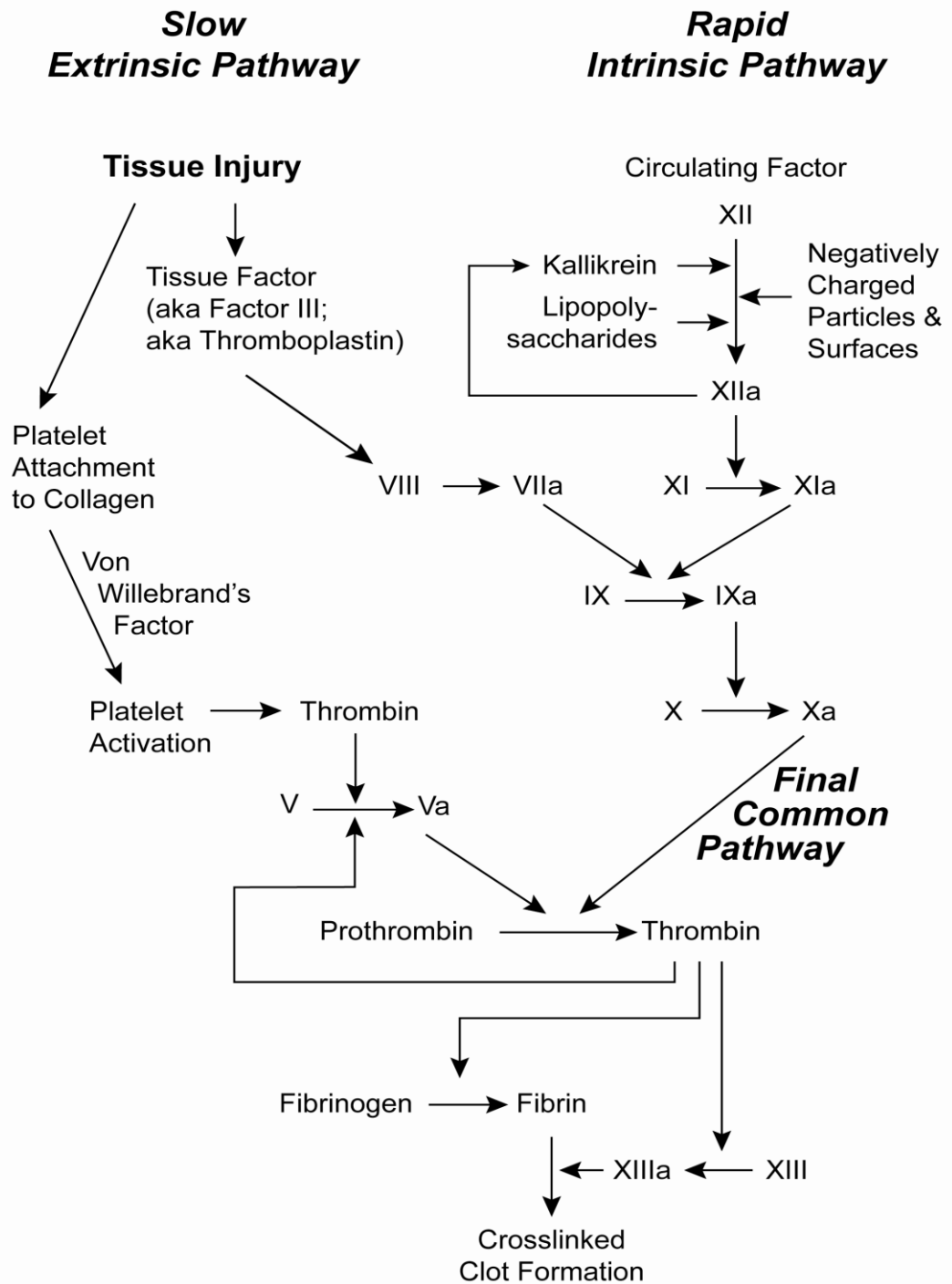


Fig 3.2. The clotting cascade.

3.3 Surface modification to attenuate the coagulation cascade

Attempts have been made to reduce the inherent thrombogenicity of synthetic graft surfaces by incorporating some of the mechanisms employed by vECs. Conversely, the use of collagen as a graft sealant at the blood graft interface has had to be tempered due to its thrombogenicity¹⁶⁰.

Membrane glycosaminoglycans may be simulated by the incorporation of heparin onto the graft surface. Results were initially mixed and dependent on the method of heparin bonding¹⁶¹ with covalent bonds with long half-life reducing the thrombogenicity of both PTFE¹⁶² and Dacron¹⁶³. A transient coating however is one reason for failure of heparin to improve short term patency¹⁶⁴. Current technology for heparin bonding has resulted in promising results for many groups (see Table 3.1). As well as discouraging coagulation heparin also reduces the proliferation of vascular smooth muscle cells in the media and intima, thus abating neointimal hyperplasia¹⁶⁵. A recent clinical trial has shown heparin-bonded Dacron to be as good as PTFE in the long term for Femoropopliteal bypass¹².

Heparin elution from graft surfaces has also been considered, partly as a result of the observation that the antiproliferative effect of drug-eluting stents (medium term) seems to outlast the drug elution. However, in the case of stents, it is now becoming apparent that this benefit may not persist in the longer term with delayed thrombosis being increasingly recognised¹⁶⁶, possibly in association with endothelial cell dysfunction and slow vessel wall healing¹⁶⁷. Hence, anticoagulant elution may be more suited to intra-vascular catheters¹⁶⁸.

<i>Year</i>	<i>Graft</i>	<i>Study type</i>	<i>Outcome</i>	<i>Reference</i>
2006	Polycaprolactone	in vitro	↓ vascular smooth muscle cell growth	165
2005	Thermoplastic polyurethane	in vitro	↓platelet adhesion; thrombin inactivation	161
2005	PTFE	retrospective clinical trial	92% 2 year primary patency for below knee bypass	169
2004	Wire coiled polymer coated	in vitro	vEC layer promotion; ↓thrombus formation	170;171
2004	PTFE	animal model	↓platelet adhesion; ↓intimal hyperplasia	172
2004	Carbon coated PTFE	animal model	↓early platelet adhesion; ↓late thrombus; ↑patency	173
2004	PTFE	animal model	↓platelet adhesion; ↓intimal hyperplasia	174
2004	Collagen	in vitro	↓thrombin generation	175

Table 3.1.

Summary of research into heparin-bonded vascular grafts in the last two years.

Additionally, platelet activity has been directly targeted with covalently bonded dipyridamole (Persantin) attached to the polycarbonate urethane graft (Chronoflex)⁴⁷, which acts by preventing cyclic adenosine monophosphate (cAMP) formation, an essential intraplatelet messenger signalling platelet aggregation. Although there was reduced platelet aggregation and a delayed thrombin reaction in vitro, this still translated to five goat carotid grafts being occluded within ten weeks. However, chronoflex may be unsuited overall for implantation due to considerable biodegradation noted within ten weeks in sheep.

ADPase (adenosine diphosphatase) was first noted as a natural antithrombogenic agent in the renal glomerular capillary wall where blood is in contact with the relatively thrombogenic glomerular basement membrane. In addition, a form of ADPase is secreted in the saliva of ticks. Platelet derived ADP (adenosine diphosphate) interacts with vEC at the CD39 receptor to cause release of EDRF. ADPase coated polyurethane grafts have better patency in a rabbit carotid model than polyurethane alone¹⁷⁶. However, recent indications are that the ADP effect on vEC is more important in small mammals than in man¹⁷⁷. It is also becoming clear that the platelet inhibitory effect of ADPase does not solely function through vEC EDRF release. Costa and colleagues have demonstrated the anti-platelet effects of ADPase in rabbit arteries where the endothelium has been destroyed beforehand¹⁷⁸.

Factor X inhibition by TFPI has been exploited by attaching it to Dacron grafts. On implantation in animal models, reduced fibrinogen adherence was noted¹⁷⁹ as well as a thinner neointima and lower thrombosis levels¹⁸⁰ compared with controls. However, the numbers included were small and it is unclear that a benefit remains in the long term as the half-life of TFPI is less than two hours, requiring constant replenishment whilst at the same time, the expression of TF increases over 12 months following implantation¹⁸¹.

Hirudin is a thrombin inhibitor which is secreted in the saliva of leeches and genetically engineered recombinant varieties have been used therapeutically as an anticoagulant. As with heparin, its presence at vascular anastomoses reduces intimal hyperplasia¹⁸², suggesting thrombin inhibition is directly linked to prevention of IH. Dacron with covalently bonded hirudin shows less thrombus formation and thinner neointima than Dacron alone¹⁸³.

Nitric oxide(NO) is released by platelets to form a microenvironment that

is unfavourable to platelet adhesion¹⁸⁴. Recently attempts have been made to manufacture NO-eluting vascular grafts due to its antithrombogenic and anti-intimal hyperplasia effects¹⁸⁵. The preliminary results are encouraging in animal models but the challenge of long-term NO production from a synthetic conduit needs to be addressed. NO effects are mediated by the cyclic 3'5'-guanosine monophosphate (cGMP) secondary messenger pathway. Phosphodiesterase inhibitors such as sildenafil cause the accumulation of cGMP, thus potentiating NO effect¹⁸⁶ and the two may have a synergistic role in future anti-platelet grafts. However, as with TFPI, the importance of the role of NO as a platelet inhibitor has considerable interspecies variability with it having little relevance in mouse models¹⁸⁷.

3.4 Electrical charge

Amongst the esoteric properties which afford thrombogenicity, the issue of surface charge is refreshingly simple. Platelets have net electronegative surface charge, and it has been known since the 1950s that the blood vessel wall also exhibits a similar surface charge, as one would expect for their mutual repulsion for each other. Sawyer demonstrated that injury to the vessel wall lead to it gaining positive charge¹⁸⁸.

PTFE has a weak negative charge too, but this is further enhanced by the fibrinous layer that forms on its luminal surface after implantation. As well as contributing to antithrombogenicity, this characteristic also has antibacterial properties, as those bacteria which are associated with graft infection have electronegative surface properties¹⁸⁹. Carbon coating to PTFE further increases its electronegativity, and is in commonplace clinical use.

However negative electropotential alone will not ensure an antithrombogenic surface. The effect of surface chemistry is of paramount importance too. Collagen is very thrombogenic despite electronegativity. Therefore although electronegativity is a prerequisite for a non-thrombogenic surface, additional surface properties are also critical in determining the platelet reaction.

3.5 Surface wettability

As with negative electrical charge, a hydrophilic surface may confer thromboresistance but that is not to say that all hydrophilic surfaces are thromboresistant¹⁹⁰. In fact, similar materials with different wettability may show no correlation with thromboresistance¹⁹¹. Van Kampen's¹⁹² assessment of poly(aminoacid) grafts revealed that platelet adherence to the wall was competing with leucocyte adherence which favoured fibrinolysis and eventual leucocytic endothelial transformation. Which component would prevail could not be predicted with surface characterisation.

PTFE's advantageous qualities include its biocompatibility, non-degradation and strength. It is mildly electronegative, but unfortunately is hydrophobic and prone to thrombosis in low flow states. One method of reducing the hydrophobicity of a material is to covalently bond hydrophilic groups to its surface. Heparin is hydrophilic, contributing to its anti-platelet adherence properties and reducing the hydrophobic nature of collagen¹⁷⁵ and PTFE (Table 3.1). Similarly, the use of compliant silicone rubber as a vascular conduit has been hampered by its hydrophobicity, affording it high affinity for platelets and fibrinogen. Julio et al³⁶. covalently bonded hydrophilic monomers to these grafts to reduce short term thrombogenicity.

Polyethylene glycol (PEG) and polyethylene oxide (PEO) are hydrophilic flexible polymers which resist protein adsorption when bonded to the vascular surface. This translates to reduced thrombogenicity when they are used to coat vascular grafts¹⁹³. The length and degree of branching of these polymers may correlate with the degree of platelet repulsion, due to their flexibility increasing thermodynamic interactions at the surface¹⁹⁴. The great challenge with respect to these groups has been firm bonding to grafts with no translation to clinical application despite in-vitro and in-vivo study for over a decade.

However before platelet interactions with the prosthesis, fibrinogen may adsorb to the blood contact surface, and become activated as well as activating platelets. Fibrinogen has bonding sites for both hydrophilic and hydrophobic surfaces¹⁹⁵. Amphiphilic surfaces can discourage fibrinogen binding¹⁹⁶. This may be due to the different microdomains effectively cancelling each others effects¹⁹⁷. They are also implicated in preventing platelet activation¹⁹⁸, possibly by interfering with platelet binding with fibrinogen. Copolymerisation of

hydrophilic polymers such as PEO¹⁹⁹ and PEG¹⁹⁸ with hydrophobic counterparts result in materials which demonstrate these antithrombogenic properties. Polysiloxane and polycaprolactone-based amphiphilic copolymers have been commercially available for use as surface modifying additives for the extracorporeal circuits of cardiopulmonary bypass²⁰⁰.

Fibrinogen adherence may be discouraged by creating conditions favourable to albumin attachment. The phospholipids membrane has a preference for albumin due to fatty acid chains, and in particular C16 chains. 16 carbon acyl groups²⁰¹ or alkyl groups form a characteristic steric conformation²⁰² which confers thromboresistance. A similar effect is seen with other specific configurations of carbon chains (C10²⁰³ and C18²⁰⁴).

3.6 Mechanical Considerations

These have been dealt with in detail in Chapter 2. They have critical relevance in considering thrombogenicity. Turbulent haemodynamics as well as excessive shear stress promote platelet activation and thrombogenesis and graft selection needs to minimise these. There is considerable overlap with the mechanisms responsible for intimal hyperplasia which is responsible for graft occlusion in the medium and long term, whereas thrombosis is likely to cause graft occlusion in the early post-operative period. The mechanical factors involved can be separated into geometric factors and graft characteristics. The former includes accurate graft calibre matching²⁹ and consideration of the angle of take off at an end to side anastomosis. Trials of tapering grafts¹⁰⁸ (to reflect the native artery) have not been successful as they ignore the relative overall increase in vessel surface area brought about by increasing branching at the same time as diameter reduction distally. Graft kinking (a particular problem in long grafts where inadvertent twisting at the time of implantation is possible²⁰⁵, as well as those which cross joints) results in gross turbulence as well as stagnant areas, providing a highly thrombogenic environment, so this needs to be minimised by the use of relatively stiff materials and external reinforcing rings. However, very stiff materials lack the viscoelasticity of arteries, promoting intimal hyperplasia and occlusion. The anastomosis itself is paramount – suturing itself causes stress concentrations and poor surgical technique may

leave excessive suture material exposed on the luminal aspect of the graft wall as a thrombogenic nidus. Even worse is poor eversion at the anastomosis, resulting in direct blood contact with the highly thrombogenic arterial adventitia.

3.7 Endothelialization

Rather than mimicking the vEC, encouraging a confluent endothelial lining to develop on the graft surface results in antithrombogenicity as well as a physiological layer that can respond to the shear forces exerted by the prevailing hemodynamic conditions.

Spontaneous endothelialisation of a synthetic prosthesis occurs by direct migration from the anastomotic edge, transmural migration of endothelial cells and by cell transformation from endothelial progenitor stem cells (EPC). The first of these is very limited in extent, with PTFE showing creeping confluent endothelialisation at a rate of 0.1mm per week from the anastomosis with rat aorta²⁰⁶. The second is responsible for the majority of confluent endothelium forming quickly in animal models. The third is only now starting to be appreciated as a mechanism of endothelial layer 'housekeeping' in native arteries, being responsible for repair of minor damage to the intima²⁰⁷. This field of study is in early infancy – the identification and origins of EPCs are yet to be defined. Despite some evidence of the endothelialisation of vascular prosthesis in some animal models this is limited in the clinical situation. There are few large animal studies such as sheep and primate models, compared with small animals such as rat and rabbit, which endothelialise more readily, and so are a poor reflection of prosthesis behaviour in humans, where the major cell type migrating into the graft are smooth muscle cells. Unlike EC smooth muscle cells do not prevent thrombogenesis but rather promote IH.

Endothelial cell adherence and differentiation is not likely to occur in high flow conditions. This means that the blood in the vessel lumen is not an efficient source of vECs. A more likely source is newly formed capillaries as a result of perigraft tissue infiltration. In addition, endothelialisation is promoted by basic fibroblast growth factor which is secreted at the site of angiogenesis²⁰⁸. A graft that is porous throughout its wall will endothelialise faster and with more confluence than a non-porous tube. PTFEs poor endothelialisation is due to its

small pore size. Hazama et al.²⁰⁹ found that standard PTFE with fibril length of 30µm did not allow for any transmural angiogenesis in rat aortas, whereas increased fibril length (and hence pore size) allowed capillaries to infiltrate the wall. The amount of cellular infiltration which correlated with thrombus free area was greatest for an intermediate pore size (fibril length 60µm). Even longer fibrils lead to a reduction of transmural infiltration. In humans there is little evidence of any endothelialisation of PTFE¹²⁵. Knitted Dacron is more porous than PTFE and forms a patchy endothelial layer after implantation in humans²¹⁰.

Animal models show spontaneous confluent endothelialisation much more readily than humans²¹¹ despite human vECs demonstrating good migration potential²¹². Apart from porosity studies, efforts have been made to enhance this in animals in the hope that it will translate to a greater endothelial coverage in human implanted grafts. Also, awareness of the difficulty of spontaneous endothelialisation has promoted the concept of endothelial cell seeding of grafts. Successful seeding requires a high uptake of vECs and has required a time consuming three stage procedure. However, a viable single stage seeding technique may be possible if a graft with a high capacity to firmly attach endothelial cells is developed. The various surface modifications undertaken to promote spontaneous and seeded endothelialisation are summarized in Table 3.2.

3.8 Conclusion

In the previous chapter an examination of how graft mechanical properties affect the ultimate performance of prostheses in small calibre vascular bypass was made. From this chapter it is clear that poor results are intimately related to unfavourable interactions between the luminal surface and blood components, causing a high rate of thrombosis. In producing the new generation of blood compatible grafts, surface properties must be carefully considered. Either a material with integral low thrombogenic characteristics or surface modification and composite coated grafts need to be considered. These modifications take the form of enhancing physical properties by addressing surface charge and hydrophilicity or by incorporating the biochemical mechanisms employed by arteries. This latter can be approached by assembling individual anti-thrombogenic constructs or by encouraging confluent

endothelialisation.

However, unlike many animal models, spontaneous endothelialisation of long graft segments does not readily occur in humans. Therefore further surface modification to form a microenvironment favourable to endothelialisation has been considered, including microporosity, extracellular matrix deposition and specific factors which promote endothelial cell adherence and proliferation. Most recently, the peptide sequences involved in the latter have been isolated and used as surface modifiers.

It is hoped that enhancing endothelialisation in animals will result in a viable endothelialising synthetic graft for humans. A concerted move away from the use of small animals as models of vascularisation and towards higher species will better represent potential graft behaviour before clinical trials. Tissue engineering advances the possibility of in-vitro endothelialisation of grafts before implantation – this technology will also benefit greatly from surface modification to facilitate rapid viable endothelialisation. This strategy accepts the difficulties encountered in achieving spontaneous endothelialisation in humans. In fact, tissue engineering as a research field has burgeoned over the years as developers have come to consider that it may be more feasible to go one step further than extra-corporeal endothelialisation and totally construct a biological conduit in vitro, than to create a synthetic product which can cope with the long list of requirements for success as a small calibre vascular implant.

3.9 Future Directions

The use of vECs from other sources has become an important field of study in the search for better vascular prosthesis. Mechanisms for this have included the harvest of cells from augmental fat and the use of endothelial progenitor cells from circulating blood²¹³. Studies using mesenchymal stem cells from the blood have proved useful in canine models and could provide a useful source of cells for clinical applications. The study of tissue engineered vascular grafts has shown many advantages over synthetic grafts but cell sources remain uncertain. Nevertheless, this has become the mode of choice for many groups attempting to develop vascular grafts. The next chapter examines this third and final approach to vascular graft development.

However the potential of segmented polyurethanes has not been fully realised. In particular, manipulation of the hard segment to optimise hydrogen

bonding and van der Waal interactions with the adjacent soft segment could result in improved mechanical properties and hemocompatibility. To this end, the experimental work presented in this thesis investigates a novel nanocomposite polyurethane with antithrombogenic properties which incorporates polyhedral oligomeric silsesquioxane into the hard segment⁵⁰.

<i>Graft</i>	<i>Modifying additive</i>	<i>Study type</i>	<i>Outcome</i>	<i>Reference</i>
PTFE	P15 peptide	in vitro	↑endothelialisation; ↓IH	214
PTFE	Anti-CD34 antibodies	animal model	Rapid endothelialisation; ↑IH	215
PTFE	Vascular Endothelial Growth Factor	animal model	↑endothelialisation; ↑IH	216
Poly(ether)urethane (Tecothane)	Cholesterol	in vitro	↑endothelialisation and resistance to shear stress; ↑endothelial precursor cell adherence	217
PTFE	Poly(amino acid) urethane	animal model	↑endothelialisation	218
Fibrin	Endothelial cell growth factor	in vitro	↑vEC proliferation; ↓early platelet adhesion; ↓late thrombus; ↑patency	219
Polyurethaneurea	YIGSR ¹	in vitro	↑endothelialisation; ↑transmural cell migration; ↑hydroxyproline production ²	220
PTFE	Tumorigenic human squamous cell line	animal model	Confluent endothelialisation by 5 weeks	221
Dacron,PTFE, polypropylene, silicone, polyurethane	titanium	in vitro	↑vEC adhesion; no increase in inflammation	222
Dacron	Collagen film	in vitro	Confluent endothelialisation	223
Dacron	Collagen	Animal model	Largely endothelialised and thrombus free at 3 weeks	224
Collagen	Heparin	in vitro	↑basic fibroblast growth factor (bFGF) binding and release	225

¹ Endothelial cell adhesive peptide sequence
² marker of collagen synthesis

Polyurethane	bFGF/Heparin	Animal model	↑endothelialisation, neovascularisation	226
PTFE	Nitrogen, oxygen (↑hydrophilicity)	In vitro	↑endothelialisation, ↑plasma protein adsorption	227
PTFE	RGD cell adhesion peptide	In vitro	↑immediate vEC adhesion; no long term advantage compared with fibronectin coating	228
Dacron	Carbon	In vitro	vEC proliferation	229
Polyurethanes and silicones	Extracellular matrix; fibronectin; glutaraldehyde preserved matrix (GPM)	In vitro	GPM provides optimal vEC proliferation	230
PTFE	Fibronectin	Animal model	↑endothelialisation (both spontaneous and seeded)	231

Table 3.2. Summary of surface modification to enhance endothelialisation (in chronological order).

4

Achieving the ideal properties for vascular bypass grafts using a tissue engineered approach

4.1 Introduction

The ideal cardiovascular bypass graft requires a broad range of characteristics including strength, viscoelasticity, biocompatibility, blood compatibility and biostability²³². It also needs to have the capability to adapt to the prevailing haemodynamic conditions, both immediately and in the long term. Till now, traditional synthetic material technologies have not been able to provide for all of these criteria¹¹, despite a large volume of materials research in this arena. Expanded polytetrafluoroethylene (PTFE) was initially successfully used for small calibre arterial bypass by Matsumoto in 1973²⁰ and since that time, no convincingly superior alternative has emerged. This has translated clinically into poor medium to long term patency of synthetic grafts when used in low flow states and small calibre (<6mm) bypass. The 5 year primary patency of PTFE grafts which cross the knee joint is less than 30%²³³, resulting in considerable re-interventions and limb loss. Therefore in cardiovascular bypass surgery, when small calibre conduits are required, every effort is made to use autologous vessels. In the case of coronary artery bypass, the internal thoracic or internal mammary artery is the first choice graft; in distal bypass surgery, the great saphenous vein is harvested and used wherever possible. However,

autologous vein is not available in a third of cases⁴ due to varicosity, previous use, incompatible calibre and diseased vein wall.

Acknowledgement of the huge difficulties involved in fulfilling the numerous ideal characteristics using traditional synthetic materials has led biomaterials research towards the rapidly advancing fields of nanotechnology and tissue engineering. Nanotechnological avenues are concerned with the incorporation of manmade molecules into traditional materials to impart novel advantageous properties such as anti-thrombogenicity and biostability⁵⁰. The mechanisms of action for these materials are not fully understood, being related to their unique quantal properties rather than the bulk properties of conventional materials²³⁴, hampering progress of their investigation and application. The graft material discussed in this thesis uses nanotechnology to attempt to confer advantageous properties to a well-established polyurethane. However, tissue engineered grafts have also been considered for several reasons. Firstly, it gives an excellent framework by which the various essential and advantageous properties of any bypass graft can be discussed. The success or otherwise of tissue engineering to fulfill these criteria is examined. Secondly, the advantages and disadvantages of the tissue engineered approach are considered. This will indicate whether it is the preferred avenue of research for small-calibre bypass grafts, or whether it is just too impractical, leaving nanotechnology as the only feasible option. Conversely if tissue-engineering is overwhelmingly advantageous and technically feasible, should effort be spent on using nanotechnology for graft development. Linked to this second point, the extent to which tissue-engineering has been developed into clinical practice and how near tissue engineered blood vessels are to clinical use is considered. The third reason for examining tissue-engineering is because the two technologies are not mutually exclusive. Investigators are currently using modifications of the nanocomposite as scaffold matrix for tissue-engineering purposes.

Tissue-engineering is an interdisciplinary field that applies the principles of engineering and life sciences to the development of biological substitutes in order to restore, maintain, or improve tissue functions²³⁵. Its ultimate trump card over synthetic materials is the inherent biocompatibility of the component biological materials. The field has captured the imagination due to the possibility of individualised specific grafts that can evolve according to haemodynamic parameters, and a large body of research has quickly built up.

Thin engineered tissues such as skin²³⁶ and cartilage²³⁷ have been used clinically over the last decade. In addition, further stimulus has recently occurred with the successful clinical implantation of the first tissue engineered hollow organ²³⁸. A human bladder was developed, but more complex organ engineering is presently limited by the inability to 'grow' the associated blood supply. Takei's group²³⁹ have used an elegant method to promote in vitro spontaneous three dimensional capillary growth in order to address this limiting factor. They have exploited the autonomous tube forming effect that collagen gel has on endothelial cells to persuade capillary budding into a collagen block from a tissue engineered microtube lined with bovine endothelial cells, using vascular endothelial growth factor (VEGF) as a stimulus. It is also now becoming clear that in the right conditions, engineered tissues can similarly promote angiogenesis, increasing their potential for manufacturing whole organs and ultimately connecting up with the host vasculature. Sekiya and colleagues tracked the autonomous organisation of ECs from random orientation to networks, along with the expression of angiogenic genes, including VEGF in sheets of cultured cardiac cells²⁴⁰.

Finally, the possibility of graft materials growing simultaneously with a patient opens up a whole new area of paediatric vascular surgery²⁴¹.

This review highlights the development of tissue engineered vascular graft development with respect to the ideal graft characteristics which are so difficult, if not impossible to obtain from synthetic materials. It concentrates on recent advances in our knowledge, and is not intended to be a general overview of tissue engineered vascular grafts as this field has already been comprehensively covered^{145;242-244}.

4.2 The major factors for consideration

The ultimate trump card of the fully tissue engineered graft is its inherent biostability, with healing properties compatible with successful permanent implantation. The graft is continually moulded depending on the haemodynamic demands placed on it¹⁴³. Thus it may be seen that the original ECM scaffolds used are not recognisable after being implanted for some time. However, as with most synthetic grafts, ECM scaffolds are vulnerable to unintended

biodegradation, leading to graft wall weakness, aneurysm and failure. This is a particular problem with elastin in decellularized xenograft scaffolds, which degrades despite glutaraldehyde-fixation due to its low opportunities for cross-linking. Tannic acid is commonly used as a fixative for elastin before electron microscopy, and this can be used to prevent its biodegradation by forming cross-linking hydrogen bonds between hydrophobic regions of the chain²⁴⁵. Unfortunately heavy crosslinking may adversely affect elastic properties. This illustrates the point that simple provision of autologous cells in an artificial ECM is not enough to automatically guarantee the desired biostability and careful selection of scaffold and cells is required.

4.2.1 Scaffold

A multitude of approaches have been utilised to achieve the common goal of viable confluent sheets of cells anchored on a tubular scaffold. The scaffolds used are either synthetic or biologically sourced. In the case of the former, a non-degrading material will result in a hybrid graft rather than a wholly tissue-engineered graft and their mechanical properties will reflect those of the scaffold, with limited capacity for adaptation to changing blood flow conditions. Few such scaffolds have resulted in a clinically successful bypass graft²⁴⁶. These will not be considered further as the properties of such materials are dominated by the scaffold, thereby cancelling the potential advantageous effects of the completely tissue engineered graft. In addition, some of the main challenges facing tissue engineering such as ready availability and initial mechanical strength do not apply to them. Biodegradable scaffolds have been shown to provide a suitable environment for adherence, proliferation and organisation of cells. They provide primary mechanical stability while the cellular structures mature. As demonstrated in fig 4.1, the scaffold initially withstands the stresses of pulsatile flow. As the scaffold begins to degrade and formation of matrix occurs, the newly regenerating cells are gradually loaded with physiological stress thereby stimulating their appropriate alignment²⁴⁷ and further stimulating tissue regeneration. Eventually the scaffold completely degrades and the regenerated tissue bears the stress. Biological scaffolds may be transplanted tissues or specifically constructed, using extra-cellular matrix

components. An example of the former is the small intestinal submucosa (SIS) vascular graft which has been implanted directly into the vasculature of pigs, dogs and sheep, and proven to remodel as well as auto-seed with EC and smooth muscle cells (SMC)²⁴⁸⁻²⁵¹. This gives the possibility of using SIS clinically as a vascular graft in cases with high graft infection risk²⁵². Perhaps the ultimate transplanted biological scaffold is an autologous vessel. Saphenous veins are commonly used for arterial bypass and are observed to 'arterialise' with smooth muscle cell hypertrophy and intimal thickening²⁵³. Clerin's group exposed the ex-vivo adaptability of small vessels, by subjecting them to extrinsic longitudinal stresses (to lengthen them) and precise internal flow programs (controlling wall thickness and vessel calibre)²⁵⁴.

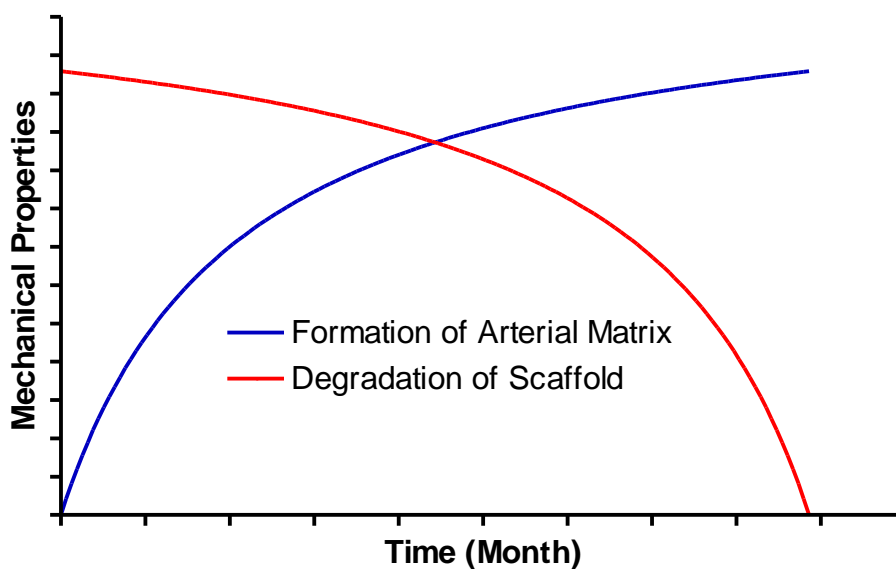


Fig 4.1. The graph demonstrates the timeline for the development of a tissue engineered bypass graft using a synthetic biodegradable scaffold, which is gradually replaced by arterial matrix.

Collagen is commonly used as an ECM, due to its high strength and the potential for auto-seeding of endothelial cells. Its use is discussed in relation to its mechanical properties later. Highly permeable biopolymers such as collagen gels are useful for holding cells in suspension and providing a favourable microenvironment for cell attachment and proliferation. These are the same roles which collagen performs biologically. They must always be matured in vitro, due to their low inherent mechanical strength. This is by promotion of collagen gel organisation and contraction around a suitable mandrel in conjunction with smooth muscle cells, resulting in a circumferential alignment of both SMC and collagen²⁵⁵ as well as application of pulsatile stress to consolidate this organisation. These processes are considered in detail below in relation to mechanical properties. However, as Isenberg points out²⁴², collagen gels perform relatively poorly with overcontraction of the gel leading to reduced matrix permeability being a frustrating problem. . Lewus and Nauman have determined that this undesirable effect is reduced by including whole collagen fibres to the hydrogel matrix²⁵⁶. To date, acceptable mechanical properties achieved in a realistic timeframe are yet to be realised.

The other major natural cell substrate is fibrin. Surprisingly, the stimulation of fibroblasts to form collagen²⁵⁷ as well as elastin²⁵⁸ may be greater within fibrin gel than collagen gel, translating to increased mechanical strength and biomimetic elasticity. Isenberg has also found fibrin gel matrix to endothelialise well with good EC retention after simulated haemodynamic shear stresses²⁵⁹.

The use of elastin directly in the scaffold is hindered by the problems described above with rapid degradation. However, recognising it's importance not only mechanically, but also in subsequent regulation of endothelialisation, Wise and colleagues²⁶⁰ used its soluble precursor, Tropoelastin, in recombinant form (ie. synthetic) in a hybrid scaffold, which maintained its mechanical properties in a rabbit model for a month. They found subsequent endothelial cell attachment and proliferation along with platelet activation properties to be superior to the biodegradable scaffold alone, or in conjunction with albumin coating. However, they have not till date shown whether the recombinant tropoelastin has inherent biostability or whether the polycaprolactone scaffold is providing this, until remodelling occurs naturally in vivo and the scaffold degrades.

4.2.2 Cells

The cells in consideration are fibroblasts, SMC and vascular EC (Fig. 4.2) which are present in histologically distinct cellular layers. Fibroblasts synthesise the extracellular matrix which is responsible for mechanical integrity; SMC have the ability to contract in response to specific haemodynamic conditions; EC present a non-thrombogenic layer at the blood-graft interface. However, there is considerable interaction between the different cell types to ensure these roles are fulfilled. This is another reason for the drive to implant grafts with all the cellular layers already present.

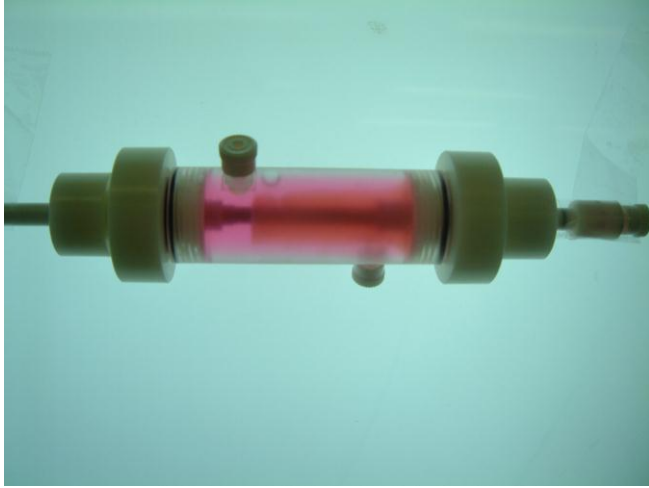


Fig 4.2. A living cellular matrix, comprising of Type I collagen & porcine smooth muscle cells, which is contracted on a central mandrel within a bioreactor.

L'Heureux²⁶¹ has cultured human fibroblasts on gelatine to form sheets which resulted in organised ECM, without the initial involvement of SMC. Repeated rolling of these sheets around a mandrel resulted in acceptable mechanical strength. The resultant conduits were endothelialised and implanted in several animal models. SMC migration from the anastomoses as well as possible transformation of fibroblasts to myofibroblasts was observed. Excellent short term and good medium term in vivo results were obtained.

Unlike the above study, most other grafts composed of cellular layers have utilised SMC rather than fibroblasts, in the common aim of replicating arterial tissue. Difficulties have centred around the contraction of SMC and cell substrates, along with culture difficulties due to the early senescence of SMC²⁶².

It is widely recognised that a rapid confluent endothelial layer protects a synthetic graft from thrombosis and early occlusion²⁶³. However, extensive endothelialisation has never been shown in clinical practice, despite the literature being replete with animal models demonstrating endothelialising grafts. This has contributed to the impetus behind endothelial seeding of grafts before implantation²⁶⁴, since physiological shear stress is a hostile environment for EC adherence and function²⁶⁵. Endothelial cells have intimate interaction with SMC, expressing transforming growth factor genes²⁶⁶, which are also responsible for SMC organisation and collagen secretion. The same growth factor signals EC apoptosis. A further role of EC is in angiogenesis, with their alignment into tubular structures. Asano and colleagues²⁶⁷ have demonstrated pore extrusion of EC via morphological changes and realignment through a collagen scaffold as a preliminary angiogenic bud. This was controlled by the shear forces exerted on EC by the blood flow.

The attachment of vascular endothelial progenitor stem cells is an exciting recent possibility²⁶⁸, aimed at rapid accumulation of appropriate cellular layers, including cell adherence from endogenous blood flow.

4.2.3 Mechanical properties

Mechanical characterisation of the artery reveals an anisotropic nature with high elasticity at low pressures and greater stiffness along with low

distensibility at high pressures²³³. This is due to the multi-laminar arrangement of collagen and elastin. Collagen provides high tensile strength - porcine carotid burst pressure is in the region of 2000mmHg²⁶⁹ - as individual fibres are gradually recruited at increasing pressures²⁷⁰ - Gupta used electron microscopy to demonstrate the straightening out of elastin fibres, until 120mmHg when additional stress was exerted wholly on collagen²⁷¹ – see Fig 3.1. The combination of strength and elasticity has been a particular challenge in potential synthetic graft development, with modification of traditional materials such as segmented polyurethanes allowing an improvement in one at the expense of the other by modification of the soft and hard segments⁴⁰. It is thought that the inequality of elasticity (compliance mismatch) between native artery and graft material may be responsible for intimal hyperplasia⁶⁶ which itself is the cause of medium to long-term graft occlusion of small calibre grafts. The common femoral artery has a compliance of 4-8 %/mmHg x 10⁻² whereas this is only 1 %/mmHg x 10⁻² in the case of PTFE⁷¹. It is essential therefore to consider an appropriate extra-cellular matrix (ECM) for TE grafts to mirror the strength and elasticity of arteries.

One principle by which to achieve this aim is to use a biodegradable hydrophilic polymer scaffold, with long term replacement by ECM. The bioresorbable scaffolds used are based on polyglycolic acid (PGA), polydioxanone or Polylactide¹⁴⁴. PGA forms a porous structure but is resorbed within 8 weeks and in order to slow degradation it is often combined with an adjunct such as polyhydroxyalkanoate, poly-4-hydroxybutyrate or polyethylene glycol¹⁴⁵. Cellular infiltration of these scaffolds is dependent on a highly porous open structure.

As discussed earlier, groups have considered collagen itself as the foundation for biological scaffolds, primarily because of the impressive strength it imparts. However, Weinberg and Bell's pioneering collagen-based scaffolds were very weak, requiring a Dacron mesh for initial strength²⁷². Berglund²⁷³ has shown that elastin makes collagen tubes stronger - it may have a considerable role in distributing the stress across the TE vessel wall. Elastin also improves the viscous nature which again is generally thought to be due to collagen. This may be because without elastin's gradual stretching influence, the abrupt pressure wave on the collagen construct may not allow sufficient time for the viscous component to manifest itself. Berglund extracted elastin scaffolds from

an animal model by targeted enzymatic digestion of ECM. However, it is very difficult to incorporate elastin into engineered structures due to its low solubility. Leach's group²⁷⁴ have used water-soluble alpha-elastin in conjunction with a 'molecular glue' to form 'elastin-like' structures with similar mechanical and cell-adherent properties. An added advantage is that the materials used are readily available off the shelf.

Collagen also derives strength from circumferentially arranged SMC layers which require prolonged culture to achieve as well as a porous collagen network. The orientation of the SMCs is paramount and can be optimised by pulsatile flow in bioreactors, causing circumferential stress as a stimulus²⁷⁵.

One way of obtaining a collagen scaffold with reasonable initial strength is by promoting the fibrous reaction against a mandrel placed subcutaneously¹⁴⁹. However, the minimum burst pressure of 200mmHg was still far below the desired magnitude for clinical use. In addition, preparation of these "biotubes" required 4 weeks of subcutaneous implantation. Physiological flow on implantation results in further collagen thickening, elastin deposition and myofibroblastic reorganisation.

Other derivatives of biological structures which may act as temporary scaffolds, to be replaced by ECM are gaining prominence. Lepidi's work²⁷⁶ on hyaluronan, an esterified hyaluronate is promising, showing rapid accumulation of organised arterial cellular and ECM components in an animal model, with biodegradation of the scaffold over four months. The cellular reorganisation is undoubtedly helped by the scaffolds ability to maintain a loosely packed ECM. However, this success in microvessels has yet to be shown in the intermediate size of vessels (3-6mm) as the strength of the construct is strongly dependent on the ECM formed²⁷⁷.

4.2.4 Blood compatibility – the endothelial lining

It is notoriously difficult to render a synthetic material non-thrombogenic, requiring the concomitant properties of hydrophilicity, electronegativity and inertness. Currently, the best hope is for the development of an endothelial lining. Unfortunately, although animal models readily endothelialise²¹¹, a synthetic graft with long confluent endothelialised sections in clinical practice is yet to be achieved. Although collagenous constructs obtained from small

intestinal submucosa have been successfully used as vascular grafts in vivo, collagen itself is thrombogenic¹⁵⁴, and gaps in the endothelial sheet or absent basement membrane may be a focus for thrombus formation. Surface modifications of collagen such as heparin-bonding can be partially successful in reducing thrombogenicity¹⁷⁵. Preliminary platelet reactivity studies have suggested that elastin exhibits less platelet adhesion than collagen²⁷⁸. These studies also uncovered good EC adhesion to both collagen and elastin.

Biologically sourced scaffolds can be seeded with variable ease, with autologous structures seeding readily compared with decellularized xenografts, especially if the latter have not been adequately treated, resulting in residual antigenicity²⁷⁹.

In keeping with the theme of replicating the biomolecular and cellular mechanisms of the structure being replaced, tissue engineering aims to provide low graft thrombogenicity via active seeding of the blood interface with endothelial cells (EC). Careful consideration must be given to the source of ECs along with the method of extraction. Enzymatic cell loosening using collagenase or trypsin requires careful timing to prevent extraction of other cell types such as SMC or fibroblasts. Mechanical stripping of endothelial linings damage EC. Recently investigated sources include veins, adipose and bone marrow.

4.2.4.1 Veins

Although endothelial cell extraction has been successfully performed from the vein wall, optimal seeding and culture on synthetic scaffolds requires a turnover time of at least seven days²⁸⁰. However the degree of adherence and function of the seeded cells depends greatly on the scaffold material used. This is perfectly illustrated by Yeh and colleagues' study of endothelial cells seeded to different metallic stent materials²⁸¹, showing the importance of considering not only attachment but also the level of function for these cells. The saphenous vein is a potential source of ECs which may be harvested if the vein calibre is too small for autologous vein bypass. Experimentally, the umbilical vein is used as a source of ECs – but this structure is not likely to be available at the time of TE graft requirement. EC can be extracted from the umbilical artery²⁸², but the yield is low, due to the size of the vessel and extraction difficult.

Of course it can be argued that using available vein as graft material is already successful in the case of small calibre vessel bypass, eliminating the need for tissue-engineering in these cases.

4.2.4.2 Adipose

Oedayrajsingh-Varma²⁸³ has shown that adipose-derived stem cells with true proliferative potential could be harvested with greater efficiency from surgically excised adipose tissue than from ultrasound-guided liposuction. However, these cells differentiated into connective tissue rather than endothelial cells and it is not clear whether the same would apply for endothelial progenitors. In fact it is becoming evident that the differentiation potential for these adipose-derived stem cells may include several different lineages, dependent on biomolecular and biomechanical environmental cues rather than it being genetically predetermined^{284;285}.

4.2.4.3 Bone marrow

This is a ready source of pluripotent stem cells, which will be available at the time of surgery. Cho and colleagues²⁸⁶, seeded small calibre decellularized canine carotids with ECs and smooth muscle cells (SMCs) of bone marrow origin before implantation and found eight week patency as well as a regenerated arterial wall. However, these cells were cultured *in vitro* for three weeks meaning that bone marrow biopsy was required separately to operation. Shin'oka's group²⁸⁷ have demonstrated endothelium-like cells on biodegrading scaffolds after fixing unselected bone marrow cells with fibrin glue and a maturation time of only four hours. However, their shear stress resistance after such short maturation is yet to be ascertained.

4.2.4.4 Endothelial progenitor cells (EPC)

The most exciting development in EC sourcing is the seeding of EPC. Pluripotent cells are easily available from every patient (bone marrow) unlike

EC, and they may also autoseed grafts from the circulation. It is thought that this latter is promoted by the use of statin therapy²⁸⁸. Apart from the bone marrow, EPC can be sourced from fat (subcutaneous/omental) and umbilical cord blood. After careful consideration of the ethical implications, embryonic tissues may in the future be used as an additional source.

EPC differentiate into EC in response to signalling from the ECM and haemodynamic conditions. Unfortunately, the number of EPC decreases in some of those patients who are most susceptible to arterial disease- the elderly²⁸⁹ and diabetics²⁹⁰. Honold and colleagues found EPC to be mobilised by granulocyte colony-stimulating factor, but their functionality was poor²⁹¹. Localised arterial damage, in particular causes the targeted attachment of endothelial progenitors, leading Sreerekha to hypothesise that the fibrin in thrombus is the homing structure²⁹². This group coated synthetic grafts with a fibrinous lining and seeded them with nucleated cells isolated and cultured from bovine blood. PTFE showed greater initial attachment of these cells than Dacron, but subsequent proliferation of these cells was faster on the Dacron graft. These cells showed functionality by synthesising nitric oxide and after 96 hours of culture, resisted the shear forces of haemodynamic flow. Lev et al. have shown an aggregative and potentiating effect of activated platelets on EPC, using human cells²⁹³. This indicates that there is a physiological role for circulating endothelial progenitors in humans.

4.2.5 Off the shelf availability

Arterial bypass grafts are required on a semi-urgent basis for the relief of critical ischaemia and in some cases, urgently after the onset of acute ischaemia which may occur after interventional radiological procedures have been attempted. One great criticism levelled at TE grafts is the long time period required before an individualised graft can be made available.

Attempts to use readily available ECM components are being made but the use of ECM gels require prolonged maturation in bioreactors after seeding with SMC to form fibrous type collagen, followed by EC seeding and further maturation to ensure confluence as well as mechanical shear resistance of 20dynes/cm². In Isenberg's fibrin gel²⁵⁹, the initial matrix maturation required 5

weeks, whilst EC seeding numbers were optimal at 2 days, with good EC alignment and retention with 10dynes/cm⁻² steady or pulsatile flow. However, even with 5 weeks matrix maturation, the mechanical strength was not uniform or adequate, with only short segments(3-4cm) of graft being useable, and even these dilating irreversibly when exposed to low pulsatile flow.

Much of the time presently required for cell seeding is attributable to the two stage procedure of cell culture followed by seeding in a bioreactor. Niklason's group¹⁴⁸ have demonstrated a direct correlation between the time for maturation and strength of the resultant graft, with their seeded biodegradable PGA scaffold having a burst pressure of 570mmHg after 5 weeks and 2150mmHg at 8 weeks¹⁴⁸.

To address this, a single-stage method aimed at simplifying and quickening the graft implantation process involves auto-seeding cells rather than relying on physical extraction of cells by enzymatic or physical means where cell yields are low and adhesive efficiency and then proliferation is limited. This latter yields different levels of differentiation of SMC lines depending on the method of extraction²⁹⁴.

Some biodegradable synthetic polymers have relatively poor cell adherence properties, making them very unlikely to auto-seed from peripheral blood. Binding these materials with collagen may enhance their cellularization capability greatly^{295;296}, leading to the possibility of auto-seeding. The collection of large numbers of specific cells and their culture for seeding purposes is itself a long process. As outlined earlier, a possible future alternative to EC harvest, culture and then seeding is auto-seeding of EPC circulating in peripheral blood which could contribute to rapid endothelialisation of scaffolds²⁹⁷. Work on animal models in this area must be interpreted with a degree of caution as endothelialisation occurs less readily in humans. Also, the number of circulating EPCs in whole blood is low and the time taken for confluent endothelialisation by auto-seeding without cell culture is high. Notwithstanding this, Shirota's department has shown effective endothelialisation with human EPCs on collagen coated polyurethane conduits after four days seeding time²⁹⁸. These cells aligned and remained confluent when subjected to flow at 30dynes/cm². The problem of low EPC numbers in circulating blood can be circumvented by rapid seeding of stem cell-rich bone marrow. Another alternative may be to persuade the bone marrow to mobilise larger numbers of EPCs, using

granulocyte colony stimulating factor and granulocyte-macrophage colony stimulating factor²⁹⁹ although there is debate as to the efficiency of the resultant EPC²⁹¹.

Other mechanisms to improve endothelialisation efficiency include surface modifications with RGD-containing peptides^{300;301} and growth factors such as basic fibroblast growth factor³⁰². The RGD moiety is also independently anti-thrombogenic³⁰³ and increases the feasibility of a single stage seeding procedure³⁰⁴.

4.3 Conclusion and future directions

Tissue-engineering of vascular bypass grafts is a fast-advancing field stimulated by the large number of bypass procedures carried out without available autologous vein and the lack of synthetic prostheses with good long term results. It is also recognised that tissue-engineering of complex organs will only be possible when the intra-tissue blood supply can be secured. The final prize is an enticing one with the possibilities of replacement organs grown to order as well as, in children, the growth of vascular bypass prostheses as the individual grows. The large list of characteristics attributed to the artery which makes it ideal for purpose can not all be satisfied within a single synthetic prosthesis. It is clear to us that the proposition of a fully tissue-engineered artery has been particularly attractive as synthetic graft development using traditional materials has reached an impasse with the realisation that the many desirable (or even essential) properties cannot be simultaneously fulfilled. However, tissue-engineering can be used to 'grow' an artery on an individual basis, demonstrating biocompatibility; blood compatibility; mechanical strength with simultaneous viscoelasticity for efficient propulsion of pulsatile flow; and the ability to react to short and long term changes to haemodynamic conditions. Endothelialisation through the graft wall can occur as part of graft healing, provided a precise porosity and pore distribution with the optimal pore size being 30µm²⁰⁶. Exact pore specifications present great challenges in scaffold engineering with the advances in computer-aided manufacture and rapid prototyping showing real potential for the future³⁰⁵. Using the micro-CT-centred screening techniques that Van Cleynenbreugel³⁰⁶ has employed on bone grafts

the resultant scaffolds need not be tested in vivo until their biomechanical and structural suitability have been assured using finite element simulations and high resolution computed tomography for structural analysis. Stem cell research is a very active avenue for investigation at present both for endothelial seeding as well as a source for all the cellular layers required in a neo-artery. Their use could potentially increase seeding efficiency; solve the cell sourcing difficulties; and reduce the time required in vitro. Ultimately, using the ability of stem cells to differentiate into different cell lines could be channelled into techniques whereby different tissue layers are engineered from the same original stem cell source. This will only be possible once the mobilisation and differentiation factors for stem cells are fully understood. A big challenge is to achieve this with the shortest possible graft preparation time, and a number of techniques are being developed to ensure this ease of availability. However, for all the appeal of a bespoke personalised graft, if the issue of quick availability is not resolved, tissue engineering will not be able to become the main mode of small calibre vascular graft production.

The concurrent rapid increase in understanding and utilisation of nanotechnology in material science has begun to show direct and indirect effects on tissue engineering. Nanofibre manipulations of established polymers can achieve the favourable properties for biological implants, by mimicking the biological with the possibility of their use as improved synthetic scaffolds³⁰⁷.

5

Materials and Methods

5.1 Background

Composite materials have become commonplace in all aspects of modern living. They involve the organised integration of two or more materials to bestow the properties of each component simultaneously. At the macroscopic level, concrete reinforced with iron rods reduces brittleness and allows skyscrapers the ability to sway considerably in the wind or at the extreme, during an earthquake. Another example is the use of carbon-fibre technology in the strengthening of the bodywork of sports cars. Epoxy resin is co-extruded with carbon fibres - or graphite - to give a light yet simultaneously strong structure. Here the integration is occurring between polymeric fibre chains at the microscopic level. However, the latest composite manipulation technology concerns the use of nanoparticles – molecular constructs measured in the nanoscale range (0.1nm to 100nm) as an additive to traditional bulk materials. Apart from the relative size, the difference between the two components is that bulk materials retain constant physical properties for all sizes, whereas nanoparticles exhibit size-dependent properties. A range of properties can be conferred, including favourable mechanical characteristics – the extreme hardness of copper nanoparticles, compared with bulk copper – or photo-optic properties, due to quantum confinement with applications in medical imaging of quantum dots, to name but a few. The attributes due to the nanoparticle are not necessarily predictable – they relate to the percentage of atoms at the surface

of the particle. In the case of bulk materials, the atoms at the surface are overwhelmed by the sheer number of atoms in the rest of the structure, this latter dictating the properties. There is a branch of physics dedicated to the special behaviour of materials at the atomic level – quantum mechanics, which acknowledges the difference with traditional (Newtonian) mechanics of bulk matter. At its most fundamental level, it explains the orbital behaviour of electrons around a nucleus – classic physics would predict electrons being drawn straight to the (positive) nucleus. The success of quantum mechanics has been in the accurate prediction of behaviour at the atomic and sub-atomic level. However, this esoteric theoretical branch of physics has not been invoked in the conceptualisation and synthesis of the polymeric material used to manufacture PCUPOSS.

Nanotechnology is concerned with manipulation at the molecular or atomic level to provide useful applications. The field was popularised with the discovery of the fullerene structure – an alternative carbon molecule to graphite and diamond. This important discovery by Harold Kroto in 1985 at the University of Sussex highlighted that different molecular configurations of the same atoms gave widely different chemical and material properties. This concept underlies the whole of nanoengineering. It is a rapidly expanding field and still very much in its infancy with wide-ranging material science applications being developed including within the medical field. So far, particular promise has been shown in the medical technology fields of novel drug delivery systems, gene therapy and tissue engineering. Yet another molecular arrangement of carbon – the carbon nanotube has so far been the most investigated nanoparticle for potential biomedical applications³⁰⁸. However, they are limited by in vivo cytotoxicity and would not be suited to prolonged implantation³⁰⁹.

PCUPOSS is a nanocomposite material covalently bonding a polyurethane with a silsesquioxane ‘nanomolecule’ with the aim of exploiting the advantages of both moieties. The initial aim was to modify polycarbonate based polyurethane to improve its biostability with a view to using it as a long term implant material, but as has been discussed above, it was not known exactly what properties would ultimately be conferred. Silsesquioxane technology was targeted due to previous incorporation of siloxane (Si-O chains) in the form of polydimethylsiloxane (PDMS) – see Fig 5.1 - into polyurethanes. This itself was stimulated by two observations: siloxane groups are biologically inert and have

similar bond properties as ether groups within polyurethanes.

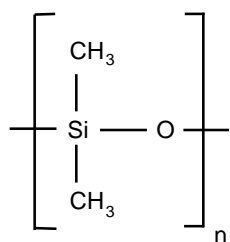


Fig 5.1. The repeating monomer of polydimethylsiloxane (PDMS). A large number of repeats (n) reduces viscosity.

Optimum levels of PDMS as a crosslinking agent as well as incorporation into the polyurethane backbone reduces biodegradation and the extent of the inflammatory response to the polymer³¹⁰. However, this incorporation also contributes to a reduction in strength despite similar bond strength as polyether. The loss of tensile properties is due to macrophase separation as a result of the poor solubility of the PDMS³¹¹.

5.1.1 Silsesquioxane

This word literally indicates one silicon atom for 1.5 oxygen atoms. It represents a class of silicone-oxygen compounds which include the polyhedral oligomeric silsesquioxanes (POSS). This latter comprises cyclical rings of alternating Si-O atoms in layers. In order to preserve the Si₂O₃ ratio, only specific ring/layer combinations are possible. PCU-POSS contains one of the most widely used POSS structures, namely the Octahedral-Dimeric Silsesquioxane – Fig 5.2.

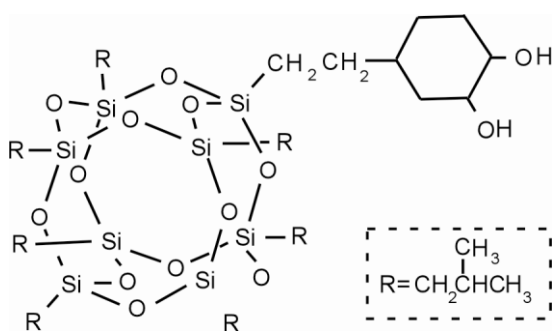


Fig 5.2. Chemical structure of trans-cyclohexanediolisobutylsilsesquioxane, the POSS moiety used in PCUPOSS.

5.1.2 Polyurethane.

This is a class of polymer with very widespread applications in all industries. This is a reflection of the huge variety of properties which can be conferred on it, depending on the constituent components. There has been widespread use of polyurethane materials as in-vivo implants due to their favourable biocompatibility. They came into prominence as medical implants from research aimed at producing the 'artificial heart', due to their high tensile strength, repetitive stress fatigue resistance and inherent low thrombogenicity.

5.1.2.1 Poly(ester)urethane

The initial polyurethanes to be evaluated had polyester soft segments. However, their use as medical implants was short-lived when it was realised that these underwent rapid hydrolysis in the biological environment, limiting them to roles where in vivo exposure was less than a few hours.

5.1.2.2 Poly(ether)urethane

When considering permanent non-degrading graft materials, polyether macroglycol appeared to be more suited, with no hydrolysis of the soft segment. A number of polyether urethanes have been produced commercially for clinical implantation – see table 1. However, ether links are susceptible to oxidative degradation when exposed to reactive oxygen species produced by macrophages. The extent of degradation is proportional to the number of ether links present, although at a much slower rate than polyester degradation. These mechanisms of degradation are discussed in detail in chapter 10.

5.1.2.3 Poly(carbonate-urea)urethane (PCU)

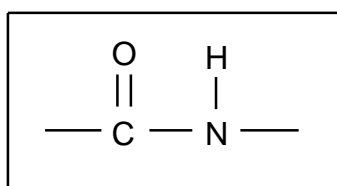
Our group has concentrated on the use of polycarbonate macroglycol.

This largely eliminates ester and ether groups, rendering the polyurethane relatively biostable. Initial in vitro biodegradation studies of PCU showed that a range of physiological solutions simulating the biological environment and its degradative mechanisms caused less degradation than polyether and polyester soft segments. However, specific hydrolytic enzymes such as cholesterol esterase as well as exposure to oxidative solutions have shown in vitro degradation. Monocyte-derived macrophages could hydrolyse polycarbonate urethanes as predicted by in vitro cholesterol esterase action³¹². However, in vivo, macrophage-derived oxidative compounds are also released which may be protective against hydrolytic degradation.

It is often stated that the biostability of polyurethanes is determined by the polyol used. However, it can be inferred from the relative biodegradative potentials of the above three PU classes that this is a simplification. If macroglycol degradative susceptibility reflected that of the PU, PCU would be highly susceptible to hydrolysis. In fact PCU is protected from degradation by the shielding effect of the hard segment. This is brought about by extensive hydrogen bonding between the carbonate groups and the hard segment at the urethane moiety.

To understand the structure of our nanocomposite, a basic understanding of polyurethane chemistry is required.

A polyurethane is a chain of repeated monomers (ie. a polymer) each linked to the next by a urethane group:



This link forms the bond within the hard segment of the polymer. Hence the term polyurethane is in a sense misleading as it does not consist mainly of repeating urethane groups. The 'co-polymer' is composed of hard segments and soft segments which exist in microphase separation – they do not mix completely with each other; giving rise to the term 'segmented polyurethane' – see Fig 5.3. A polyurethane with a preponderance of hard segment is described

as 'crystalline' whereas if the soft segment dominates, it is termed an 'amorphous polyurethane'.

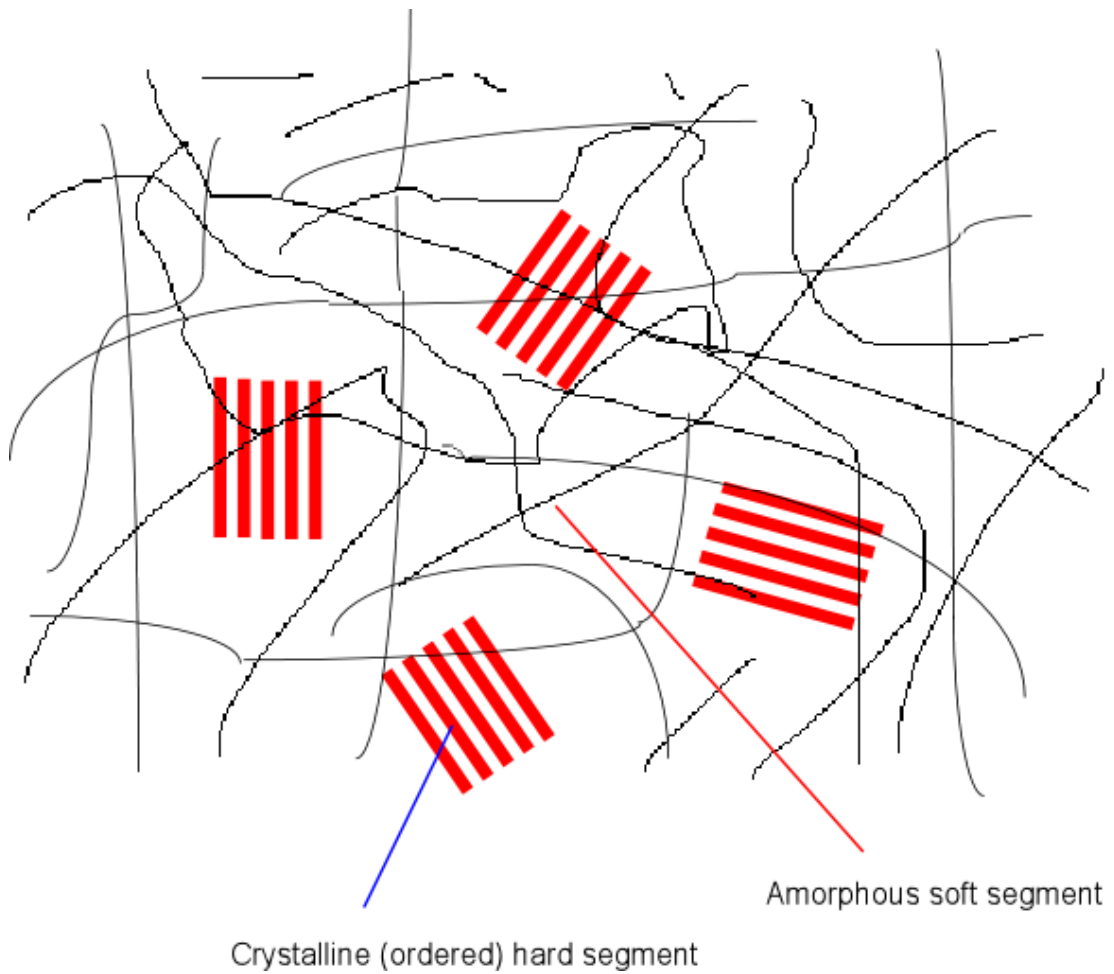


Fig 5.3. Molecular schematic to describe the segmented structure of polyurethanes. The ordered hard segments are highly polar groups with strict alignment and strength. These float in a 'sea' of soft segment, which allows considerable movement. Hence the combination can be elastic and simultaneously strong.

The hard segment incorporates a urea bond, formed by reacting -NH_2 groups of a diamine with -NCO groups on a diisocyanate; or a urethane bond by reacting diol -OH groups with the -NCO , whereas the soft segment is a macroglycol such as polyester, polyether, polycaprolactone or polybutadiene which is also reacted with the diisocyanate - the -OH groups of the macroglycol with -NCO on the diisocyanate - to form further urethane links. The hard segment is the highly ordered and tightly packed crystalline component with polar groups capable of multiple H-bonding and van der Waal attractions to adjacent groups whereas the soft segment forms an amorphous matrix with random intertwined coils within which the hard segments float. One consequence of microphase separation is that an increase in the hard segment to increase strength will affect the soft segment too resulting in a reduction of elasticity as a result of increased 'virtual crosslinking' of the crystalline segments with each other and with the matrix. Although it is not clearly understood at present, it is also thought that microphase separation is also responsible for the low thrombogenicity seen with many polyurethanes, due to irregular nanoscale surface geography³¹³.

The oxygen atom of hydroxyl groups is slightly electronegative due to its propensity to pull electrons away from its neighbouring hydrogen atom. The cyanate group consists of a carbon atom with electron-greedy nitrogen and oxygen either side of it, making it relatively electropositive, and therefore readily reacting with the oxygen of the hydroxyl group. The result of this reaction is to leave the carbon satisfied but the adjacent nitrogen remains electronegative. The nitrogen donates a pair of electrons to the hydrogen atom of the hydroxyl group which is now next to it, forming a urethane bond. This reaction is summarized in Fig. 5.4.

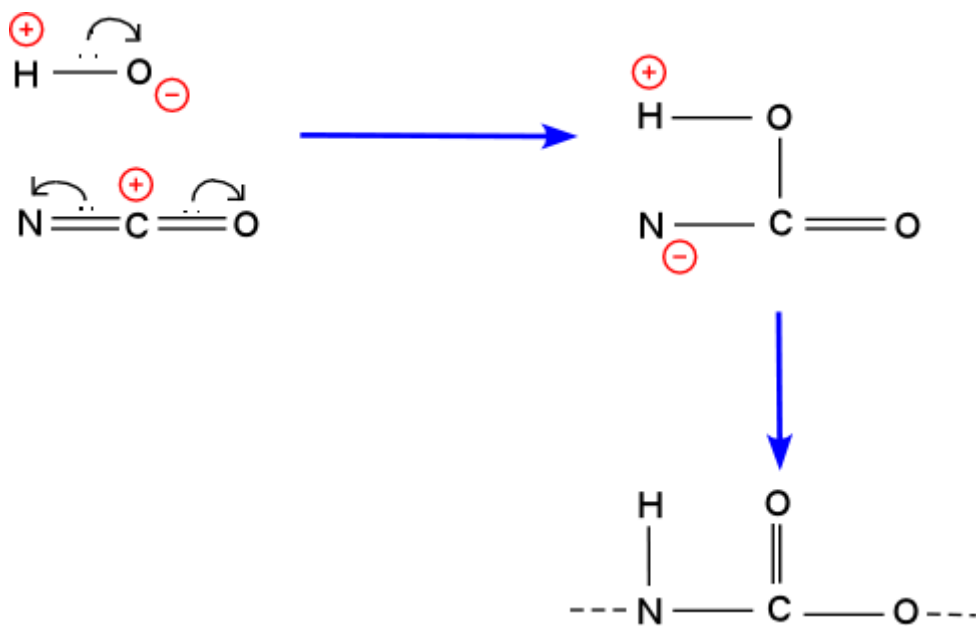


Fig 5.4. The formation of the urethane bond. See text for details.

5.2 Synthesis of PCU-POSS

72g of dry poly-hexamethylene carbonate diol (2000 molecular weight) is mixed with 2g of trans-cyclohexanediolisobutylsilsesquioxane (Sigma-Aldrich) – the POSS, in a 500ml reaction flask equipped with a nitrogen inlet and mechanical stirrer. The mixture is heated to 125°C to dissolve the POSS in the polyol and then cooled to 60 °C gradually by removal of the heat source. Constant stirring is performed throughout. 18.8g of flake methylene diisocyanate (MDI) are added to the polyol blend and then reacted, under nitrogen, at 75 °C for 90 minutes to form a pre-polymer. This consists of POSS moieties with MDI attached at each of its hydroxyl groups, and polycarbonate with MDI reacted to the diol groups on either end. 156g of dry dimethylacetamide (DMAC) is slowly added to the pre-polymer to form a solution, which is then cooled to 40 °C. Chain elongation is carried out by drop-wise addition of a mixture of 2g ethylenediamine and 0.05g diethylamine in 80g dry DMAC. The former's two amine groups cause chain extension by the formation of urea groups, and the latter having one amine, terminates the predominantly linear chain. Finally a mixture of 4g 1-butanol and 80g DMAC are added slowly to the polymer solution.

5.3 Tensile Stress Testing of Graft Material

5.3.1 Introduction

Tensile testing is the universally recognised technique for mechanical characterisation of any material. However, testing of small elastic specimens with low magnitudes of failure requires high attention to detail to ensure accuracy and reproducibility. The basic premise is to apply a strain to the sample, monitoring extension and stress within the material. The strain may be gradually increased until the sample breaks to give information about material strength. Standard apparatus for tensile testing is designed for larger specimens than the 5mm graft and require considerable modification. Also a consideration of the biological environment is required to validate the test

procedure. The viscoelastic behaviour of a tissue depends on the temperature of the environment, so testing needs to occur at 37°C.

5.3.2 Stress-strain behaviour

This relationship fundamentally describes the mechanical behaviour of the overall graft. It requires the appreciation of any possible directional anisotropy. This relates to the mechanical properties in one direction being different to those in another direction. Therefore it is of paramount importance to measure tensile properties in the circumferential plane, and compare the results with the longitudinal direction. In reality, grafts are never subjected to steadily increasing deformation. Nevertheless, it provides baseline data on the strength and elastic properties of the material.

Stress is a ratio of applied load on the material to its cross-sectional area (Force/Area). The highest stress achieved before the material breaks is termed the 'ultimate strength' or 'ultimate tensile strength'. This is not necessarily the stress immediately before fracture of the sample – see Fig 5.5

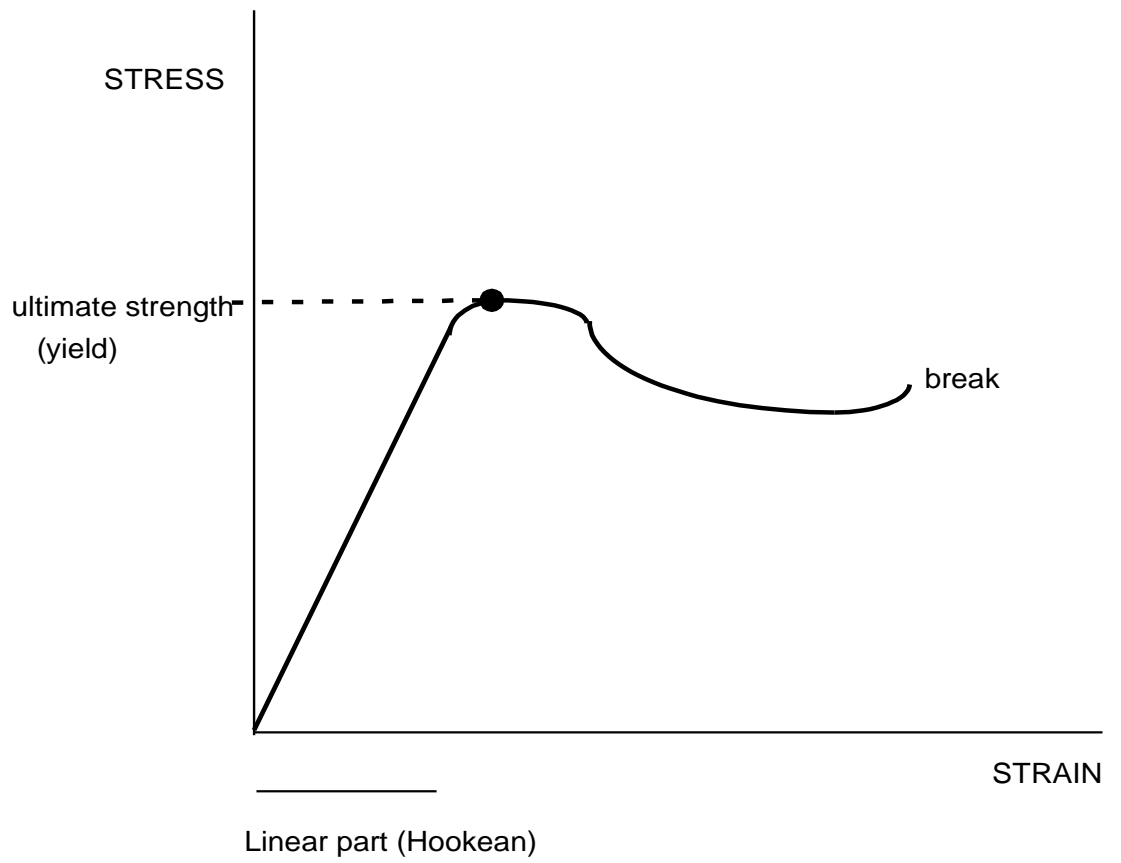


Fig 5.5. A typical stress-strain curve.

Strain relates to another ratio – that between the stretched length and the original unstretched length, and so has no units. The initial relationship in the curve above is linear, following Hooke's Law, which states that for an elastic material, the stress is proportional to the strain. The relevance of this portion is that removal of the stressor would result in a reduction in strain exactly along the same line. It is important to know the pattern of stress unloading as pulsatile flow entails a continuous loading and unloading of stress on the vessel wall.

Artery segments do not distend and relax along the same line on the stress-strain curve. They do not show linear stress-strain relationships as discussed in chapter 2. The extrusion-coagulated grafts may be considered to be foams, due to the high pore density and size which is demonstrated by scanning electron microscopy in chapter 6. It is not strictly accurate to speak in terms of stress with foams as the specimen cross-section thickness is largely pores, rather than the polyurethane material. Instead, force may be used to show the same relationship with strain. Force-strain characteristics for foams have a characteristic shape – Fig 5.6

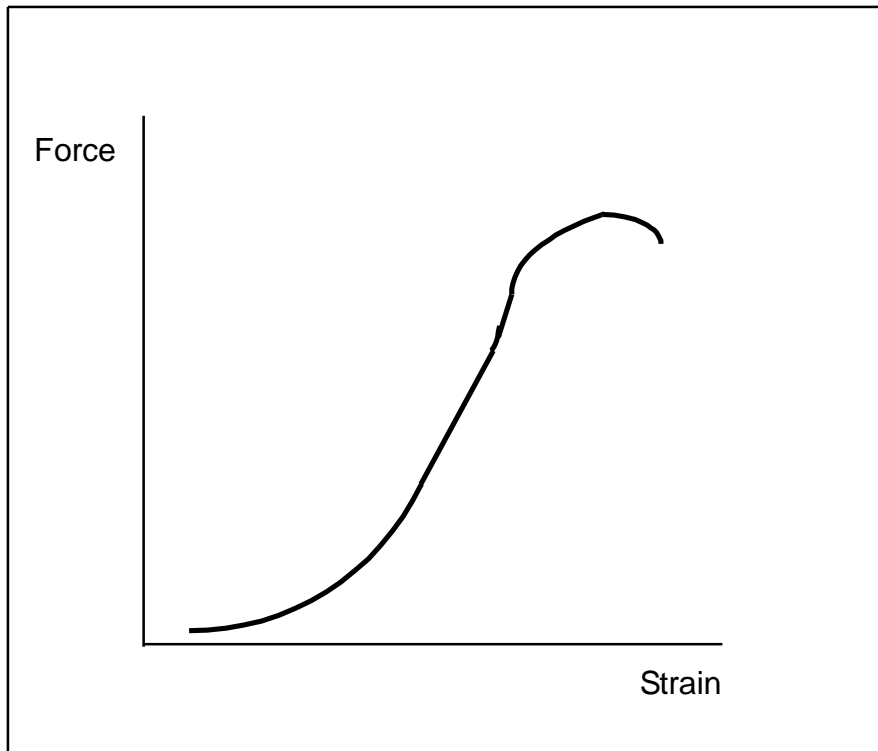


Fig 5.6. The typical tensile test curve for foam structures.

In fact, this curve is not dissimilar to the more commonly performed compression test of a foam – see Fig 7.1. The initial part of the tensile curve simulates the J-shaped curve found for arteries and one reason for the selection of highly porous polymer constructs (ie. foams) as alternative compliant grafts.

5.3.3 Stress Relaxation

This is defined as the reduction of stress over time under a constant strain. It is a measure of the viscous component of mechanical properties. Together with elongation, it demonstrates viscoelasticity of the test sample. In many polymer applications it is a highly undesirable property. Generally speaking, these include applications which require long periods of strain maintenance such as the screw-top lid on a plastic jar. However, viscoelasticity is an inbuilt feature of the arterial wall as discussed in chapter 2. The usual way of quantifying the results of a stress relaxation test is by plotting the decay of stress with time. Dividing the stress at a given time by the strain gives an apparent modulus, which can then be re-plotted as a function of time³¹⁴.

5.3.4 The longitudinal sample

The traditional sample for tensile testing is ‘dog-bone’ shaped – see Fig 5.7.

The wide ends are placed within the grips of the apparatus. The reason behind this shape is to ensure that the highest stress concentrations do not build up at the grip ends themselves. It must be assumed that application of any grip will place additional stresses on the sample in the vicinity of the grip margin, potentially weakening the graft at this point. Hence on applying strain, the sample can fail prematurely at the grip edge, misrepresenting the actual ultimate tensile strength of the material. By widening the ends of the sample, the stress concentrations are greatest in the central narrow part which is unaffected by the grips (stress = force/area). This area is known as the ‘gauge length’.

Extraction of the ‘dog-bone’ from the graft is not a simple affair. The graft

is first opened longitudinally. However using a template and cutting the sample out of the graft with a scalpel blade introduces variable stresses to the edge, as it is impossible to follow the template smoothly with the same pressure throughout. The method used is punching the sample out of the graft wall using a razor-sharp cutter and a mechanical press. The cutter needs to be sharpened regularly to ensure that the cutting process is identical for each sample. To eliminate this possible variable, some authorities recommend that the cutter design should not be razor-sharp, accepting the slight side-shear that will occur, as this will at least be the same for all samples cut.

Even with this technique there is the possibility of non-uniformity due to the elasticity of the graft and its shape-memory for a tubular form. The pressing action of the cutter on the graft can stretch it as it cuts. To preserve uniformity of the cut edge, the graft material was sandwiched between two polyurethane sheets. This ensured the specimen was flat without being stretched. The sheet above the sample was 0.5mm thick whereas the sheet below was 3mm thick. The cutter depth was set such that at its lowest point it rested 2mm within the substance of the lower sheet to ensure it has completely transected the graft sample. The press was lowered manually with a swift action.

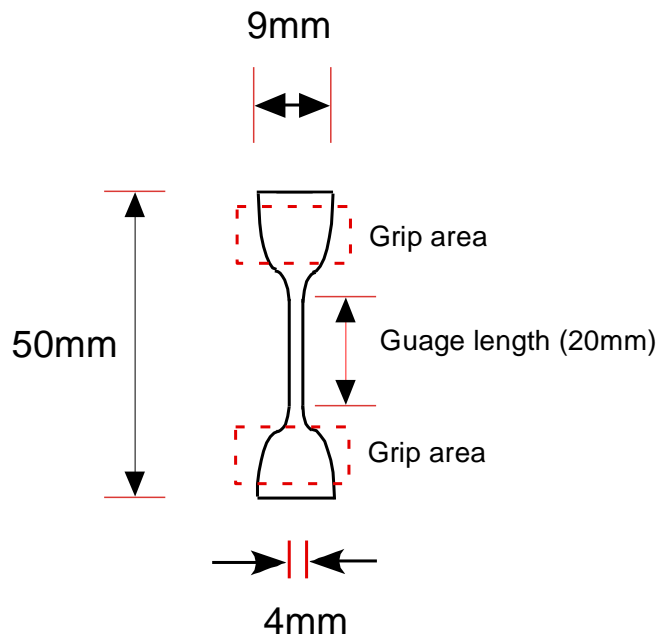


Fig 5.7. The dimensions of the dogbone specimens used (not actual size).

5.3.5 The testing grips

The ideal grip characteristics are to be as light as possible whilst offering a secure grip with no slipping of the specimen³¹⁵. The grips used were constructed specifically for the graft material using pairs of flat blocks of nylon which could be opposed together tightly using thumb-bolts with the 'dog-bone' end sandwiched within them. These ensured no slippage in the tensile range before failure. The relative advantage which the graft specimens had was that they were not brittle, so the grip strength could be high without fear of sample breakage. In addition, due to the low force range in which the graft specimens were to be tested, the errors created by the slight 'give' in the load cell and load frame were negligible. The upper grip rested on two screw threads projecting upwards from the lower grip, to align the two grips precisely, and to prevent any stress on the sample at the start of the test. Fig 5.8a and 5.8b show the grip set-up. To further ensure vertical alignment and prevent side loading or bending moments, the samples were loaded into the upper grips first, then allowed to hang down before inserting into the lower grips. However, this was not adequate to ensure that the specimens were placed exactly neutrally, without initial slack. An alternative technique was also used, whereby a template was made of the dogbone from inelastic acetate, which was then placed alongside the dogbone in the grips. The template was pre-cut across the narrow area of the dogbone, and the length held by surrounding flanges.

5.3.6 The circumferential sample

The extrusion-coagulation process used may result in anisotropy of the graft. Testing in the circumferential direction is necessary for comparison with the longitudinal characteristics.

The problems posed here are due to the small size of the specimens involved. One method of circumferential stretching is to place a hoop of test material between two pins and pull the pins apart (Fig 5.9).

However, the pins would need to be very small themselves. A suitable grip for this was designed using stainless steel links from a wristwatch bracelet, along with the pins which hold the links together (Fig 5.10a and 5.10b).



Fig 5.8a. The longitudinal sample held in the neutral position within the nylon block grips.

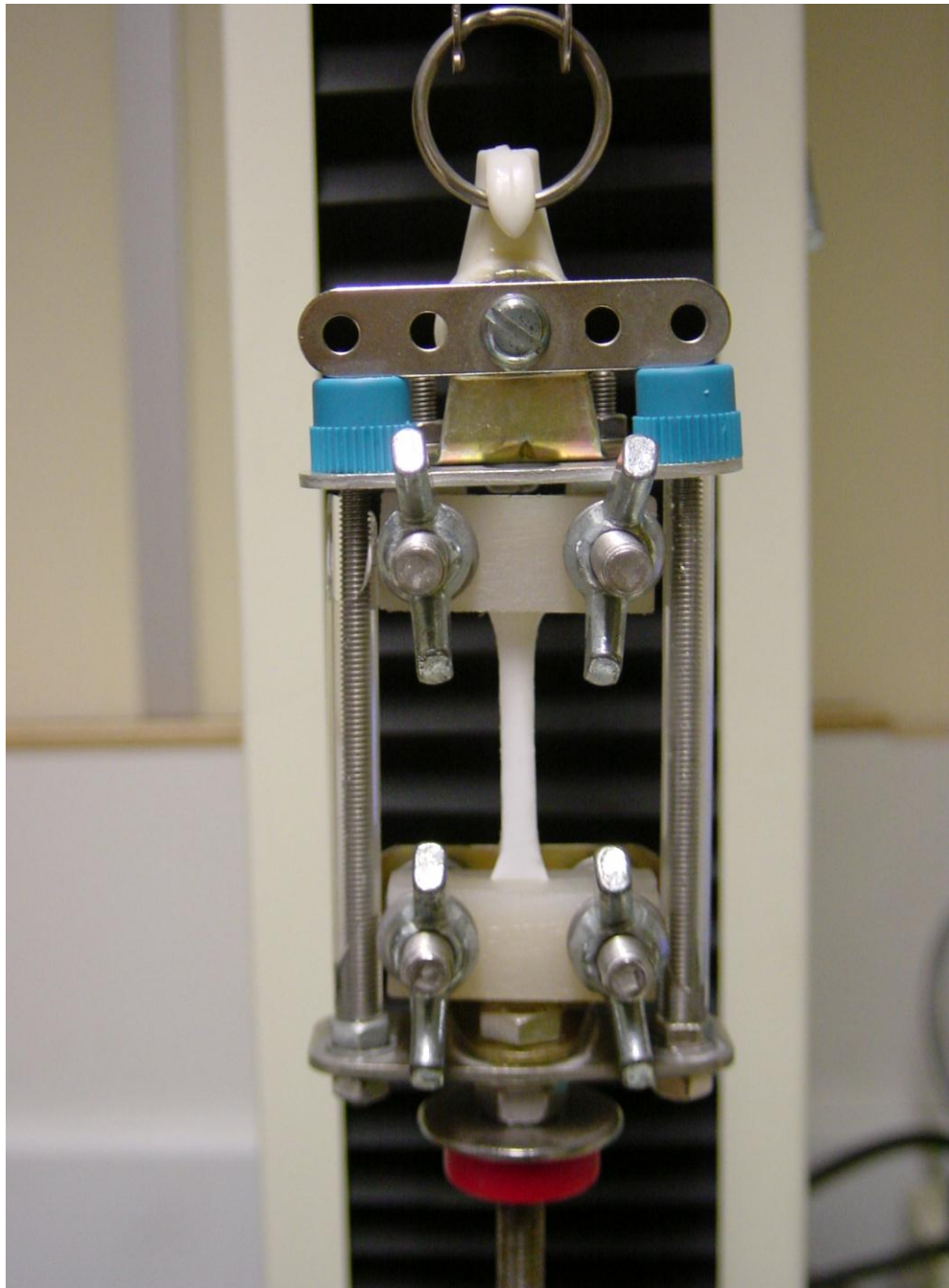


Fig 5.8b Close-up of the grips used for longitudinal dogbone samples

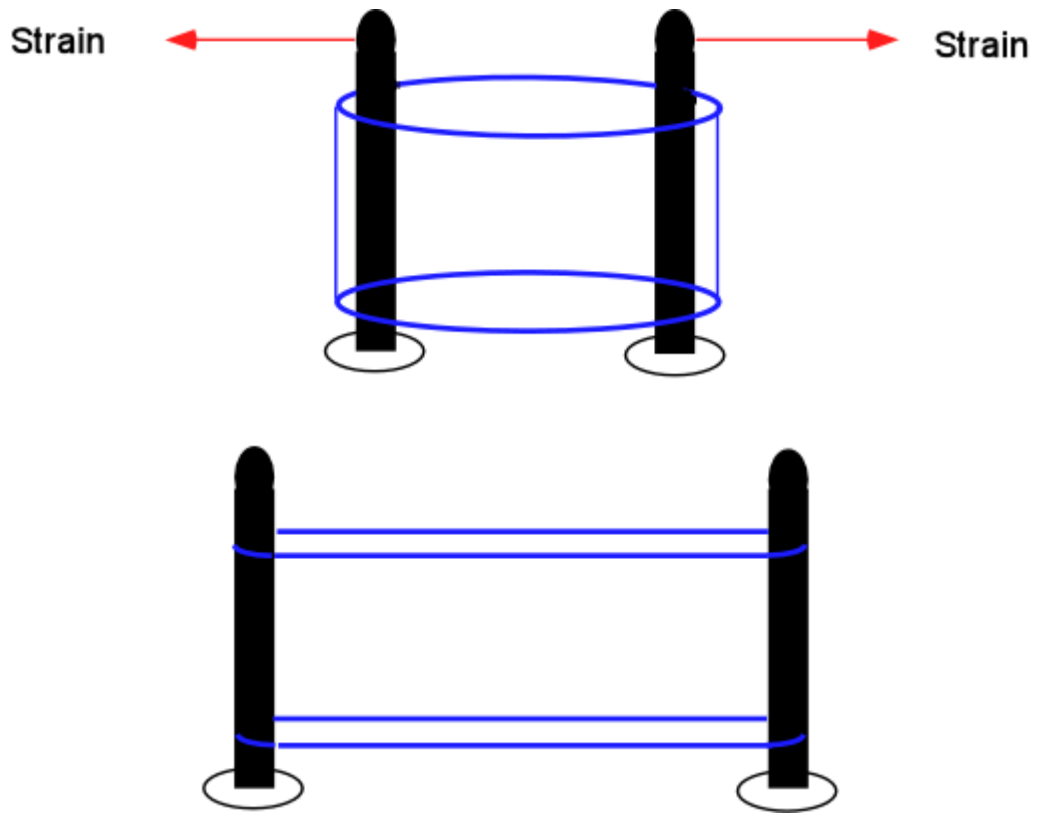


Fig 5.9. The concept of hoop testing of tubular structures.

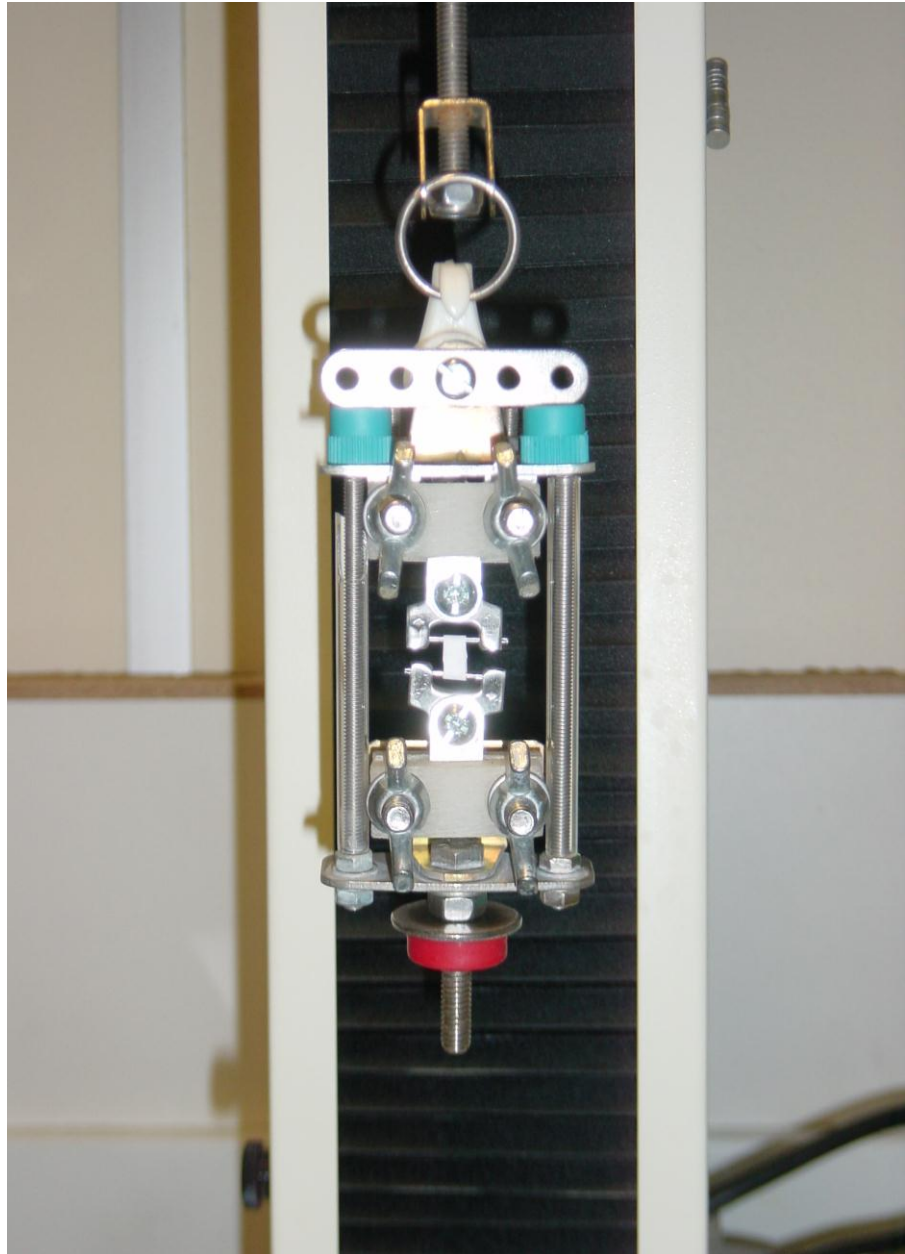


Fig 5.10a. The use of links and bracelet from a stainless steel wrist-watch band to design the rig for hoop testing of circumferential samples.

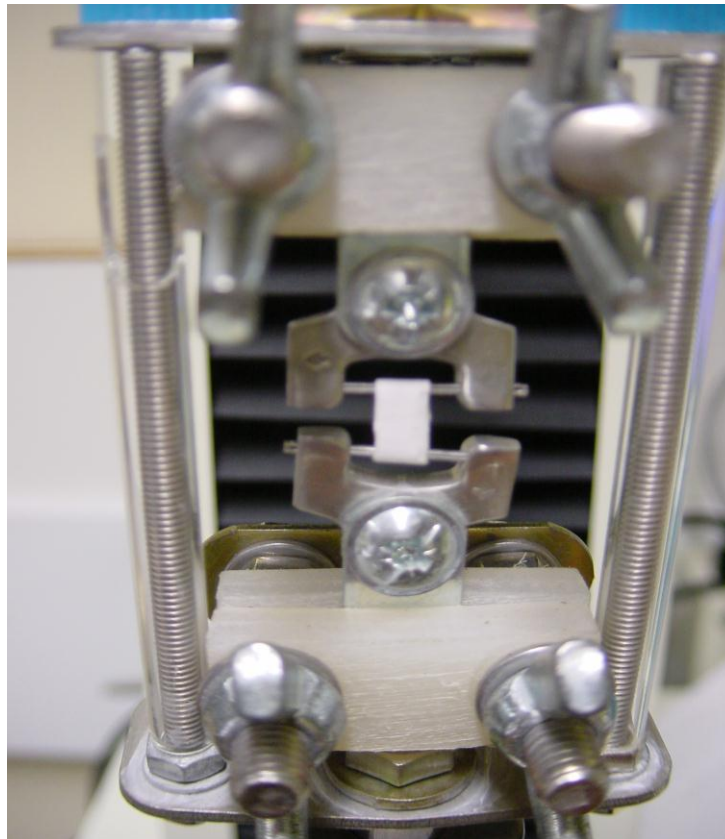


Fig 5.10b. Close-up of the hoop testing rig.

One difficulty when using this system is assessing the starting point for the test. The hoops neutral position is circular in cross section, but the pins can be moved further apart before stress is exerted on the material itself. To prevent a pre-stressed starting point, it was decided to start the test with the hoop resting on the upper pin, but not in contact with the lower pin. This was difficult to perform due to the buoyancy provided by the water environment. Another difficulty arising from this issue was determination of the initial unstretched dimensions for calculating strain. An approximation would be to use

$$\pi \times \text{radius} \quad (1)$$

which is half the circumference. A justification for this approximation follows:

Imagine a thread looped to make a circle with radius r . The length of that loop of thread is

$$2 \times \pi \times r \quad (2)$$

If opposing ends of the circle were now pulled taut, they would effectively leave a double thread whose length must be half the length of the original thread

$$\pi \times r \quad (1)$$

Another concern is that the stress due to the pins themselves will be very large at high strains such that they will tear through the hoops, underestimating true strength. For this reason, it was decided to manufacture a cutter for small 'dogbone' specimens to be pressed in the circumferential direction as well. This was created from the casing which surrounds quartz crystals on electronic circuit boards. These were selected due to their sharp edge as well as their appropriate size. The cutter consisted of two such cases in parallel, held 4mm apart. This cutter worked well initially but quickly became blunt, so a new cutter was made to order.

5.3.7 The environmental chamber

Viscoelastic properties of a material are dependent on the temperature used. This can be explained in terms of the entropy in the system. Stretching an elastic material involves alignment of its molecules and an overall reduction of disorder, which is against the universal trend towards an increase in disorder (entropy). This discrepancy manifests as the force with which the elastic material attempts to contract back to its original state. At higher temperatures, the entropy of the molecules is greater due to their greater energy and so strain is resisted more than at low temperatures. It is therefore essential to test the graft samples at the in vivo temperature.

A clear perspex tubular tank surrounding the grips was filled with water at 37°C immediately before the test was carried out. This tank was screwed into the base of the lower grip with an intervening O-ring to ensure a watertight seal – Fig 5.11.



Fig 5.11. The tensile test including environmental chamber filled with water at 37°C.

5.3.8 The Tensillometry Machine

The Hounsfield H5K-S UTM is a benchtop mechanical testing machine with a 250N load cell attached with a force accuracy of +/- 0.5N. It is a vertical Universal Testing Machine consisting of a single screw load frame with a 750mm extension limit. A PC with operating software for the machine is attached.

5.3.8.1 Method

5.3.8.1.1 stress/strain and tensile strength

The 'dog-bone' sample was secured in the upper grip with thumb-bolts. The upper grip was placed on the guide-rail to align it with the lower grip and the lower end of the sample was secured in the lower grip without tension. The ensemble was then threaded through the base of the water-tank and then screwed onto the testing frame. The load cell was latched onto the upper grip via a hook and loop, ensuring that no strain was applied to the sample. The environmental chamber was filled with water at 37°C. Hounsfield operating software was used to extend the sample at 60mm/min until it failed. A tensile force/extension curve was generated and ultimate stress and elongation recorded.

This procedure was repeated for six longitudinal and six circumferential samples.

5.3.8.1.2 stress relaxation

A 70% elongation strain was applied to three longitudinal and three circumferential samples in the environmental chamber. The reducing force was recorded manually using a stopwatch at five second intervals to start with and then gradually over longer intervals until no further stress relaxation was seen over 90 seconds.

5.4 Compliance measurement

5.4.1 Introduction

As outlined in the review of mechanical properties previously, the concept of arterial compliance is necessary due to the complex nature of elasticity of all biological tissues. In particular, the elastic character is determined both by the degree of stretch that has already been exerted on the vessel (preload) and also, the rate at which the vessel is being stretched. It follows that compliance may be considered as the degree of further distensibility at any given preload, and cannot be stated without including a description of the preload under which it is measured.

Different groups have used a variety of methods to determine compliance³¹⁶. Arterial waveform analysis with mathematical algorithms allow for the determination of overall compliance for the whole arterial tree; pulse wave velocity and pressure/distension relationships can be used to consider short vessel segments individually. The assessment of local graft segments extra-corporeally can be grouped into quasi-static and dynamic tests. The former involves slowly increasing the pressure within the conduit being tested and monitoring the rate of distension change. The result is usually stated at 120mmHg to present uniformity and allow comparison. However, this test, although useful for mechanical characterisation when formal tensile testing data is not available, does not truly reflect compliance as it assumes a purely elastic sample, with no viscous component. For simplicity, it neglects the increased stiffness of arterial specimens at high rates of pressure change. The elastic character of vessels tested in this way may be a significant overestimate due to the low rate of pressure change utilised compared with the physiological pressure waveform of pulsatile flow.

For this reason, a more rational assessment of viscoelastic material elasticity is to test it in the environment in which it works – ie. in-vivo. This may be non-invasive testing of compliance, using ultrasound for distension data and a percutaneous blood pressure sensor. However, for grafts at an early stage of development, it is ethically desirable to address mechanical properties before implantation. To achieve this, the graft requires placement within a biomimetic flow circuit. Real time pressure and distension data with pulsatile flow can be

used to calculate compliance:

$$C = \frac{d_{\text{sys}} - d_{\text{dias}}}{d_{\text{dias}}} \times \frac{1}{p_{\text{sys}} - p_{\text{dias}}}$$

(C is compliance; d_{sys} is systolic diameter; d_{dias} is diastolic diameter; p_{sys} is systolic pressure; p_{dias} is diastolic diameter)

The strain proportion is worked out as a percentage by multiplying by 100 and the percentage compliance is calculated. A further multiplication factor of 100 converts the compliance to the universally used units of %/mmHg ($\times 10^{-2}$).

In fact, this method defines volumetric compliance, which is a composite of radial (or circumferential) compliance and longitudinal compliance³¹⁷.

5.4.2 Method overview

An 8cm length of prosthetic graft was mounted horizontally on a fixed frame and tied with 3/0 silk via bespoke PTFE interconnects to silicon rubber tubing. The graft and frame were immersed in a waterbath at 37°C. The proximal graft end was connected via tubing to a jacketed reservoir which was held at variable height to control mean pressure in the circuit. The distal graft end was connected via tubing to the inflow channel of a phantom pulse generator (Harvard apparatus Model 1421, South Natick, MA, USA). The output from the pump poured into the reservoir. Ultrasound with wall tracking software was used to visualise and measure the inner wall movements resulting from the flow in the circuit. Fig 5.12 shows a schematic diagram of the circuit set-up.

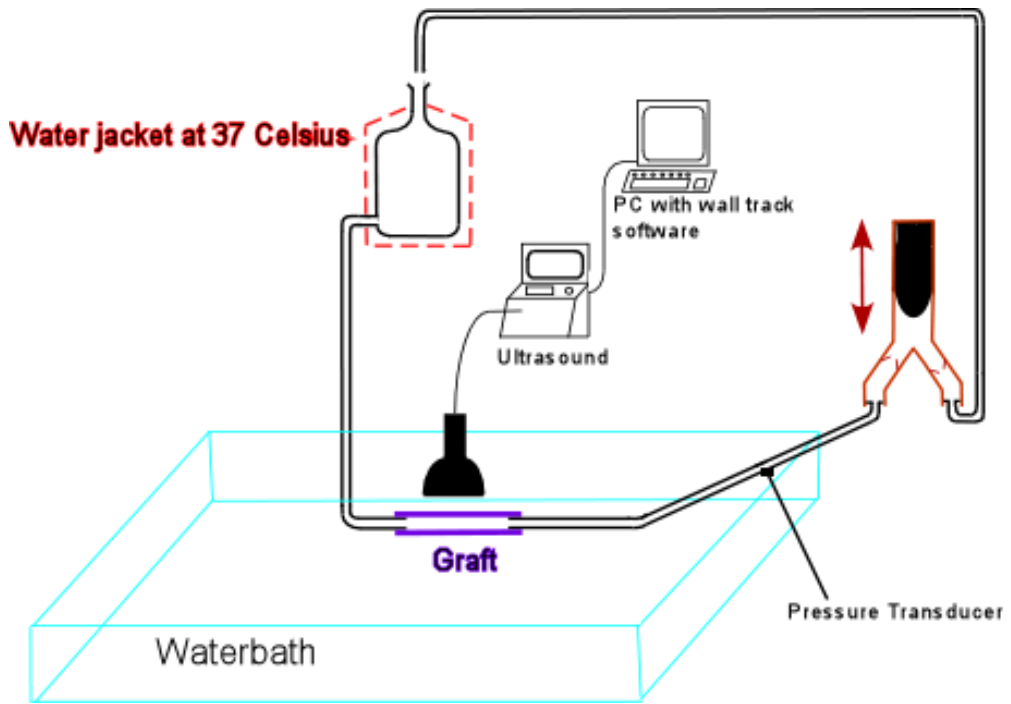


Fig 5.12. Schematic diagram of the flow circuit used to measure dynamic compliance.

5.4.2.1 Fluid in the circuit

600ml of fluid was needed to fill the circuit. Initially, in order to achieve the non-Newtonian properties of blood, donated packed red blood cells made up with SAGM (Sodium/adenine/glucose/mannitol) additive – see Table 5.1 - from the London Transfusion Service was used. The blood was collected in a CPD (citrate/phosphate/dextrose) anticoagulant solution – see table 5.2. 300mls of plasma was removed after centrifugation from 450mls of donated blood and the cells resuspended in 250mls of SAGM. These units were one day past their expiry date, so as to be clinically obsolete and would otherwise be discarded. Blood from different blood groups were not mixed. The blood was warmed in the jacketed fluid reservoir to 37°C over ten minutes, during which time the outlet was clamped. A mercury thermometer monitored the temperature of the blood and at 37°C, the clamp was removed to allow the blood to fill the circuit. All air bubbles were eliminated by coaxing them upwards into the reservoir.

Component	Concentration (mmol/L)
Sodium chloride	150.0
Adenine	1.25
Anhydrous glucose	45.4
Mannitol	28.8

Table 5.1. The composition of SAGM additive.

Component	Concentration (g/L)
Sodium citrate (dehydrate)	26.3
Dextrose (monohydrate)	25.5
Citric Acid (anhydrous)	3.27
Monobasic sodium phosphate (monohydrate)	2.22

Table 5.2. The composition of CPD anticoagulant.

5.4.2.1 Consideration of blood's viscous flow in the circuit.

The use of a blood product in the flow circuit was aimed at modelling the mechanical graft/blood interaction which would occur in vivo. Blood is a suspension of cells in plasma, with its own viscoelastic properties. This means that its physical behaviour is dependent on the rate of stress exerted, and in particular, its flow characteristics are dependent on shear rate. This property is termed 'Non-Newtonian' behaviour, unlike homogenous fluids such as water, which exhibit 'Newtonian' behaviour – see Fig 5.13. Blood's viscosity is therefore increased in low flow states. At the same time, viscosity will determine the shearing forces at the vessel wall to some extent. It is this point which suggests the rationale for the use of a fluid which demonstrates the viscous properties of whole blood.

However, a number of additional factors would question the need and validity of using blood products in the circuit.

When considering flow in an artery with an internal diameter greater than 100µm, the effect of viscous forces are greatly overwhelmed by inertial forces on the cellular components which are the principle determinant of the flow characteristic³¹⁸. There is an important difference between the two parameters. Viscosity relates to the ease with which one lamina of fluid slips over the adjacent laminae and is greatly influenced by plasma rheological properties. However, the inertial forces to consider in larger vessels relate to the rigid structure of cells and their proportion in the blood, as well as the attractive forces between red cells which are all dependent on the flow velocity. The inertial force is given by the product of mean flow velocity and vessel diameter.

Although it is true that blood's viscosity is dependent on shear rate, the shear rates in the circulation are sufficiently high to ensure minimum (and constant) viscosity. This means that flow conditions keep the blood's properties at the right side of the shear stress/ shear rate graph. It is therefore not important to consider variable viscosity in the flow circuit, where both vessel diameter and flow rates are high, and the use of fresh blood would not greatly contribute to the accuracy of measurements.

Furthermore, our initially chosen alternative was to use donated blood, after warming it to 37°C. Its viscosity would be expected to be lower than that of

fresh blood due to the age of the red cells³¹⁹. Also, blood viscosity is greatly dependent on the haematocrit level³¹⁸. Donated units of packed cells have a variable haematocrit which may be 25% greater after extraction of plasma and resuspension in SAGM. In order to address haematocrit standardisation, a variable amount of isotonic solution would be required each time the circuit was filled. This was impractical and in view of the reasons outlined above, the precise non-Newtonian behaviour of blood seemed irrelevant. Therefore, the viscosity of whole blood was determined by testing a 2ml citrated sample of freshly donated blood in a rheometer using a 4° cone and plate system at a constant shear rate of 200s⁻¹. This rate reflected the magnitude of wall shear rate to be found in physiological conditions³²⁰.

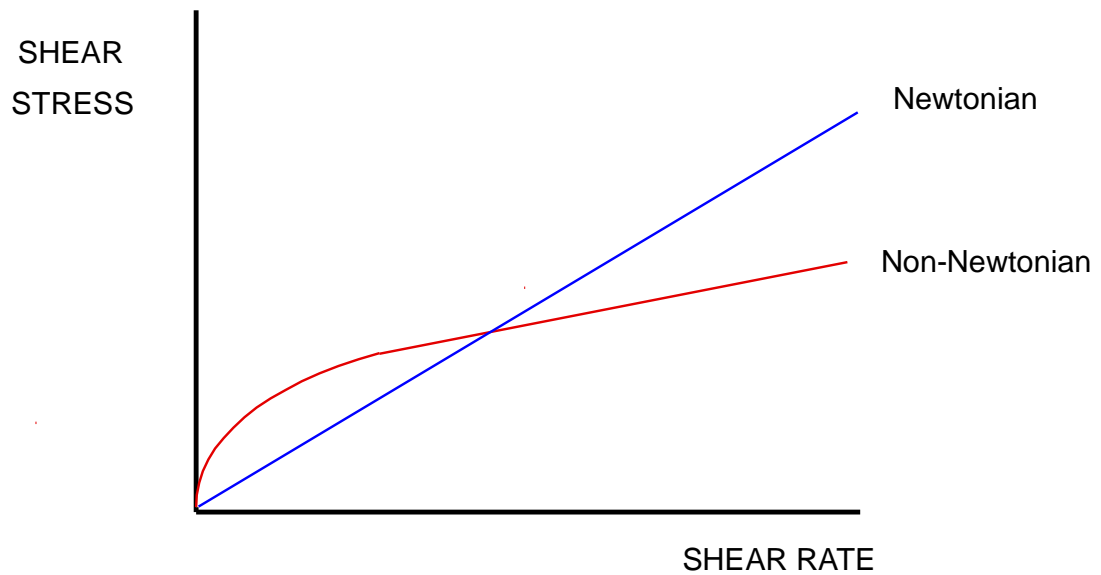


Fig 5.13. The viscous relation to shear rate for Newtonian and Non-Newtonian fluids. The gradient of the lines correspond with viscosity, so a Newtonian fluid maintains the same viscosity for all shear rates, whereas a Non-Newtonian fluid (blood) has a low viscosity at high shear rates (high flow rates).

5.4.2.2 The biomimetic pulsatile flow generator

The Harvard Apparatus Model 1421 is designed to simulate the pulsatile output from the ventricular system of the heart with features to minimise haemolysis. It utilises a positive piston actuator, which in combination with ball-type unidirectional valves ensure that there is a constant flow rate even when there are variations of resistance in the flow circuit – Fig. 5.14. All materials which come into contact with the blood in the circuit are inert – silicone rubber, acrylic plastic and PTFE. The ball valves are stainless steel, coated with silicone.

The systolic phase (piston compression) comprises 35% of the cycle duration, with diastole (rarefaction) taking up the remainder, to closely model the cardiac output. The pump has been previously validated as the pulsatile source for a laboratory model of the circulatory system by Levy and Zieske³²¹.

Both pulsatile rate and pulse pressure can be varied independently when using the pump. A pulse pressure of 40mmHg was used throughout the testing as an approximation of the physiological norm. The ‘afterload’ was provided by the height of the blood in the reservoir, which was physically moved to manipulate mean pressure.

The piston was lubricated after each hour of use using Fomblin®, a perfluorinated polyether high performance inert lubricant.

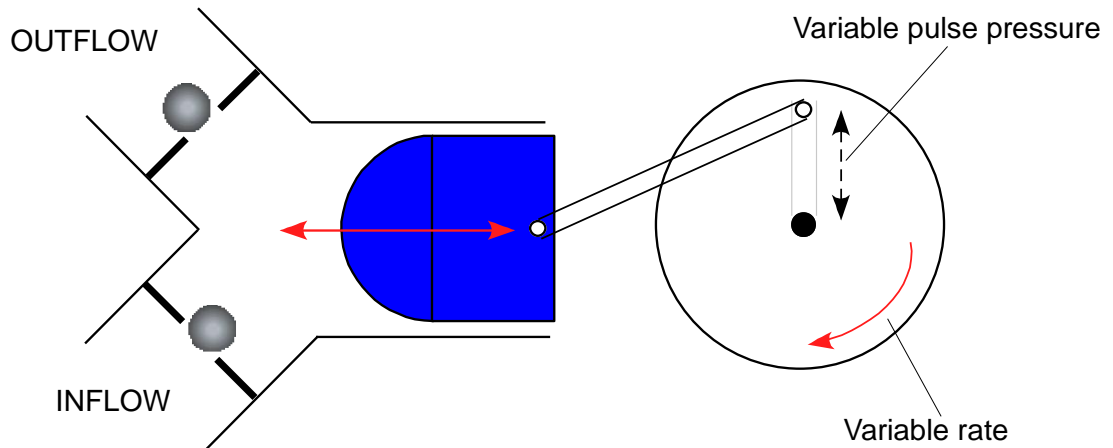


Fig 5.14. Schematic diagram of the biomimetic pulsatile flow generator used in the circuit.

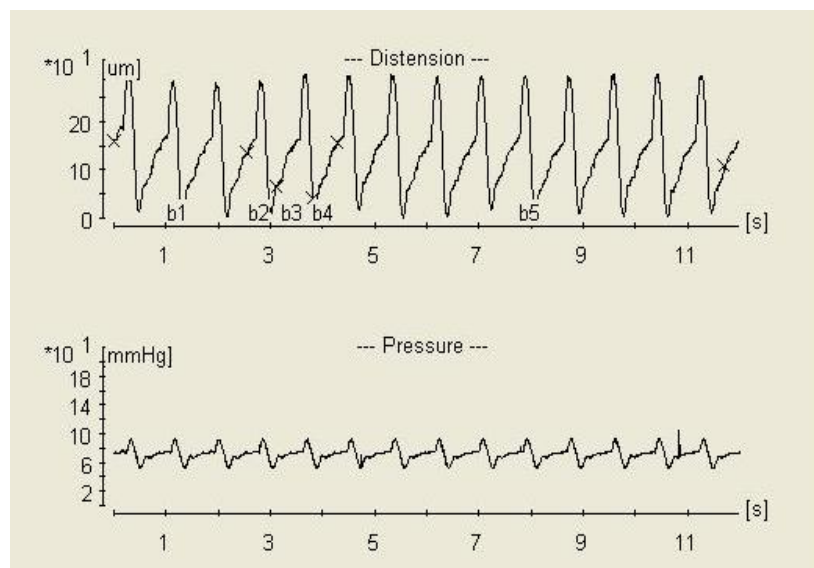


Fig 5.15. Distension and pressure waveforms through the compliant grafts in the biomimetic pulsatile flow circuit used for compliance testing. The waveform data was generated from the wall-tracking duplex and Millar probe placed within the graft respectively.

5.4.2.2.1. Consideration of the biomimetic waveform

As a result of the pump's output and the influence of the tubing, interconnects and graft in the circuit, the pressure waveform as measured by a Millar Probe catheter transducer placed within the graft was not completely representative of the pressure waveform within a human artery – see Fig 15.15.

5.4.2.3 Accessory tubing

All of the tubing used was made from silicone rubber, which although elastic, had negligible distensibility in the physiological pressure range. This was verified by connecting samples of the tubing into the circuit in place of the test sample to show, using the ultrasound probe, that there was no distension up to the maximum systolic pressure used.

5.4.2.4 Ultrasound

A 50mm 7.5MHz linear array probe connected to a Doppler ultrasound machine (Picus, Pye Medical) was aligned longitudinally along the graft with its tip within the waterbath. This position was adjusted to give the sharpest possible B-mode image of the graft wall edge. The sharpest possible image corresponded with visualisation of the wall at its maximum width, indicating its true diameter.

'Linear array' relates to the linear arrangement of piezoelectric crystals along the probe length which vibrate to produce parallel streams of ultrasound waves. This allows a two dimensional image of the graft length to be built up – Fig. 5.16. The B-mode setting is used to show this two dimensional image by converting the reflected ultrasound signal into a signal whose intensity (brightness) is proportional to the energy of the reflected signal received.

The M-mode (motion mode) setting provides a continuous temporaneous ultrasound image for a single piezoelectric reflected signal, which is plotted on a linear time-frame.

A trackerball interface was used to select the exact point along the length of the graft segment at which the wall movement was to be assessed in real time. This point was principally determined by the clearest signal with least reflections. Reflections were also eliminated to a large extent by electronically dampening the reflected signals outside the area bounded by the graft walls. Reflections in the region of the graft wall could be reduced significantly by thoroughly degassing the graft by prolonged emersion in de-ionised water before testing, until the graft no longer floated in water. This required 24 hours, and could be speeded up by immersing in absolute ethanol for 30 minutes instead.

5.4.2.5 Wall Track System

M-mode ultrasound gives a visual representation of wall movements resulting from pulsatile flow. The principle role of the Pie Medical Wall Track System II (WTS) is to provide an automated continuous calculation of anterior and posterior inner wall movement leading to distension data without any user interface. This is particularly important for small calibre grafts as the movements concerned are very small ones, leaving great scope for user error if manually measured from the M-mode image.

The software also eliminates a large proportion of reflections by analysing signal similarity and paradoxical movements. However, this feature is not fool-proof, and every effort was made to minimise reflections. It was also critically important that the ultrasound wave passes through the full diameter of the graft, so as to ensure that the distension is in the plane of the wave so that wall movements were not underestimated – see Fig 5.17. In practice, a non-centred graft resulted in a considerably noisy distension waveform.

Another advantage of the wall track system was that each time distension readings were repeated, the same signal points could be sought out to represent the inner walls. This had two important consequences. Firstly, it reassured that exactly the same points on the wall were being assessed with each measurement, allowing fair comparison. If the measuring point was set manually each time a reading was taken, it was an impossible task to be completely consistent, due to the constant pulsatile movement of the graft wall. The second consequence was that once a crisp ultrasound image was obtained

and the WTS picked out the true wall edge, the investigator could carry out a series of measurements without rechecking the computed edge, provided neither the ultrasound probe nor the point along the graft length used for measurement was moved. For these reasons, manual edge recognition and human judgement were eliminated. Measurements were only pursued if the WTS automatic edge detection concurred with manual positioning. If this was not the case, the reading was rejected, and repeated after addressing the cause. Once a series of measurements was started, no changes were made to probe position, graft position or measuring point. If there was an unforeseen mishap, such as leak from the tied graft end, the whole series of measurements were abandoned and repeated.

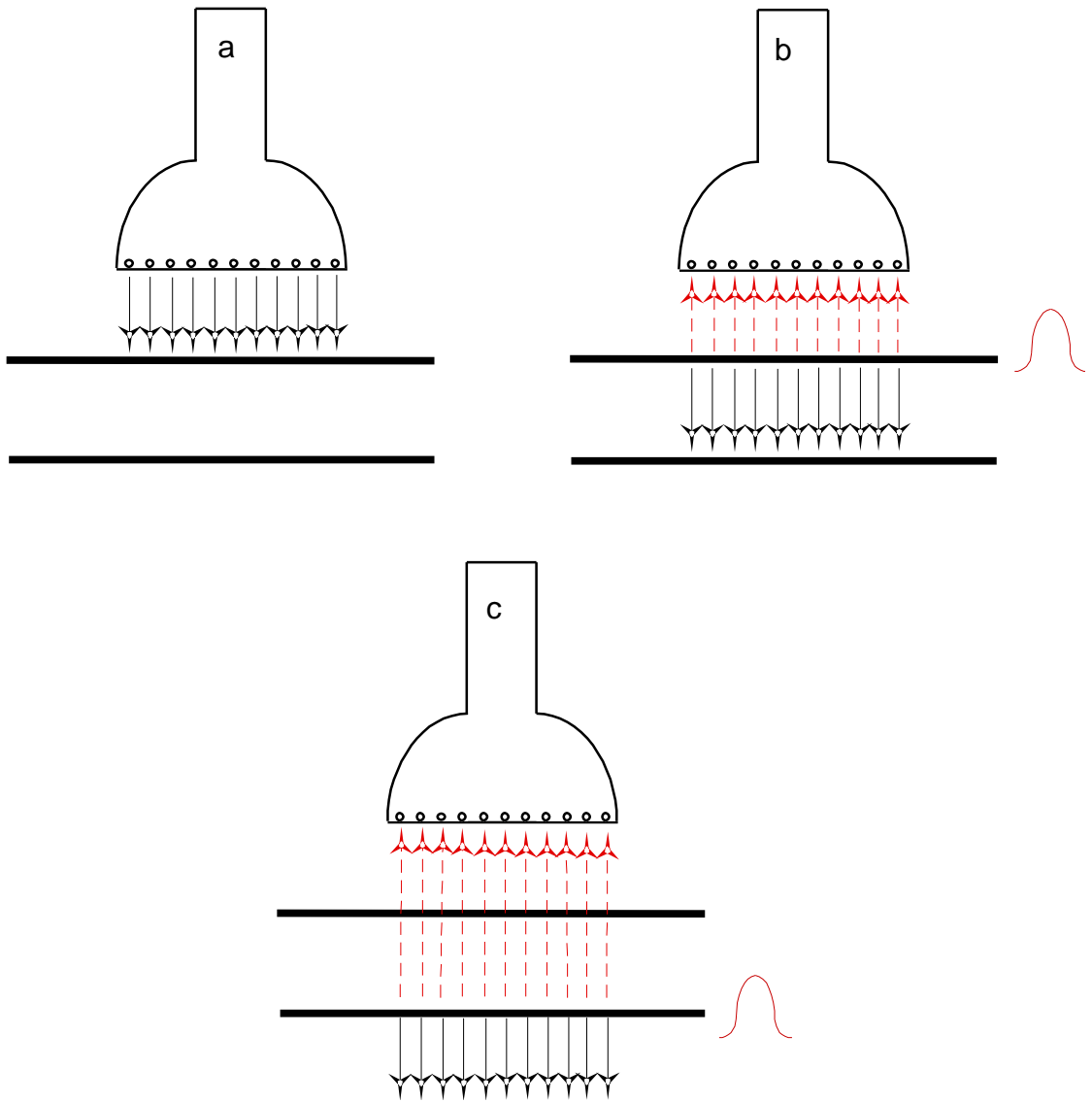


Fig 5.16. A two dimensional image of the graft can be built up by utilising a linear array of piezoelectric crystals emitting parallel waves.

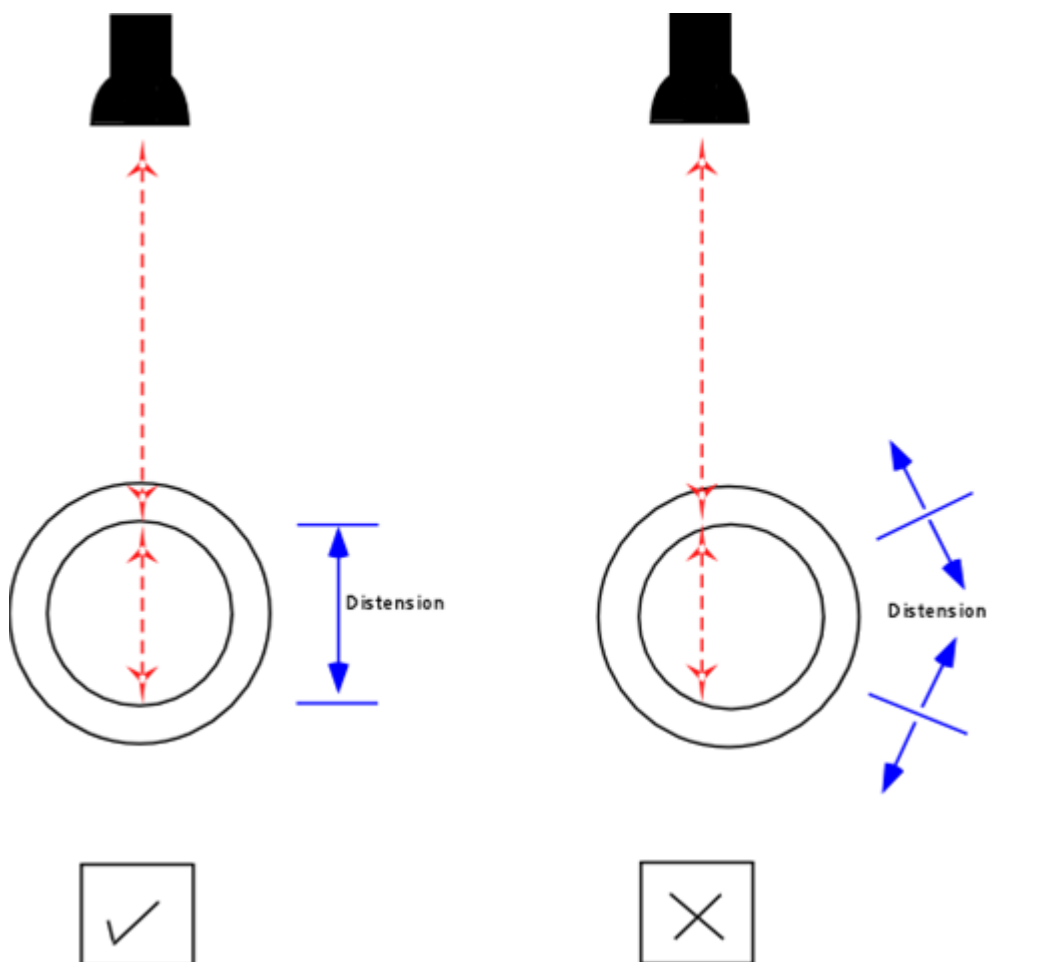


Fig 5.17. By centering the graft precisely under the ultrasound probe, distension will be in the plane of the ultrasonic wave, leading to accuracy of measurement and elimination of a noisy signal.

5.5 Burst Strength Testing / Longitudinal Strain

A high pressure syringe pump (Harvard Apparatus PHD 2000 Programmable) containing freshly de-ionised water (pH 7.0) was connected via a transducer (Honeywell Component No. 22PCCFB6G) to highly compliant non-porous latex tubing lining 8cm lengths of vertically suspended graft (Fig 3) with distal clamping and weighted to ensure 10% longitudinal stretch. The transducer was pre-calibrated by connecting it to a standard clinical sphygmomanometer and a voltmeter to record voltage readings at 0mmHg, 100mmHg and 200mmHg from which offset and gain figures were calculated and entered into a personal computer with bespoke software for recording the pressure at a sample rate of 10Hz. The transducer was connected via a 10v power source to the personal computer. Water was expelled from the pump with the graft unclamped to allow the apparatus to be filled completely, whilst ensuring all air was eliminated from the apparatus. The clamp and weight was applied and the graft was filled till the pressure within it was 0mmHg. Parallel horizontal marks were made with a permanent marker on the anterior wall at the midlength of the graft. 0.2ml/minute infusion rate was used to raise the pressure slowly until the graft failed. A 2 megapixel digital camera (Olympus Camedia) was used to take serial images of the pre-drawn marks at regular pressure intervals.

Image analysis software (Carl Zeiss KS400 Version 3.0) was used to measure the gap between the marks to indicate longitudinal strain as a result of circumferential stress.

6

Extrusion-phase inversion of a small calibre compliant graft.

6.1 Introduction

A multitude of different methods have been utilised to manufacture porous grafts for vascular bypass. These include salt leaching¹³², electrospinning³²², electrospaying with phase-inversion³²³, excimer laser ablation³²⁴, the replamineform method³²⁵, dip-coating and extrusion³²⁶. Each method has its benefits and drawbacks.

6.2 Techniques currently used for polymeric vascular graft construction

Electrospinning can achieve a precisely controlled overall porosity, but is only possible using highly viscous polymers which are able to 'spin' into a flowing fibre from the 'Taylor Cone'. This cone is generated by an electric field applied to a metal capillary through which the polymer extrudes. The electrostatic repulsion effect due to the electric field allows the spun fibre to be whipped and thinned simultaneously to be collected on a surface (See Fig. 6.1). The degree of thinning can thus be accurately controlled. If a low viscosity polymer is subjected to the same electric field, a spray effect is generated as

the electrostatic repulsion forces the droplet to disperse in an aerosol – this is known as electro spraying and is generally used for thin sheet formation with lower mechanical strength than would be required in a potential vascular graft

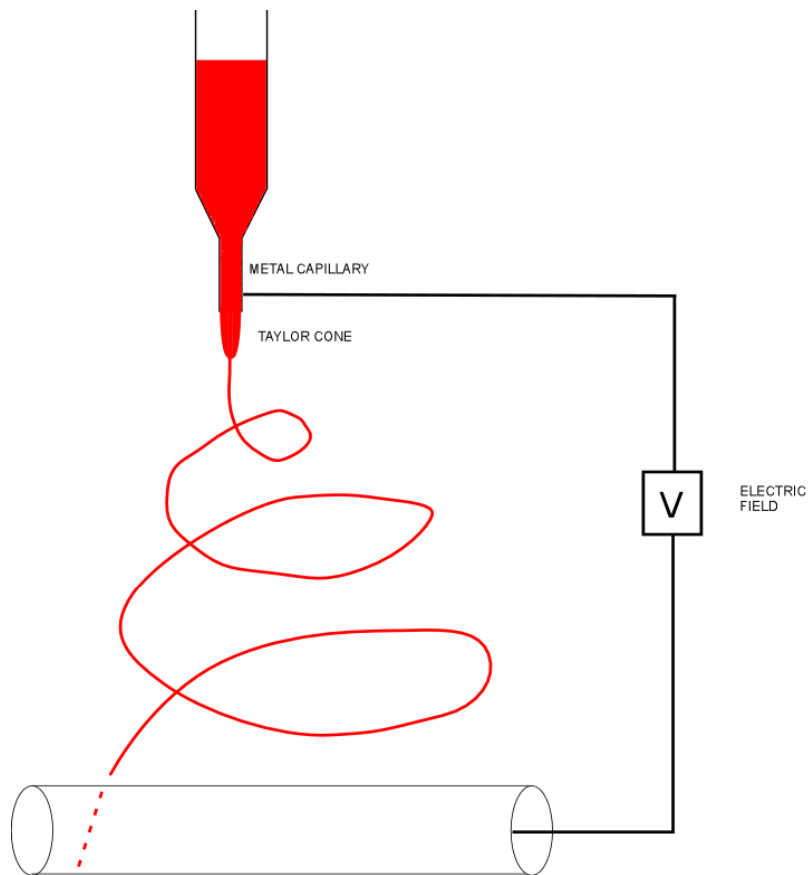


Fig 6.1. Electrospinning as a method of producing a porous graft from a liquid polymer.

Salt leaching methods are usually used as a method of imparting porosity. They entail the formation of a product incorporating a salt in crystalline form which can be ionised in solution and washed out to leave pores where the crystals previously existed. It is commonly combined with polymer casting where the solvent is evaporated from the polymer solution. As the pore size is reflected by the original crystal size, in theory the pore size is controllable. However in practice many problems were encountered when considering this method of imparting porosity to the nanocomposite polymer. Firstly the crystal size required for ideal microporous graft formation was an order of 10 magnitudes smaller than the smallest available salt crystals, requiring mechanical grinding and ultra-fine sieve separation to produce crystals smaller than 100nm in size. In addition, the salt particles need to be uniformly distributed throughout the polymer solution, which was difficult to achieve. Even if this could be managed by thorough mixing with an electric homogeniser, the salt aggregated at the bottom of the polymer if not used immediately. However, immediate use is never possible as agitating the polymer for mixing results in a large number of bubbles which need to be excluded – the fastest way was to apply vacuum suction to the polymer – requiring at least one hour.

Excimer laser ablation is used commonly by ophthalmologists for ablation of the cornea and lens with minimal thermal damage to surrounding tissues. It is the ability to generate defects of extremely precise size that makes it suited to pore formation in cast polymer. However, the formation of pores by such mechanical means will inevitably lead to structural weaknesses at the pore edge which could theoretically be propagated into critical cracks and macroscopic weakness on repetitive stress cycles. Long term fatigue testing results are required to assess the safety of this method.

Porosity is desired as a structural mechanism – to provide graft elasticity³²⁷; to enhance adherence of endothelial cells to the graft lumen; as well as encouraging transmural support for successful cellular integration³²⁸. Neovascularisation through the wall may also have a role in limiting neointimal hyperplasia and atherosclerosis, by preventing hypoxia of cells attached to the lumen³²⁹. However, very high porosity adversely affects handling properties by requiring graft pre-clotting before implantation; increasing thrombogenicity; and causing massive fibrovascular infiltration³³⁰ which soon leads to a loss of compliance.

Dip-coating actually refers very simply to the immersion of a scaffold into polymer in order to coat it. This requires an additional process to solidify the result. This may be by casting (ie. solvent evaporation) or phase inversion by swapping the solvent for a non-solvent. Freehand dip-coating can cause great variability between grafts produced, and for adequate quality control, a mechanised dipping process is necessary. Kannan has produced microvessels from the nanocomposite using a semi-mechanised dip-coating followed by phase inversion³³¹. His work involved dipping mandrels (green needles) via a mechanical arm into polymer solution, then allowing a capillary action to act and distribute a thin coating of polymer uniformly before dropping into a coagulant. This gave good results in terms of wall uniformity and mechanical properties. The technique used for the manufacture of small calibre vascular grafts was essentially a modification of this method which has already been proven using the nanocomposite.

6.3 Extrusion-phase inversion

Strictly speaking, extrusion refers to the pressured drawing of a material (usually a polymer) through a template to form a three dimensional model with a cross section mirroring the template. This requires a highly viscous polymer which will hold its shape after drawing out. The pressure is usually provided by a screw system pump. The technique used here depends on a layer of polymer coating a mandrel as it passes through it, with shape being given by the exit aperture. In this respect, this is extrusion. However, the viscosity of the polymer is much lower than that used in typical extrusion. If phase inversion is not immediately commenced, the polymer will flow off the mandrel.

The concept of phase inversion can be best explained by consideration of the nanocomposite as pure polymer with a variable amount of solvent in which it is dissolved. The lower the amount of solvent, the higher the viscosity (ie. the more solid). Phase inversion relates to the controlled removal of solvent by swapping it for a non-solvent – see Fig 6.2.

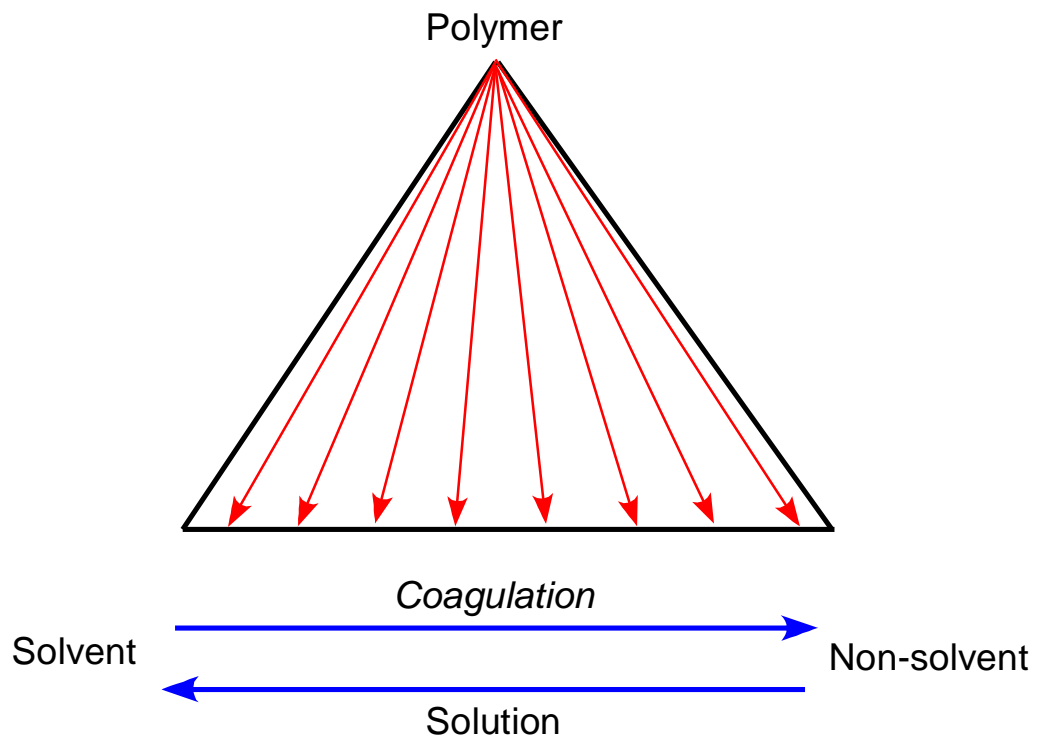


Fig 6.2. The ternary model of phase inversion. The polymer can exist in a solid phase, dissolved phase or any intermediate phase, depending on the amount of solvent present. A non-solvent can exchange with the solvent to control the polymer phase precisely, making the system a combined interaction between three constituents.

The technique of extrusion combined with phase inversion is not novel – it is used in the manufacture of the Chronoflex graft which is commercially available as a vascular access graft, utilising the patented method of Charlesworth³³². However, this is a horizontal extruding system which requires a constant rotational torque during phase inversion to ensure evenness of the graft walls. The idea of using a vertical extruding system relying on gravity for a uniform graft wall thickness lead to the development of a novel bench-top extruding device. However, it had proven impossible to produce uniform lengths of graft with the integrity required for any research use.

My initial aim was to examine the reasons for the failure of this device, correct the problems and achieve tubular conduits with sufficient integrity for subsequent in vitro and in vivo research.

6.3.1 Technique

A mechanical arm driven vertically downwards at 10mm/sec by a motor was positioned such that it held a 5mm diameter stainless steel cylindrical mandrel within the exit aperture of a polymer chamber (Fig 6.3). This latter structure, encased within a perspex block, was also made from stainless steel, comprising of a circular 5mm entry aperture superiorly; a luer-lock syringe compatible polymer introduction channel laterally (Fig 6.4); and a 6mm circular exit aperture inferiorly which could be supplanted by a 5.5mm aperture adapter (Fig 6.5). The perspex block was held in a bracket to allow the descending mandrel to pass through the entry and exit apertures.

With the mandrel's base centrally placed and level with the exit aperture (Fig 6.6), nanocomposite was injected slowly into the polymer chamber. For this step it was imperative that the syringe contained no air bubbles. The syringe was allowed to settle for 15 minutes after drawing up polymer to ensure that any air bubbles which were present could rise to the nanocomposite's surface and be excluded.

A vertical column of coagulant solution was placed directly below the exit aperture leaving a 5mm gap between the two. The cover was opened and the mandrel driven downwards vertically into the coagulant at 10mm/sec

immediately afterwards (Fig 6.7). A pressure switch on the mechanical arm ensured it stopped descending when it reached the polymer chamber. The alignment was checked during this extrusion by visually comparing the layers of nanocomposite coating either side of the mandrel within the coagulant solution in the moments before coagulation occurred. This was undertaken in two planes perpendicular to each other about the longitudinal axis of the mandrel, and was facilitated by viewing against a natural light background.

The column was undisturbed for 20 minutes after which time the mandrel was disconnected from the mechanical arm and placed en-bloc bathed within the coagulant solution in the fridge at 5 °C for a minimum of 12 hours. Thereafter, the mandrel was removed from the coagulant and dried with paper towels, before transferring to an absolute ethanol bath for degassing over 10 minutes, thereby facilitating removal of the formed tube from the mandrel. This latter step was carried out by gently loosening the conduit from the rod along its whole length with small circular and longitudinal stresses after which the whole tube easily slid off without excessive strain.

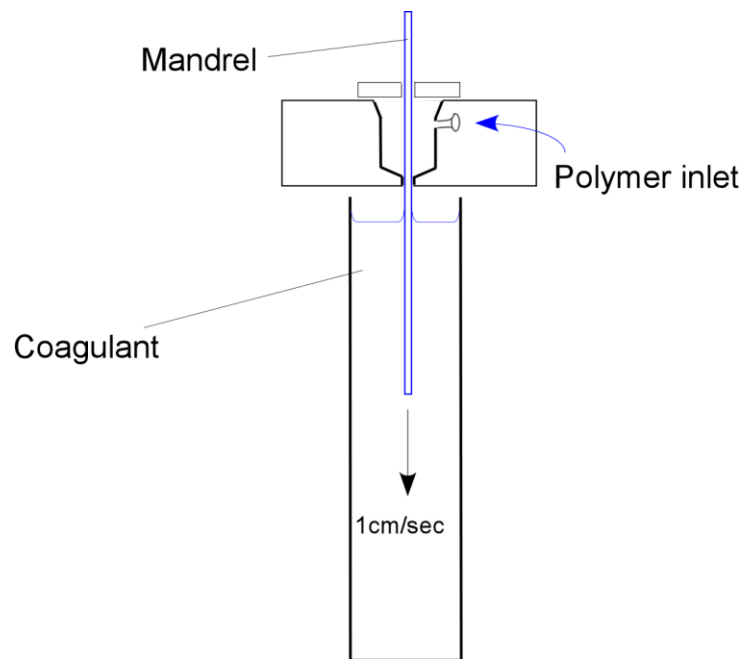


Fig 6.3. The bench-top extrusion-phase inverter device.

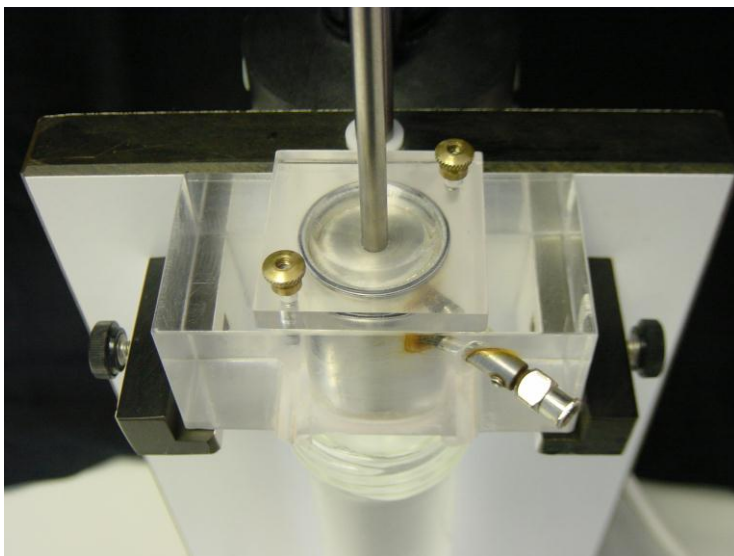


Fig 6.4. The polymer chamber, showing the entry aperture through which the mandrel fits snugly. The polymer inlet can be seen on the right side of the perspex block.

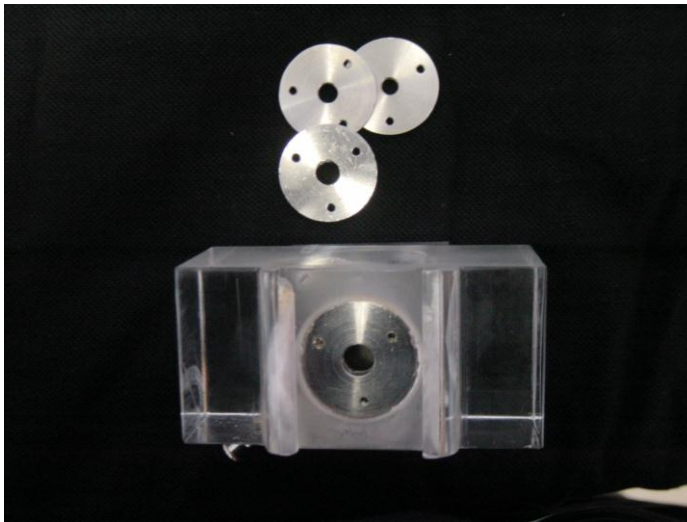


Fig 6.5. The undersurface of the polymer chamber showing the exit aperture along with three adaptors for varying the aperture size.

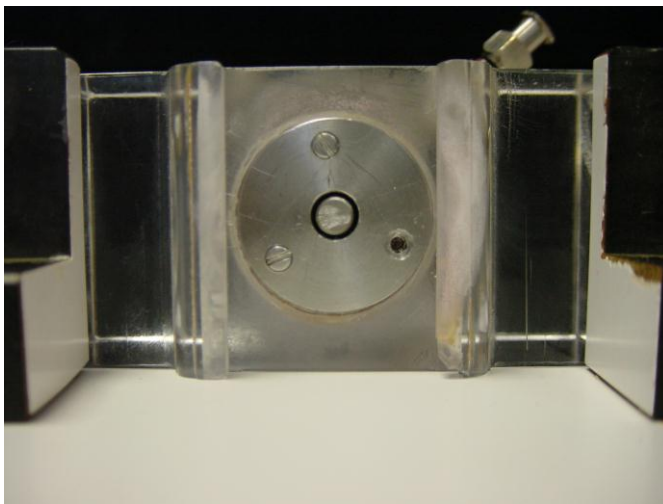


Fig 6.6. The mandrel is positioned such that there is an equal gap around it in all directions. Its lower level is flush with the lower border of the exit aperture.

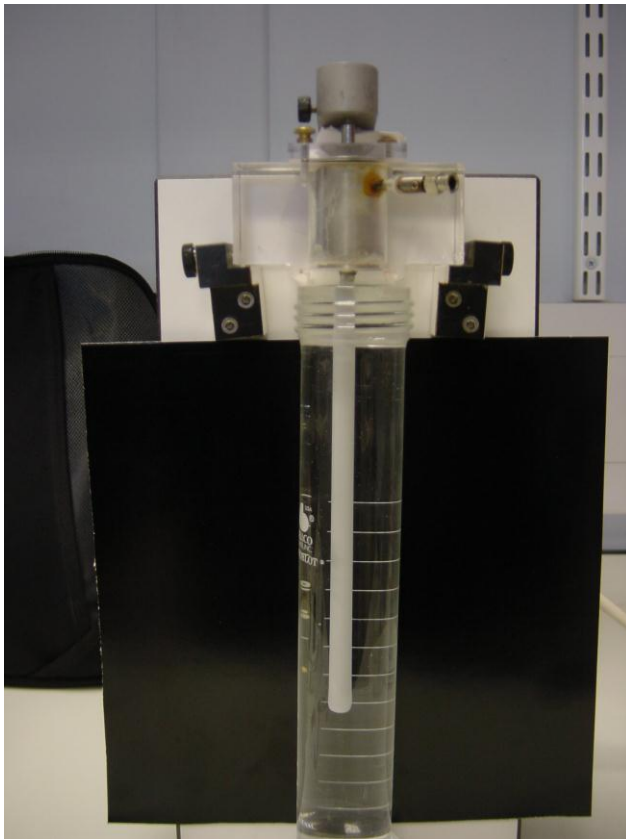


Fig 6.7. The mechanical arm has lowered the mandrel through the polymer chamber, in so doing coating it with the nanocomposite. The exit aperture controls the thickness of this coating which further descends into the coagulant solution, causing phase inversion.

To assess for ideal extrusion conditions, the process was repeated for different concentrations of DMAC and ethanol in distilled water and coagulant temperature range from 0 to 50 °C, using scanning electron microscopy to visualise the detail of the wall cross section and pores.

6.3.2 Troubleshooting

It was apparent that the greatest control of wall thickness was achieved when the mandrel was used to drive the polymer through the exit aperture, as opposed to the polymer running down the mandrel wall. This required high enough viscosity to prevent the polymer from spontaneously dripping out from the exit aperture when the mandrel was in place. This always occurred from the right side of the exit aperture, which was near the polymer entry port. Therefore the polymer was leaking out even before the polymer chamber could be filled. In order to exploit the effect of gravity to form a uniform wall, it is necessary to have an equal weight of nanocomposite in the polymer chamber surrounding the mandrel. These concepts are illustrated in fig 6.8.

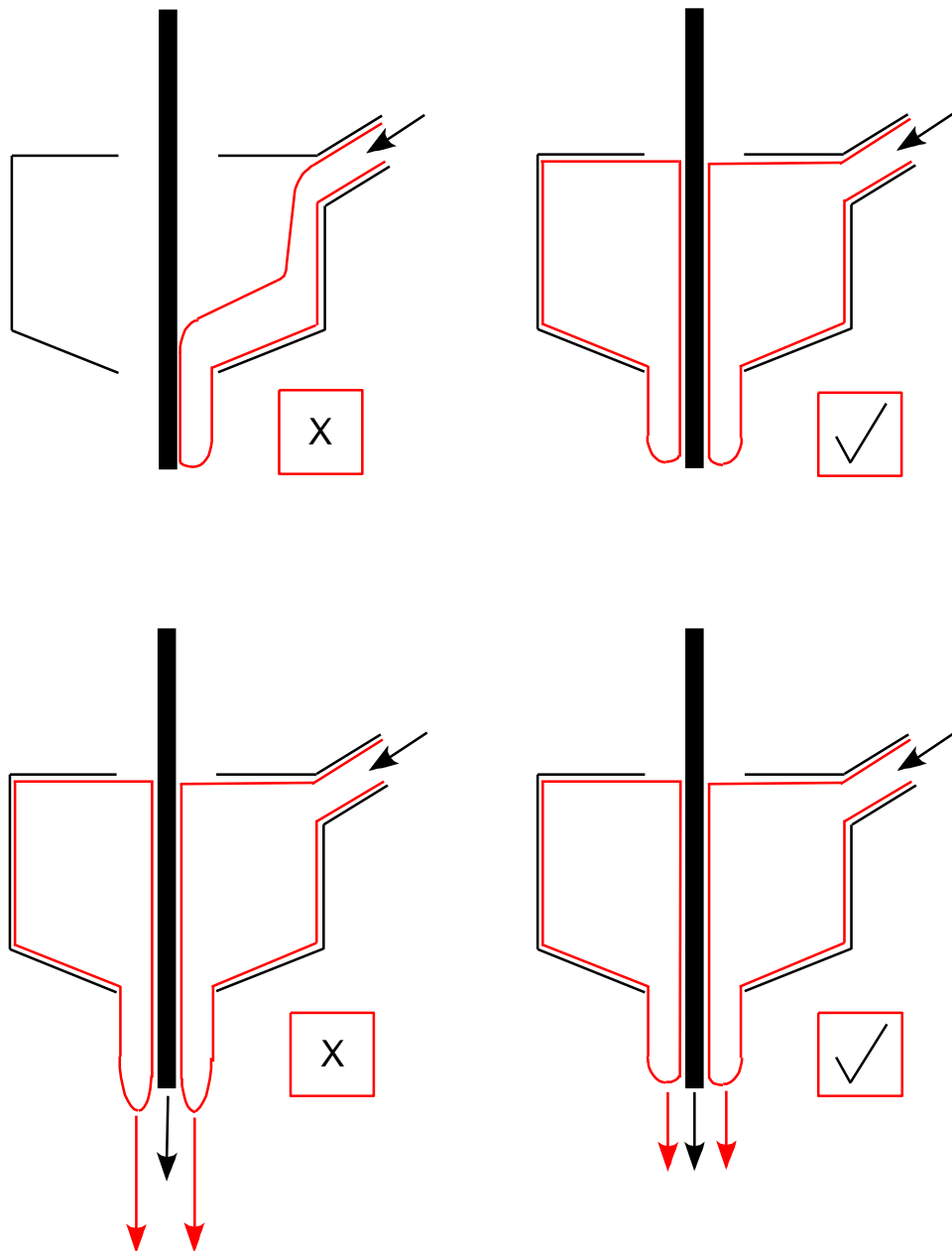


Fig 6.8. The polymer must not be so viscous that it starts to pour past the mandrel before the polymer chamber has had a chance to fill up (above). It must also be driven down by the mandrel into the coagulant rather than slide down the mandrel (below).

6.3.3 Rheological consideration

Clearly the flow characteristics of the polymer used was paramount. Furthermore, the flow of different batches of polymer would need to be identical to ensure identical product dimensions and to proffer a fair comparison between different polymers. Therefore rheological testing of the polymer solutions was undertaken.

6.3.3.1 Inter-batch variability

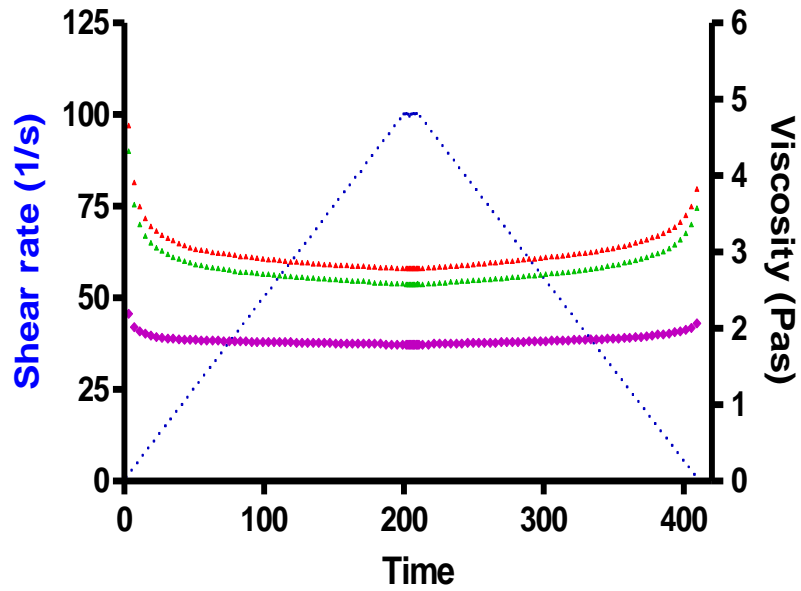
In theory, different batches of polymer synthesised using the same protocol would be identical to each other. However, this assumes several things. Firstly it assumes that the raw materials obtained from the suppliers are identical each time. It assumes that there is no transformation of the raw materials due to suboptimal storage. It also depends on there being no change in the flow properties of the polymer on storage. These natural assumptions make it important to investigate different batches of “the same polymer”.

Rheological testing of the polymer was undertaken using a Bohlin CVO Rheometer (Malvern Instruments, Malvern, United Kingdom), a typical cone and plate tester – see Fig. 6.9.



Fig 6.9. Bohlin CVO Rheometer – 4° cone and plate type, with full rheological testing capabilities including temperature adjustment using a Peltier plate system.

Shear rate-dependent viscosity of the three batches



- shear rate
- Viscosity batch 1
- Viscosity batch 2
- Viscosity batch 3

Fig 6.10. The viscosity of the three batches of nanocomposite when measured using an up-down shear rate ramp

Three batches of the nanocomposite were tested. One batch which was five months old, as well as two batches made on consecutive days, using the same raw materials.

The test performed was a simple one. The rotation of the cone was programmed to exert a gradually increasing shear rate from 0 to 100 s^{-1} via a shear ramp and then back down to 0. The behaviour of the fluid under these conditions of shear are of interest, and one way of quantifying this is to use the rheometer to measure the shear stress on the fluid as a result of this applied shear rate. Viscosity is defined by the ratio of shear stress: shear rate (analogous to elastic modulus = stress:strain) and is an appropriate measure of flow behaviour.

The first observation was that for the majority of the test, the fluid behaviour appeared Newtonian – the relationship between shear stress and shear rate was constant ie. the viscosity was the same, whatever the level of stress applied to the polymer – see Fig 5.12. However, at the very lowest shear rates, the viscosity appeared to creep up significantly. This may be artifactual with frictional forces such as air resistance acting on the rotating cone coming into prominence at the lowest shear rates. A Newtonian behaviour would be expected in a homogenous solution like the dissolved nanocomposite.

Figure 6.10 shows that batch 3 had considerably lower viscosity than either batch 1 or 2 which has serious implications for quality control of the product, since identical procedures were followed during synthesis. This may be because of the difference in reagents used, or due to the prolonged storage of batch 3. To investigate the effect of storage, batch 1 was retested using identical parameters after four months – Fig 6.11.

The effect of storage of batch 1 on viscosity

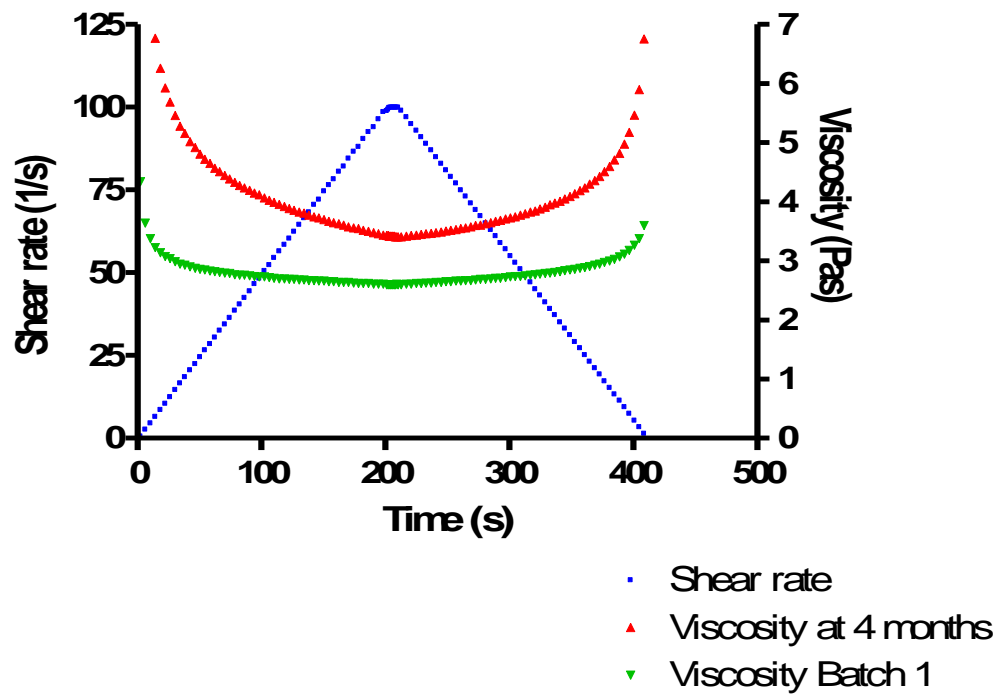


Fig 6.11. The increase in viscosity seen after storage of nanocomposite (batch 1) for four months.

These results show that after storage, there was in fact an increase in viscosity, rather than the reduction which we would expect if storage was the cause of the difference between the three batches. Therefore, the differences seen were more likely to be due to small variations in the original raw materials used, if one assumes the manufacturing process was completely standardised. Despite an airtight container, an increase in viscosity may be due to evaporation of DMAC from the polymer solution into the air-space within the bottle. An equilibrium within the airspace is not maintained due to the repeated opening of the container each time a sample of nanocomposite was required. A second observation was that there was a non-Newtonian aspect to the polymer's behaviour after prolonged storage – the viscosity was no longer constant through the range of shear rates and there was a definite reduction in viscosity at high shear rates. Due to these results, it was decided that every batch made would have a baseline viscometric test and used to make conduits within two weeks of synthesis. Viscosity of 3 PaS was achieved for each batch produced. This was accepted as the standard as at this viscosity, no polymer flowed out of the polymer chamber when the 5mm mandrel was in place for ten seconds which was enough time for the polymer chamber to become uniformly filled with polymer. Modified polymers were synthesised to the same viscous profile by manipulating the amount of DMAC used to dissolve them.

As well as using solvent to standardise the viscosity of the polymer solution and so prevent it from leaking from the exit aperture, the perspex block was redesigned to incorporate an exit aperture cover which was a simple PTFE sliding cover running in a groove under the block – Fig 6.12 and 6.13.

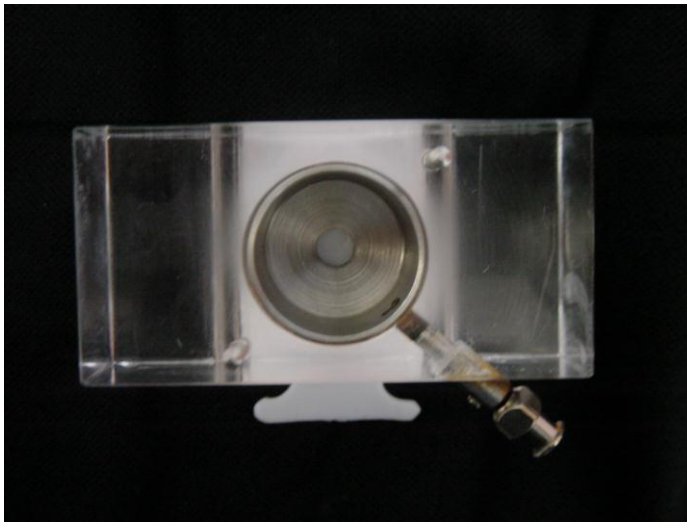


Fig 6.12. Exit aperture cover closed.

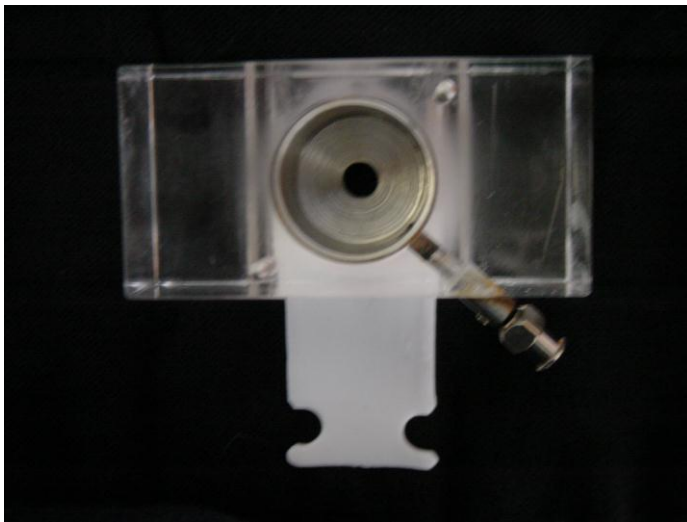


Fig 6.13. Exit aperture open.

The amount injected was important as too little gave a very short thin graft. Too much was wasteful as it resulted in a large globule of polymer at the dependent end of the mandrel. To determine the optimum amount of polymer, a graft was produced using a range of polymer amounts. The uniformity of the wall was assessed by image analysis (Carl Zeiss KS 400 version 3.0), and variability >10% from the mean was rejected. The length of uniform-walled graft was recorded along with the mean wall thickness along the usable length. The results are summarized in table 6.1. The balance between incomplete coverage of the mandrel and excessive polymer wastage was found when using 3.5ml polymer per graft.

Amount of polymer (ml)	Usable length (mm)	Mean wall thickness (mm)	Notes
2.0	11	0.42	Incomplete coverage of mandrel
2.5	18	0.50	Incomplete coverage of mandrel
3.0	69	0.54	No excess polymer after coating
3.5	86	0.54	Small excess after coating
4.0	64	0.59	Large excess globule
4.5	65	0.60	Large excess globule

Table 6.1. The effect of amount of nanocomposite injected on the uniform usable length of conduit produced.

6.3.4 Reproducibility of graft manufacture

Using distilled water at 0 °C as the coagulant, 5 conduits were extruded with a 5.5mm exit aperture and a further 6 with a 6mm aperture. Extrusions were consecutive with no selection of 'best specimens'. The image analysis software was used to measure the uniformity of wall thickness at 72 points distributed equally around the circumference, so assessing the reproducibility of the extrusion process. The results are summarised in Table 6.2, fig 6.14 and 6.15.

	Mean wall thickness(mm)	Minimum (mm)	Maximum (mm)	Standard Deviation	Coefficient of variation
Thin 1	0.33	0.25	0.44	0.05	0.15
Thin 2	0.34	0.27	0.4	0.026	0.08
Thin 3	0.34	0.2	0.43	0.057	0.17
Thin 4	0.34	0.22	0.42	0.046	0.14
Thin 5	0.32	0.23	0.4	0.04	0.12

	Mean wall thickness(mm)	Minimum (mm)	Maximum (mm)	Standard Deviation	Coefficient of variation
Thick 1	0.48	0.38	0.6	0.067	0.14
Thick 2	0.52	0.37	0.72	0.107	0.21
Thick 3	0.52	0.48	0.59	0.030	0.06
Thick 4	0.5	0.37	0.61	0.063	0.13
Thick 5	0.51	0.43	0.62	0.048	0.09

Table 6.2. The variation of wall thickness for each graft based on image analysis at 72 equally spaced points around the circumference

Thickness of thin walled grafts (with standard deviation)

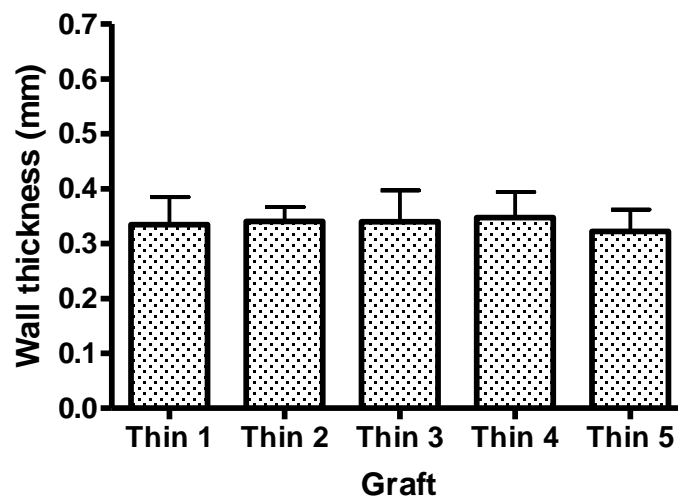


Fig 6.14. The intra and inter-graft variation in wall thickness for the thin-walled grafts.

Thickness of thick-walled grafts (with standard deviation)

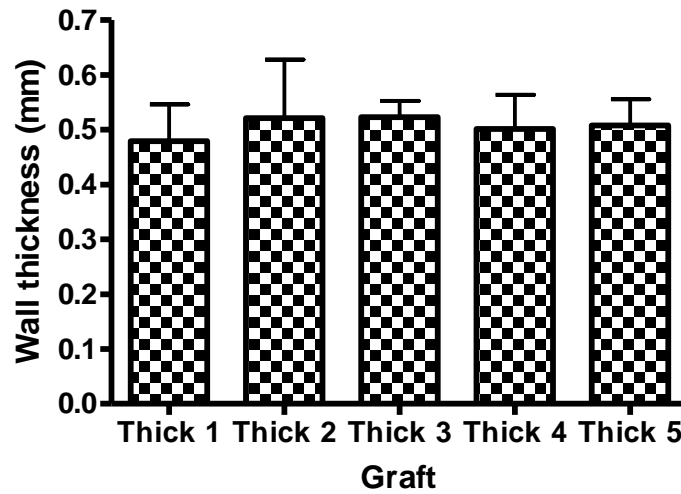


Fig 6.15. The intra and inter-graft variation in wall thickness for the thick-walled grafts.

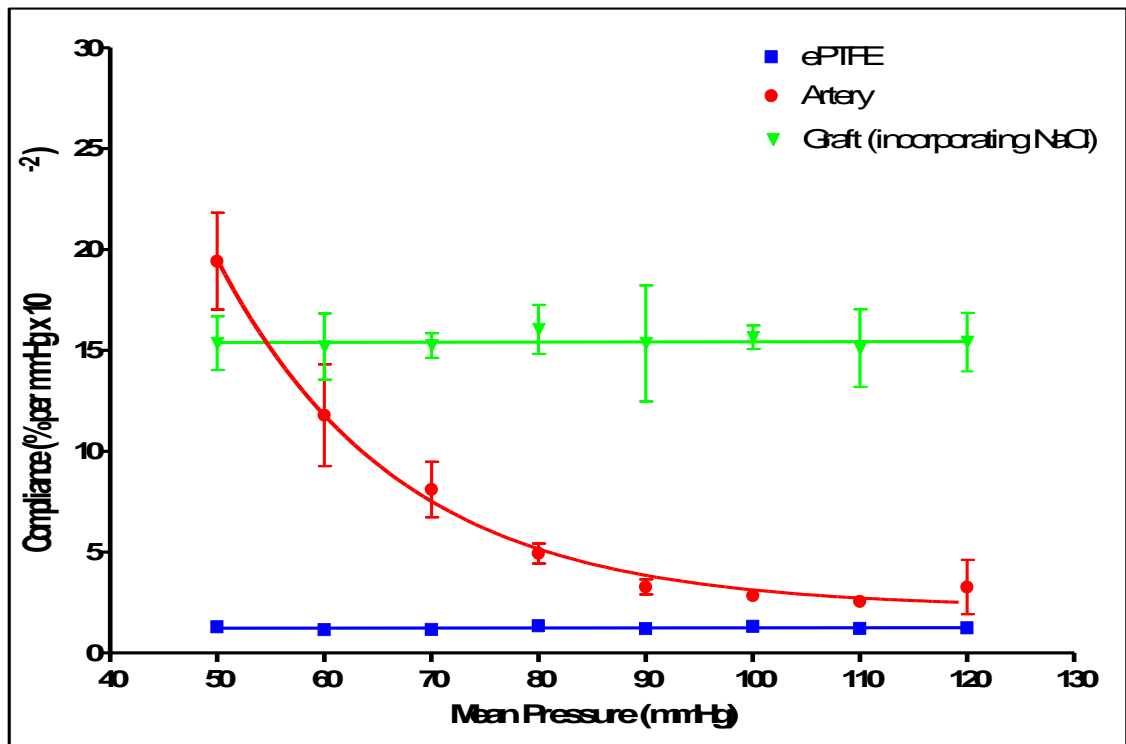


Fig 6.16. The compliance of grafts manufactured from PCUPOSS using 5% $\text{Na}(\text{HCO}_3)_2$ filler and surfactant (n=6). Compliance characteristics of human external iliac artery (n=6) and PTFE (n=1) were measured by Mr Mike Mikhael and Mr William Khor and have been included with permission for comparison.

6.4 PCUPOSS incorporating porosifier and surfactant.

Initial attempts to produce a graft were utilising the PCUPOSS with 5% finely ground sodium bicarbonate ($\text{Na}(\text{HCO}_3)_2$) thoroughly mixed in along with Tween 20 surfactant. The coagulant used was water at 50°C. The reason for this was to impart uniform porosity through the wall of the resultant phase inverted graft. The $\text{Na}(\text{HCO}_3)_2$ would not dissolve in the polymer solution as DMAC is not a solvent for it. Instead, $\text{Na}(\text{HCO}_3)_2$ crystals would float in the polymer and during phase inversion, the water would cause them to dissolve, leaving pores in the space they previously occupied. The surfactant would aid the penetration of water through the polymer. This is therefore a salt leaching technique which is being used to impart porosity. The Chronoflex prosthesis used a similar technique of using a water soluble porosifier and a surfactant to impart porosity throughout the graft. The sodium chloride grinding was achieved using a standard mortar and pestle until a finely ground powder resulted. The resultant graft was highly porous. As a result, its compliance was found to be extremely high, averaging $15.4\%/\text{mmHg} \times 10^{-2}$ – Fig. 6.16.

Physiological flow in a healthy human achieves a typical mean pressure of 80 to 100mmHg with a pulse pressure of 40mmHg, suggesting that matching arterial compliance would require a value nearer $3\text{-}5\%/\text{mmHg} \times 10^{-2}$. Therefore the compliance of this graft was unnecessarily high. This would cause excessive dilatation of the graft during pulsatile flow with consequences on both blood flow profile as well as wall stress. Firstly, the flow of blood from the artery into the relatively dilated graft would cause a calibre mismatch, concentrating stress at the proximal anastomosis as explained in Chapter 2, as well as flow separation, abnormally low wall shear stress as well as pooling and stasis of blood. This would be similar to the behaviour of flow experienced at the distal anastomosis between artery and PTFE graft, as would be expected to lead to the same pattern of intimal hyperplasia as the heel and toe of an end-to-side anastomosis. Secondly, the high degree of distension during each cycle of pulsatile flow would make the graft susceptible to fatigue, due to the repeated rapidly changing stresses.

This graft had several other major problems. It required pre-clotting with blood due to the high porosity. This is a time consuming and messy affair during bypass surgery. The idea of promoting clot formation on the lumen of a graft

designed to be anti-thrombogenic is somewhat perverse. Drying the specimens in an oven at 60°C caused them to rapidly shrivel. Air drying also led to corrugation and reduction of internal diameter. This could be due to the collapse of pores with weak inter-porous walls. This theory suggests that the inter-porous walls were so weak that it was the surface tension of the water lining the pores which kept the pores from collapsing. Although the burst pressure of the graft was not tested formally, it was clear during the compliance testing that the grafts were bursting at mean pressures of only 140mmHg. This is within the physiological range for many hypertensive patients. In summary, a less porous structure was required.

6.5 PCUPOSS grafts

To test the theory that the problems with the porosifier/surfactant-incorporated PCUPOSS were due to the high porosity of the grafts, it was decided to manufacture grafts from PCUPOSS without any porosifier.

All the grafts produced were 18cm in length with a minimum of 10cm useable length with uniform wall thickness. The 6mm aperture adaptor was used to ensure thick-walled prostheses. The coagulant solution was deionised water at 50 °C. Surprisingly, these grafts also shrivelled on drying. If the assumption that phase inversion without the aid of a porosifier would lead to a graft with low porosity was correct, this would mean that the grafts instability in air was not due to pore collapse. To investigate the cause of this instability, scanning electron microscopy (SEM) was undertaken for PCUPOSS grafts made with and without porosifier. This required sequential dehydration of the grafts using graded solutions of ethanol, causing them to shrivel. Despite the shrivelling, it was apparent from the SEM images that the grafts were highly porous even without porosifier – Fig 6.22.

This finding led to the hypothesis that pore size and distribution was a result of the precise dynamics of exchange between solvent and coagulant. It would follow that affecting these dynamics would influence the pores. One way of doing this would be to modify the coagulant solution.

6.6 The effect of coagulant temperature on porosity

Coagulant temperature may have a bearing on the rate of exchange of solvent and coagulant. Therefore the extrusion-phase inversion process was repeated for temperatures between 0 and 50 °C. The results were all dehydrated with serial ethanol solutions in order to prepare them for SEM– see Fig. 6.17-6.22. Grafts extruded into warm coagulant solutions were susceptible to shrivelling on dessication. Only conduits formed in coagulant at 0 °C showed no distortion after storing in dry conditions. This allowed unimpeded visualisation of the pore structure. The wall was composed of four distinct layers – Fig 6.23 – comprising from lumen outwards: a lumen skin with small pores – Fig 6.24; large interconnecting pores in high density forming the majority of the cross section; small pores in high density near the outer edge; a non-porous outer skin with microscopic ridges throughout – Fig 6.25.

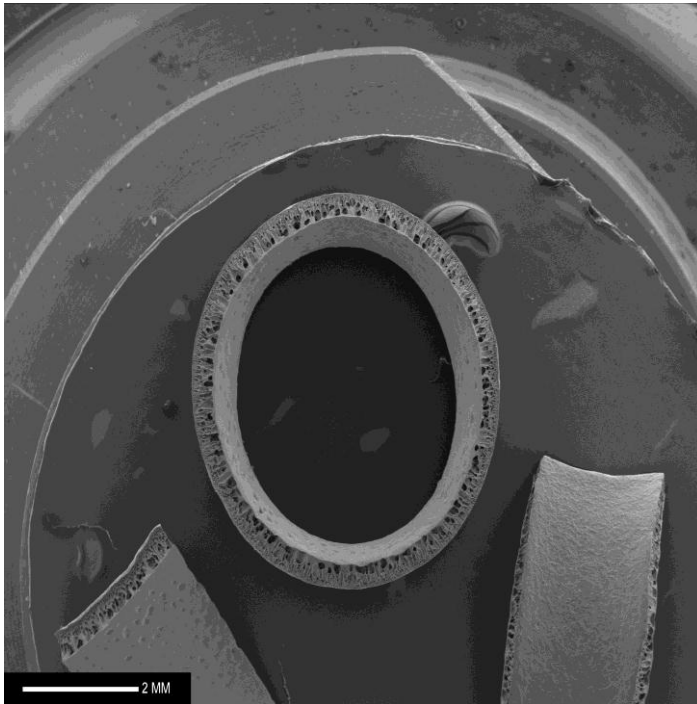


Fig 6.17: Coagulant is deionised water at 0°C (scale bar 2mm)

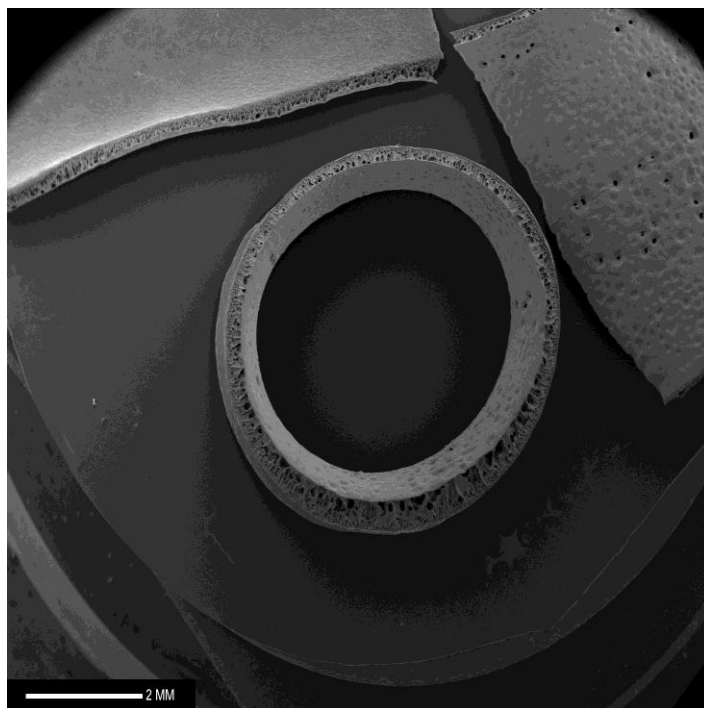


Fig 6.18: Coagulant is deionised water at 10°C (scale bar 2mm)

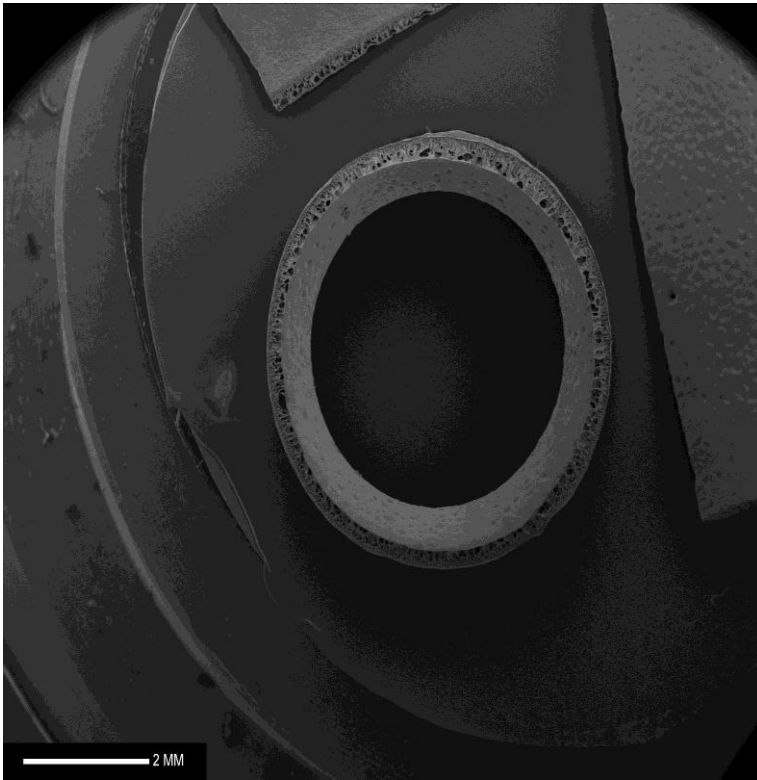


Fig 6.19: Coagulant is deionised water at 20⁰C (scale bar 2mm)

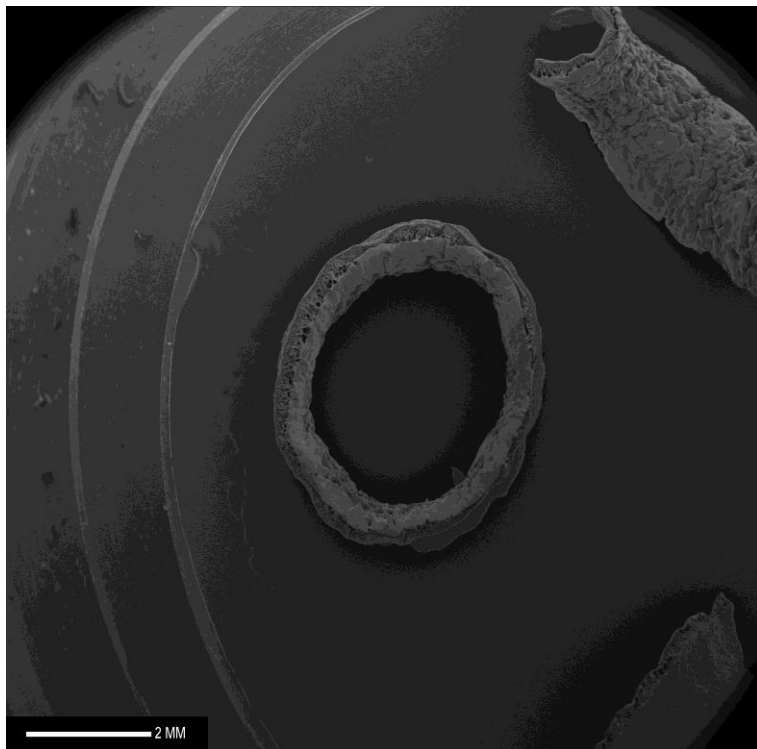


Fig 6.20: Coagulant is deionised water at 30⁰C (scale bar 2mm)

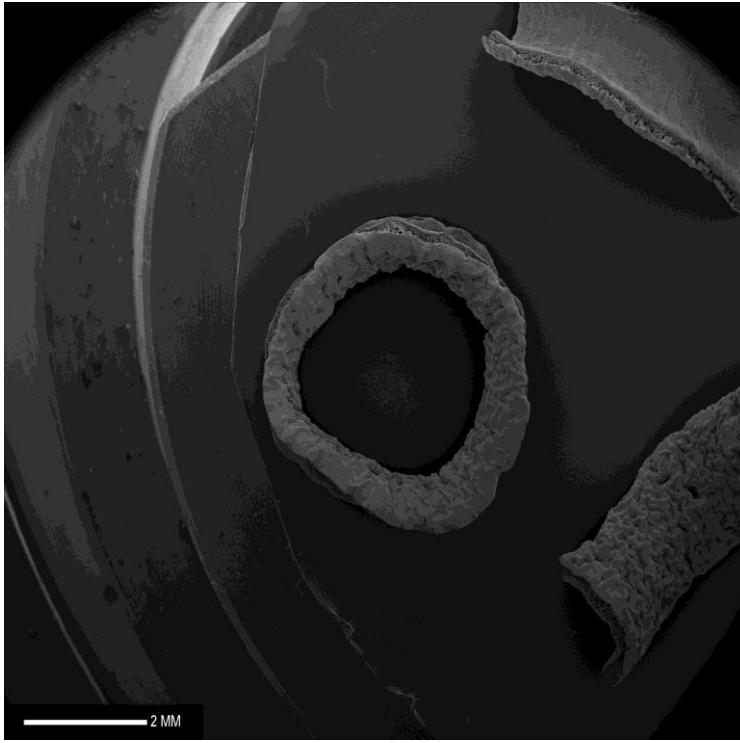


Fig 6.21: Coagulant is deionised water at 40°C (scale bar 2mm)

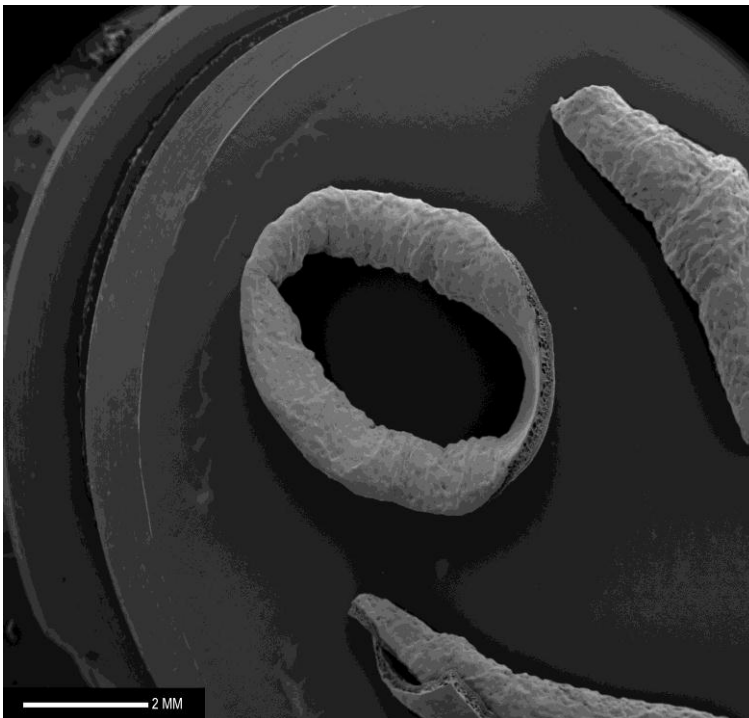


Fig 6.22: Coagulant is deionised water at 50°C (scale bar 2mm)

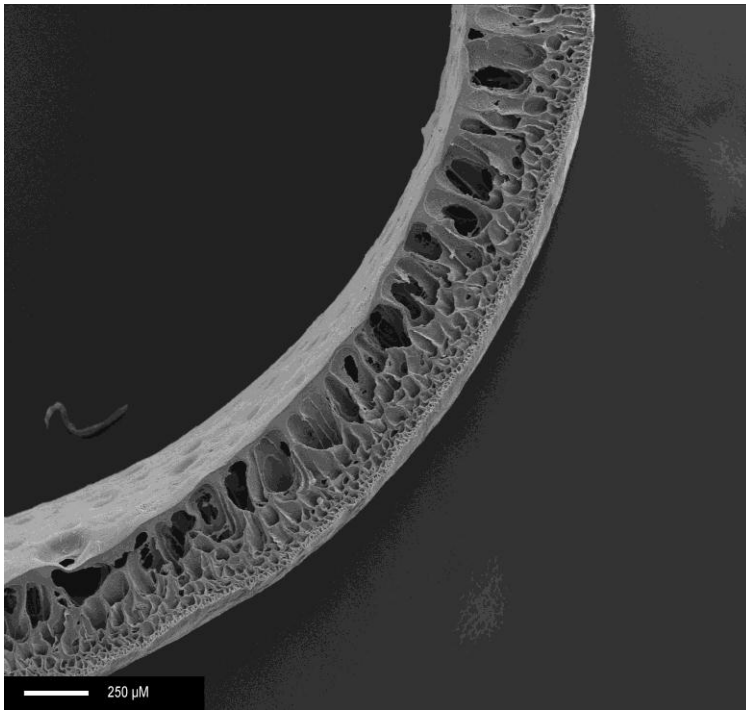


Fig 6.23: Four-layered structure of the graft wall (scale bar 250microns)

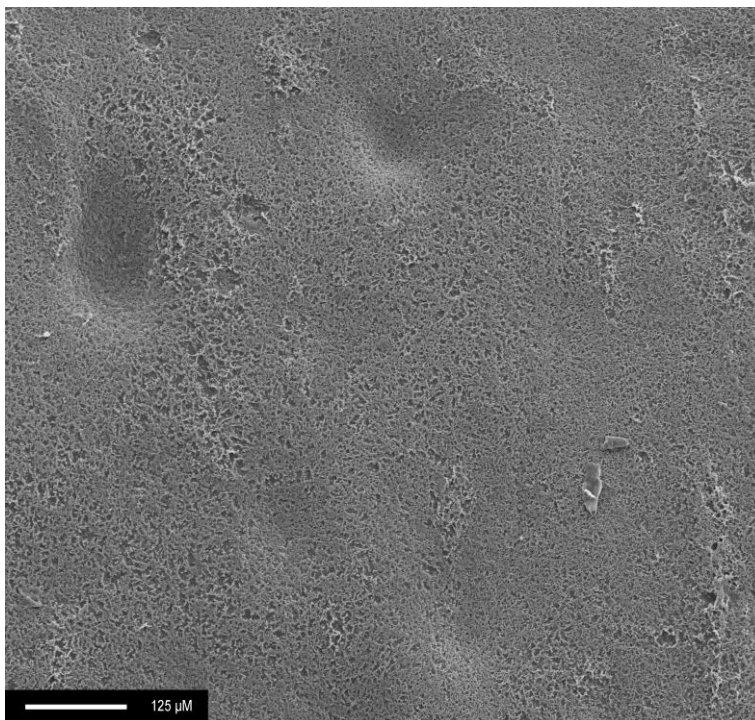


Fig 6.24: Lumen of graft (scale bar 125 microns)

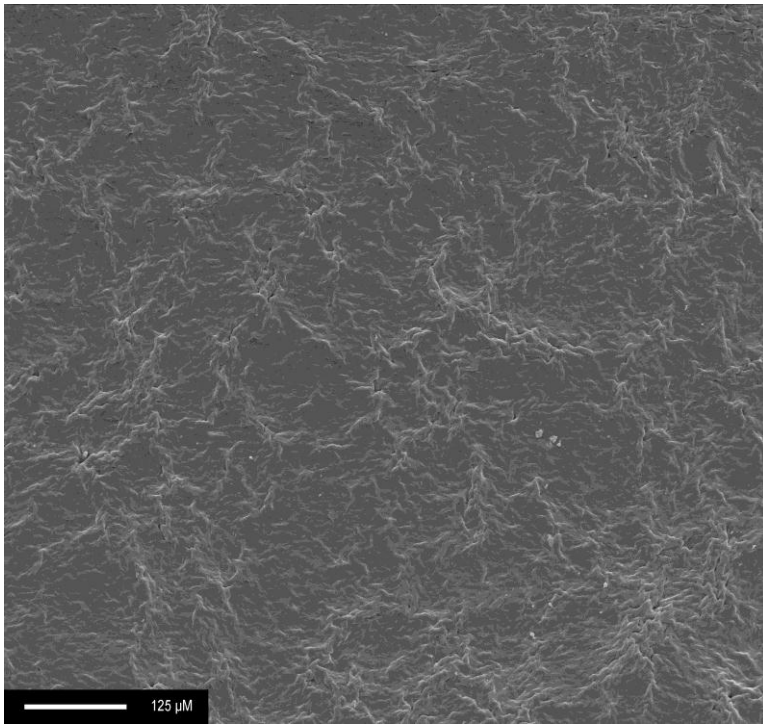


Fig 6.25: Outer skin of graft demonstrating microscopic ridges throughout the surface (scale bar 125microns)

However, an alternative explanation to optimisation of exchange dynamics exists for the relative resistance to shrivelling of grafts coagulated at higher temperature. This was initially realised by accident when a graft was extruded using a mandrel which had been pre-heated in an oven at 100 °C. The polymer was seen to slip rapidly down the mandrel faster than the mandrels descent into the coagulant. It was clear that the high temperature resulted in a reduction in the nanocomposite's viscosity. Therefore, it is possible that the graft stability seen at low temperature coagulation is simply due to an effective reduction on the polymers viscosity which in turn results in a thinner graft. To investigate the effect of temperature on the nanocomposite further, further rheological tests were performed using a peltier plate to heat the polymer while continuously measuring viscosity. The results are shown in fig. 6.26.

This confirmed the exponential reduction in viscosity with increasing temperature. Image analysis was used to measure the wall thickness of grafts phase inverted at the different temperatures. As the pore size and distribution could not be analysed directly by SEM, alternative methods were required.

Direct visual analysis was attempted by close-image photography of the cross section of the grafts. However, the resolution of this method was not good enough to uncover small changes in porosity – Fig 6.27. Therefore an indirect method of assessing overall porosity was sought. Graft density is a good indicator of the amount of nanocomposite in the conduit. Therefore it has an inverse relationship with overall porosity. However, density (mass per unit volume) requires an accurate measurement of graft volume. This presents great difficulties in itself. Measuring the dimensions of the graft requires very precise cross sectional thickness measurement throughout the length of the graft. This is possible using image analysis for individual cross sections, but in order to factor in the slight wall thickness changes through the length of the graft, the graft would require cross sectional measurements at many points along its length. The alternative method for measuring volume is using a volume displacement technique in a fluid. However, immersion in water will not give an accurate volume due to the displacement of air within the pores which would occur on immersion. This would lead to an under-estimate of volume. To simplify the problem, it was decided to use unit weight as a measure of amount of nanocomposite and hence inverse relation with porosity. This is an industrially accepted standard for the quantification of porosity of irregularly

porous foam structures. The graft can also be considered to be a foam due to its open pore structure. Therefore, the weight of 1cm length of graft was measured for each coagulant temperature, using bench-top electronic scales.

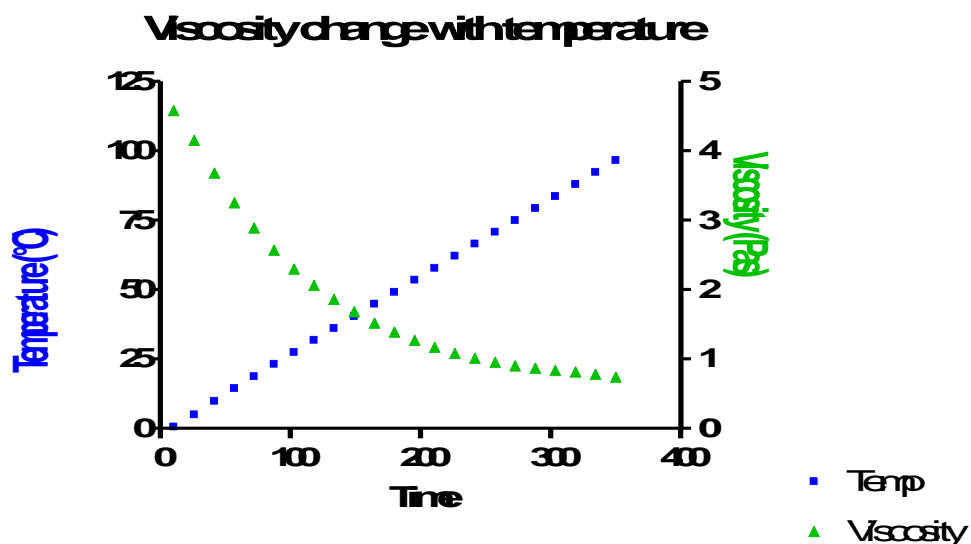


Fig 6.26. The temperature dependence of viscosity for the three nanocomposite batches.

0°C	30°C	50°C
0.034	0.031	0.022
0.034	0.033	0.028
0.035	0.030	0.024
0.034	0.031	0.024
0.034	0.029	0.021
Mean 0.034 grams	Mean 0.031 grams	Mean 0.024 grams

Table 6.3. The actual and mean weight (grams) of 1cm lengths of graft extruded into water coagulant at different temperatures. Lighter grafts resulted from higher temperature coagulation suggesting greater porosity at high temperature coagulation, in view of the similar graft dimensions.

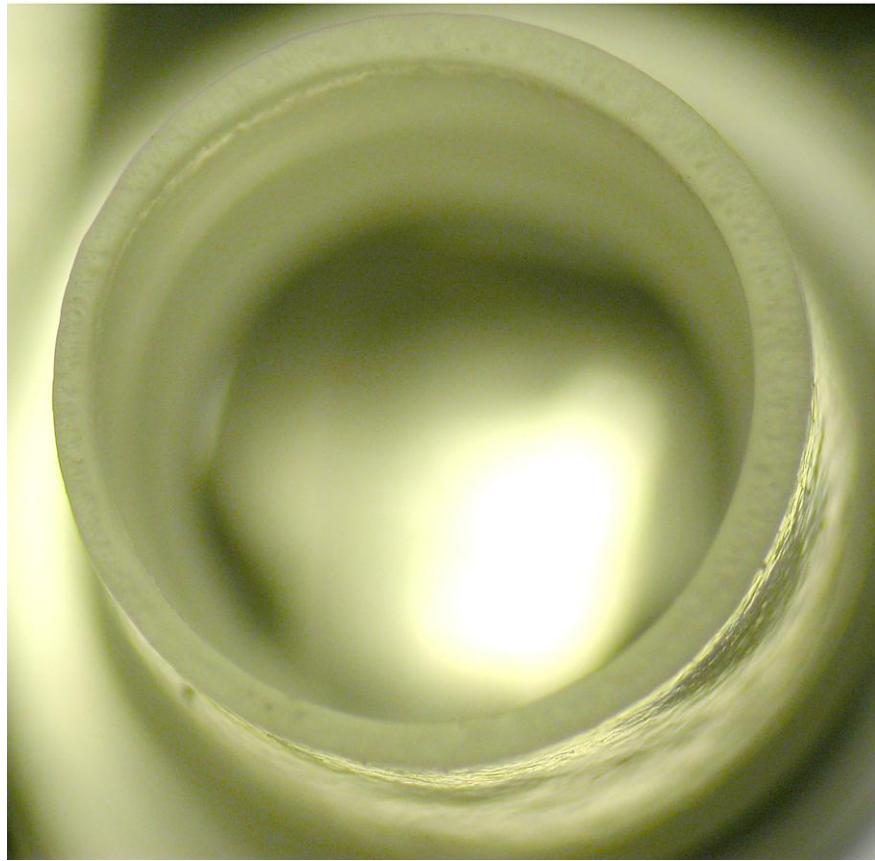


Fig 6.27. High resolution macro-photography in an attempt to show the specific pore structure of the graft cross section.

The effect of temperature does not act by modifying the thickness of the grafts formed. Therefore the exit aperture size is directly responsible for the wall thickness of the grafts and there is no difference in the behaviour of the polymer once it has coated the mandrel and is lowered into the coagulant (whatever the coagulant temperature).

Although four distinct laminae were observed, these are not separate entities, as they were produced en-bloc in a single step extrusion process. This removed the possibility of weaknesses developing between the different laminae due to relative shear stress during the prolonged repetitive strains involved in physiological flow. Preliminary attempts at increasing the burst strength of these conduits by dip-coating the completed graft secondarily in polymer solution was abandoned after it was evident that the interface between the resultant two coaxial tube structures showed signs of separation after prolonged exposure in a biomimetic pulsatile flow circuit. This illustrates the advantage of the single en-bloc manufacturing process. Soletti's group³³³ recently reported their coaxial polyurethane tube with a cast/salt-leached inner tube covered by an electrospun fibre, which was claimed to have no detectable "delaminations". However, this scanning electron microscopy observation was not repeated after haemodynamic conditions.

6.7 The effect of DMAC in the coagulant

In order to investigate the dynamics of The effect of increasing concentrations of DMAC in the coagulant solution was to visibly slow the coagulative process. This resulted in an increase in maximum pore size at the luminal aspect, but did not noticeably affect the other layers.

20% ethanol caused some shrivelling on drying, but below this concentration, ethanol's effect was to increase the luminal surface pore size as well as increase the uniformity of pore size at the lumen. These results are summarized in Table 6.4. Ethanol's effect of reducing variation in pore size has been shown previously by Chen et al¹³², albeit at much higher concentration than here. Khorasani and Shorgashti³³⁴ have found a similar pore size standardising effect with alcohols. However, at very high alcohol concentrations, the expected reduction in size and number of the largest pores (which they

have termed “macrovoids”) was not seen with our polymer. This may reflect the different technique used for phase inversion - Khorasani coated glass plates with polymer which were then immersed in waterbaths; alternatively, the properties of the polymer itself may be responsible; also, Khorasani used N,N-dimethylformamide (DMF) rather than DMAC as solvent. Very high ethanol concentrations rendered our developing graft unstable at the phase inversion stage.

Additive to coagulant	Maximum pore size (microns)	% large pores in wall cross-section	Lumen surface pore size (microns)
5% DMAC	236	89	0-4.5
10% DMAC	389	85	0-13.5
15% DMAC	278	87	0-13.5
20% DMAC	347	89	0-18
5% EtOH	250	60	4.5
10% EtOH	390	88	6.7
15% EtOH	305	92	8.9
20% EtOH	305	85	22.3

Table 6.4. Effect of different coagulants on composition of the graft wall

6.8 The mechanical and physiological implications of the grafts' pore structure.

High porosity in the graft wall allows for a highly compliant prosthesis. It can be described in terms of pore size and pore density, and a comprehensive description requires both parameters to be addressed. However, phase inversion resulted in a graft with changes in porosity through the wall. Therefore an overall pore size or distribution is not meaningful. Overall, the pore size was greater near the lumen than the outer wall. This means that the principle elastic strain due to blood flow will be exerted at the lumen, compressing the vessel wall, rather than radial expansion of the outer aspect. The static outer wall would allow optimal incorporation into the surrounding tissues on implantation³³⁵. Low porosity of the outer aspect may reduce fibrovascular infiltration from the surrounding tissues which is responsible for loss of compliance properties after infiltration. However, a complete absence of pores resulting in a smooth outer surface can cause a florid capsule formation around the prosthesis resulting in a profound loss of compliance³⁷. This may be a frustrated cellular attempt at successful integration of the graft into its surrounding tissues as a result of a smooth surface providing no tethering

points. The graft provides plentiful tethering points via its regular expanse of ridges and troughs on its external surface. We have preliminary results showing absent external capsular formation on implantation of this nanocomposite in an animal model.

Low porosity of the luminal aspect is associated with poor spontaneous endothelialisation as well as reduced neointima formation³³⁶. The relative importances of both of these graft healing characteristics have been extensively explored with groups investigating grafts with both high and low porosity and a pore size of 10 to 45 microns is required for spontaneous endothelialisation⁸¹. However, spontaneous endothelialisation is only seen in animal models of synthetic vascular prostheses¹²⁰; implantation in humans result in a fibrinous neointimal lining without confluent endothelialisation¹²⁵. To date, endothelialisation of a synthetic prosthesis in humans has yet to be achieved and this challenge has been approached by some groups with attempts to actively seed endothelial cells to grafts prior to implantation²⁶⁴. At the same time nevertheless, work continues to explore the endothelialisation characteristics of animal vascular models. Lumsden et al.³³⁷ showed that a non-porous lumen in PTFE grafts was associated with reduced NIH in canine and baboon models. Their experimental design ensured no potentially confounding difference in the surface chemistry between porous and non-porous PTFE segments within the same conduit.

6.9 Conclusion

A small calibre microporous conduit has been developed using an extrusion-phase inversion technique. This method is an amalgamation of two well-established methods. The benefit of using this hybrid method is to ensure uniformity of the conduit wall by utilising the constant downward force exerted by gravity in combination with the precise extrusion enabled by a careful alignment between the descending mandrel and the exit aperture. By modifying the exit aperture, it is possible to change the wall thickness. This is important as it presents variables to manipulate when attempting to achieve the optimal mechanical properties.

This technique shows that it is possible to create a porous conduit by

phase inversion without the use of a porosifier. Although a porosifier has been shown by others to make the pore size uniform, this was not the case with the nanocomposite. This was largely due to the difficulty in grinding the porosifier into uniformly small crystals. This resulted in large cavities which made the graft very weak and inappropriate for physiological stresses.

Another variable which affected overall graft integrity was the coagulant used. Although some pore size equalising effect was seen with ethanol, this was much less than that shown by Chen¹³². Ethanol did appear to slow phase inversion down, as did the introduction of DMAC into the coagulant solution – in both case, this caused an increase in the size of the outermost pores only. The greatest beneficial effect was seen on using low temperature phase inversion. This ensured the grafts maintained their form on natural drying and imposed dehydration. This has profound implications for graft storage as well as demonstrating better graft integrity – if the pores rely on water's surface tension to prevent their collapse, the interporous wall must be very weak.

As the basic biostability, cytotoxicity and thrombogenicity of the nanocomposite has been previously demonstrated, the grafts may now be tested for mechanical performance, in order to assess their potential for subsequent in vivo implantation, which is the ultimate aim for these conduits manufactured in the laboratory.



Mechanical characterisation of the graft

7.1 Introduction

The reasons for mechanical characterisation of any novel material are outlined in the introduction to this thesis. The primary objective of mechanical characterisation in this case was to observe the behaviour of the material under stress. This was a necessarily vague aim, as until the investigations were completed, the material's properties could not be predicted or second-guessed. It could be surmised that because the material is a polyurethane, high strength is expected. However, this holds true for cast sheet preparations, but introducing porosity as for the phase inverted coagulated conduits weakens the material, whilst increasing elasticity. Equally, the latter material could be expected to be more elastic than the cast sheet. Compression studies would be required for complete characterisation but were not performed as the principle stresses from haemodynamic flow are tensile.

Secondary objectives were more focused. A comparison of the graft's properties with the current industry standard synthetic graft, PTFE was sought. The reproducibility of the mechanical properties was analysed as a method of batch testing for the extruded grafts. Any difference in tensile properties between the longitudinal and circumferential directions (mechanical anisotropy) was investigated. Finally, although industry-standard reproducibility was not expected from conduits made from a small bench-top device, mechanical characterisation could give an indication of whether the product had the structural integrity to be able to consider progressing to the next stage of

development, namely animal model work.

7.2 Tensile testing protocol

There are several international standards for materials testing which could be applied to the nanocomposite cast sheet and graft. As a result, any appropriate protocol is accepted in the scientific community, as long as it is clear as to which standard is being used. The ISO 37 standard for tensile testing of rubber (vulcanized or thermoplastic)³³⁸ was selected as it was designed specifically for very elastic materials which are simultaneously strong. The protocol allowed for the same test conditions for both cast sheet and porous graft; also it prescribes the use of ring specimens for circumferential tensile testing, which was simpler than trying to cut any measure tiny dogbone samples across the graft circumference; thirdly the dogbone cutter for Type 2 samples (Fig 5.7) was readily available in the department. The test was conducted at 500mm/min as stipulated in the protocol. However, this standard was subsequently substituted for ISO 7198 – Cardiovascular implants; tubular vascular prostheses³³⁹. This was because of concerns over the high load arm speed (500mm/min) which was associated with a high level of sample slippage within the grips. Furthermore, haemodynamic flow would not cause stress at this higher rate. This standard uses a load arm extension rate of 50mm/min and is specific to vascular grafts, incorporating the functional tests described in chapter 8 too.

7.3 Porous sample testing

A foam may be considered to be an aggregation of hollow cellular structures which may or may not be interconnected. The graft wall porosity was high and can be described as a foam structure. Most foam structures are utilised for compressive rather than tensile purposes. As a result they are usually characterised using compressive forces and unlike tensile testing, the behaviour of foams in compression is well recognised.

The typical compression stress-strain relationship for a foam is given in

Fig 7.1.

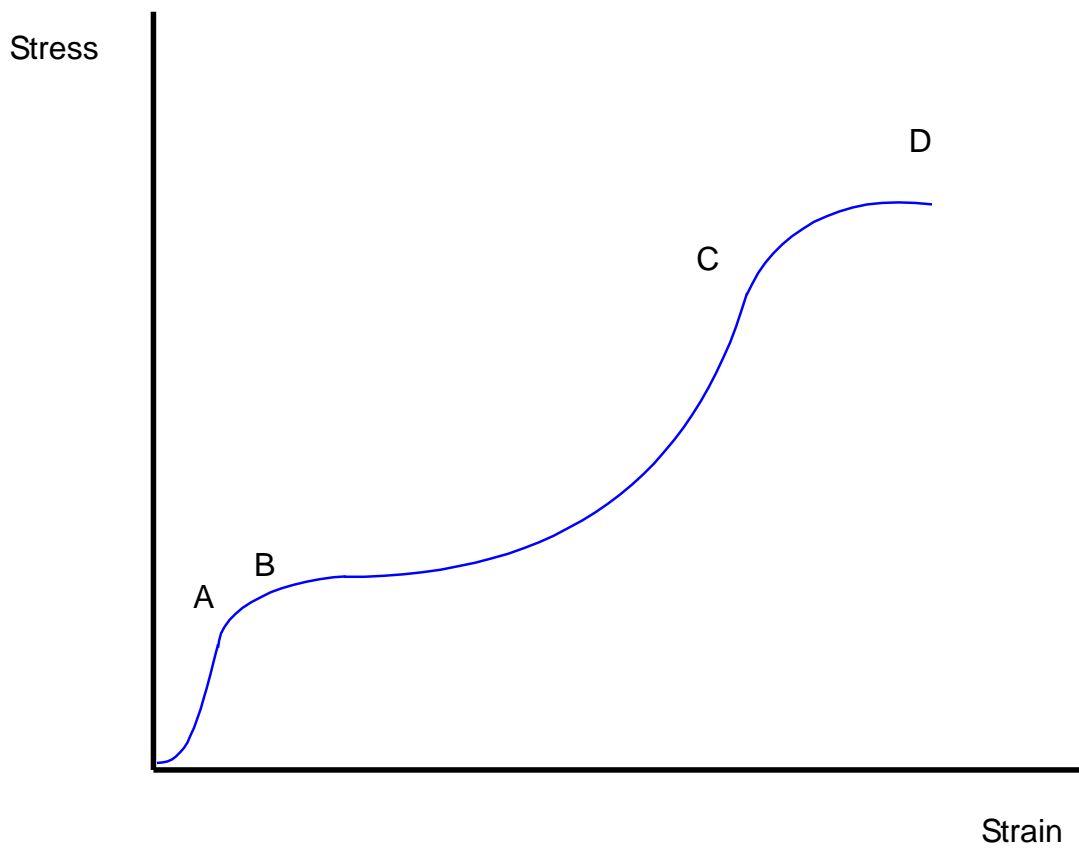


Fig 7.1. The typical stress-strain relationship found on exerting compressive forces to a foam.

To aid understanding of this curve, a honeycomb illustrative model is used - Fig 7.2.

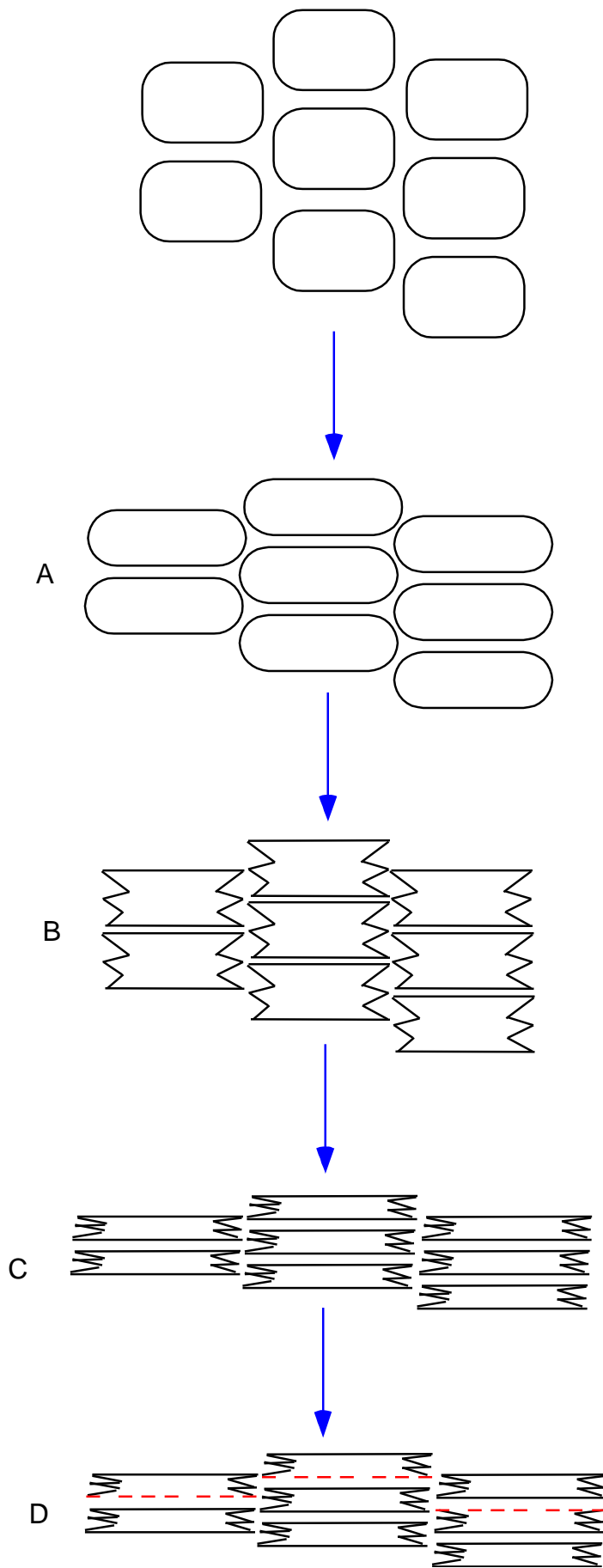


Fig 7.2. Compression of a foam structure.

The points A-D on the stress-strain curve correspond with the letters in figure 7.2. During the initial stages, the cells are compressed together (A) until the point when the cell edges parallel to the axis of compression buckle (B). Here there is a sudden easing of stiffness, manifesting as a reduction of elastic modulus – the gradient of the curve suddenly falls. Further compression increased the buckling effect, causing a tighter organised crystalline structure (C). This is reflected in an increased elastic modulus. Finally, if further compression is possible, the cell edges perpendicular to the compressive force may fracture, with failure of the overall structure (D).

The tensile behaviour of foam structures are not similarly predictable. When tensile tests are conducted on foams, the force applied is often described rather than stress. This is because the cross-sectional area of a foam is not the same as the area over which stress is applied. Instead the area is determined by the pattern of porosity, and stress is applied to the material only. Furthermore, stretching a porous sample causes such elongation and flattening of the pores that the whole specimen becomes much thinner than a non-porous structure with the same initial dimensions. Therefore the stress measurements calculated using graft sample thickness were valuable for comparison between different graft specimens; however, they were unlikely to be fully accurate.

7.4 Failed Tests

As discussed in the methodology of tensile testing, for a tensile test to be deemed accurate and successful, a number of criteria needed to be observed. Overall, only one in four tests conducted was deemed successful.

7.4.1 Noise

There was a particularly high incidence of premature test abortion on the Hounsfield tester. It was observed that at whichever rate of ascent of the test arm (50-500mm/min) the action was not smooth. The test was programmed to abort at the moment when there was a reduction in force. This criterion was set to detect a sample with a flaw such as a defect caused by an air bubble leading to early failure. It ensured that even a slightly weakened sample could not be

passed as a successful test. There were multiple reasons for this 'roughened' curve (which I have termed 'noise'), with contributions from critical weaknesses in the samples; extremely high sensitivity of the load cell; poor lubrication of the load arm; as well as minute oscillatory waves initiated in the water of the environmental chamber which exerted very small forces on the sample. This jerky motion is demonstrated in fig. 7.3 in the bitmap format generated by the Hounsfield software.

Despite the micro-oscillations, the test represented in Fig 7.3 completed to breakage of the sample. However this was often not the case. Fig 7.4 shows a typical example of premature halting before sample failure.

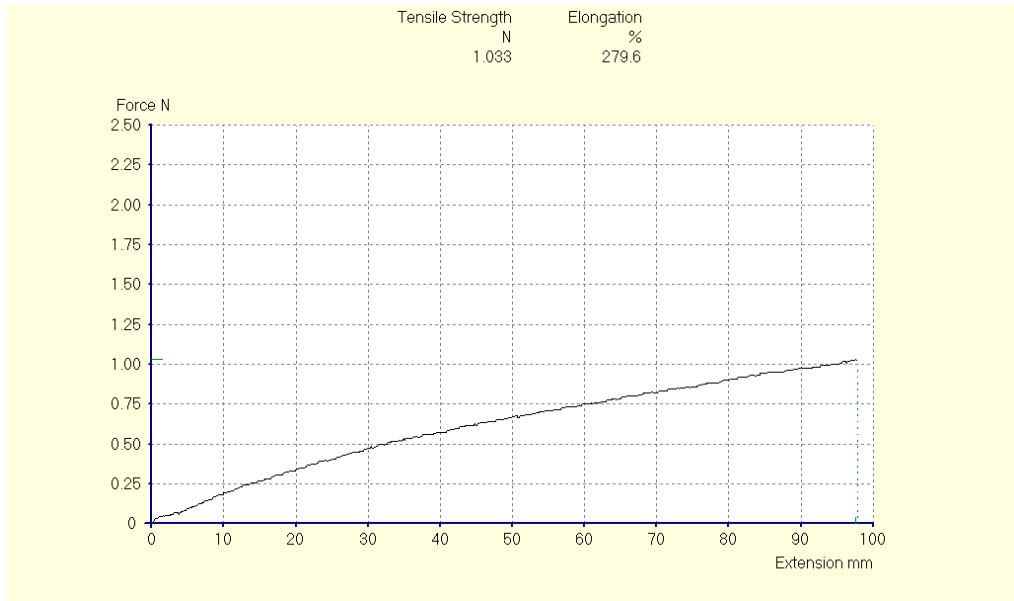


Fig 7.3. The serrated appearance of the tensile test curves generated with initial samples on the Hounsfield Universal Tester.

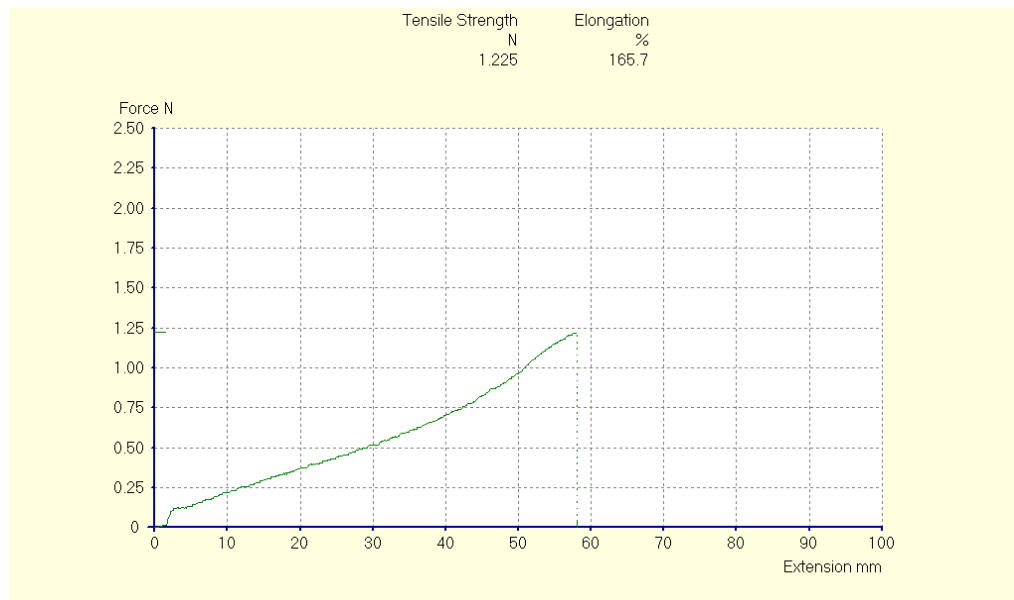


Fig 7.4. Premature halting of tensile test – the sample had not achieved its failure point.

The strain achieved was only 165.7% compared to the range for samples which were tested to failure within this group of tests (n=10) of 193.1% to 279.6% with mean strain at failure of 240.4%.

7.4.2 Initial graft placement

A further error demonstrated in Fig 7.4 was in placement of the graft for initialising the test. This is represented by the test curve not starting at the axis origin. At test commencement an extension of 2 mm occurred without any increase in stress. This indicates that the slack in the specimen was not completely taken up at the start of the test. The result was (a small) inaccuracy in strain determination and confusion as to the initial shape of the curve. When considering this in the context of small calibre graft function, the behaviour of the graft at low stress was critically important to investigate accurately as this is the order of stress which the graft would be constantly exposed to in haemodynamic flow.

The ring specimens presented a problem when it came to establishing the starting neutral position. The rings had shape memory which held them in a hoop structure when no force was exerted. However, this could not be defined as the neutral position, as the pins were able to pull apart for approximately one millimetre before force was being exerted. This is demonstrated in Fig 7.5. The test represented in fig 7.7 was started with the graft already under slight tension (approximately 0.3N). This was an avoidable error.

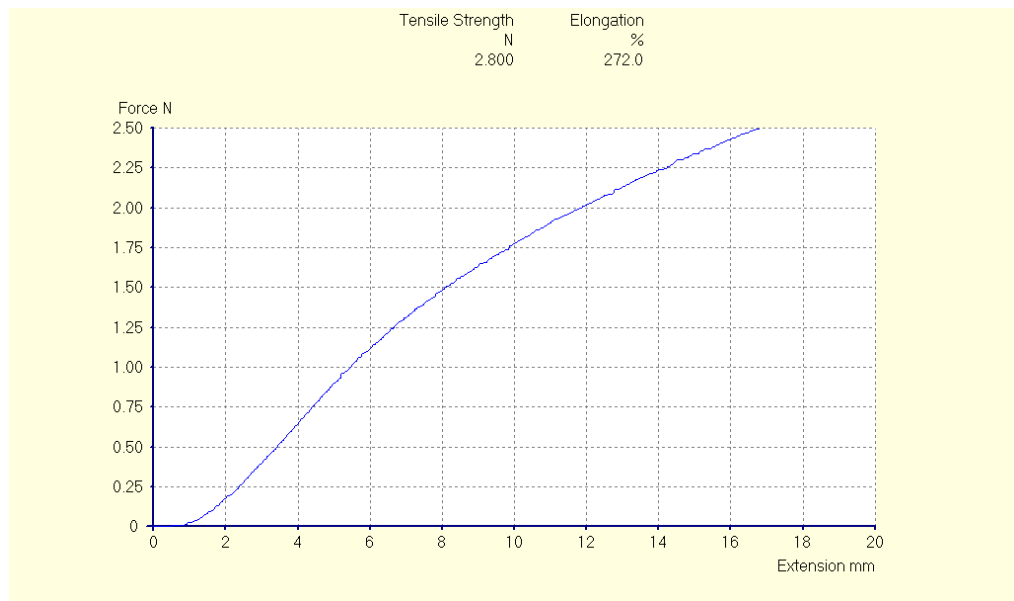


Fig 7.5. Typical tensile test obtained from a ring specimen when the pins were aligned at the initiation of the test such that they were both in contact with the ring, but without deforming it. This results in an extension of approximately one millimetre before significant stress is applied to the sample.

7.4.3 Slippage

This was a fundamental problem at the interface between sample and grip. The grip design was neither optimal for the cast sheet, nor the porous graft. A tight grip on small samples without concentrating pressure unduly within the area of test was a great challenge, and the commercially available grips for the Hounsfield tester were not adequate. Fig 7.6 shows obvious slippage of the sample within the grips. When this occurred, it was almost exclusively at the beginning of the tensile test, with the test usually continuing to completion without further slippage. This observation led to the hypothesis that the slippage was occurring due to poor initial ‘purchase’ between the PTFE blocks in the grip and the sample. In order to increase the friction across the area of the sample within the grips, thereby increasing the purchase, squares of printed circuit board (PCB) were interposed between the graft and the grip. This mainly eradicated the problem with slippage although the new sandwich arrangement introduced an additional interface at which relative movement was possible.

Slippage was far less frequent as a result, but when it occurred, it was even more dramatic with visible displacement of the PCB relative to the PTFE block – Fig 7.7. Excoriating the PTFE block surface would have improved the friction without adding another interface but risked damaging the bespoke grips irreversibly.

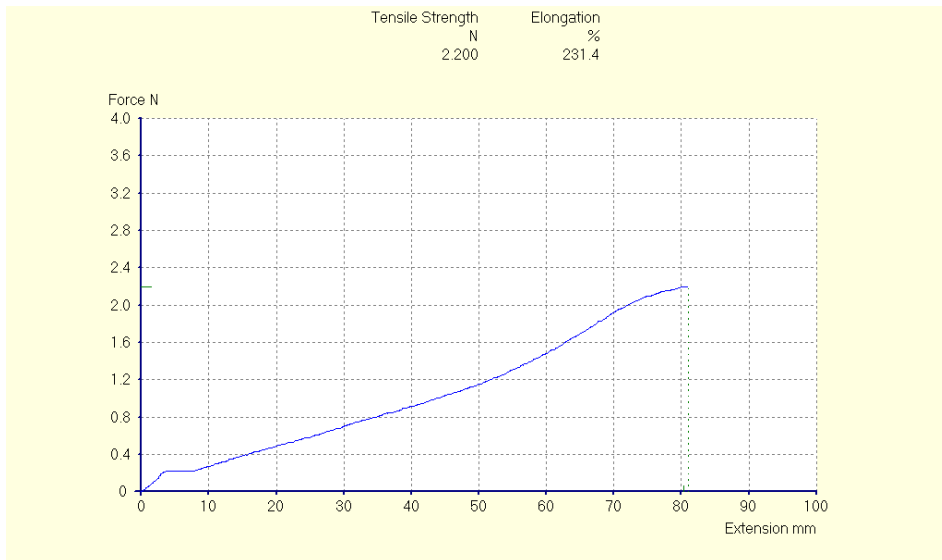


Fig 7.6. Slippage of the graft within the grip leading to a period of apparent extension with no increase in load. The initial steep gradient before the slippage may represent the graft not being placed exactly perpendicularly in the grips, hence the stress was not uniformly across the whole cross section of the sample. The placement error may also have contributed to there being residual force on the specimen before commencement of the test, as one side of the specimen could still have appeared slack to the investigator’s eye.

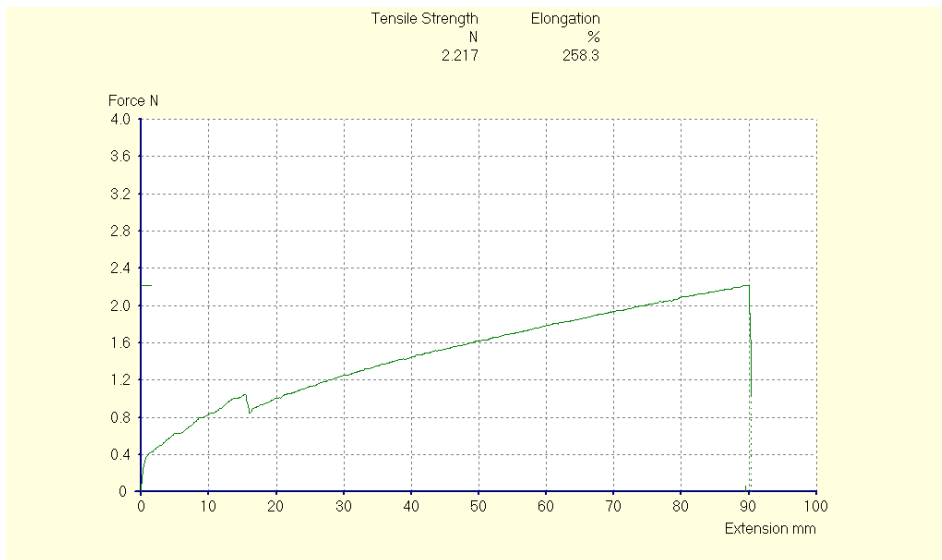


Fig 7.7. Dramatic slippage of the PCB within the PTFE blocks leading to a sharp decrease in stress during the tensile test.

7.5 Tensile test results

7.5.1. PTFE

One of the principle attributes of PTFE contributing to its success as a vascular conduit is its mechanical strength. Fig 7.8 shows the typical stress-strain relationship obtained for a longitudinal specimen of commercially available small calibre expanded PTFE (4mm diameter carbon-impregnated IMPRA[®] Carboflo[®] thinwall vascular grafts – C R Bard, Tempe, Arizona). Although the highly crystalline structure endowed it with an extremely high tensile strength, the elasticity in the physiological range was very low. There were two distinct phases of elastic modulus (E) – an initial low modulus lasting for 10-15% elongation of the specimen followed by extremely high elastic modulus. These results were extremely reproducible for repeated tests – see table 7.1.

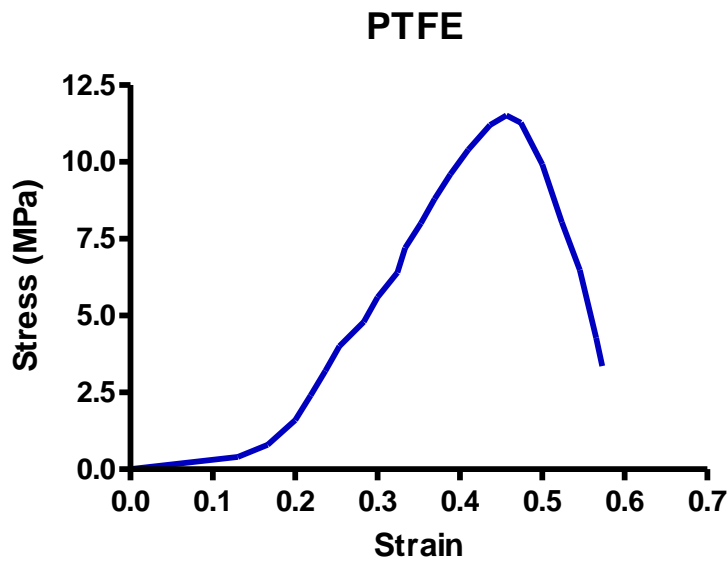


Fig 7.8. Tensile test of expanded PTFE.

Specimen	Initial E (MPa)	Final E (MPa)	Transition strain	Ultimate Strength (MPa)
1	2.51	42.25	0.17	11.52
2	2.43	40.88	0.13	11.27
3	2.58	43.21	0.14	11.52
4	2.6	42.76	0.13	11.59
5	2.55	41.09	0.15	11.47

Table 7.1. Youngs Modulus (E) and Ultimate Tensile Strength for five sections of 4mm ePTFE sourced from same graft.

7.5.2 PCUPOSS cast sheet

Initial testing of the nanocomposite cast sheet showed even greater strength and great distensibility, with graft failure occurring at nearly ten times the original length. However, at low stress, the elasticity was low (Fig 7.9).

These results were similar to those for simple PCU sheets – Fig 7.10 but incorporation of POSS was expected to increase the ultimate strength considerably.

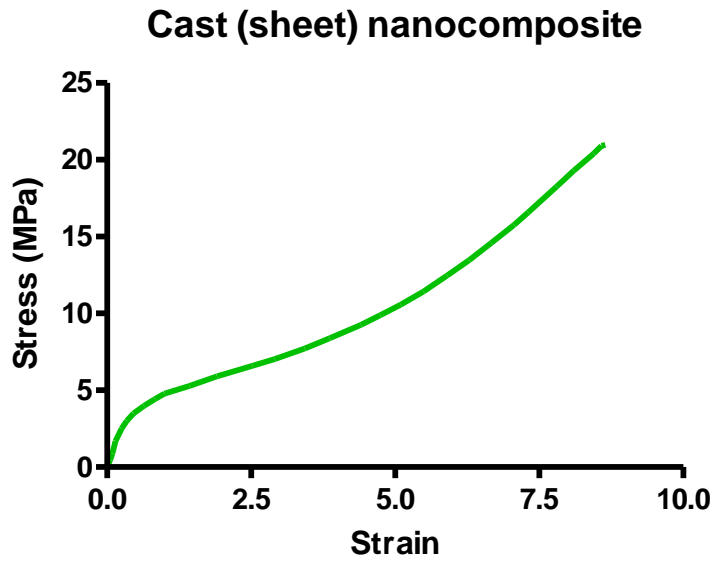


Fig 7.9. Tensile test of initial cast sheet of 2% POSS nanocomposite.

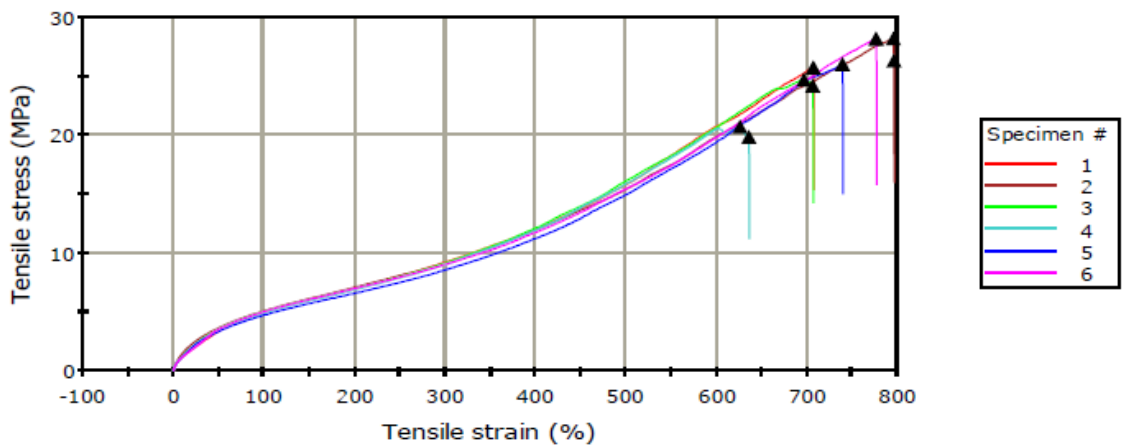


Fig 7.10. Tensile test of PCU with no POSS moiety incorporated. The maximum stress achieved was in the range 20.74 - 28.17 MPa; SD 2.745; mean 25.57 MPa.

Due to this lower than expected strength, further examination of the polymer synthesis method was undertaken, as it was felt that the ideal stoichiometry was not being realised. It was noted that there was a fine powder-like layer on top of the cast sheets being produced, even when using fresh reagents to manufacture the polymer. One theory was that this was unreacted MDI. This would certainly affect the stoichiometry of the preparation, as would spontaneous dimerisation of the MDI reducing the availability of NCO groups for reaction with diamine or diol – Fig 7.11.

MDI dimerisation was avoided by storing the solid flakes at 0°C and each batch of MDI was examined by melting it – pure MDI was completely translucent; however any dimerisation led to significant opacity in the solution, which was then rejected. Improving the polymer manufacture process thus led to a threefold increase in ultimate tensile strength – fig 7.12.

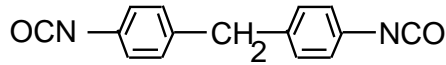
Compared with initial nanocomposite sheets as well as with PCU, this resulted in a threefold increase in maximum stress to the range 58.05 – 68.68MPa; SD 3.908; mean 65.29 MPa.

7.5.3. PCUPOSS graft

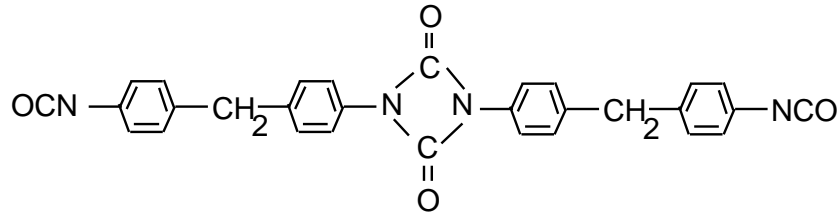
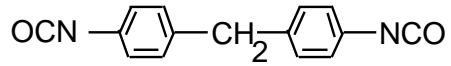
Once the extrusion-coagulation technique could produce consistently uniform conduits, they were subjected to tensile testing. However from the outset, there appeared to be considerable variation in the results obtained. This was in stark comparison to the strict reproducibility of tensile testing of multiple cast sheet specimens as demonstrated in Fig 7.10 and 7.12. Most of the initial samples resulted in J-shaped stress/strain curves – Fig 7.13 and 7.14. This curve represented a desired property, suggesting that aneurysmal change would not occur prominently at high stress levels. These samples showed much greater elasticity at low stress than either PTFE or the cast sheet. Introducing porosity reduced ultimate tensile stress compared with the cast sheet greatly, but this still remained above physiological levels. Mechanical anisotropy was suggested with testing in the circumferential direction revealing lower ultimate strength than longitudinal testing. Extrusion processing of polymers is known to cause this pattern of mechanical anisotropy. The EDXA results confirmed that the anisotropy seen was not due to a molecular redistribution of the POSS nanocage, leaving the hypothesis of polymer chain alignment expected from

extrusion and preserved during phase-inversion. However, the graft elasticity was similar in circumferential and longitudinal directions. The initial stress-strain behaviour suggested very little difference in elasticity (as shown by the gradients of the graphs near the origin) between the thin and thick-walled grafts. Once appreciable strain has developed, however, the elastic modulus for the thicker specimens were higher than their thinner-walled counterparts, suggesting lower distensibility for the former.

MDI



MDI



4,4' MDI

Fig 7.11. Spontaneous dimerisation of MDI stored at room temperature in its solid state. This can be avoided by storing at 0°C or in melted state at 50°C.

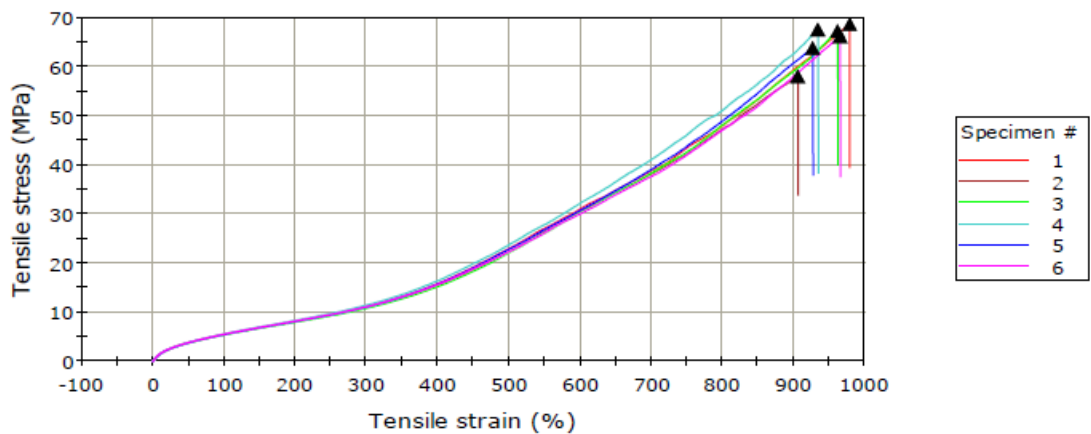


Fig 7.12 Tensile test of the POSS-incorporated nanocomposite, using non-dimerised MDI.

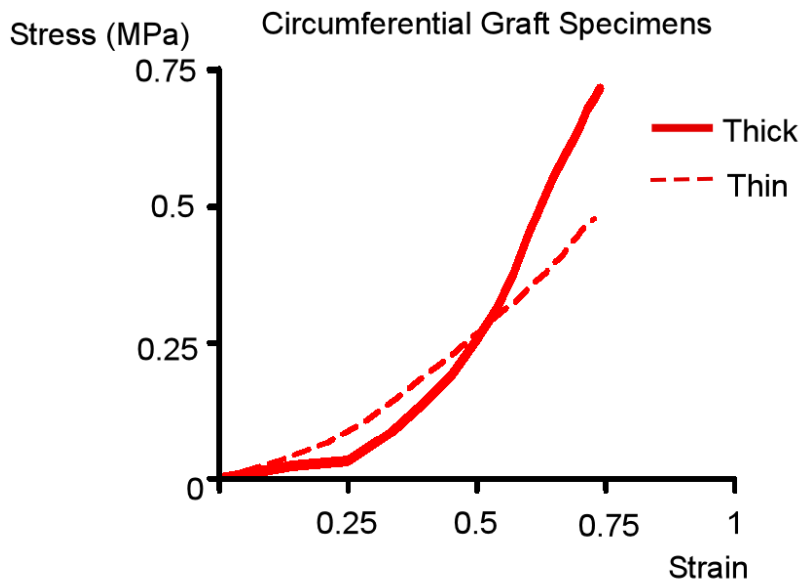


Fig 7.13. Tensile test of thin and thick-walled porous grafts in the circumferential direction.

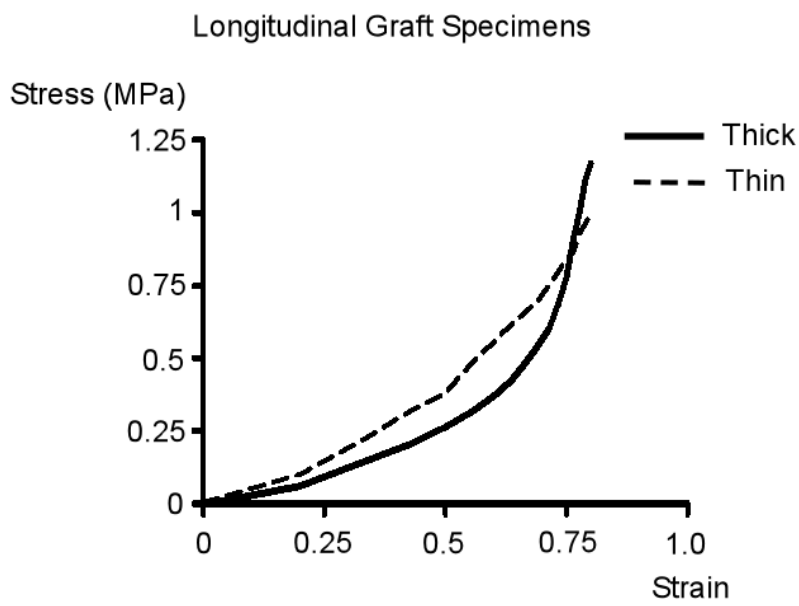


Fig 7.14. Tensile test of thin and thick-walled porous grafts in the longitudinal direction.

However, many other samples demonstrated convex curves, as in Fig 7.3. This was a worrying finding, as it showed that the final product was not reliably reproducible despite all previous attempts at standardisation of the manufacturing process. Furthermore, convex curves were more likely to be prematurely terminated due to oscillatory noise than concave curves; hence by selectively discarding these results, this was introducing a reporting bias. The standardisation of graft manufacture was revisited. There was variation occurring at least one of the steps leading to test results:

- a. polymer synthesis
- b. graft manufacture
- c. test specimen preparation
- d. tensile test

In order to formally evaluate the extent of this variability, 6 thick-walled and 6 thin-walled grafts were manufactured from a single batch of polymer which had been synthesised 48 hours previously and stored in a dark dry cupboard. The reasons for these conditions have been discussed in Chapter 6 when considering polymer batch testing. At this stage, it had not been realised that there was significant dimerisation of the MDI leading to unfavourable stoichiometry of the final polymer. Longitudinal and circumferential (ring) specimens were prepared from each graft and dimensions were collected pre-testing, along with dry weight data after completing the tensile tests. The test protocol was changed to follow ISO 7198³³⁹, the first difference being the change in load arm extension from 500mm/min to 50mm/min. This rate was of the order experienced in haemodynamic flow, and it was hoped that there would be less slippage of the graft within the grips at this more gradual extension. Also this new standard did not include the stipulation that the test should be terminated if there was a reduction in force. This removed the bias against convex curves which were previously being prematurely terminated more frequently than those with J-shaped (concave) curves. In this way, variation at each of the four stages which may have accounted for the differences in the end results was addressed. The option to alter circumferential testing from ring specimen testing to dumbbell testing was not taken up however, as the dumbbell specimens would need to be very small, requiring a new bespoke

cutter as well as causing difficulties in specimen thickness measurement. Also, testing very small specimens usually results in inflated results for ultimate tensile stress³³⁸.

In fact none of the curves obtained after changing the test conditions as above were J-shaped. The ring specimen curves were all sigmoid shaped, being concave initially with a convex shape after an inflection point – see Fig 7.15 and 7.16.

The dogbone specimens were similar although the initial J-shaped curve was subtle (Fig 7.18) or even absent (Fig 7.17). One explanation for this slight difference is that the pronounced initial J-shape of the ring specimens would have had significant contribution from the uptake of slack from the circular specimen before strain was fully manifesting as stress across the test sample.

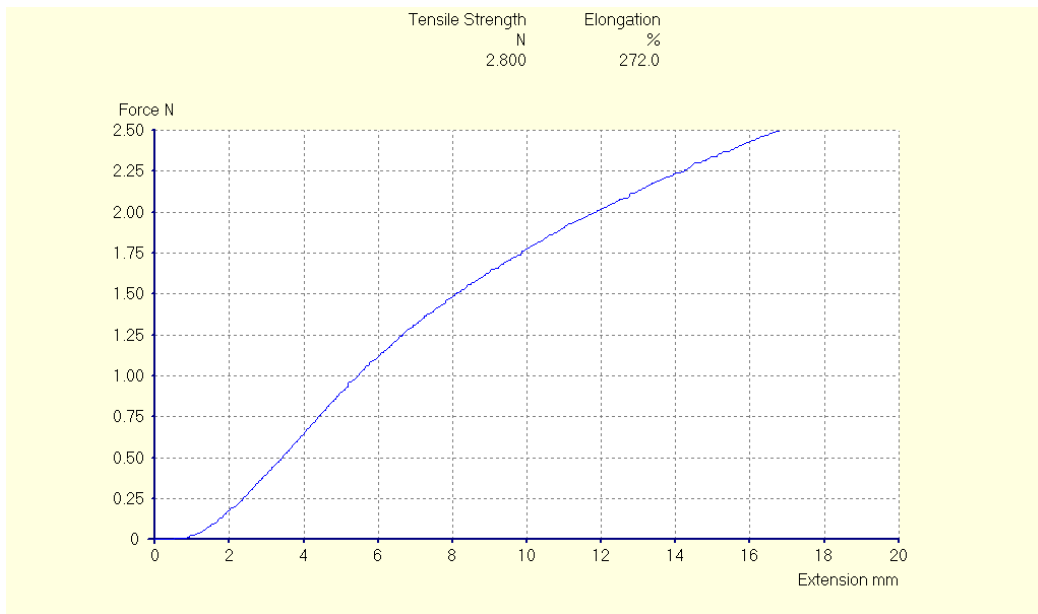


Fig 7.15. Typical tensile test curve for a thin-walled ring specimen.

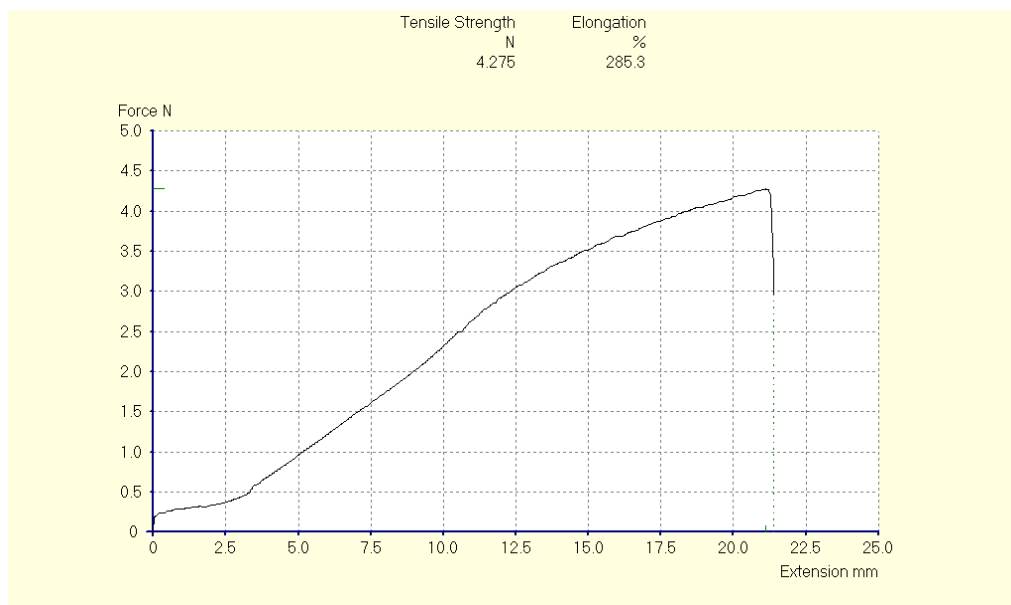


Fig 7.16. Typical tensile test curve for a thick-walled ring specimen

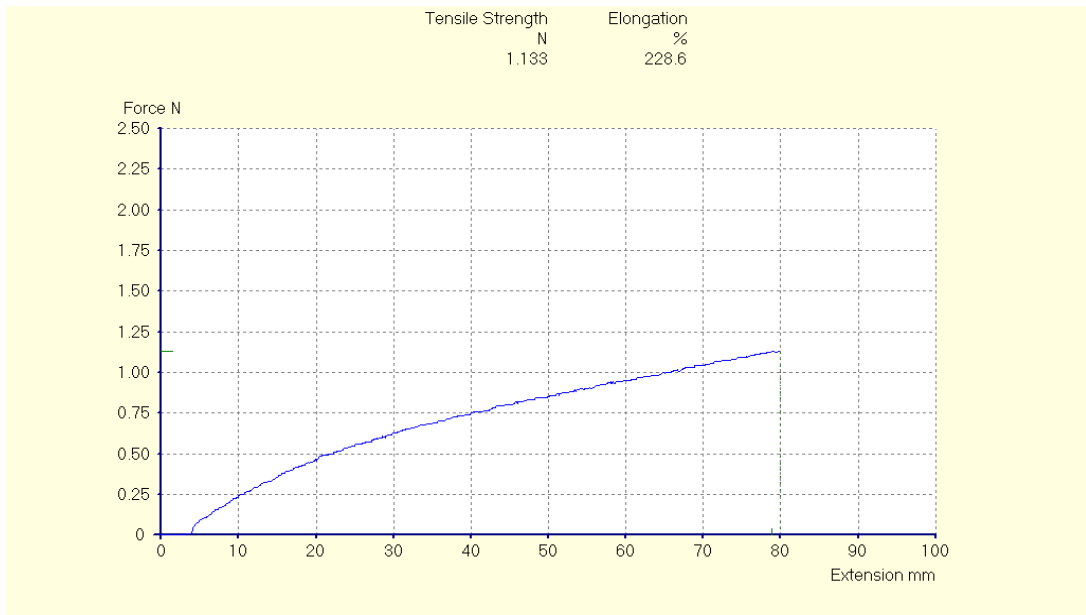


Fig 7.17. Typical tensile test curve for a thin-walled dogbone specimen

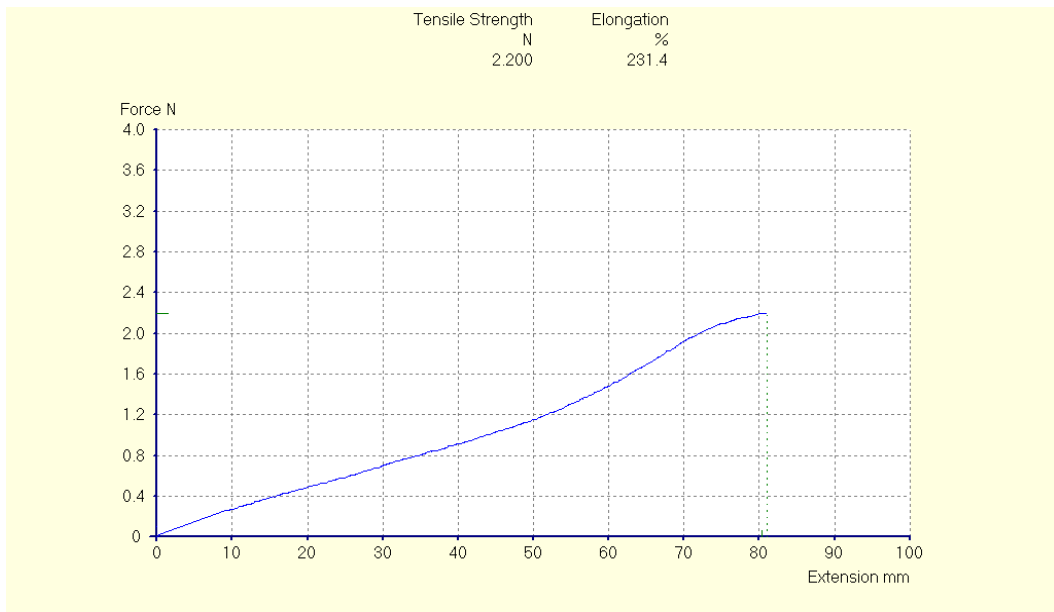


Fig 7.18. Typical tensile test curve for a thick-walled dogbone specimen

Ring specimens	Mean thickness (mm)	Dry weight (g)	Ultimate Tensile Force (N)	Ultimate Tensile Stress (MPa)	Ultimate Strain (%)
t1	0.4	0.007	2.8	0.698	272
t2	0.43	0.0074	2.732	0.641	265
t3	0.36	0.0072	3.016	0.832	305
t4	0.39	0.0074	2.467	0.635	230
t5	0.38	0.0067	2.616	0.696	246
t6	0.41	0.0072	3.032	0.737	305
f1	0.53	0.0106	4.515	0.851	272
f2	0.58	0.0109	4.275	0.742	285
f3	0.53	0.0107	4.3	0.819	268
f4	0.56	0.0102	4.135	0.738	283
f5	0.54	0.0097	3.884	0.725	276
f6	0.55	0.0089	3.376	0.609	203

Table 7.2. Results obtained from circumferential tensile testing of ring specimens taken from thin-walled (t) and thick-walled (f) grafts.

Dogbone specimens	Mean thickness (mm)	Dry weight (g)	Ultimate Tensile Force (N)	Ultimate Tensile Stress (MPa)	Ultimate Strain (%)
T1	0.36	0.0283	1.332	0.927	228
T2	0.33	0.0244	1.225	0.92	166
T3	0.31	0.0219	1.168	0.943	193
T4	0.27	0.0165	1.033	0.967	280
T5	0.29	0.0217	1.133	0.99	229
T6	0.35	0.0267	1.482	1.05	274

F1	0.73	0.0544	2.624	0.895	254
F2	0.63	0.0454	2.068	0.827	234
F3	0.47	0.049	2.2	1.169	231
F4	0.76	0.0427	2.217	0.733	258
F5	0.62	0.0411	2.007	0.811	226
F6	0.56	0.0405	2.017	0.895	250

Table 7.3. Results obtained from longitudinal tensile testing of dogbone specimens taken from thin-walled (T) and thick-walled (F) grafts. The shaded samples were technically failed tests due to graft slippage (T2) and sample failure occurring at the grip edge rather than within the test area (F1).

7.6 Addressing mechanical anisotropy

7.6.1 Ultimate Tensile Stress

These results confirmed that there was a significant difference in ultimate strength between longitudinal and circumferential tensile testing, as suggested in the preliminary testing ($p=0.0001$; 2 tailed unpaired t-test). However, there was still apparent variation in the ultimate stress achieved. This could be because of inaccuracies in the measurement of the sample thicknesses. This lead to the consideration of whether specimen thickness was a valid parameter by which to base the stress across the test segment which was effectively a non-uniform foam. Unlike weight, graft thickness was not an accurate measure of the amount of polymer in it, as this measure was dependent on porosity as well. A better measure of amount of material in the sample was its weight.

Figs 7.19 and 7.20 show the relationship between wall thickness or dry weight of the tested specimens and tensile strength for samples of different wall thicknesses. There was a stronger linear correlation between the dry weight and tensile strength than wall thickness for both longitudinal (R^2 value 0.9561 vs 0.856) and circumferential (R^2 value 0.9059 vs 0.6165) test specimens. This was especially true for the circumferential specimens.

Longitudinal strength of different graft specimens

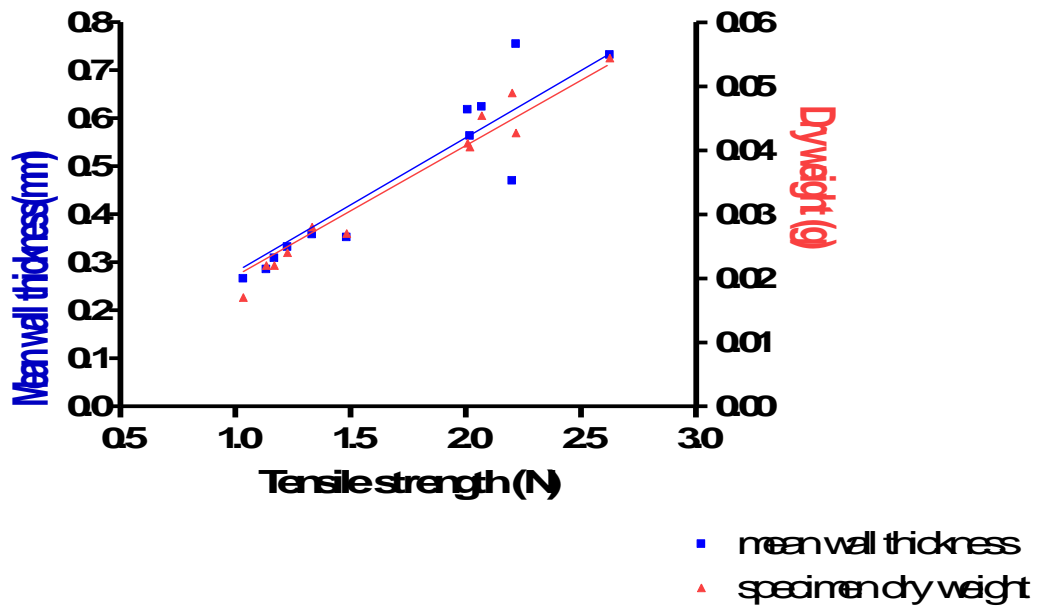


Fig 7.19. The linear relation between graft specimen dimensions and longitudinal strength.

Circumferential strength of different graft specimens

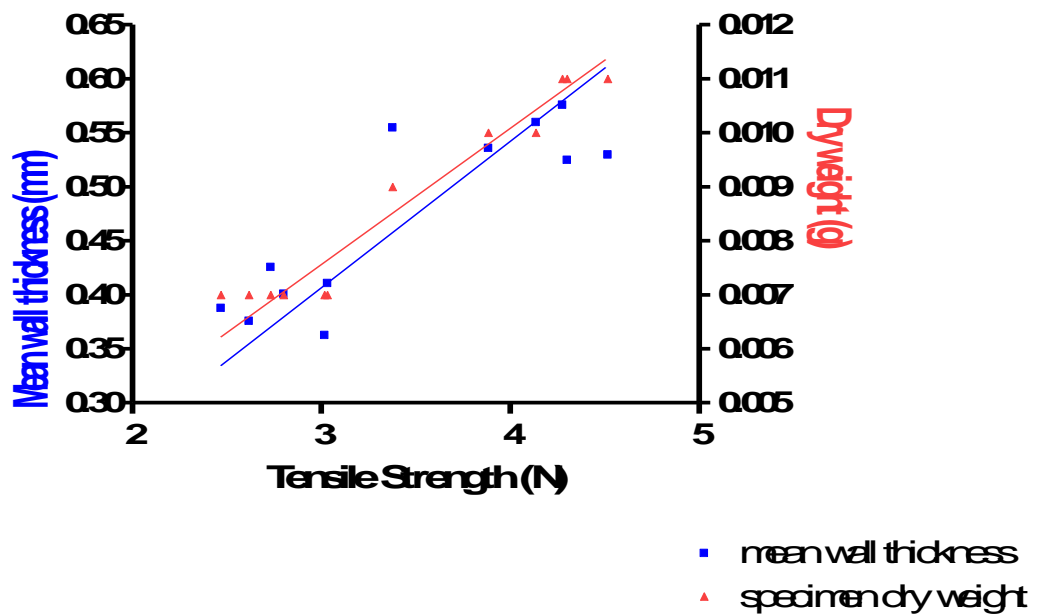


Fig 7.20. The linear relation between graft specimen dimensions and circumferential strength.

Therefore, one reason for lower ultimate stress for circumferential specimens could be because of a consistent over-reading of thickness measurement in these specimens compared with longitudinal samples. To investigate this, it was necessary to compare the measured thickness of each sample with the weight. As longitudinal and circumferential samples were of different sizes, unit weights were considered, by dividing the sample weight by the flat area of the specimen – 255mm² for longitudinal dogbones and 62.8mm² for circumferential rings. The relationship between measured thickness and unit weight are demonstrated for dogbone and ring specimens in Fig 7.21 and 7.22 respectively.

These two best fit lines suggest that there is no large difference between thickness measurements for longitudinal and circumferential specimens. In fact, the small gradient difference shows a slightly lower measurement of thickness for circumferential compared with longitudinal specimens rather than over-reading. Furthermore, the best fit line correlated better with the measured data in the case of the circumferential rings than the longitudinal dogbones ($R^2 = 0.85$ and 0.79 respectively).

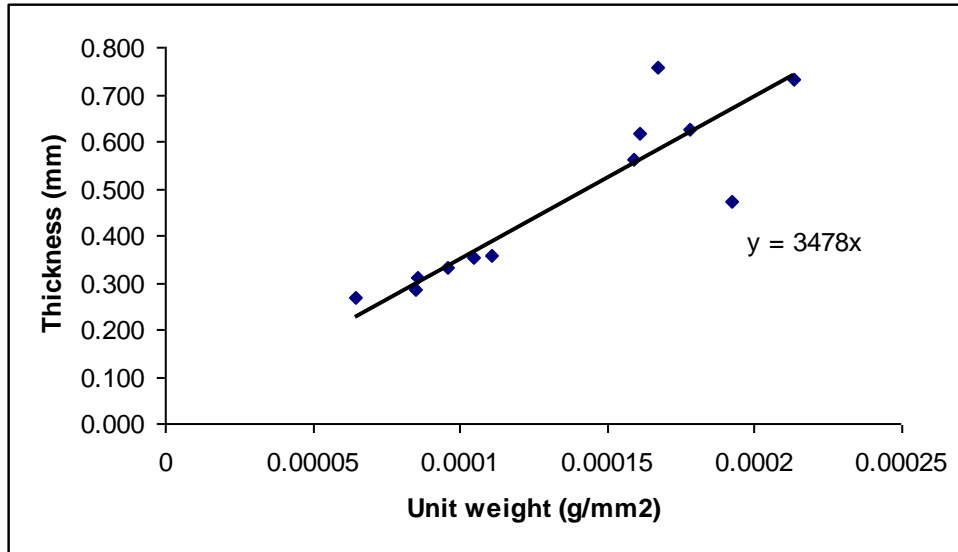


Fig 7.21. The direct correlation between measured thickness and unit weight for longitudinal graft samples.

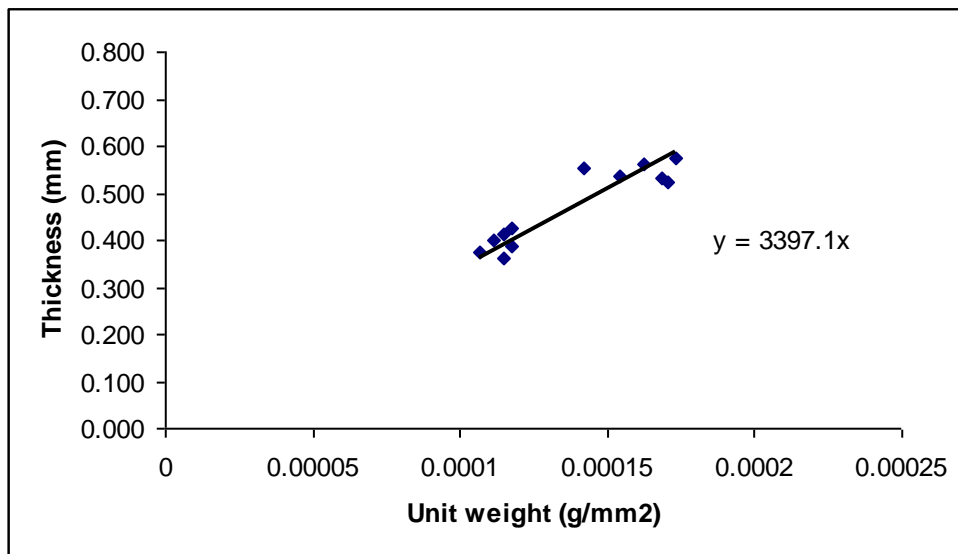
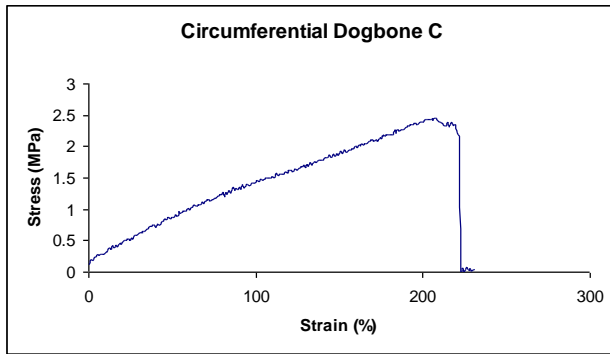
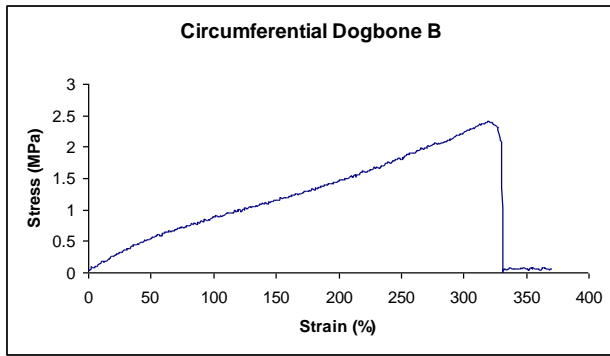
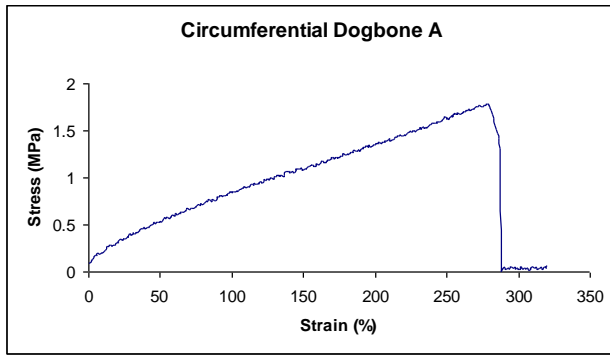


Fig 7.22. The direct correlation between measured thickness and unit weight for circumferential graft samples.

7.6.2 Curve shape

Using different types of sample (dogbone and ring) for longitudinal and circumferential testing respectively introduces a possible reason for the difference in the curves generated in tensile testing. One hypothesis for the sigmoid shaped curve for ring specimens is that the initial hoop shape of the specimen is responsible for gradual application of stress to the wall as the hoop is flattened out. This is not the case for the dogbone specimens where the strain is taken up as stress in the wall immediately and uniformly. In order to test if the initial concave shape (J-shape) is due to the ring configuration, a smaller specimen cutter was commissioned and used to cut specimens in the circumferential direction across the longitudinally opened graft. Although the stress calculations were not felt to be accurate as the size of the specimens did not allow for precise thickness measurement, all of these curves were similar to the longitudinal dogbones, rather than the circumferential rings – see Fig 7.23. Therefore, it was concluded that the sigmoid curves generated from the ring specimens were artifactual and that there was no real difference in the shape of the tensile curve in longitudinal and circumferential directions.



7.23. Tensile testing in the circumferential direction using a dogbone cutter.

7.7 Viscoelasticity

Standard tensile testing gives an indication of the distensibility of the graft material under the conditions of the test. However, it does not acknowledge the effect of any viscous element on the material's character. Significant viscosity influences the elasticity demonstrated during the tensile test, with the magnitude of this effect being dependent on the rate of graft extension. Almost all materials exhibit some degree of viscoelasticity, and especially biological tissues. Polymers are well known for their viscous component. Stress relaxation is one way of demonstrating viscous nature. It relates to the dissipation of stress which occurs once a defined strain is applied. Fig 7.24, 7.25, and 7.26 show this phenomenon for PTFE, thick-walled longitudinal dogbone specimens and thin-walled dogbone specimens respectively after they have been rapidly extended (500mm/sec) to 70% strain.

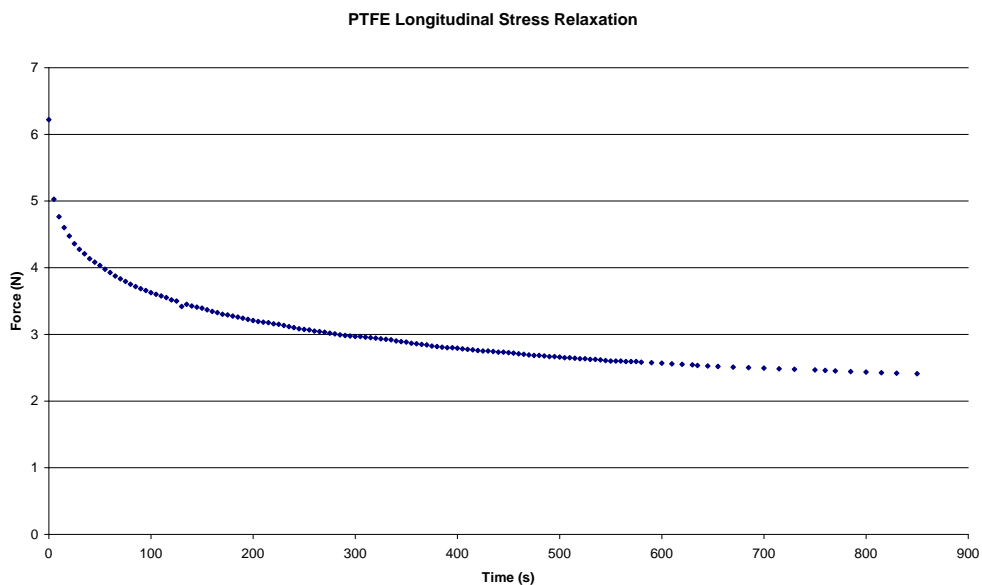


Fig 7.24. Stress-relaxation of a PTFE longitudinal dogbone specimen.

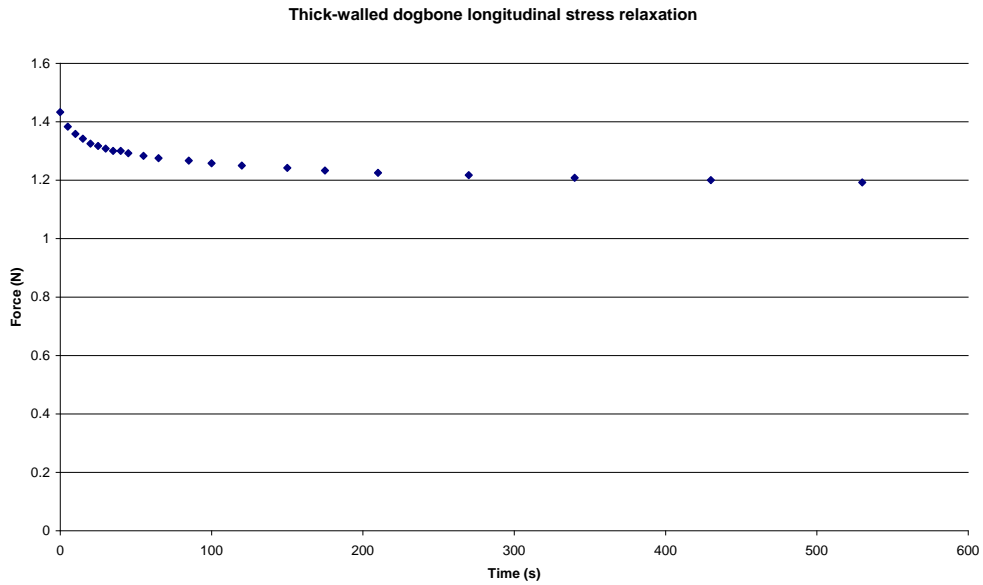


Fig 7.25. Stress-relaxation of a thick-walled longitudinal dogbone specimen.

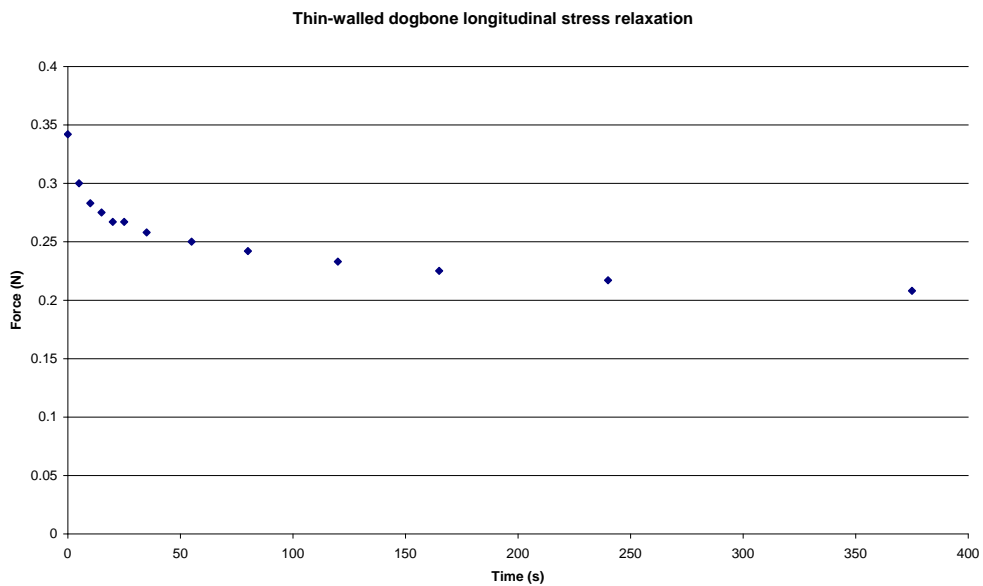


Fig 7.26. Stress-relaxation of a thin-walled longitudinal dogbone specimen.

Another way of demonstrating viscosity is to apply and maintain a predetermined force to the material. In a viscous material, in order to maintain the force, continuing deformation of the material will be necessary. This phenomenon is termed 'creep'. Therefore if tensile forces are applied to the material, a constant force will cause gradual elongation of the material.

There are several implications of the viscous element in material characterisation. Firstly, the viscosity is of course a fundamental mechanical characteristic. Secondly, viscosity affects the tensile test with the result being

dependent on the rate at which the tensile test was performed. An extension rate of 50mm/min was used as it was indicated in the standard being followed, and this was a reasonable magnitude when considering haemodynamic pulsatile flow. However, it is clear from the stress-relaxation curves that the graft may achieve a higher elastic modulus and ultimate tensile stress if the tensile rate is higher. Thirdly, exerting repeated tensile forces as in haemodynamic flow may magnify the effect of the viscosity or even set up complex unpredictable oscillations of forces. Therefore, simple tensile testing may not give much real indication of the graft's true behaviour in haemodynamic conditions.

7.8 Conclusion

Basic mechanical characterisation of the graft material was undertaken via tensile testing. The results have been presented in the form of an investigative journey as the methodology and even the polymer used evolved during the course of the study.

Although some initial tensile tests gave J-shaped curves, it became clear that once the graft manufacturing and testing processes were fully standardised, the curves obtained were not J-shaped, but convex. The explanation for the initial results was the methodology being used (ring specimens rather than dogbones for circumferential specimens) and also the automatic premature termination of tests detecting a reduction of stress during the test, which resulted in a selection bias against convex results.

The porous grafts were far more elastic than either ePTFE or PCUPOSS cast sheets in the physiological range of stresses. This was at the expense of graft strength. Simple tensile testing does not predict how the graft will behave in haemodynamic conditions. Elasticity cannot be translated directly into compliance data due to the viscous element that has been demonstrated here. Similarly, ultimate stress does not have a simple relationship with haemodynamic stress as blood pressure exerts forces in all directions simultaneously (circumferential, radial and longitudinally). Therefore dynamic testing of the graft is essential, and studied in chapter 8.

8

The functional mechanical properties of porous poly(carbonate) urethane based nanocomposite grafts.

8.1 Introduction

The fundamental mechanical characterisation described in the previous chapter affords a description of how the nanocomposite graft material behaves under stress. However, this is not tailored to the specific use for which the graft is intended. Although the information is essential for a baseline in developing any new material, the surgeon who will ultimately use the graft will not be able to easily use the information as the results do not immediately translate to an indication of mechanical safety under the physiological stresses of pulsatile flow. In order to undertake this translation, some understanding of the stresses acting on the graft wall is desirable, and this has been discussed in chapter 2. However, analysis of flow velocity profiles and viscoelastic interaction with the graft wall would be required to quantify the precise stress vectors. Each of these is in itself a complex field requiring sophisticated theoretical models which have not been conclusively described so far, and simpler alternatives have been sought. One such alternative is to simulate the potential stresses on the wall by mimicking pulsatile flow. This removes the need to define exactly what the stresses are and where they act. The flow circuit used here and described in detail in Chapter 5 does this. Another option is to simplify the components of pulsatile flow down to its constituents. The measurement of burst pressure

addresses the maximum radial/circumferential stresses which the graft can bear, and is a direct indicator of graft strength, given in units familiar to a surgeon (mmHg). An additional layer of complexity is in the measurement of graft durability which has not been considered here. This requires pulsatile testing over the period of the required lifespan of the graft. In this case, an expectation of 30 years use is reasonable. However, insistence on thirty years of mechanical testing before consideration for clinical use would be counter-productive. Accelerated life testing can be achieved by increasing the frequency of the pulsatile cycle even to 20Hz. However such rapid stresses have a huge effect on the behaviour of any viscoelastic material. For this reason, fatigue testing has not been effectively performed for the grafts which have been used clinically. Partly as a result of this, long term mechanical weaknesses have only been uncovered after a period of implantation, and even now, it is not clear what the lifespan of PTFE and Dacron grafts is.

8.2 Compliance

8.2.1 Compliance of lower limb arteries

The compliance of human external iliac artery was found to range from almost $20 \text{ \%}/\text{mmHg} \times 10^{-2}$ at a mean pressure of 25mmHg to less than $5 \text{ \%}/\text{mmHg} \times 10^{-2}$ at 100mmHg mean pressure by Tai using a similar flow circuit to the one used here.

Bergel's classical measurement of Young's modulus in the canine arterial tree showed reducing distensibility more distally along the aorta³⁴⁰. However, the difference was prominent at lower pressures only. He did not find a significant difference in elasticity between the abdominal aorta and either carotid or femoral arteries. However, Tai³⁴¹ has measured human superficial femoral artery compliance in-vivo, demonstrating a drop from $14.1 \text{ \%}/\text{mmHg} \times 10^{-2}$ in the common femoral to $1.9 \text{ \%}/\text{mmHg} \times 10^{-2}$, suggesting a reduction of compliance distally. Using the ultrasound probe with wall tracking, human arterial compliances were re-evaluated in a healthy volunteer – Table 8.1.

Artery	Systolic diameter (μm)	Diastolic diameter (μm)	Diameter difference (μm)	Pulse Pressure (mmHg)	Compliance (%/mmHg x 10 ⁻²)
Femoral	8611	8478	133	45	3.486
High SFA	6878	6780	98	45	3.21
Low SFA	3929	3901	28	45	1.595
Popliteal	4065	4035	30	45	1.65
AT	3118	3097	21	45	1.51
PT	3667	3647	20	45	1.21
DP	2742	2728	14	45	1.14

Table 8.1. Non-invasive dynamic compliance as measured in a healthy young adult volunteer at a brachial blood pressure of 110/65 mmHg. SFA – superficial femoral artery; AT – anterior tibial artery; PT – posterior tibial artery; DP – dorsalis pedis artery.

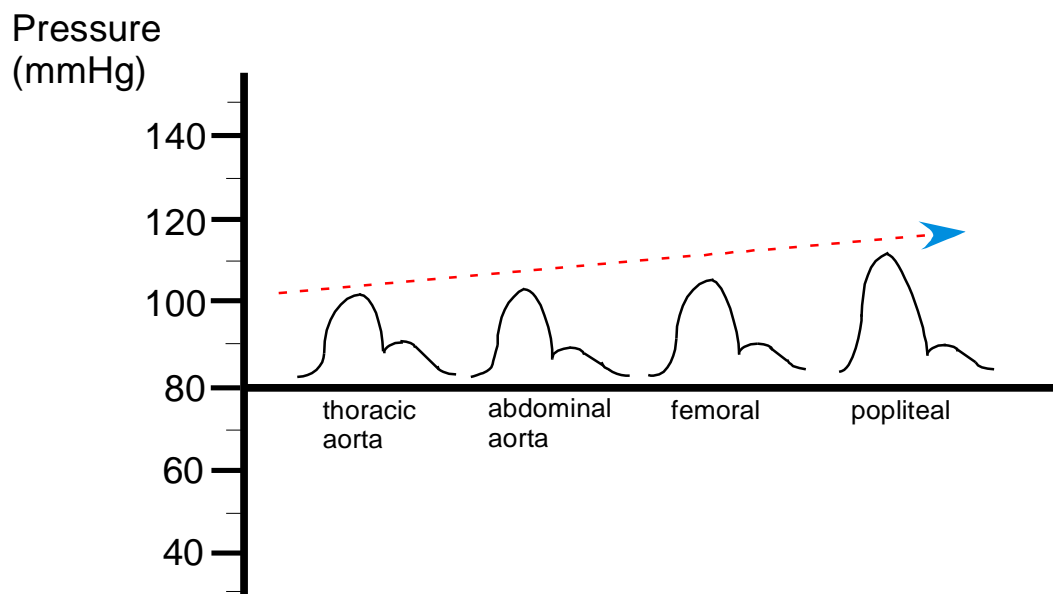


Fig 8.1. The increase in systolic pressure along the arterial vasculature resulting in increased pulse pressure in the smaller arteries. Concept for diagram taken from Nichols and O'Rourke³⁴².

Brachial systolic and diastolic blood pressures were measured simultaneously and assumed to be equivalent to the pressure in the vessels being measured. In fact in young healthy individuals, there is a slight increase in pulse pressure distally, due to an increasing systolic pressure – see Fig. 8.1. However, the assumption is reasonable in those with arterial disease, including the elderly. In young people however, assuming brachial pressures are the same as distal pressure can result in an overestimation of compliance measurements in the smaller vessels, relative to the more proximal larger ones.

A circular cross section was assumed for each vessel, so the maximum internal diameter measured was defined as the true diameter. As can be seen in table 1 there was an apparent increase in internal diameter from the low SFA to the popliteal artery. It was also difficult to visualise the low SFA. The scan was performed in the presence of a vascular technician, who then verified the diameters independently. There was a general trend towards reducing compliance distally. The compliance figures are considerably less than those found by Tai for the external iliac artery. However, these latter studies were performed on excised specimens without the physical constraints of surrounding tissues. Furthermore, the in-vivo assessment corresponded to a mean pressure of 80mmHg – at this mean pressure, Tai's own findings were a dramatic reduction of compliance to the order of $5\%/mm\text{ Hg} \times 10^{-2}$. Cheng's measurement of femoral compliance in 21 healthy volunteers was of the same order of magnitude as found here ($6.04 \pm 4.14\%/mm\text{Hg} \times 10^{-2}$)⁹⁵. The majority of patients requiring distal bypass prostheses with have mean pressures of at least 80mmHg.

It is also evident from these results that there was a large drop in compliance along the SFA with the upper SFA being far more elastic than distally. Taking all these different sources together, it can be seen that there is decreasing compliance distally in the lower limb arterial tree. The rate of decrease is somewhat variable between individuals. These figures do not support the theory of compliance mismatch being fully responsible for IH, as the distal anastomosis is especially vulnerable but has the least compliance mismatch. However, bearing in mind the difference in compliance between implanted and explanted artery, it is not known whether the compliance of PTFE reduces after implantation, possibly to zero, thereby bringing compliance mismatch back into play.

8.2.2 Compliance of PCUPOSS grafts

ePTFE is a rigid material with compliance in the region of $1 \text{ \%}/\text{mmHg} \times 10^{-2}$. In order to minimise progressive intimal hyperplasia, compliance akin to superficial femoral artery is desired. However, at the same time, using high degrees of porosity to achieve elasticity can result in poor mechanical strength, and a balance between the two mechanical properties is required. This is illustrated by our early attempts to include $\text{Na}(\text{HCO}_3)_2$ porosifier and surfactant in the nanocomposite solution during phase inversion. The rationale behind this was to produce hyperelastic grafts ($10\text{-}20 \text{ \%}/\text{mmHg} \times 10^{-2}$) which would match the highest compliances achieved by Tai. The result was very compliant weak conduits which burst at mean pressure of only 140mmHg. This pressure level is easily achieved in the hypertensive patient. The compliance results from 5cm lengths of 5mm diameter of this weak graft is shown along with our own measurement of explanted swine common femoral artery compliance in Fig 6.16 which is reproduced here again as Fig 8.2. The arterial segment was of the same dimensions and prepared immediately after slaughter with a saline wash followed by gluteraldehyde preservation to preserve mechanical properties. It was tested within 6 hours of explantation.

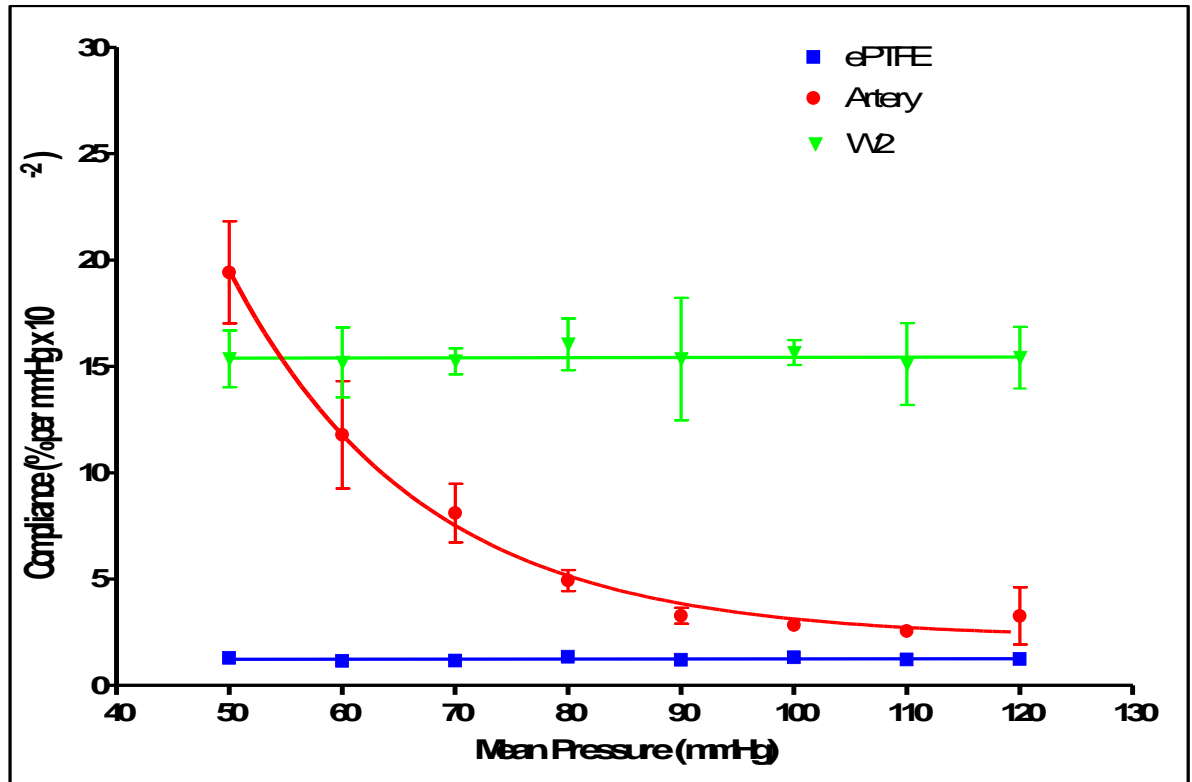


Fig 8.2. The hyper-compliant conduit achieved by using 5% Na(HCO₃)₂ porosifier and surfactant mixed in with the polymer solution before extrusion/coagulation. The coagulant used was de-ionised water at 50°C. This graft matched the compliance at low mean pressure of the explanted swine common femoral artery but failed at a mean pressure of only 140mmHg. The standard deviations shown relate to 3 readings taken at equally spaced points along the graft.

The integrity of grafts manufactured from PCUPOSS without any porosifier using deionised water at 0°C as coagulant appeared much stronger from basic handling observations, tensile testing and behaviour on dehydration and its compliance was determined using the flow circuit described earlier. A compliance of the order 3-6%/mmHg x 10⁻² was hypothesised as the desired range for compliance matching at the proximal (femoral) anastomosis. 6 grafts of each wall thickness were tested – Table 8.2.

Compliance as a function of mean pressure within PCUPOSS graft

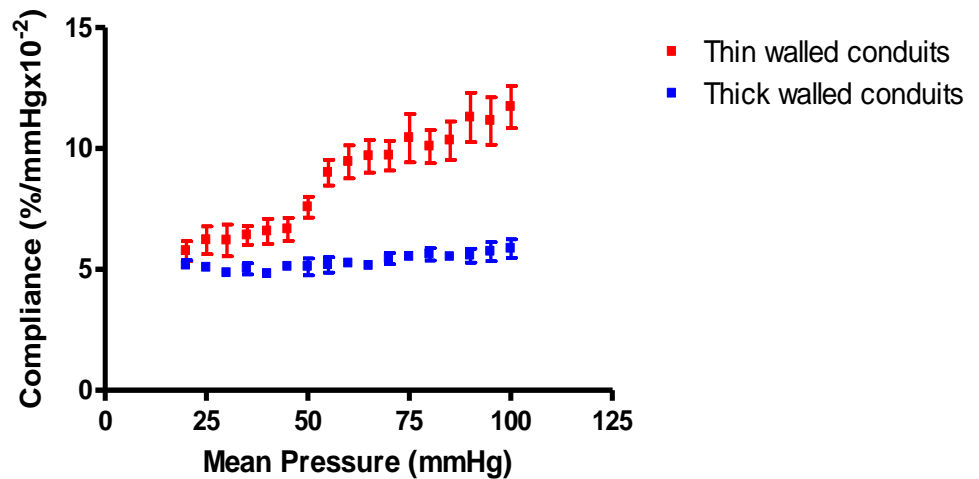


Fig 8.3. The compliance profiles of thick and thin-walled 2% POSS conduits.

Fig 8.3 shows the compliance range for PCUPOSS tubes. The thin grafts were more compliant than their thicker walled counterparts, as would be expected from the derivation of compliance (C) from elastic modulus (E) which demonstrates an inverse proportion relationship between wall thickness and compliance. The derivation for this relationship is shown in equations 4 and 5 in chapter 2.

Other groups manufacturing polymeric vascular conduits have made similar findings³²². Arterial wall thickness also shows a link with compliance - a direct correlation has been made between arterial stiffness and intima-media thickness, stimulating measurement of the latter to assess cardiovascular risk⁶⁰. However, in this case, it is not due to a mechanical mass effect; rather a result of cellular adaptation to the prevailing haemodynamic conditions, similar to IH.

The thick walled conduits were in the predetermined desired range. However, it is important to consider the compliance across the range of pressures. As discussed in chapter 2, arterial compliance reduces at higher stresses in vivo. In physiological terms, at high blood pressures, the vessel is stiffer. This is a consequence of the gradual recruitment of collagen at higher

pressures. It is a safety feature preventing over-distension in the face of the repetitive abrupt changes in stress involved in pulsatile flow. This variation of elastic properties is one reason why it is not adequate to consider elasticity of the arterial material at a single stress level, requiring the concept of incremental elastic modulus or compliance.

The ideal graft would conform with arterial compliance at all physiological pressures, not just for reasons of compliance matching but also to prevent over-distension. The bypass prostheses in current use do not have the problem of over-distension due to their inelastic status. However, development of elastic alternatives requires incorporation of the composite model demonstrated in arteries by way of the complementary systems of elastin and collagen. The issue has been addressed at both molecular and macroscopic levels.

At the macroscopic level, Sonada developed a compliant graft with a coaxial "tube inside a tube" system⁷⁴. This was effectively a microporous compliant graft made from poly(ether)urethane with a less porous outer sleeve. The wall thicknesses of each was designed to confer the high compliance due to elastin (inner conduit) at low pressure and low compliance due to collagen (outer sleeve). This concept is demonstrated in Fig 8.4.

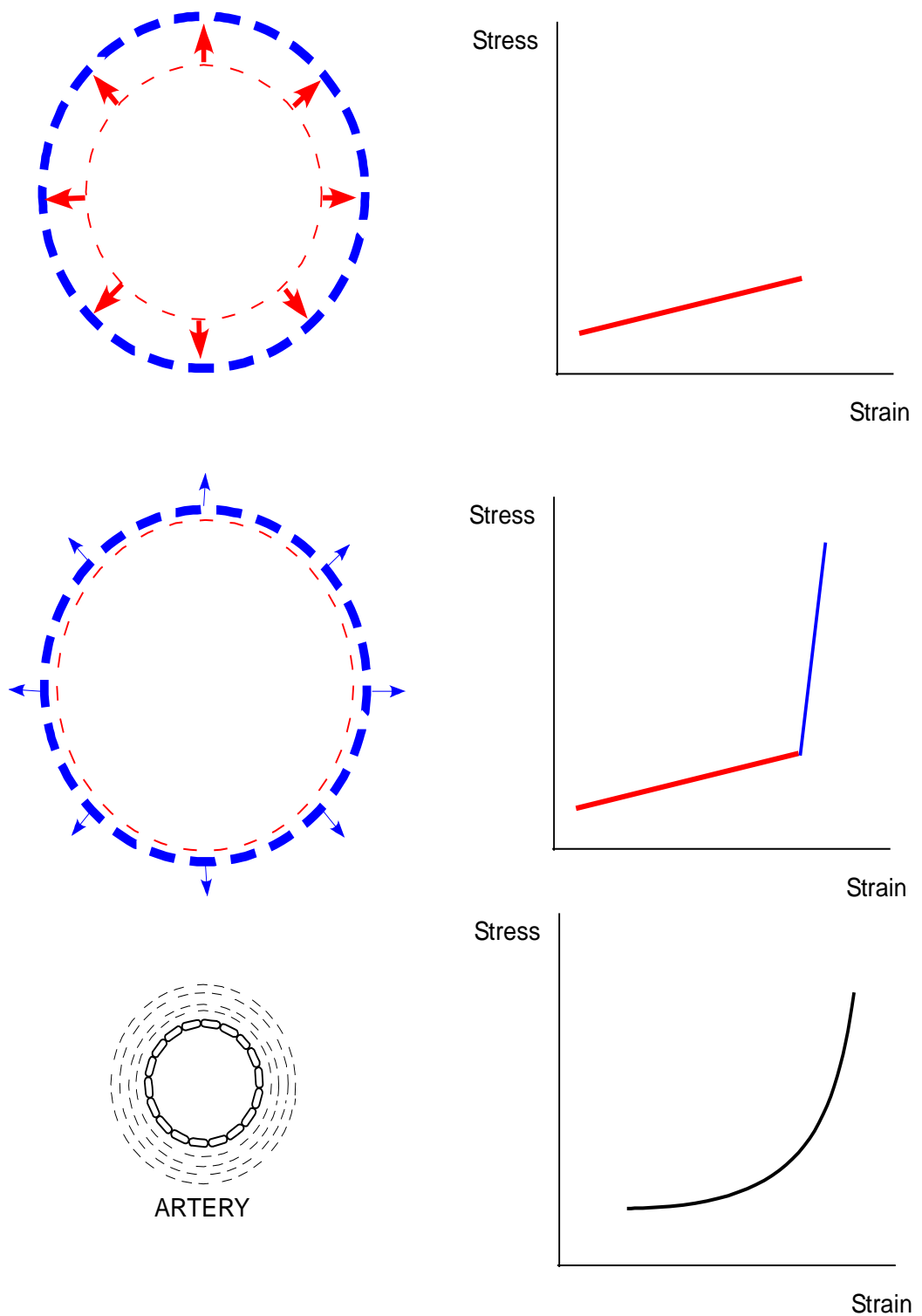


Fig 8.4. Initial distension of highly compliant inner conduit until the less compliant outer sleeve is abutted results in a composite stress strain relationship which can approximate the 'J-shaped' stress-strain curve of artery.

Theoretically, the same behaviour can be expected of elastomeric polymers via the phenomenon of strain crystallisation. The initial high distensibility is due to the aligning of the hard segment chains within the soft segment matrix. Once the former is aligned longitudinally along the plane of extension, the subsequent distensibility is low, representing the stretching of the hard segment chains themselves.

However, the thin walled grafts were displaying the opposite phenomenon. At higher mean pressures, there was an increase in compliance. This quality may predispose these grafts to aneurysmal behaviour over time. It is also represented by the convex shape obtained in the tensile test curve for the same graft – Fig 7.15 and 7.17. The thick-walled grafts showed a uniform compliance of $5\%/mmHg \times 10^{-2}$ which is also represented by the linear (Hookean) elastic relationship shown in the initial part of the tensile tests for this graft – Fig 7.16 and 7.18.

In order to understand the reasons for the increasing compliance of 2% POSS thin grafts, the original shape of the stress-strain relationship needs to be reconsidered – Fig 8.5.

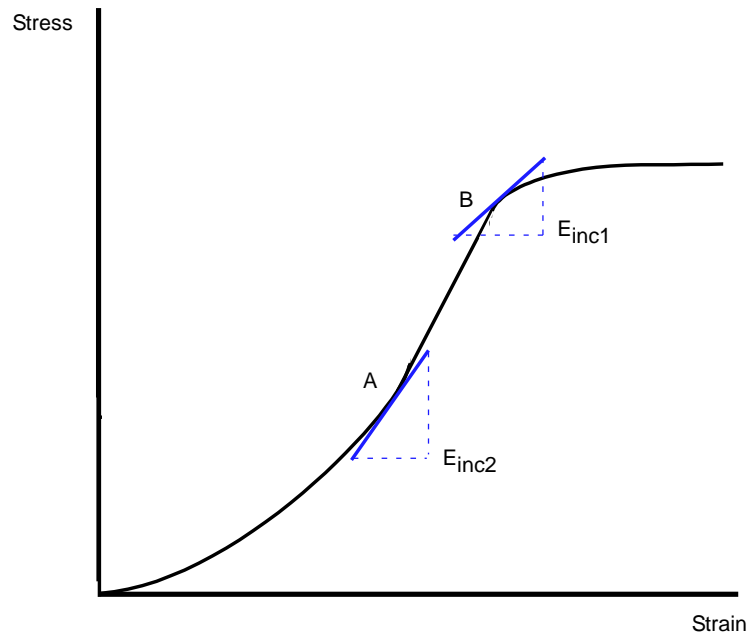


Fig 8.5. The typical sigmoid curve generated from tensile testing of polymeric samples. Tangential points are included to demonstrate the incremental elastic modulus at different parts of the curve.

This shows that there is a varying incremental elastic modulus (E_{inc}) at different points along the curve, as given by the gradient of the tangent. Therefore $E_{inc2} > E_{inc1}$. It can be seen that until point A, there is an increasing E_{inc} . Between A and B, E_{inc} is constant and subsequently, it falls. The relationship between E_{inc} and compliance is inversely proportional as seen in equation (3), so at the lowest pressures, compliance is reducing, followed by a section of uniform compliance and finally, at the highest pressures before failure, the compliance increases.

From this it can be seen that it is desirable to remain in the range between the origin and point B, as the region of increasing compliance is immediately before mechanical failure. This would suggest weakness and therefore unsuitability of the thin walled 2% POSS conduit for physiological use. However, the compliance graph needs to be seen in the context of the tensile test for the same graft, represented in the previous chapter – Fig 7.15, 7.17 and 7.23. These are not typical polymer stress-strain relationships. In each instance, the inflection point B arrives early in the tensile test with the majority of the stress loading until failure of the sample occurring after this point. In fact there is a long period of Hookean (uniform) elasticity after inflection point B. Therefore it is not a foregone conclusion that the 2% POSS grafts would not be able to withstand high pressure haemodynamic flow over the long term.

It was hypothesised that the reason why thin PCUPOSS grafts did not show the desired reduction in compliance through strain-crystallisation at higher mean pressure may be due to the highly porous structure with the very thin interpore walls failing at relatively low stress, and in doing so, rapidly increasing the stress across the remaining graft wall. If the pore structure resulting from the coagulation-phase inversion technique was to be utilized, a stronger but equally compliant polymer was required. As the introduction of POSS to the PCU polymer has been shown in tensile testing to strengthen the nanocomposite structure a new polymer was synthesised with an increased concentration of MDI and POSS, with the aim of strengthening the soft segment. Due to stoichiometric considerations, 6% POSS was the next level of nanomolecule incorporation to maintain the polyurethane chemistry. The results are shown in Fig 8.6.

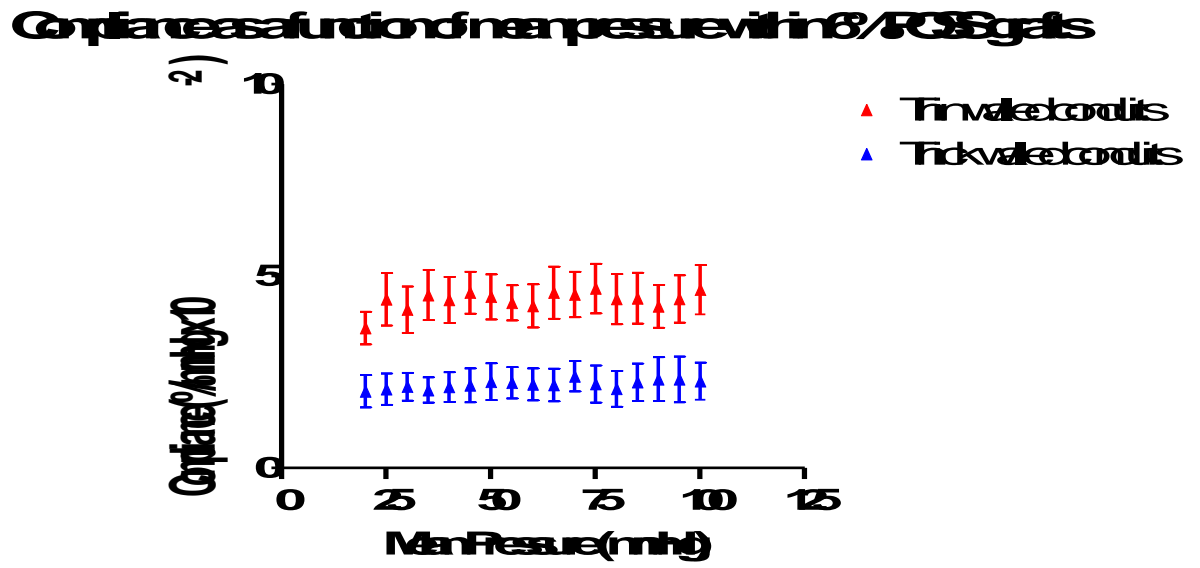


Fig 8.6. The compliance profiles of thick and thin-walled 6% POSS conduits

Just like the thick-walled 2% POSS conduits, the thin-walled 6% conduits demonstrated uniform compliance through the range of pressures, correlating with the favourable section of the tensile curve between point A and B (Fig 8.5). However, the 6% POSS grafts were less compliant than their 2% POSS counterparts at comparable dimensions. So although for the same wall thickness, there is the desired shift towards the left in the tensile curve, the aim of doing so whilst simultaneously maintaining high compliance, was not achieved.

Increasing the proportion of hard segment would theoretically give a similar effect as increasing the proportion of POSS, as the hard segment acts to strengthen the relatively weak soft segment. The polymer was synthesised with increased MDI and ethylene diamine to investigate this. As expected, the consequence of increasing the hard segment proportion in the nanocomposite was to reduce its compliance – Fig 8.7. This is also what occurs when the hard segment is increased in traditional segmented polyurethanes³⁴³. Thick walled equivalents were discounted from further testing as poor compliance was expected.

Compliance as a function of mean pressure within 2% POSS grafts with increased hard segment proportion

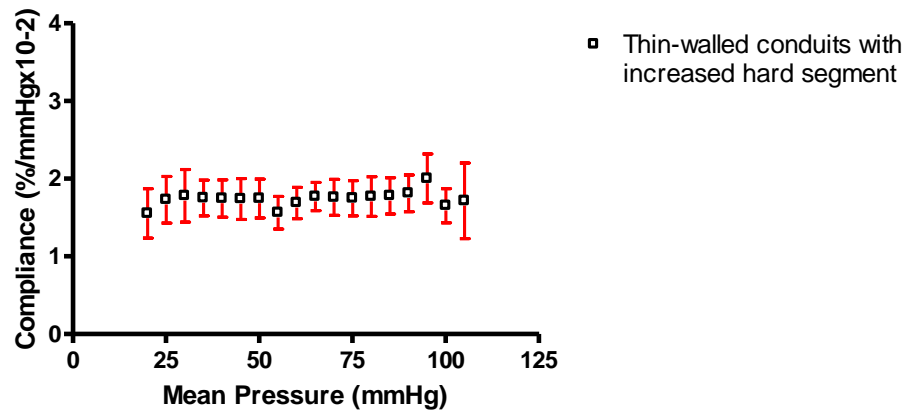


Fig 8.7. Increasing the hard segment results in a reduction of compliance.

Rather than increasing the hard segment, hard segment modification was then considered. Disrupting the strict linearity and hence crystallinity of this phase was achieved by replacing the ethelene diamine chain extender with 1,3 diaminocyclohexane. The effect was to create branched hard segment chains rather than straight chains. Fig 8.8 shows the compliance of grafts made from this polymer.

Compliance as a function of mean pressure within grafts with a disrupted hard segment

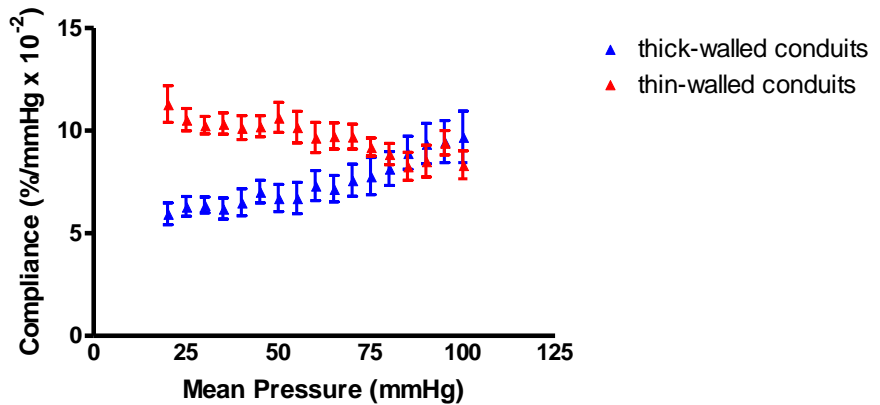


Fig 8.8. Chain-disruption of the hard segment results in a maintenance of compliance.

The thin-walled grafts showed the desired feature of reducing compliance at higher mean pressure. The effect of this improved safety profile on the burst strength of the graft compared with the original linear chain hard segment graft was investigated.

8.3 Burst Pressure

Fig 8.9 shows the burst pressures obtained for each graft type.

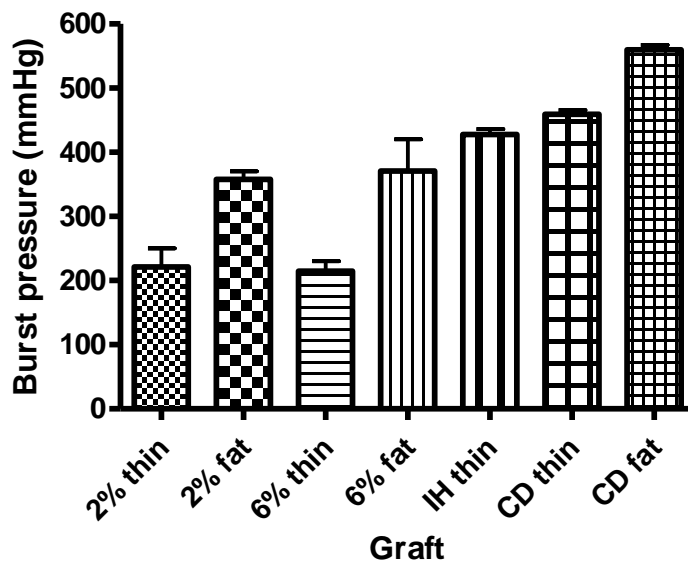


Fig 8.9. Burst pressures and standard deviations for each graft type.

The strength of the final structure is determined by the pore structure as well as the precise alignment, H-bonding and 'virtual crosslinking' between the amorphous and crystalline phases. The cast sheet with no pores is very strong (tensile strength $\geq 60\text{MPa}$) suggesting a high degree of interaction between the hard and soft segments. However, this method of manufacture allows copious time for the two phases to achieve optimal order. In contrast, coagulation is a considerably faster process with coagulant rushing into the polyurethane substance in exchange for solvent¹³² with a solid structure forming within

seconds. This may not give the time required for positioning of the two phases, which along with the porous character may lead to a weak conduit. These are possible reasons for the low burst pressures obtained for the 2% and 6% POSS thin walled conduits. The latter did not achieve the expected increase in strength over the 2% POSS graft. On the other hand, increasing the total proportion of hard segment did double the burst pressure to 400mmHg. In comparison, the burst pressure for the internal carotid artery is approximately 5000mmHg²³². PTFE was introduced by Gore as a vascular prosthesis with a burst pressure of 600mmHg⁵¹. One way to strengthen the conduits is to increase their wall thickness, as the maximal force applicable to a cylindrical vessel, f is given thus:

$$f = Pd/2t$$

where P is the burst pressure, d is the vessel diameter and t is wall thickness. As f and d are constant, the burst pressure P would ordinarily be directly proportional to wall thickness t ; however, this is only true for a cylinder with a homogenous wall whereas our grafts demonstrate a gradient of porosity through the wall. Nevertheless, an increased wall thickness did lead to a dramatic loss in compliance.

Hence, without modification of the hard segment, a stronger yet simultaneously compliant graft was not possible using this the extrusion-coagulation manufacture technique. A higher POSS concentration in the hard segment did not significantly affect strength for the porous structure. Increasing the hard segment proportion did strengthen the graft as would be expected, at the expense of a further loss of compliance. Chain-disrupting the crystalline phase however produced grafts which had both enhanced compliance and circumferential strength. Both of these could be as a result of optimisation of the interaction between the amorphous and crystalline phases due to the branching hard segment providing a greater surface area for that interaction. In particular, hard segment disruption may cause a stronger graft via increased H-bonding and van der Waals forces between the two phases.

Polycarbonate exhibits greater in vivo biostability than either polyether or polyester⁴⁰ and would be highly desirable as a long term biological implant. Nanotechnology has previously been used to toughen polycarbonate³⁴⁴, and

despite the high porosity of the graft walls and the thin walls necessary for optimal compliance, a polycarbonate-based polyurethane is strong enough to handle the expected range of blood pressure. Many patients requiring vascular bypass surgery will be hypertensive, so the upper limits for the expected range will be more than 140/90. However, 400mmHg will never be achieved clinically by this group of patients, although blood pressures of 400/320 have been noted in powerlifters during their sport!

8.4 Viscoelasticity

Fig 8.10 and 8.11 demonstrate viscoelastic loops which result from pulsatile flow through a single 2% POSS thin conduit. These recordings were taken after a steady state had been achieved during pulsatile flow. From a single loop, the elastic distension ratio (EDR) was calculated and these are shown in Fig 8.12.

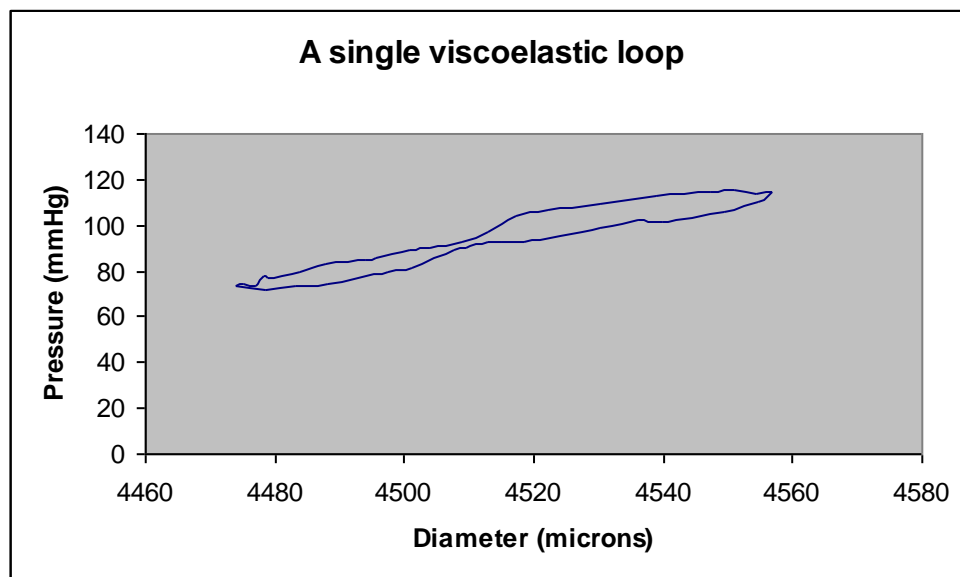


Fig 8.10. A single viscoelastic loop measured during steady pulsatile flow through a 2% POSS thin conduit.

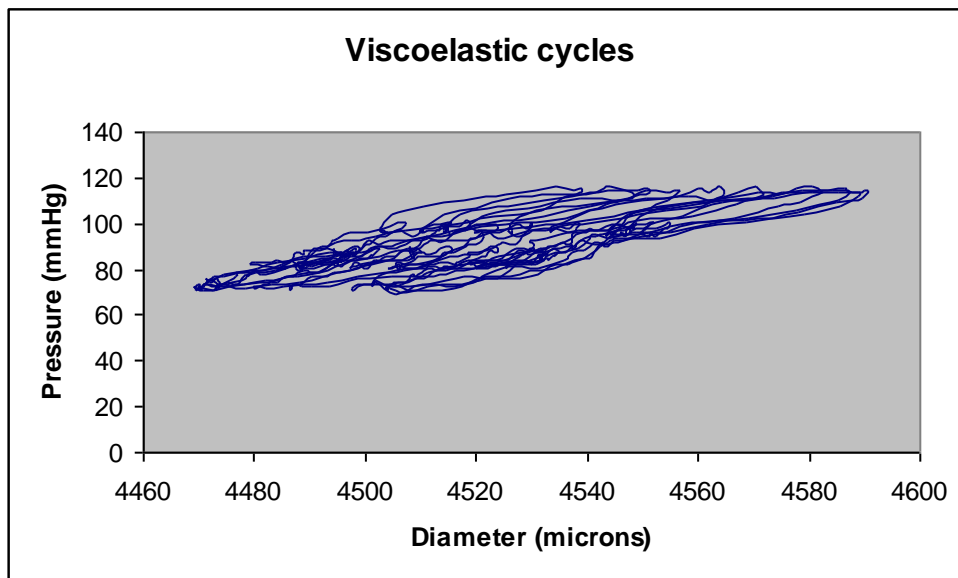


Fig 8.11. Fifteen consecutive viscoelastic cycles during steady state pulsatile flow through a 2% POSS thin conduit. The area within each loop was similar, with the demonstrated variation being caused by lateral conduit wall movement due to the pulsatile flow.

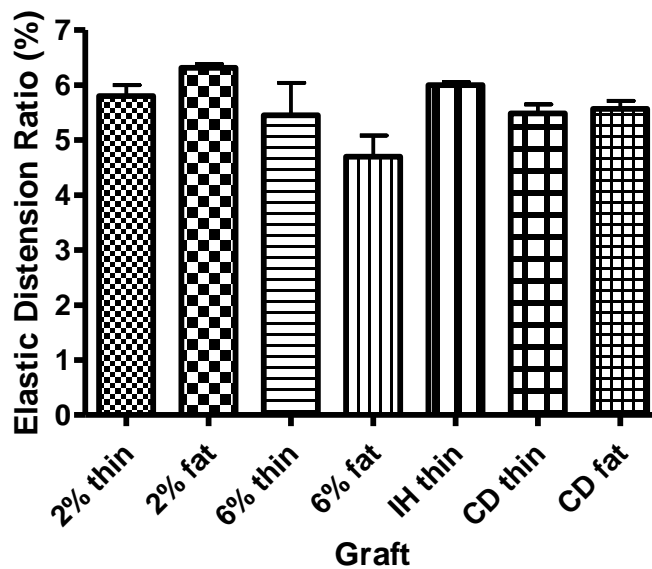


Fig 8.12. Elastic Distension Ratios for each graft type with standard deviation.

The overall EDRs were comparable with human arteries. Shau et al³⁴⁵ found EDR for brachial, radial and dorsalis pedis arteries to be 6.34%, 6.15% and 5.6% respectively. As with the artery, the diameter at any point during systole was higher than the same pressure in the diastolic phase. The difference between the two (quantified by elastic distension ratio) indicates the energy imparted into the vessel wall. In the case of an artery, excessive loss of pulsatile energy into the wall results in a requirement for increased ventricular work and even cardiac failure³⁴⁶. For this reason, the pulmonary artery does not demonstrate significant viscous behaviour. It is also why excessive viscosity of smaller calibre grafts should be discouraged.

The role of the viscous component is to smooth the coupling between a pulsatile mechanical output from the heart and a steady non-turbulent stream at the peripheries. A further advantageous consequence of storing energy in the wall is that the diameter change during the cardiac cycle is lowered. In addition as viscous behaviour is dependent on the rate of change of stress, the strain on the wall at times of high cardiac output is not greatly increased, due to the increase in heart rate. These limits safeguard against excessive stress and over-distension.

8.5 Longitudinal strain

Figs 8.13-8.18 show the lengthening that results from intraluminal pressure for each graft type.

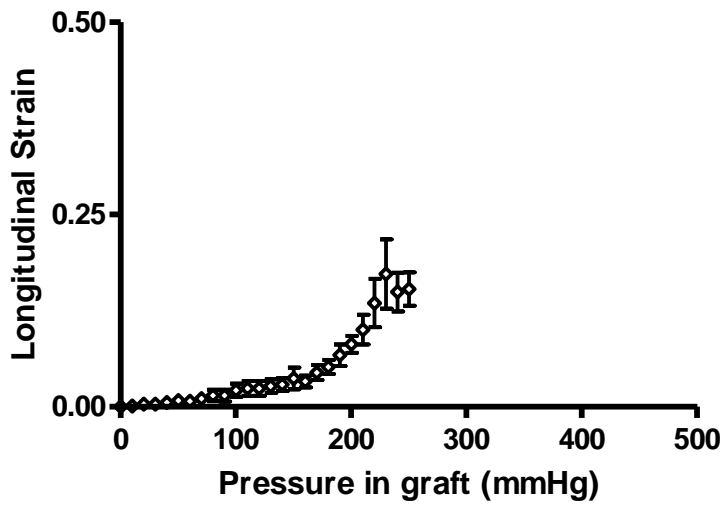


Fig 8.13. Longitudinal strain due to pressure within the grafts: 2% POSS thin

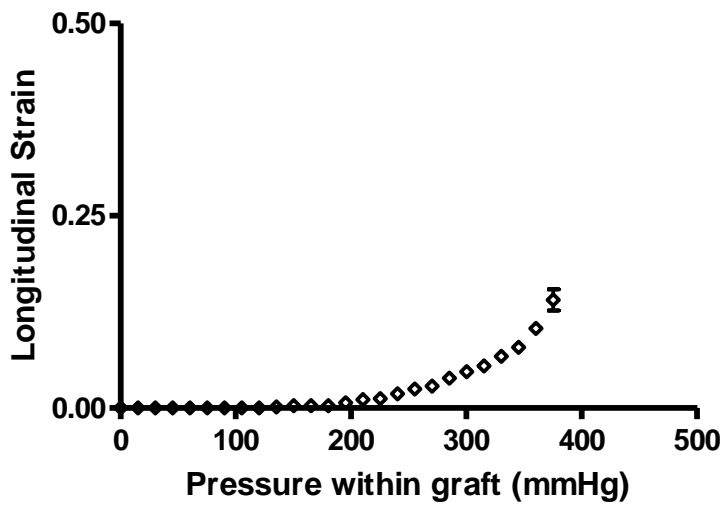


Fig 8.14. Longitudinal strain due to pressure within the grafts: 2% POSS fat.

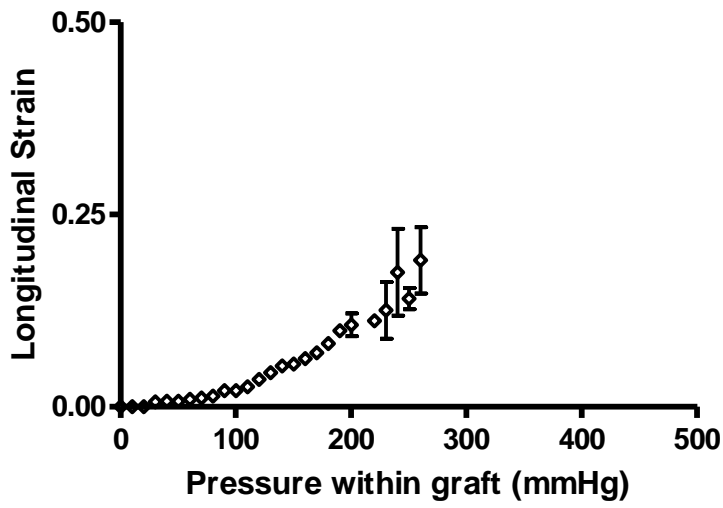


Fig 8.15. Longitudinal strain due to pressure within the grafts: 6% POSS thin

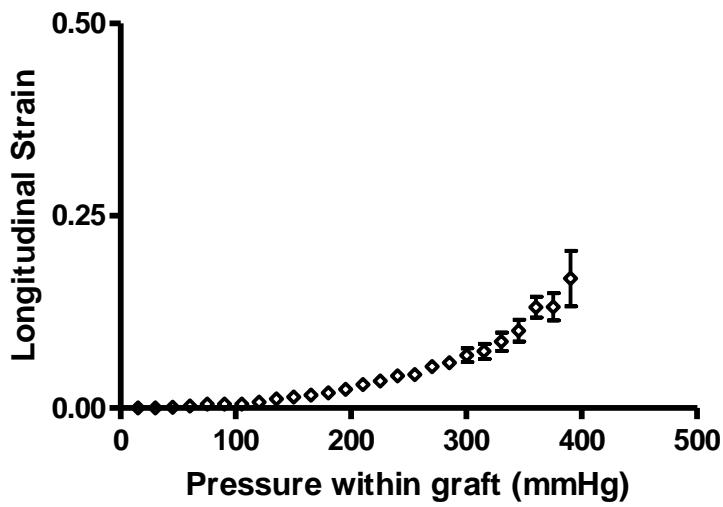


Fig 8.16. Longitudinal strain due to pressure within the grafts: 6% POSS fat.

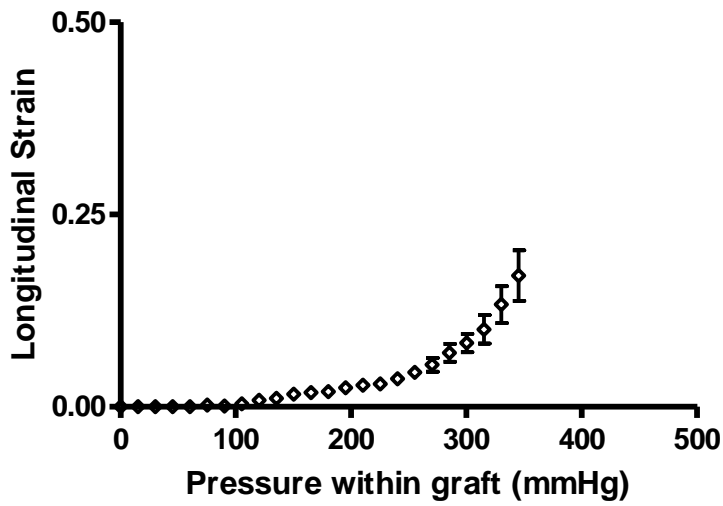


Fig 8.17. Longitudinal strain due to pressure within the grafts: 2% POSS thin with increased hard segment.

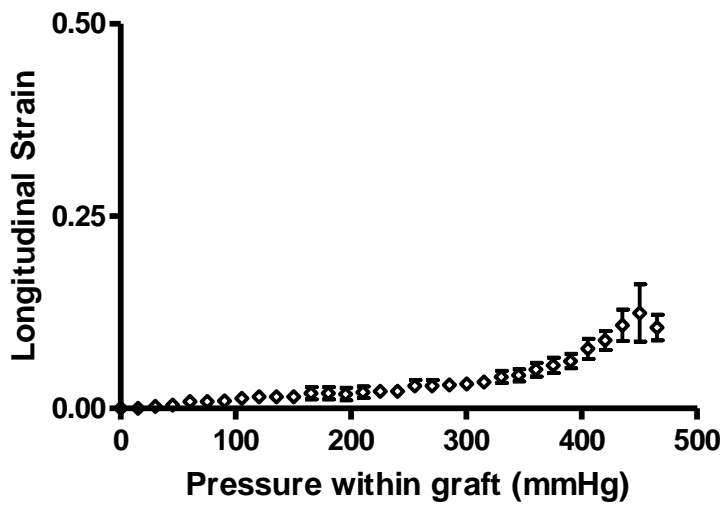


Fig 8.18. Longitudinal strain due to pressure within the grafts: 2% POSS thin with hard segment chain disruption.

The strains calculated are small within the physiological blood pressure range, provided an initial 10% longitudinal stretch at implantation. The thick walled tubes demonstrated less elongation than their thin walled counterparts. Both hard segment modifications resulted in lower elongation for a given pressure than the unmodified nanocomposites. The chain disrupted conduits showed especially low longitudinal strain, even at pressures over 400mmHg despite being the most compliant. This suggests anisotropy of the material, or different elastic properties depending on the orientation being tested²³². Furthermore, the 6% POSS conduits showed greater longitudinal strain than their 2% counterparts. In view of the lower circumferential compliance of 6% tubes, this shows a further accentuation of anisotropy. It may be that increased POSS concentration may serve to align the hard segments circumferentially, reducing elasticity radially but not longitudinally. Anisotropy is a feature of all biological tissues including arteries³⁴⁷. It is of critical importance when considering vascular grafts as significant elongation would result in oscillation of the whole conduit during pulsatile flow. This puts additional stress on the anastomoses, hinders optimal incorporation into the surrounding tissues and adds to turbulence of flow. At the extreme, it can cause buckling of the graft. The fact that the CD thin conduits reveal such anisotropy infers that the two phases are aligned to promote circumferential stretch but to discourage axial lengthening when compared with the other polymers. It has been demonstrated that there is significant longitudinal movement during pulsatile flow through the human aorta, carotid, brachial and popliteal arteries in vivo³⁴⁸. This appears to be greater for the intima-media than the adventitia, causing a relative shear stress between wall layers. However, this is only partly due to circumferential stressors. The viscous nature of the arterial wall is also responsible for longitudinal shear which would be most pronounced at the intima since this is the blood/vessel interface at which the shear stress is being exerted.

8.5 Conclusion

Incorporation of POSS into a polycarbonate-based-polyurethane has produced a non-thrombogenic nanocomposite with greater biostability than previous poly(ether) and poly(ester) urethanes. Although cast sheets of this

material are extremely strong, in this form at low stress levels, their distensibility is negligible, making compliance mismatch inevitable when used clinically for small artery bypass. A highly porous structure increases compliance but reduces the strength of the resultant graft. Porous grafts were manufactured and their mechanical properties were tested.

No increase in strength occurred at higher levels of POSS. However increasing the hard segment component increased burst pressure from 200mmHg to 400mmHg. Increasing the proportion of POSS or hard segment in the nanocomposite caused a reduction in compliance. As with increasing the hard segment, the effect of increasing wall thickness was to increase strength at the expense of a loss of compliance. However, modification of the hard segment by chain disruption techniques have lead to a 5mm diameter conduit with a compliance of $5\%/mmHg \times 10^{-2}$ - similar to the superficial femoral artery; a viscous component providing energy capacitance during pulsatile flow, thereby reducing stress at the vessel wall and smoothing the pulsatile output from the heart to a non-turbulent stream at the periphery. The burst pressures for such grafts is well in excess of the levels that would be expected clinically and they are not at risk of elongation and buckling when implanted into the vasculature provided a 10% longitudinal stretch.

The favourable mechanical and biocompatibility studies make the chain disrupted graft ready for in vivo evaluation. However, modification of the extrusion process or additional external reinforcement such as microfibre electrospinning will be required to strengthen the grafts further before human trials can be considered.

Conduit	Hard Segment characteristic	Wall thickness	Number tested
2% thin	2% POSS	0.33mm	6
2% fat	2% POSS	0.58mm	6
6% thin	6% POSS	0.33mm	6
6% fat	6% POSS	0.58mm	6
IH thin	2% POSS with increased hard segment	0.33mm	6
CD thin	2% POSS with chain disrupted hard segment	0.33mm	6

Table 8.2. Summary of all conduits tested. The basic polyurethane consisted of a polycarbonate soft segment with hard segment containing 2 or 6% silsesquioxane. The hard segments were further modified by increasing their proportion overall (without adding more POSS) and by interrupting their three dimensional structure.

9

The methodology of burst pressure measurement

9.1 Introduction

When polytetrafluoroethylene was introduced as a vascular bypass graft material in 1975 by Impra and Gore, its burst pressure was assessed to be in the region of 600mmHg⁵¹. However, after its clinical use commenced, a number of cases of aneurysmal dilatation were reported, leading to an examination and optimisation of the sintering process used during graft manufacture, as well as the emergence of externally reinforced PTFE prostheses.

As discussed earlier despite the poor long-term patency of PTFE in small calibre (<6mm) bypass, no suitable alternative has been forthcoming. However, there is an ongoing large volume of research into synthetic materials for vascular implantation. We have seen how in terms of mechanical characteristics, the ideal prosthesis would demonstrate similar viscoelastic properties to native artery, whilst simultaneously being able to cope with physiological blood flow. This latter is both in terms of absolute pressure and also defatiguability in high cycle testing.

Segmented polyurethanes are at the forefront of material research for potential vascular prostheses²⁴⁴, due to their combination of elasticity and strength. As detailed in chapter 5, this is a result of their dual phase

configuration with crystalline hard segments floating in an amorphous soft segment with virtual crosslinking with van der Waal interactions and hydrogen bonding between the two. Additionally, polyurethanes have a low inflammatory response in vivo unlike rubber and traditional silicone rubbers. However, at present there are no polyurethane prostheses in general clinical use as vascular prostheses due to their long term biodegradation, poor thrombogenicity profile and the difficulties in producing polyurethane with the combination of high compliance and strength⁴⁰.

Although polyurethanes are elastic, they have high elastic moduli – the distensibility at the low pressures found physiologically is low. In order to increase their distensibility, various methods have been used to impart porosity to the conduit walls. Porosity is also desired to promote graft healing after implantation by transmural fibrovascular infiltration and in vivo endothelialisation after implantation²⁰⁶, with an ideal pore size between 10 and 45µm⁸¹. However, a very high pore size causes over-exuberant fibrous infiltration and a loss of elasticity⁸⁰. In most cases, the degree of porosity required to simulate arterial distensibility in vitro is high. Unfortunately, a highly porous graft is much weaker than its non-porous counterpart. Therefore careful assessment of burst strength is critical in the progress of a potential graft through to the phases of in vivo work and subsequent clinical trial.

A multitude of different methods have been used to measure burst pressure in tubular conduits. These methods usually consist of subjecting the grafts to increasing intraluminal pressure until they burst. However, the rate of pressure increase, the mechanism used to provide this pressure and the interface between the graft and the pressurising fluid vary considerably.

Porous PCUPOSS grafts have been subjected to burst pressure testing using water at varying rates of infusion. Their burst strengths have been measured with and without a highly compliant latex sleeve inside the graft to transmit pressure to the graft wall. The aim was to discover whether the differences in methodology caused any difference in the results obtained.

9.2 Materials and Methods

2% POSS-incorporated grafts were manufactured by the extrusion-phase

inversion technique described in chapter 6.

9.2.1 Burst pressure assessment

A high pressure syringe pump (Harvard Apparatus PHD 2000 Programmable) containing freshly deionised water (pH 7.0) was connected via a transducer (Honeywell Component No. 22PCCFB6G) to 8 cm lengths of graft with or without a non-porous latex tube lining. This was vertically suspended with distal clamping and weighted to ensure 10% longitudinal stretch. The transducer was precalibrated by connecting it to a standard clinical sphygmomanometer and a voltmeter to record voltage readings at 0mmHg, 100mmHg and 200mmHg from which offset and gain figures were calculated and entered into a personal computer with bespoke software for recording the pressure at a sample rate of 10Hz. The transducer was connected via a 10v power source to the personal computer. Water was expelled from the pump with the graft unclamped to allow the apparatus to be filled completely, whilst ensuring all air was eliminated from the apparatus. The clamp and weight was applied and the water infused at 0.2ml/min; 50ml/min and 100ml/min in those grafts with latex lining. For the graft without latex inner lining, an initial infusion rate of 0.2ml/min was commenced, and this was gradually increased to take account of the percolation of water through the wall at high pressure and ensure an increasing intraluminal pressure. Figure 9.1 summarizes the different methods.

The infusion was continued until the graft material burst, and the burst pressure recorded.

9.2.2 Data collection and statistical analysis

6 grafts were subjected to each method and mean and standard deviations (SD) of burst pressure and flow rate were calculated. One way ANOVA parametric variance analysis with Tukey post test analysis was undertaken to compare the results of the different methods.

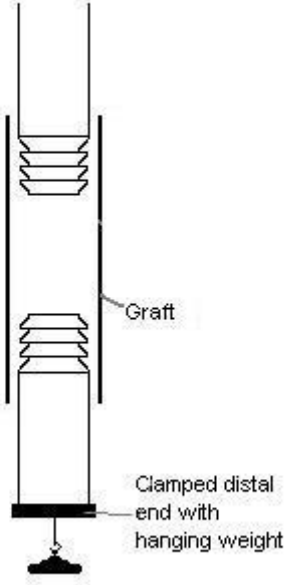
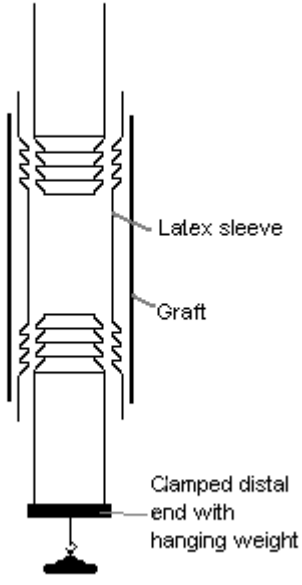
<p>Initial infusion rate: 0.2 ml/min Final infusion rate: 4.0ml/min</p>	<p>Infusion rate: 0.2 ml/min 50 ml/min 100 ml/min</p>
	

Fig 9.1. Summary of the different burst pressure measuring techniques.

9.3 Results

Fig. 9.2 shows the burst pressures for each method used. The statistical summary of comparison is tabulated in table 9.1. The use of a latex inner lining resulted in a significantly increased burst pressure. An infusion rate of 0.2ml/min produced a lower burst pressure than 100ml/min. There was no significant difference in burst pressure between 0.2ml/min and 50ml/min or 50 and 100ml/min.

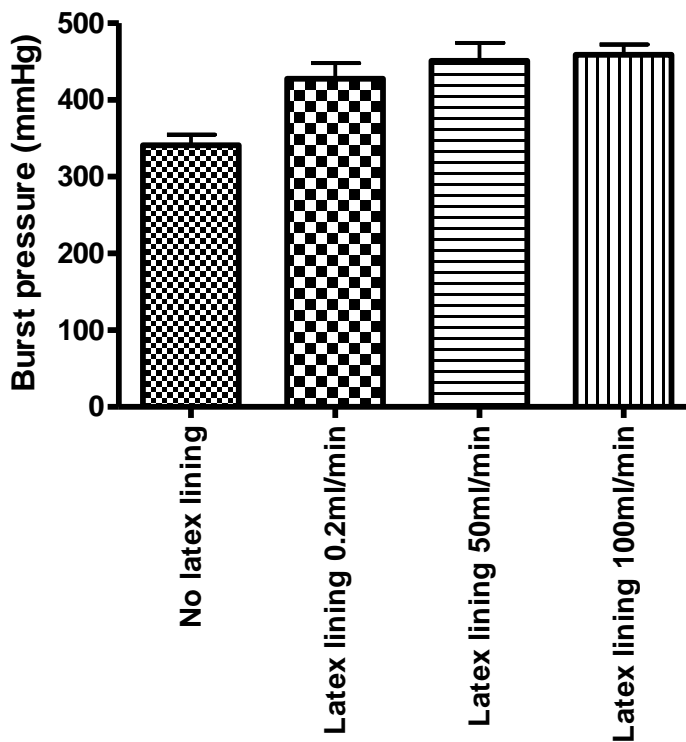


Fig. 9.2 Burst pressures obtained via the different measuring techniques. Data are mean \pm SD of six experiments.

	P value
No latex lining vs Latex lining 0.2ml/min	P < 0.001
No latex lining vs Latex lining 50ml/min	P < 0.001
No latex lining vs Latex lining 100ml/min	P < 0.001
Latex lining 0.2ml/min vs Latex lining 50ml/min	P > 0.05 (N/S)
Latex lining 0.2ml/min vs Latex lining 100ml/min	P < 0.05
Latex lining 50ml/min vs Latex lining 100ml/min	P > 0.05 (N/S)

Table 9.1. The significance of the differences in results between the four different methods. (N/S) = non-significant

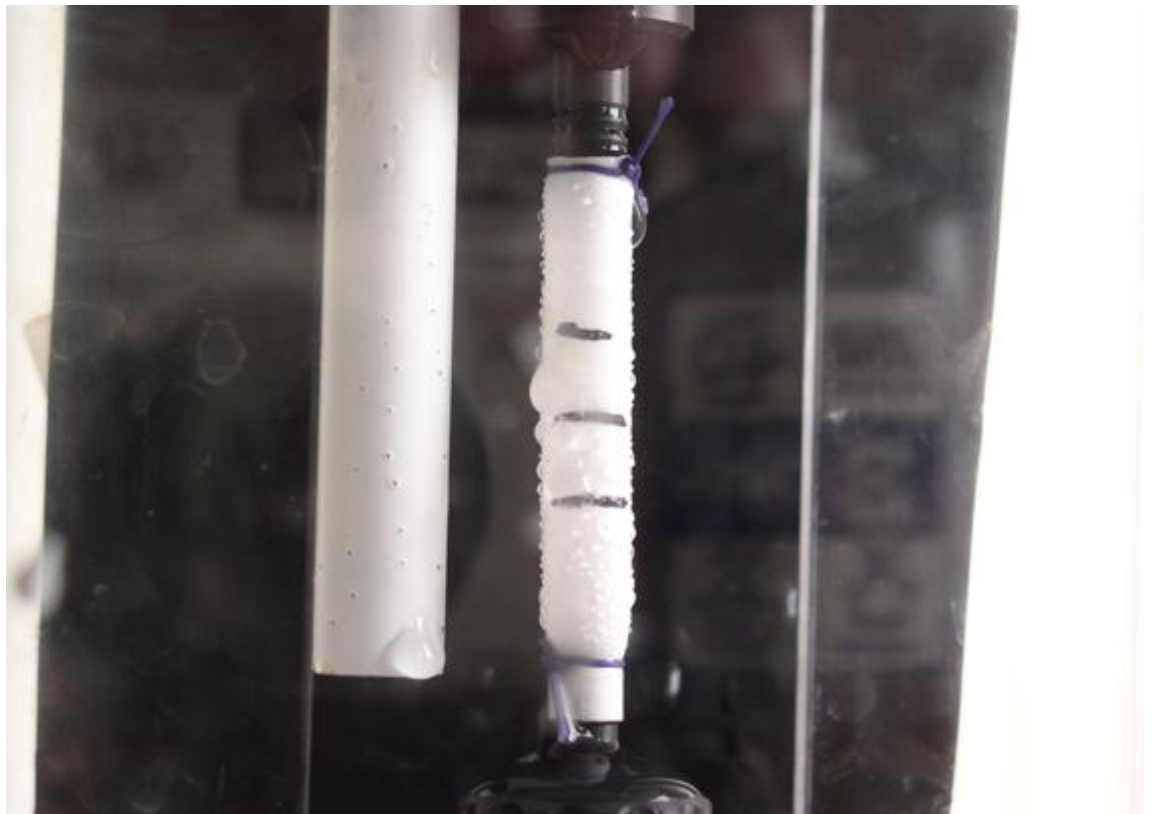


Fig 9.3. Subjecting a graft with an interconnected porous structure to intraluminal pressure of 300mmHg leads to 'sweating' of water through the wall.

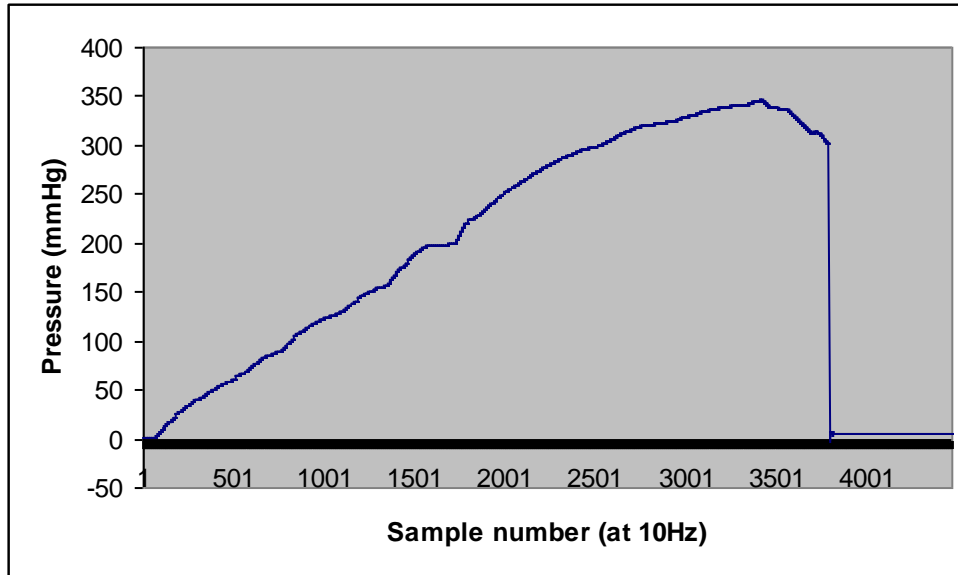


Fig. 9.4 The aneurysmal point is a more accurate term than burst pressure, defined as the point at which further infusion at the same rate does not result in any increase in pressure (in this case 347mmHg).

Fig. 9.3 shows an example of the percolation of water through the conduit wall at high pressure when a latex lining was not used. Fig. 9.4 shows how a peak pressure is reached before a reduction of pressure occurs despite continuing infusion, due to aneurysmal dilatation of the graft.

9.4 Discussion

The conduits tested had an open porous structure. This interconnected network of pores is a prerequisite for transmural migration of cells to promote endothelialisation. However, when pressurised, the effect is to force water through the pores leading to sweating through the graft wall – see Fig. 9.3. There are several consequences that follow. Firstly, the rate of infusion needs to be increased to ensure the intraluminal pressure continues to increase. Secondly, the degree of sweating increases in line with increasing pressure, due to the stretching of the interporous walls. This causes the pores to increase in size, raising the overall permeability of the wall. At very high pressures, fracture of the interporous walls occurs causing coalescence of pores into larger cavities. Due to the interconnecting nature of the pores, the pressure is instantly equalised between adjacent pores. On coalescence of two pores, this same pressure is in effect exerting stress on a larger balloon. The wall tension increases in proportion to the increased radius as given by Laplace:

$$T = \Delta p r / 2$$

where T represents tension in the pore wall; Δp is the change in pressure; r is pore radius. This increase in tension makes it likely that the new cavity will also burst and coalesce into a larger cavity. This mechanism eventually leads to the graft bursting.

In practice, blood will interact with the graft wall differently to water. Its progress through the open pore network will be impaired due to the larger size of particles involved. This will result in a non-uniform distribution of pressure across the graft wall. Also, the blood will leave a thin layer of clot on the luminal surface, effectively closing the pore system. This is an argument for using a non-porous latex sleeve which tests the strength of the whole wall thickness.

However, porous grafts are now being developed which are designed to discourage thrombus formation⁵⁰. In addition, thrombus cover may not be uniform, leading to patches which are vulnerable to pore coalescence.

Graft failure due to the redistribution of tension across large cavities due to pore coalescence is analogous to the mechanism by which Dacron grafts weaken. Dacron prostheses consist of knitted or woven fibres. Initial strength is lost due to the fraying and eventual breakage of a single fibre. This may be initiated by yarn slippage within the canvas causing an area of increased localised stress³⁴⁹. This leads to greater strain on the remaining fibres, as the same stress is exerted on fewer fibres³⁴⁹. The initial fraying of a single fibre by biodegradation³⁵⁰ can occur despite the high crystallinity of Dacron, resulting in excellent biostability of the overall structure. Hence, high burst pressures demonstrated initially in the laboratory under static testing conditions, may be inaccurate, when compared to the implanted graft under high cycle pulsatile flow.

The higher burst pressures obtained when a latex sleeve is used suggests that the circumferential stress is being exerted equally across the whole wall rather than being concentrated through pores. However, the pore structure may make a non-porous lining essential due to the rapid transmural leaking of water. This is especially true for highly porous structures and those materials that are less porous but have very high burst pressures, such as expanded PTFE. Some groups have tested burst pressures at much greater rates of pressure increase than here, by connecting the conduits being tested straight to high flow gas supplies. The high infusion rates may be necessary in the methodology due to porosity allowing the gas to escape through the graft wall as fast as it is infused. At such high rates, the time between the development of a flaw and the subsequent rupture is almost negligible. By contrast, we found that slow infusion gradually lead to a point when subsequent continued infusion at that rate resulted in a reduction in pressure. We recognised this as the moment at which aneurysmal change was developing and at that infusion rate, no further pressure increase would occur before the graft would burst – Fig. 9.4. However, we found that if the rate of infusion was dramatically increased at this ‘aneurysmal point’ a further increase in pressure was possible.

Similarly to our findings, McClurken et al.³⁵¹ noted that a constant

infusion of water into a latex balloon which was lining a PTFE graft, such that the sample burst over 10-20 seconds led to a point where massive dilatation started to occur causing a drop in pressure, so that at the moment the graft actually burst, the pressure was much lower than at its peak. Our proposal is that a very high infusion rate could continue to increase pressure in the conduit despite the distension, thereby overestimating burst strength.

A viscoelastic component to the vessel wall properties also results in different mechanical behaviour depending on the rate of distension³⁵². Although previous studies have shown the grafts to have viscosity comparable with human artery, this experiment has not quantified the relative importance of viscosity.

Graft strength is the most fundamental characteristic of bypass grafts in development and therefore its accurate measurement is of paramount importance. The philosophy of measurement required by regulatory agencies such as the Food and Drug Administration (FDA) is to test above and beyond the limits which would be expected physiologically. At the same time, the FDA advocates a "least burdensome approach" to testing, recognising the large number of tests required to show graft safety³⁵³. These two philosophies are demonstrated by the FDA's approval of methods utilising water or saline rather than blood for burst pressure testing. In addition, although the difference in results due to different methodology for our grafts did not place them at risk of bursting in the physiological range of blood pressures, the difference is still very important as burst pressure is a fair indicator of structure, including any flaws, which is intimately related to the long term fatigue strength. For this reason, although precise qualitative guidelines are not given, the FDA is unlikely to approve synthetic grafts with burst pressures just above the physiological range.

In the reported literature, there is considerable variation in the methods used to measure burst strength which may lead to a discrepancy between results and subsequent graft performance after implantation. Table 9.2 shows the methods described for reporting burst pressures for vascular grafts and anastomoses in papers catalogued on Medline over the last ten years. The importance of the method used has often been unrecognised, on occasion leading to the omission of significant methodology which may affect the final result.

Graft/Anastomosis	Method of burst pressure testing	Infusion rate (ml/min)	Burst pressure (mmHg)
Biodegradable polyester scaffold ³⁵⁴	Phosphate buffered saline (PBS) via syringe pump; no lining	0.67	>120
Seeded carotid acellular matrix ³⁵⁵	Media perfusion solution via peristaltic pump at 15rpm	Not applicable	1402 (mean)
Chitosan-blended polymer membrane-covered stent ³⁵⁶	Saline via syringe pump	4ml/min	>500 (reached limit of apparatus)
Glue adhesive anastomosis ³⁵⁷	Saline via hypodermic syringe	Variable (manual)	440(mean)
Crosslinked acellular porcine carotid ²⁶⁹	Distilled water via air pressure	Not given	2200 (approximate)
Heparinized acellular porcine carotid ³⁵⁸	Water via syringe pump	0.8ml/min	3440
Fibronectin tubes ³⁵⁹	Growth media via syringe	10mmHg/2min	187 (mean)
Haemostased ends of explanted porcine arteries (ultrasound, diathermy and clips) ³⁶⁰	Saline via hypodermic syringe	Variable (manual)	Range 128-854
Solder/laser treated rat femoral artery aneurysm ³⁶¹	Saline via syringe	Variable (manual)	>502
Heparinized acellular porcine carotid ³⁶²	PBS via syringe pump	45mmHg/min	Minimum 1912
Cryopreserved deendothelialised allograft vein with subsequent endothelialisation ¹³¹	'Fluid' filled syringe pump	Not given	2300 (approximate)

Haemostased ends of internal thoracic artery branches using harmonic scalpel ³⁶³	Air via hypodermic syringe	Variable (manual)	Range 210-350
Explanted canine carotid ³⁶⁴	High pressure nitrogen gas supply	Not given	Range 2600-5400
Porcine splenic artery anastomoses using protein-based solder ³⁶⁵	Syringe driver; fluid used not indicated	Not given	<1200
polyethylene glycol derived adhesive on collagen, carotid and PTFE defects ³⁶⁶	Water via syringe driver	5ml/min	<840
Seeded bioabsorbable polymer scaffolds ¹⁴⁶	PBS - system not described	Not given	Range 50-326
Hybrid polymer/tissue engineered grafts ³⁶⁷	PBS via syringe pump	3mmHg/sec	>240
Microporous polyurethane ¹³²	Air pressurized device	300mmHg/sec	Approximate range 1710-2200
Rat femoral artery anastomosis – sutures, sleeve, laser ³⁶⁸	Saline via syringe pump	2ml/min	Range 140 - >1500
Protein solder and collagen patch repair of porcine arteries ³⁶⁹	PBS via syringe pump	Not given	Range 100-600 (approximate)
Diathermy haemostasis of animal arteries and veins ³⁷⁰	Not described	100mmHg/sec (artery); 10mmHg/sec (vein)	Range 195-771

Table 9.2. Methods used and results obtained for burst pressure testing of tubular conduits over the last ten years. A Medline search was undertaken for the key-term “burst pressure”.

9.5 Conclusion

Using a latex sleeve increases the burst pressure obtained. This is due to the pores being negated by the non-porous sleeve. However, the mechanism by which graft failure occurs in-vivo may not be via pore coalescence, due to initial clot formation followed by a confluent neointimal layer. In addition, with highly porous grafts, it may be very difficult to maintain an increasing intraluminal pressure due to transmural leakage, leaving no option but to use a non-porous lining.

A high infusion rate overestimates burst pressure. The discrepancy may be even greater when using the very high infusion rates associated with gas cylinder pressure, but we cannot confirm this as our maximum infusion rate was 100ml/min.

When burst pressure is measured, the precise method including infusion fluid, infusion rate and the use of lining materials needs to be carefully considered and described when reporting the results. Although the use of blood as the infusion fluid may be more physiologically realistic, this reduces the high burden of proof requested by standards agencies and changes a purely mechanical test into a functional one.

10

In vivo durability testing

10.1 Introduction

In vivo studies of the developing graft can only be pursued once rigorous in vitro examination is complete and the results are satisfactory. The particular properties that require attention include cytocompatibility of the synthetic material, biostability of the graft, blood compatibility and mechanical integrity. Each of these factors can be solely responsible for catastrophic failure of the graft and there is no point in continuing to animal work if in vitro results in each area are not favourable.

However there are other critical factors which are not easily explored in vitro, relying on animal models to test them. This group of properties include durability and fatigue-resistance, which are particularly pertinent due to the constantly changing repetitive stresses of haemodynamic flow in a biological environment. A crude simulation of pulsatile flow at 37°C can be made, including accelerated inflation testing to attempt to demonstrate mechanical integrity over many years in a far shorter time-period (accelerated life testing), but this itself leads to a number of problems. Firstly, it is impossible to create the true biological environment, so mechanical stresses and biodegradative stresses cannot be applied simultaneously in a quantifiable realistic manner. Secondly, although it is an attractive proposition, accelerated inflation changes the behaviour of the graft, as it's viscoelastic nature by definition means that the level of distension(strain) due to inflation pressure(stress) is dependent on the rate at which the stress is applied and released (inflation cycle rate). In order to correct for this, accelerated cycle tests may be carried out at higher

temperatures than 37°C. This can then independently affect the biostability of the grafts. It is for this reason that investigators have moved to animal models without formal consideration of fatigue testing.

In reference to material fatigue it is worthwhile to consider the case of Dacron development for several reasons. This material has now been implanted in humans for long periods of time. Also, it is used as an aortic graft, where the shear stresses are greatest, making failure due to fatigue a real risk. Dacron fibres were found in vitro to have an extremely strong crystalline nature. Within ten years after introduction into clinical practice of the double-veloured crimped textile prosthesis which we are familiar with, structural failures were being identified within the knitted structure, in the form of defects due to dropped stitches, in particular in the dipped valleys formed by crimping³⁷¹. These defects were due to problems inherent in the manufacturing process for Dacron grafts, but fatigue was implicit in the resultant graft aneurysms, as failure due to structural weakness alone would have been uncovered soon after implantation. These problems were neither uncovered in vitro nor suspected in vivo, as the time required for graft failure to develop was six to ten years. The mechanism of failure is presumably the increased concentration of stresses in the fibres around the defect, as well as the room available for further yarn slippage, enlarging the defect and thereby risking false aneurysm. Further slippage also weakens the structure generally, giving rise to aneurysmal dilatation of Dacron itself. Subsequently further improvements were made to the textile manufacture.

10.2 Biodegradation studies of the graft

10.2.1 Biodegradation of PCU: in vitro assessment

Simulation of the biological environment has proven to be difficult. The ideal in vitro test would expose the material to the various degradative mechanisms present in the biological environment in isolation as well as in combination. It would also quantify what time period of biological exposure corresponds with the test protocol. This latter is practically impossible, not least because the level of degradative stress in vivo is dependent on physiological conditions such as level of inflammatory response to the graft material. An alternative philosophy is to present a biodegradative regime that outstrips that

which would be reasonably expected in vivo. This latter direction was taken by my preceding investigators. This method precludes the application of combined biodegradative and haemodynamic stresses – the two are likely to act synergistically to accelerate biodegradation. Wiggins' group³⁷² have shown in vitro that oxidative solutions cause faster degradation when multidirectional dynamic mechanical stresses are applied to polyetherurethane samples.

The works of Zhao³⁷³ have also shown that successful biodegradation is reliant on the synergy between pre-stressing of the graft material and biologically derived degraders including oxidative, peroxidative and hydrolytic agents. In particular, natural proteins such as human plasma α_2 -macroglobulin and caeruloplasmin are involved in creation and propagation of surface cracks (environmental stress cracking) via oxidative mechanisms. Macrophages are involved in auto-oxidation and monocytes stimulate free radical generation. Ubiquitous enzymes (phospholipase A₂) and macrophage-derived enzymes (cholesterol esterase) are also involved in hydrolytic degradation.

Labow's review³⁷⁴ of macrophage activity in response to polyurethane grafts highlights several important points. Firstly, it is the presence of polyurethane itself which stimulates the differentiation of monocytes into macrophages. The monocyte's primary oxygen free radical secreting role and peroxidative function is swapped for the lysosomal secretion of the macrophage along with its phagocytic efficiency. As differentiation into macrophages is a result of subacute or chronic inflammation as would be expected with an implanted graft, this questions the role of free radicals in biodegradation. Along with cholesterol esterase, other minor esterases are secreted which also cause ester hydrolysis. Although the upregulation of cholesterol esterase is a well documented response to polyurethanes, the biomolecular trigger for this upregulation, which occurs at the ribonucleic acid level, is not known. The oxidising mechanism of macrophages is also due to lysosomal secretions, offering the intriguing possibility that macrophage secretions are tailored to the nature of the foreign body – poly(ether)urethane stimulates oxidising agents and poly(ester)urethane causes hydrolytic action. In addition, polyether-based polymers are slightly susceptible to hydrolysis at the urethane group, as opposed to the ester groups themselves for poly(ester)urethanes. Labow also highlights the synergy between the different degrading agents, pointing out the increased degradation of polyurethane when applying sustained strain to the material and pretreating it

with α_2 -macroglobulin before oxidising.

These synergistic biodegradative and mechanical mechanisms point to the major deficiency of Salacinski et al.'s¹⁴² use of physiological degradation solutions to assess biostability of poly(carbonate-urea)urethane (PCU), on which the current nanocomposite is based. The test material was exposed to plasma fractions (incorporating proteins which act as surface crack propagators), free radical generators, oxidising agents and hydrolytic enzymes individually, but not in combination. After 70 days of exposure, they found no evidence of surface cracking of PCU whereas poly(ether)urethane (PEU) showed multiple cracks on SEM. This correlated with changes in molecular weight of PEU on exposure to the various plasma fractions. Oxidising solutions, and in particular peroxidation actually resulted in an increase in molecular weight for PCU. This same phenomenon was observed in vivo and in vitro with the Biospan® (aliphatic polycarbonate soft segment) prosthesis. Christenson and colleagues³⁷⁵ have shown via attenuated total reflectance-Fourier transform infrared spectroscopy (ATM-FTIR) that the oxidative degradation is associated with soft segment disruption as well as increased crosslinking. The increased molecular weight may be a result of this increased crosslinking. In vivo, the mechanism for this may be free radical damage to both soft and hard segments – see Fig. 10.1 and 10.2.

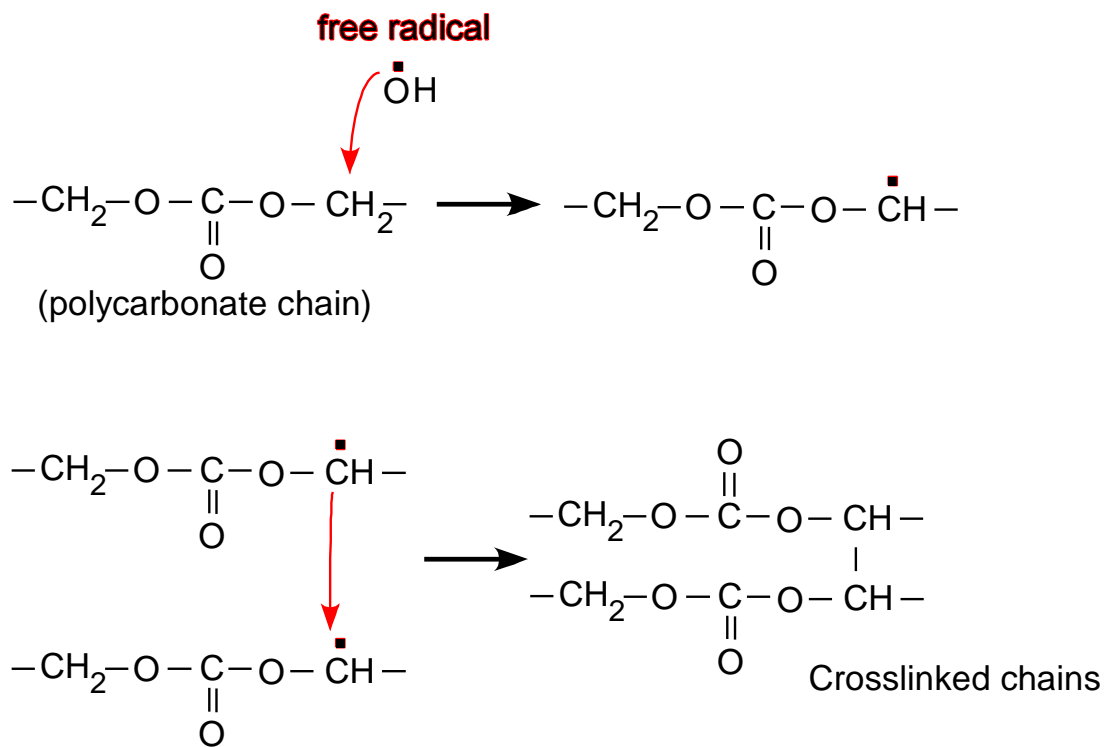


Fig 10.1. The mechanism of free radical stimulated oxidative crosslinking of adjacent polycarbonate soft segments.

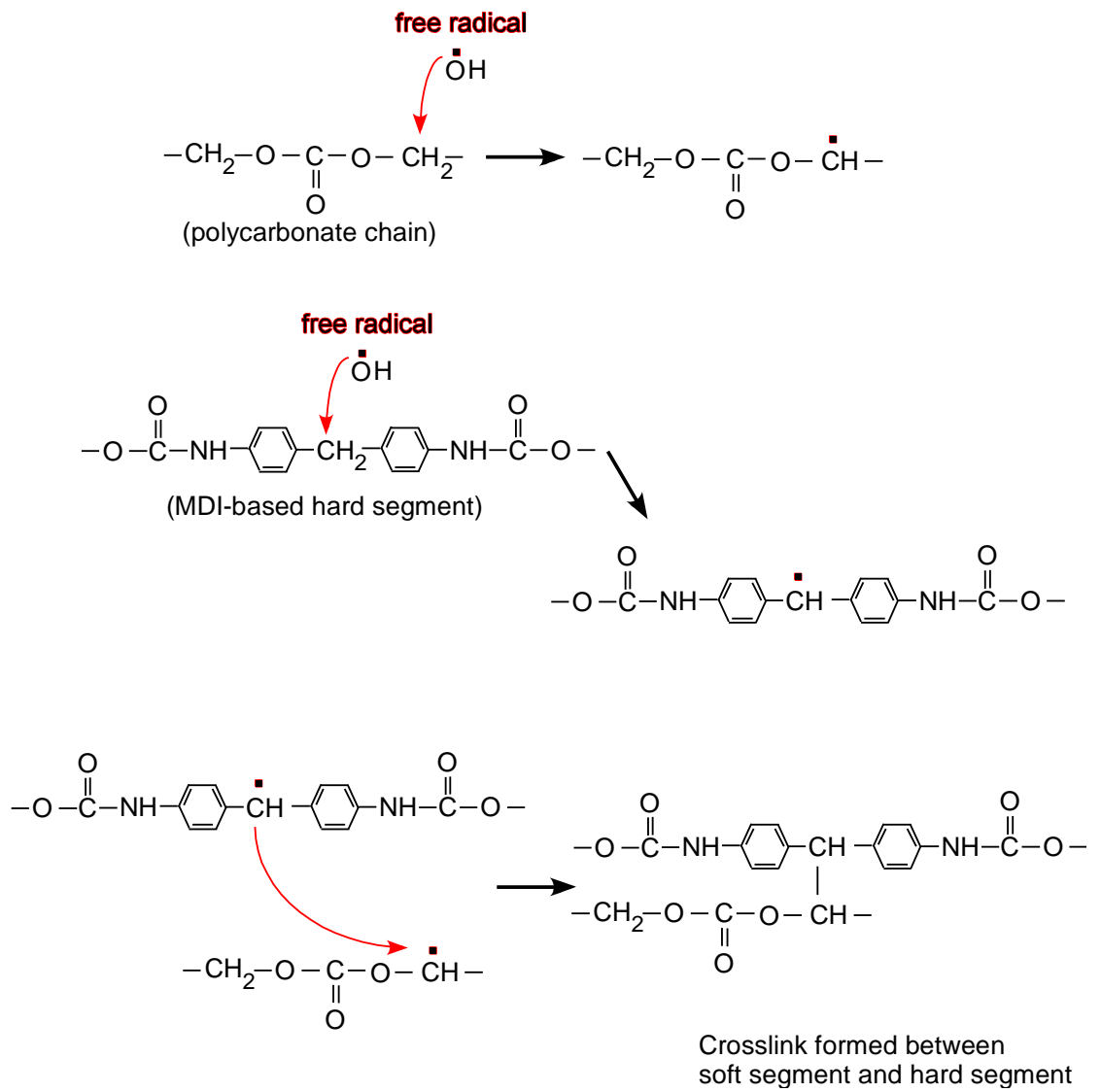


Fig 10.2. Free radical mediated crosslinking between polycarbonate soft segment and the hard segment.

Peroxidising solutions also caused a reduction in elastic modulus of the PCU¹⁴², suggesting degradation which adversely affects mechanical properties, which was confirmed by showing an associated reduction of ultimate tensile strength. This is also in keeping with increased crosslinking, causing a reduction of chain flexibility.

In fact, repeated macrophage derived free radical damage is thought to be a principle trigger for breakdown of soft segments³⁷⁵ which occurs via a combination of oxidative and hydrolytic mechanisms – Fig 10.3.

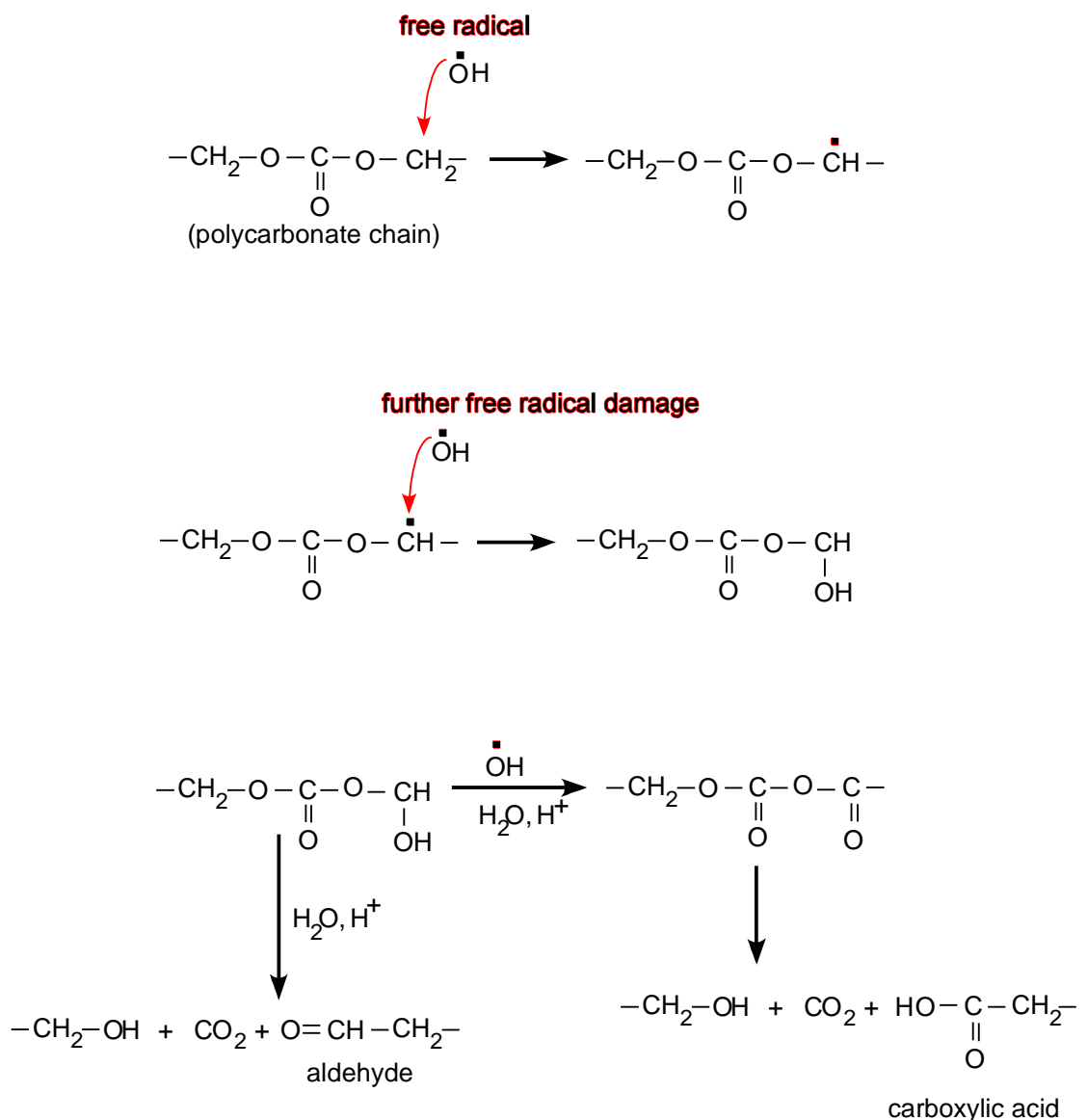


Fig 10.3. After initial (oxidative) free radical damage, polycarbonate soft segment degradation is caused by a combination of oxidative and hydrolytic means.

These phenomena are more pronounced in polyether-based PU due to the higher susceptibility of the ether groups to deprotonation, making the initial free radical assault more likely. These results appear to show some oxidative degradation of PCU. A more drastic effect on mechanical integrity was found when PEU was exposed to oxidising solutions with complete fragmentation of the graft material in one such solution. The unexpected loss of mechanical integrity in PCU on peroxidation was explained by suggesting that the peroxidative environment was in fact promoting hydrolytic degradation as well – supported by the degradation mechanisms discussed above. Therefore, the initial aim of separating out the different degradative mechanisms in vitro was not completely fulfilled. However, this apparent undesirable result did not preclude PCU from being tested in vivo, as it was pointed out that significant peroxidative conditions are not usually encountered physiologically.

In vitro hydrolysis alone caused no degradation of PCU, with minor compliance changes with PEU. However, it is known that an acid environment favours hydrolytic breakdown. Furthermore, such an environment could be reasonably expected after graft implantation due to lysosomal secretion and attempts at phagocytosis and cell membrane lysis, especially if associated with infection. The protocol used would be more stringent by hydrolytic degradation in an acidic environment.

The degradative solutions used in vitro needed in vivo validation in order to quantify how the in vitro results translate in terms of implantation time. It was demonstrated that PCU was more resistant to degradation than commercially available PEU, but this did not indicate whether there would be long term degradation of PCU after implantation. Therefore, Seifalian et al.'s long term animal model⁸² to assess degradation of PCU which followed was of paramount importance.

10.2.2 Biodegradation of PCU: in vivo assessment

PCU was implanted in an aorto-iliac canine model⁸². The high flow haemodynamic parameters ensured a rigorous mechanical test simultaneous to

the in vivo exposure. 18 month and 36 month biodegradation was assessed. There were no macroscopic signs of dilatation or weakness after 36 months. Mechanical properties were preserved over that time with no significant difference from pre-implantation levels in either circumferential strength or compliance. Pitting, etching and environmental stress cracks were not observed on SEM. ATM-FTIR was used to observe the 1740cm^{-1} peaks, representing the C=O, and hence soft segment degradation (Fig 10.3) and showed no difference across the anastomosis. It would seem that in this model at least, there was good biostability and durability over the long term, equating with a preservation of the favourable pre-implantation mechanical properties. However, the same material was subsequently implanted in an ovine carotid interposition model by Aldenhoff et al.⁴⁷ for 10 weeks, and in each instance, there was dilatation of the conduits with wall breakdown and curvature within that short time. This study contributed to the shift of emphasis away from considering Chronoflex® as a permanent vascular implant.

10.2.3 Biodegradation of PCUPOSS: an in vitro assessment

In order to progress with polymer biostability and hence make a reasonable case for animal model work, the in vitro biodegradation profile for PCUPOSS needed to be shown to be better than for PCU. Kannan repeated the biodegradative solutions experiment on PCUPOSS³⁷⁶. He found that plasma proteins, free radicals, hydrolytic, oxidative and peroxidative environments had no effect on the hard or soft segments. However, the hydrolytic and peroxidative solutions did reduce the number of Si-O bonds in the sample, as evidenced by fourier transform infrared spectroscopy (FTIR). This was interpreted to mean that the peroxidation caused degradation within the POSS moiety, but the POSS function of improved interaction between soft and hard segment via cross-linking and hydrogen-bonding was preserved despite the siloxane bond degradation. As with PCU before, there was no evidence of any surface cracking on SEM, although some slight shearing of the crystalline peaks and pitting of the surface was noted with exposure to plasma fractions, as well as significant shearing of the surface with peroxidative solutions. Further evidence of the preservation of the soft segment structure was provided in the form of

maintenance of elasticity and burst strength as well as no significant change in glass transition temperature (T_g) as measured by Differential Scanning Calorimetry (DSC). This latter test did however show a reduction in melting point (T_m) for one peroxidative solution. Kannan's interpretation was that the vulnerable soft segment was not affected by the degradative solutions due to its shielding by the hard segment, with POSS an adjunct to this shield. However, the POSS was being degraded by the peroxidative solutions, without any impact on mechanical properties. It is this last point which indicates that PCUPOSS could resist biodegradation better than PCU.

10.3 Which is the most suitable animal model?

It is widely recognised that a rapid confluent endothelial layer protects a synthetic graft from thrombosis and early occlusion. For this to occur, transmural capillary ingrowth is required as a supporting medium³²⁸ or even a direct source of endothelial cells³⁷⁷. However, such autonomous endothelialisation has never been achieved in clinical practice. This means that the results of animal studies where endothelialisation has occurred can not be applied to human trials. In particular, good patency of grafts which have endothelialised after being implanted in animals may not be reflected in humans. The literature is replete with animal models demonstrating endothelialising grafts, but few have translated to successful trials with ePTFE being the only commercially successful small calibre graft since its introduction in 1973²⁰. As a result, emphasis has turned towards facilitating endothelial seeding of grafts before implantation as well as tissue engineering of bypass grafts and endothelial progenitor cell adherence from circulating blood. Endothelialisation of both PTFE and Dacron® have been shown to improve patency in humans^{378;379}.

The behaviour of the implanted nanocomposite grafts without preceding in vitro endothelialisation is of interest. In order to validate any animal study, a careful consideration of which species will best model human vascular behaviour.

Much of the assessment of graft behaviour in vivo has been undertaken

on small animals – rabbit and rodent. In both cases, PTFE graft healing behaviour is similar to humans with a fibrinous lumen lining with minimal endothelialisation within 30days^{206;380}. However, the aorta of both is only 1.2-1.5mm in diameter^{206;381} and so more appropriate for microvessel studies than our graft.

A host of large animals have been popular for arterial bypass graft implantation studies including pig, sheep, goat, dog and baboon²¹¹. Larger animal models are generally considered more representative of human physiology with primates thought to be the most accurate reflection. This however, is not necessarily the case when considering the vascular system.

Clowes addressed the endothelialisation potential of baboon vasculature, showing that there was rapid confluent endothelial coverage of PTFE of intermediate porosity (60µm internodal distance), as a result of transmural capillary infiltration³⁷⁷. This is in stark contrast with humans where the same PTFE does not allow capillary infiltration to cross the whole width of the graft wall, resulting in failure to endothelialise³⁸².

Anatomical and growth considerations need to be taken into account when considering suitability of animals. Pigs are often discounted from long term studies of implanted grafts because of their phenomenal growth rate through most of their lifespan. Subspecies which have reduced growth rates are very expensive³⁸³. However, porcine investigations in the short term have shown the development of a neointima which includes cells that superficially appear like endothelial cells, but closer investigation reveals that they do not stain positive for von Willebrand factor; nor do they have the characteristic intercellular junctions of endothelium³⁸⁴.

Sheep and goat models have femoral and carotid vessels which are of an appropriate calibre for our study. The sheep carotid is particularly convenient for access, subsequent doppler access and presents a long unbranched length. The sheep is particularly popular in cardiac valve models, where valve and cardiac haemodynamics are adjudged to be similar to humans'; however, the downside is that this model has a high intravascular calcification rate compared with humans. Poole-Warren et al. showed that, as with humans, the principle mechanism of endothelial lining of PTFE grafts in sheep was the limited in-growth from the anastomoses with the artery³⁸⁵. James and colleagues showed that an endothelial lining was critical for short term patency of PTFE conduits in

the ovine model³⁸⁶. In fact, all six of the unseeded PTFE carotid interposition grafts implanted were occluded within 13 weeks. No systemic anticoagulation was used at the time of the implantations or post-operatively. The ovine model is therefore a very exacting one, equalling or even more stringent than the clinical scenario.

Canine models have enjoyed prominence due to similar healing properties as humans. However, unlike humans they endothelialise very readily and graft implantation studies are of little value. Dixit et al. compared dog and human endothelial cell behaviour, finding human endothelial migration at the anastomotic junction to be greater than canine counterparts. However, the emerging picture was complex and questions remained about the model used to illustrate the EC behaviour. Firstly, this group found similar migration rates for ECs on polystyrene and Photofix, a decellularized bovine (collagen) pericardium. This would suggest that the in vitro Photofix conditions were not close to the biological state. Next the human and canine EC types were morphologically and biochemically different. Human umbilical vein endothelial cells (HUVECs) are significantly larger and rounder than Canine endothelial cells (CECs) with the higher migration rate and distance of the former being haphazard with poor confluence and high senescence during the experiment. CECs on the other hand proliferate faster than their human counterparts. The critical issue of strength of adherence of the ECs was not addressed, and CEC attachment may be far more robust than HUVECs, which would correspond with the gaps noted in HUVEC migration patterns. The HUVECs showed greater secretion of prostacyclin (a powerful anti-aggregatory prostaglandin and hence their chosen proxy for EC function), but this fell off quickly compared to the sustained release over time in canine cells²¹². In summary, there are considerable differences between the two and Dixit discusses that one explanation of the success of canine endothelialisation may be high levels of spontaneous endothelialisation from circulating cells, which would fit with the findings of this limited study.

It is apparent that an animal model that endothelialises the graft surface spontaneously is a poor representation of the clinical state. For this reason, canine and baboon models need to be discounted. Furthermore, the biostability of PCU in the canine model demonstrated by our group⁸² relative to the ovine model⁴⁷ questions its validity in a durability study. Porcine models are unsuitable

for long term implantation due to their rapidly increasing size. Small animals have vascular healing properties akin to humans, but larger vessel diameters are necessary. This leaves the ovine model, which is suitable in terms of healing properties, surgical access, vascular anatomy and a long adult phase with no increase in size. Perhaps most importantly it has already been shown by Aldenhoff⁴⁷ to be a hostile biodegrading environment for a conduit closely related to PCUPOSS, in the context of favourable in-vitro biomimetic degradation testing as well as a falsely reassuring canine model. The downside of using this model for durability studies is that it is associated with high levels of early occlusion of prosthetic grafts, potentially bringing a premature end to the study period. The converse argument is that it is ideal for testing permanent vascular prostheses as the high early occlusion rate is due to the lack of endothelialisation of vascular prostheses during healing; a characteristic the sheep shares with humans. Ultimately, as the aim of the model is to show whether PCUPOSS is better able to cope with the biological environment than its predecessor (PCU), it makes sense to use the stringent model which is already known to degrade the latter.

10.4 Method

10.4.1 Animal model protocol

All animals were cared for as per the guidelines provided in the Care of Laboratory Animals Handbook. 8 sheep (mean weight 56kg) were sedated by intramuscular administration of 0.2mg/kg xylazine and 10mg/kg ketamine, before anaesthetising with halothane gas. A duplex doppler was used to identify the right internal carotid artery of each animal and the blood flow rate within the artery as well as the arterial diameter was recorded. Differentiation was made from the external carotid artery by the presence of branches of the latter. The hair overlying the carotid artery was shaved bilaterally and each carotid was exposed in turn. 5000iu multiparin (heparin sodium) was administered and allowed to circulate for 5 minutes before clamps were applied. With control of either end of the internal carotid, proximal and distal soft clamps were placed. A 5.5cm segment of unbranched common carotid was excised, at least 0.5cm

distal to the carotid bifurcation. 5cm length of 4mm diameter prosthesis was anastomosed in its place in an end-to-end fashion using a continuous 6/0 prolene suture, starting with the proximal anastomosis. Before the distal anastomosis was fashioned, blood was flushed through the graft by transiently releasing the proximal clamp, and once the proximal clamp was reapplied, the graft was flushed out with heparinised saline. The distal clamp was also transiently released to allow back-flow to flush out the distal vessel before the distal anastomosis was formed in the same way. This procedure was repeated immediately before the final suture was placed to complete the distal anastomosis. Any suture-hole bleeding was curtailed by applying gauze swabs to the anastomotic areas. The blood flow within the graft was assessed by duplex immediately after resumption of flow and 30 minutes later. The wound was closed in layers using absorbable sutures and dressed with a transparent bio-occlusive dressing. The animals were recovered and kept in free grazing conditions. Individual water troughs were provided for each animal, filled with 150mg aspirin dissolved in 100mls of water at dawn daily, which was only refilled with water once the initial water had been consumed. The animals were sacrificed on the same day after a minimum of 17 months (520 days).

10.4.2 Scanning Electron Microscopy

This was performed on the explanted grafts to look for evidence of surface pitting, fissuring, cracking, balding and weakness propagation, compared to pre-implantation controls.

10.4.3 Histological and Immunohistological Analysis

Grafts were embedded in wax and Haematoxylin and Eosin (H and E) as well as trichrome staining was performed along with immunostaining using anti-von Willebrand factor antibody and CD31 antibody (Alrich). Sequential thin slices were cut and mounted on slides for light microscopy.

10.4.4 Mechanical testing

Two grafts were used for post-implantation mechanical testing.

Compliance was measured for mean pressures between 20 and 100mmHg using a pulse pressure of 40mmHg in the flow circuit previously described. The graft was then placed in the burst pressure apparatus, using a latex lining sleeve and an infusion rate of 0.2ml/min until it failed. The fibrous capsule was removed from the second graft and the burst pressure measured in the same way. The results were compared with compliance and burst pressures for identical control grafts which had not been implanted.

10.4.5 Chemical Analysis - Fourier Transform Infra-Red spectroscopy (FTIR)

This is a powerful technique used to examine the covalent chemical bonds present in a sample. It works on the principle that different chemical bonds have characteristic patterns of vibration. When electromagnetic radiation is focussed on the vibrating bond, any wave of the same frequency as the vibration will be absorbed by the sample and not passed through to the detector. Most of this wave frequency falls in the infrared spectrum. Fourier transform maximises the absorption data extraction by beaming multiple infrared frequencies simultaneously at the sample, and varying these frequencies. The absorbance is computationally calculated.

10.4.6 Thermal Analysis

10.4.6.1 Thermal Gravimetric Analysis

This test is used to demonstrate the degradation temperature of a polymer by exposing the polymer sample to an increasing temperature ramp whilst simultaneously monitoring the sample weight. Therefore it is a measure of thermal degradation. An inert gas environment is used to ensure chemical degradation such as oxidation does not occur.

TGA measurements were performed using a TGA Q500 (TA instruments, USA). Samples (about 10mg) were heated to 600 °C at a heating rate of 10 °C under a nitrogen purge to determine the temperature at which the residual weight of the sample became 95% of the original weight.

10.4.6.2 Differential Scanning Calorimetry (DSC)

This test investigated the amount of energy required to increase the temperature of the graft sample (ie. heat capacity). At phase transition points it is the energy required to complete the transition, even without any further increase in temperature. Water exists in both solid and liquid forms at 0°C as represented by the stable ice/water mixture. Heat energy is required to enable the transition of ice to liquid even though the temperature of the water has not increased.

Unique to polymers with an amorphous component is the glass transition point (T_g). This represents the temperature boundary between the glassy phase and the rubbery phase of the polymer. The glassy phase is a hard but brittle polymer, whereas the rubbery phase is soft and elastic. In the case of PCUPOSS (and all polyurethanes) the glass transition point relates to the amorphous soft segment. The contribution of the hard segment to glass transition is due to its soft-segment shielding role. Unlike the main phase transitions between solid and liquid (melting) and liquid and gas (vaporisation), T_g does not involve absorption or release of energy by the polymer. It simply reflects a change in heat capacity of the polymer.

DSC measurements were performed on a Mettler Toledo 822e (UK) DSC. Heating scans were acquired from -50 to 250 °C at a rate of 5 °C/min.

10.4.6.3 Dynamic Mechanical Analysis (DMA)

Whereas DSC is limited to demonstrating T_g of the overall polymer, DMA can give more detail pertaining to soft segment and hard segment behaviour as well as a more accurate T_g . This information is obtained by monitoring the material behaviour under a small oscillating (sinusoidal) force during an increasing temperature ramp. By measuring the resultant strain, the elastic (storage) modulus can be demonstrated. By monitoring the phase delay in converting the oscillating stress to resultant strain which is given by the phase angle δ , the loss of energy to the environment can be demonstrated (loss modulus), which is related to the viscoelastic property of the polymer and is

comparable to the loss of energy demonstrated in the viscoelastic hysteresis loop during pulsatile flow. This loss of energy is quantified by 'tan δ ' which is the ratio of storage modulus to loss modulus.

Dynamic Mechanical Analysis was performed using a TA-Q800 DMA (USA). DMA measurements were conducted at a heating rate of 3°C/min and the frequency of 1 Hz in the tensile mode.

10.5 Results

10.5.1 Numbers of grafts

8 grafts were implanted as internal carotid grafts in eight animals. 2 animals died before the end of the study period. One death was at 29 days due to a chest infection. The other death was at 91 days with the cause undetermined from post-mortem. On explantation of the remaining 6 grafts, 4 were visibly fully patent, one appeared partially occluded and one was occluded. These results, along with the duplex flow rates and vessel calibres measured are shown in Table 10.1.

No.	Weight (kg)	Common Carotid Diameter (mm)	Flow in artery (ml/min) X	Flow in graft on implantation (ml/min)	Flow 30 min after implantation (ml/min) Y	Y/X	Implantation (days)	Outcome
1	46.7	3.8	360	288	342	0.95	91	Died, fully patent
2	46.1	3.6	420	315	370	0.88	545	Fully patent
3	50.5	3.7	452	407	475	1.05	630	Fully patent
4	47.2	3.9	380	247	304	0.80	605	Fully patent
5	44.6	3.7	510	393	403	0.79	29	Died, fully patent
6	48.5	4.1	335	285	328	0.98	523	Fully patent
7	45.1	4.0	350	210	290	0.83	662	Occluded (thrombus)
8	43.0	3.6	390	321	321	0.82	549	Partially occluded

Table 10.1. Graft summary for each sheep, including duplex results pre and post-implantation.

10.5.2 Gross appearance of grafts

A loose external fibrous capsule surrounded each graft – Fig 10.4 and 10.5. This was not adherent to the graft surface and was removed easily by cleaving it longitudinally. A thin uniform neointima was visible over the lumen surface of each patent vessel – Fig 10.6 and 10.7. No thrombus was evident. The neointima was not thickened at the anastomoses.

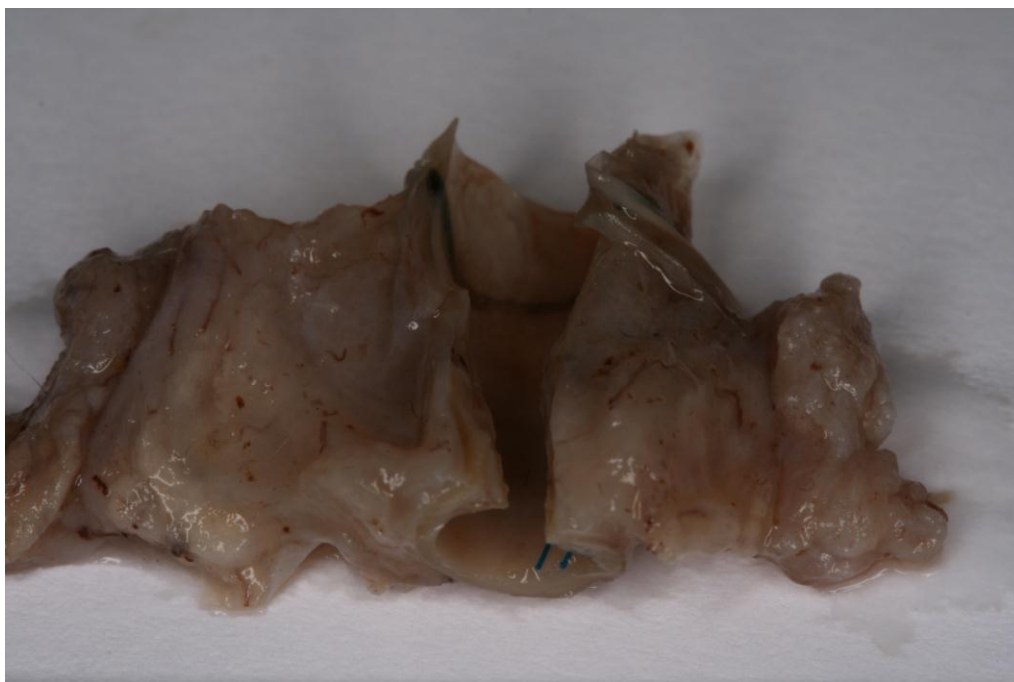


Fig 10.4. Uniform smooth lining on the lumen seen on longitudinal cleavage of the graft. The prolene suture (blue) at the anastomotic line is visible.

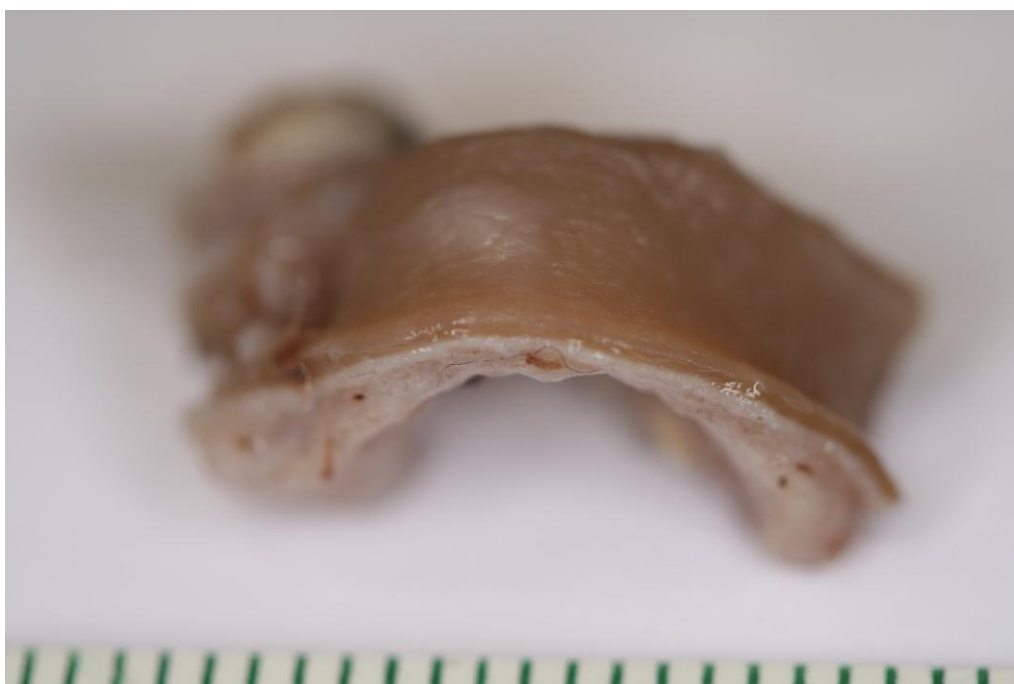


Fig 10.5. Close up of the smooth, uniform lumen lining of the explanted graft.



Fig 10.6. The fibrous capsule surrounding the explanted graft.

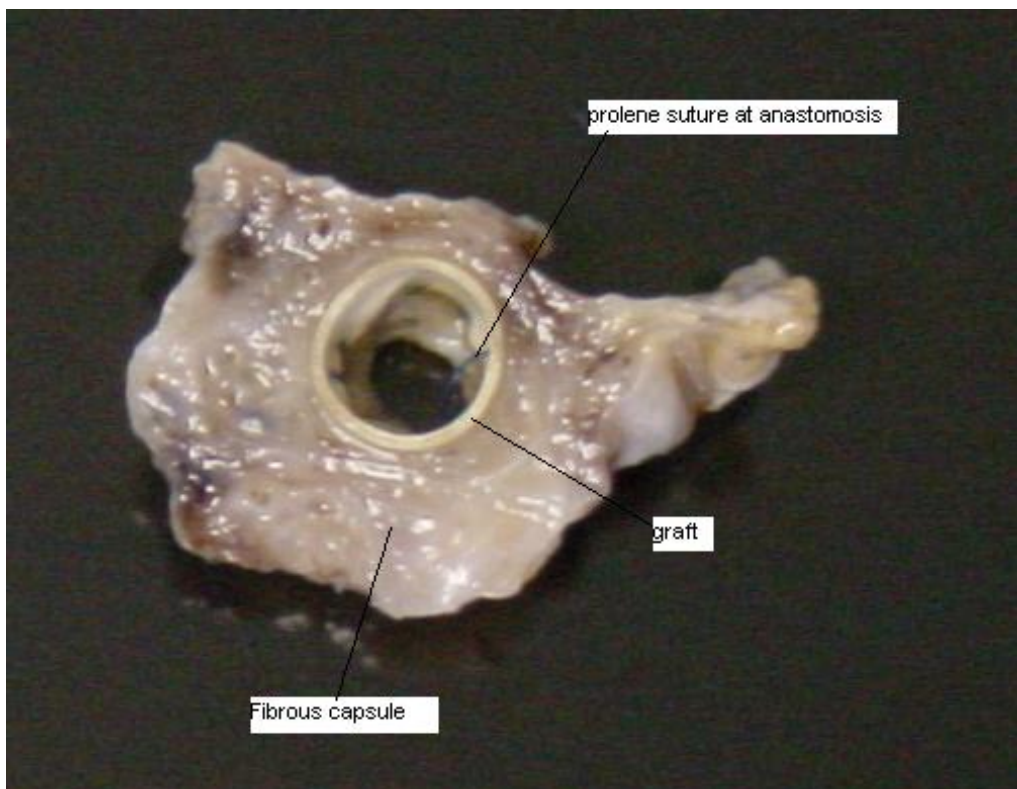


Fig 10.7. Cross section of the explanted graft, showing the florid fibrous capsule. The section has been cut near the anastomotic line, showing the

native artery and suture line.

10.5.3 Scanning Electron Microscopy

Ultrastructural analysis confirmed that there was no physical breakdown of the graft material (Fig 10.8). Lumen analysis showed a regular longitudinal lattice of ridges(Fig 10.9) which on closer observation showed interspersed endothelial cell-like structures in varying states of flattening (Fig 10.10).

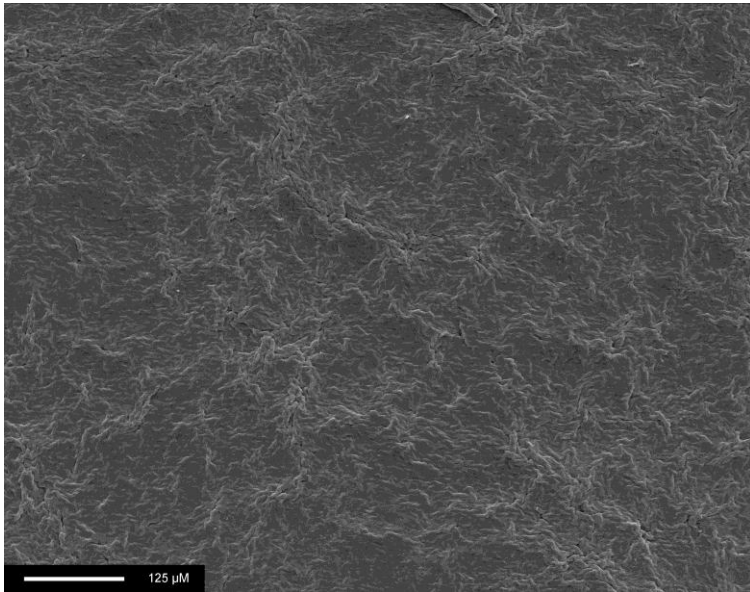


Fig 10.8. Outer Surface SEM of the explanted graft showing no evidence of pitting, fissuring, cracking or balding. Scale bar is 125 μ m

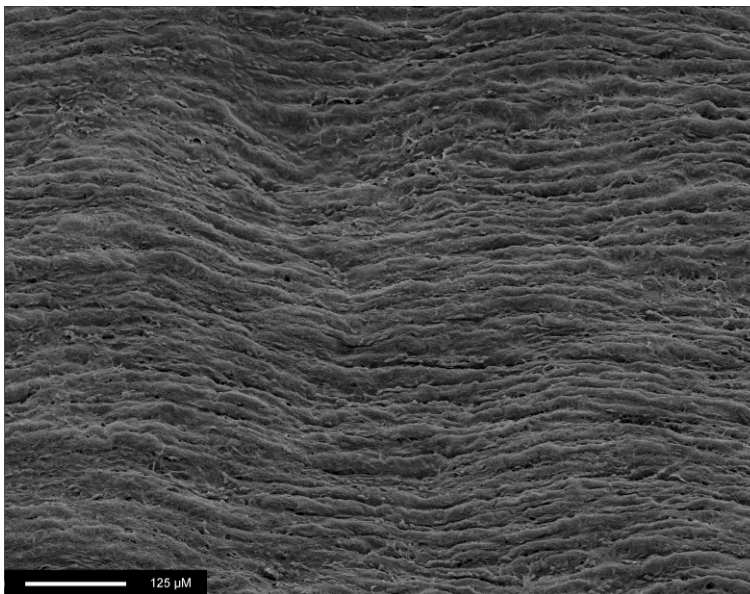


Fig 10.9. Inner lumen SEM showing ultrascopic ridges covered with a lattice structure. Scale bar is 125 μ m

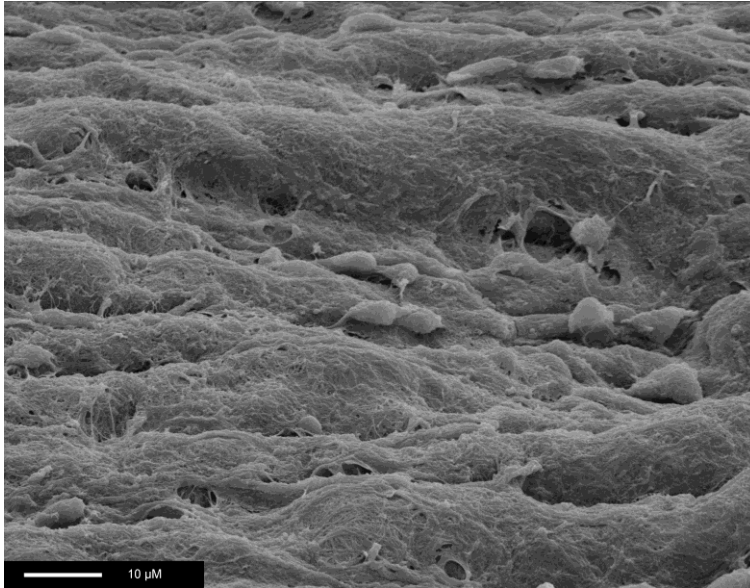


Fig 10.10. Higher magnification SEM of the ultrascopic ridges of the lumen lining of the explanted graft showing cell-like structures on the surface with varying degrees of flattening. Scale bar is 10µm.

10.5.4 Histology

There was a dense cellular layer immediately adjacent to the graft lumen, with endothelial-like cells within this layer – see Fig 10.11. A loose fibrin-like layer was present on the luminal side of the cellular layer. There were occasional cells within the fibrinous layer. These had the appearance of myofibroblasts. Erythrocytes could be seen within the loose neointima as well. There were periodical aggregations of erythrocytes bound within connective tissue borders within the graft material itself. These had the histological appearance of immature capillaries growing through the wall of the graft.

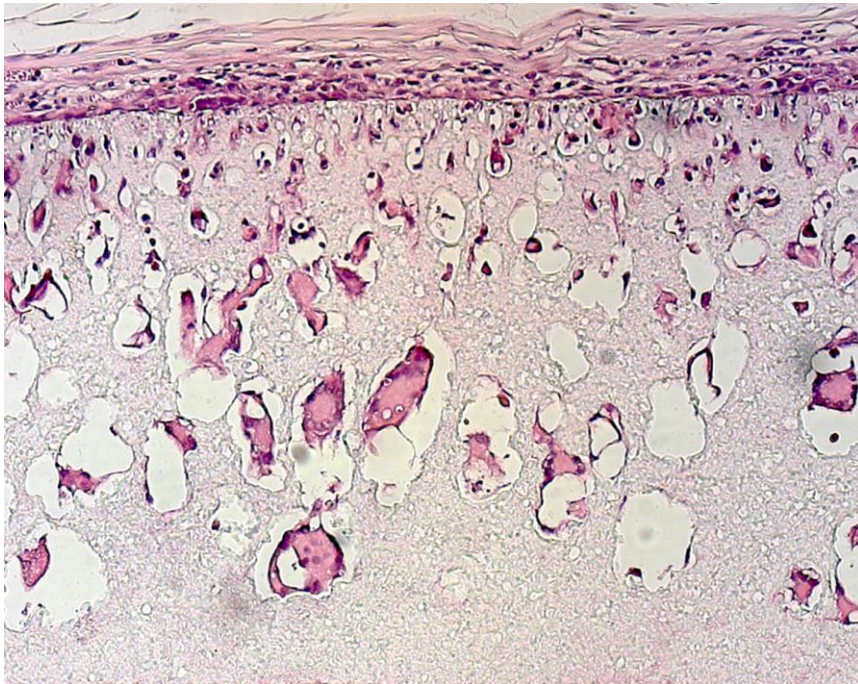


Fig 10.11. H&E staining of the graft wall, showing the lumen (superior).

10.5.5 EC characterisation

CD31 antibody immunostaining suggested two areas of increased uptake, namely the surface of the fibrinocellular lining of the graft as well as lining occasional small tubular cellular structures noted within the pores of the graft (Fig 10.12). However, the stain was taken up by the graft non-specifically, and it

could not be definitively shown that the staining was identifying endothelial structures.

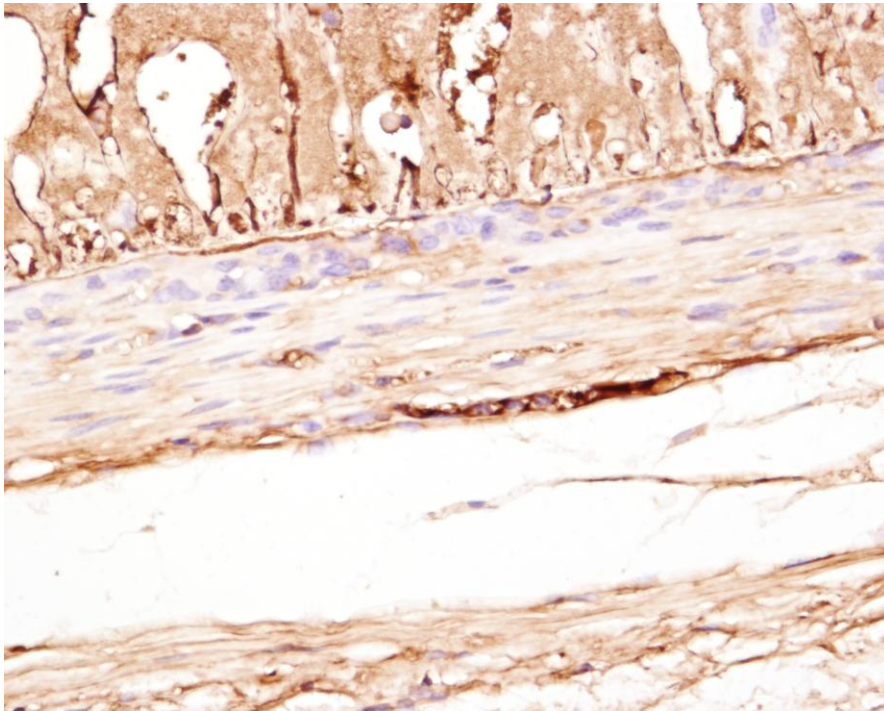


Fig 10.12. CD31 antibody staining showing uptake throughout the slide including the graft wall. There is a concentration of uptake at the blood contact surface on the periphery of the fibrinocellular layer which developed within the graft lumen. There is a second increased uptake in cellular tubular organisations within the pores.

Anti-vWF immunostaining showed a clear increased uptake in the graft lumen without the associated uptake elsewhere. This was even evident in areas when the fibrin layer was thin or non-existent (Fig 10.13). This immunostain also highlighted the small tubular structures within occasional pores of the graft (Fig 10.14).

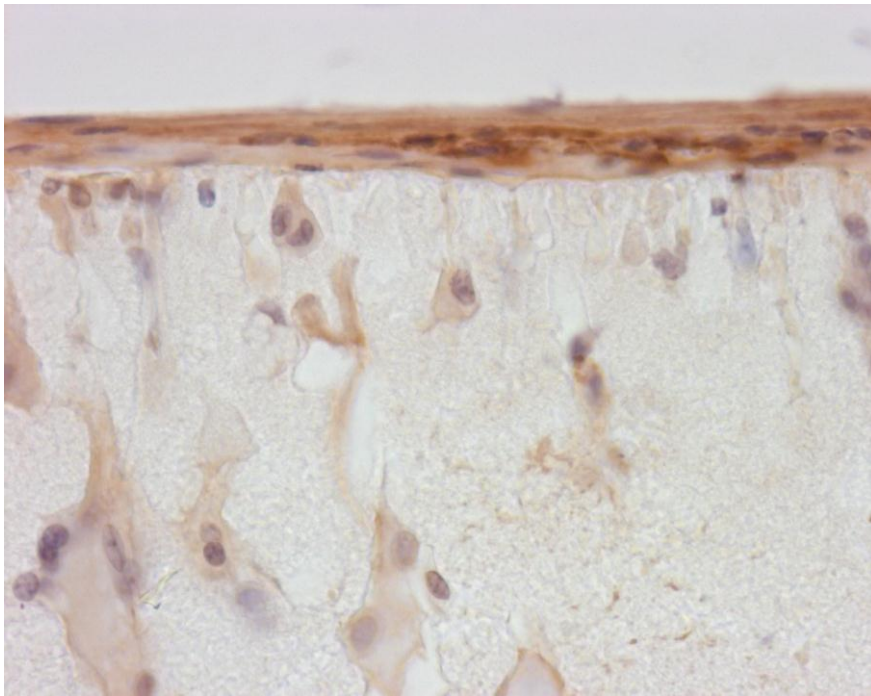


Fig 10.13. The immediate graft wall luminal surface where the fibrinous layer is not present showing increased uptake of the anti-vWF immunostain.

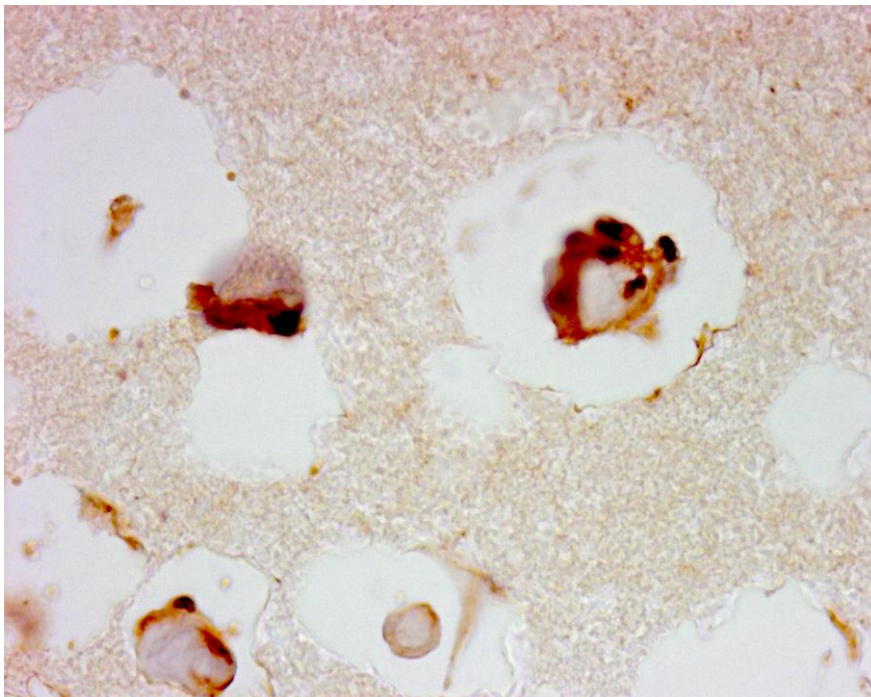


Fig 10.14. Small tubular cellular structures within the graft pores which immunostain heavily with anti-vWF.

10.5.6 FTIR Analysis

Fig 10.15 shows the spectroscopy result for the pre-implantation and post-implantation grafts. There is no significant difference in either peak location or size for the two. The main peak of Si-O (1240cm^{-1}) is not attenuated as Kannan found with in-vitro hydrolytic and peroxidative degradative solutions³⁸⁹. Replicating his findings from the in-vitro study, the polycarbonate soft segment (-NHCO- bonds at 1740 cm^{-1}) was completely preserved.

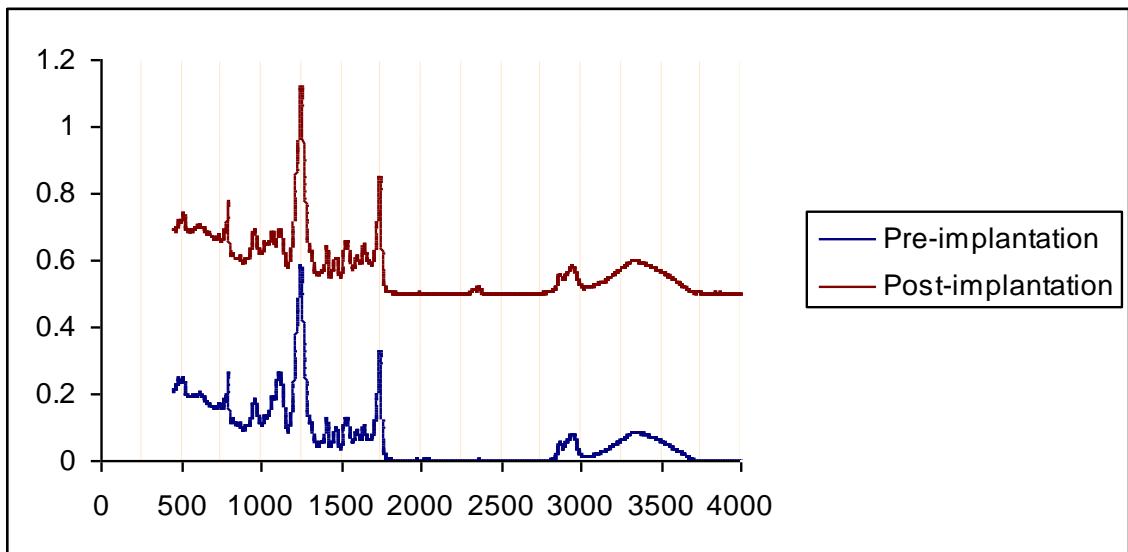


Fig 10.15. FTIR analysis of the pre and post-implantation grafts showing preservation of the Si-O peak at 1240 cm^{-1} and the -NHCO- bonds at 1740 cm^{-1} .

10.5.7 Compliance of graft pre and post implantation

Fig 10.16 shows the compliance of the explanted graft with and without the fibrous capsule attached. For comparison, the compliance measurements of the original conduits are included. It shows that the fibrous capsule resulted in a dramatic loss of compliance. However, removal of the capsule returned the compliance to the level of the pre-implant graft, suggesting that the biological environment did not cause a loss of compliance due to structural degradation.

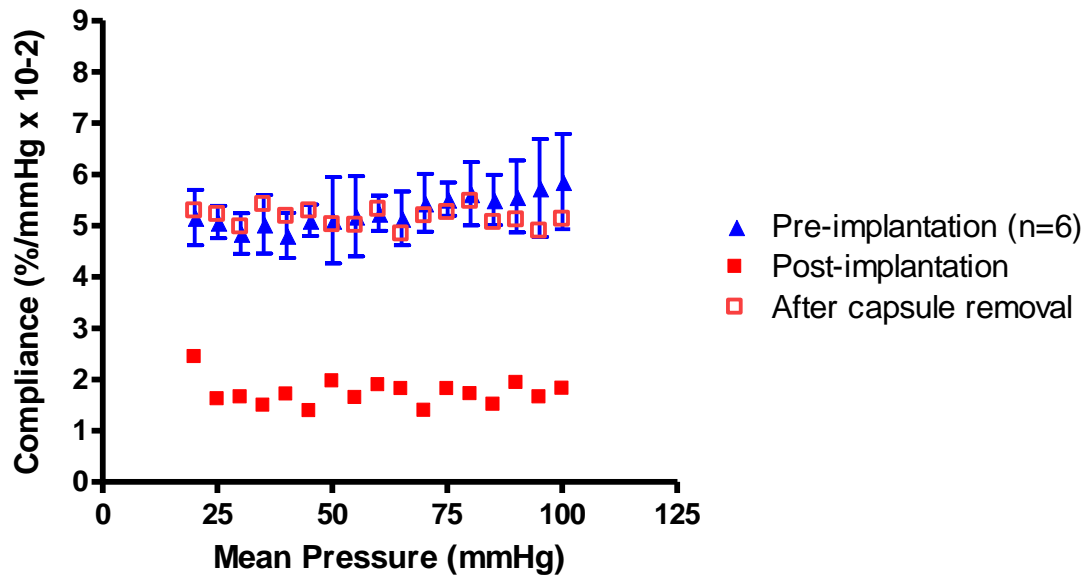


Fig 10.16. The compliance of the post-implantation graft compared with the pre-implantation graft. The results are shown for the graft alone and with the fibrous capsule attached.

10.5.8 Burst strength pre and post implantation

The graft strength is shown in table 10.2.

(n=6)	Pre-implantation	Post-implantation	Capsule removed
Burst pressure (mmHg)	358 (+/-15)	874	363

Table 10.2. Burst pressure for the graft pre and post-implantation. The post-implantation burst pressure was obtained with and without the fibrous capsule.

10.5.9 Thermal Gravimetric Analysis

This showed two distinct temperatures at which the sample degraded as a function of increasing temperature; approximately 275 and 425°C for both pre and post-implantation grafts – Fig 10.17. These two represent the thermal degradation of the soft and hard segments respectively. It is evident that there was no change in soft segment thermal degradation after the prolonged period of implantation.

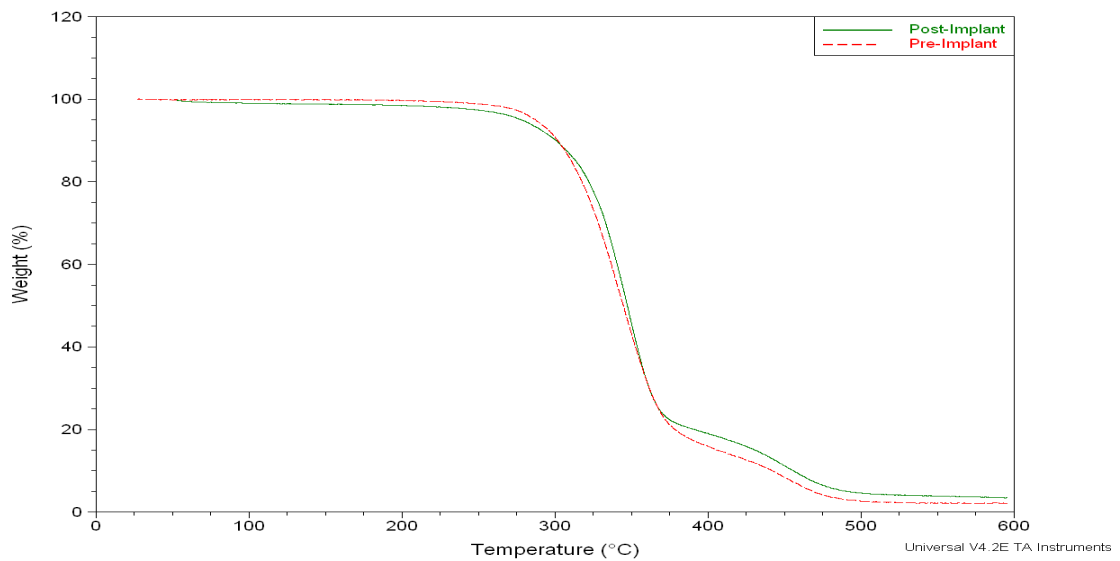


Fig 10.17. TGA results for the pre-implantation and post-implantation grafts, showing the two distinct points of increasing weight loss as the temperature is increased – approximately 275 and 425°C. This is the same for both samples.

10.5.10 Differential Scanning Calorimetry

The DSC results are shown in Fig 10.18. As per Kannan's investigations³⁸⁹, the T_g for both samples were not significantly different (-37°C). This low T_g means that the grafts are well within the rubbery form at biological temperatures. The test was terminated before a clear melting point (T_m) was reached.

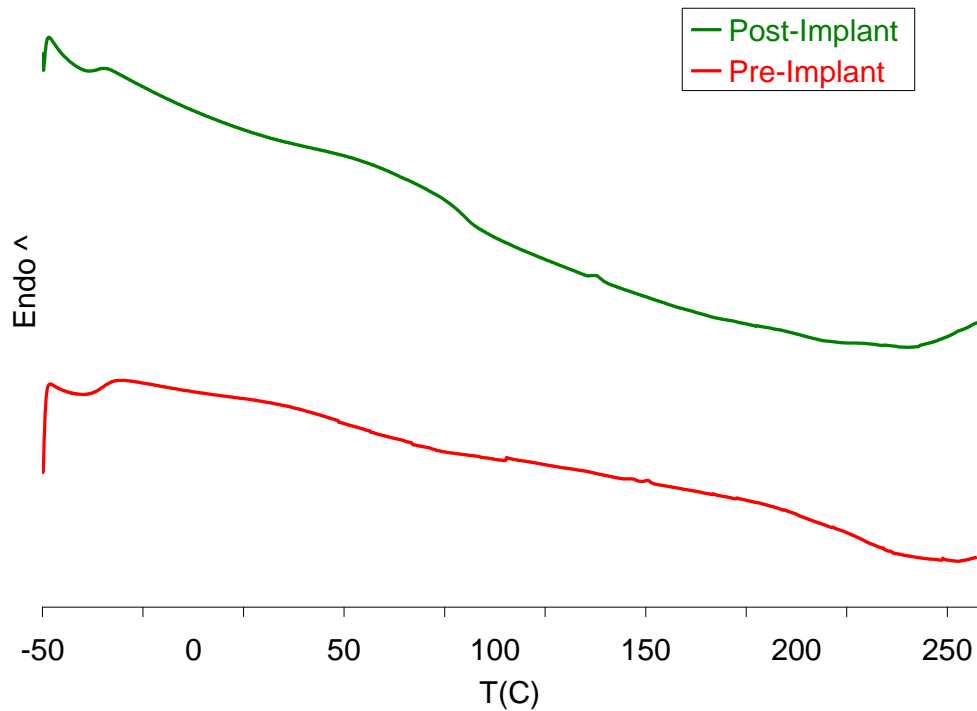


Fig 10.18. DSC thermograms for pre and post-implantation grafts. There was no significant difference in T_g . The test was terminated at 250°C which was before the melting point (T_m) was reached.

10.5.11 Dynamic Mechanical Analysis

Fig 10.19 to 10.21 show the DMA results for pre and post-implantation grafts. These demonstrate a difference of just 4°C in T_g between the two, which is not a significant difference. The T_g is clearly identifiable, suggesting a high degree of cross-linking between the soft and hard segments. The storage and loss modulus in the glassy region is higher in the implanted conduit, indicating an increase in crystallinity compared with the original graft. However, in the biological temperature range, and throughout the rubbery phase there is no significant difference. The $\tan \delta$ value which represents the ratio of storage modulus to loss modulus is identical for the two grafts.

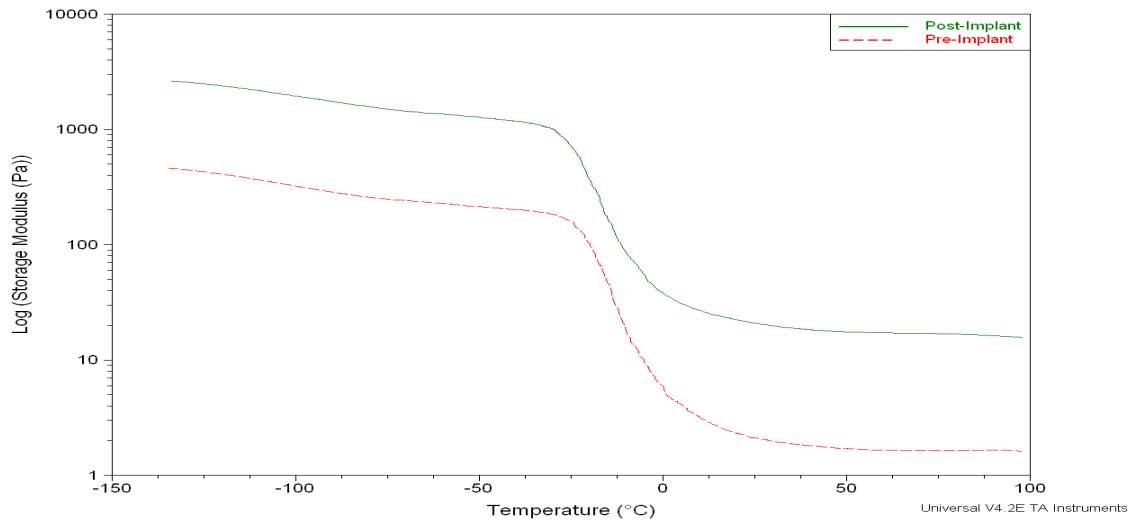


Fig 10.19. DMA result showing the storage modulus from the glassy phase, through the T_g into the rubbery plateau for the pre and post-implantation grafts. The increase in storage modulus after implantation is significant in the glassy phase.

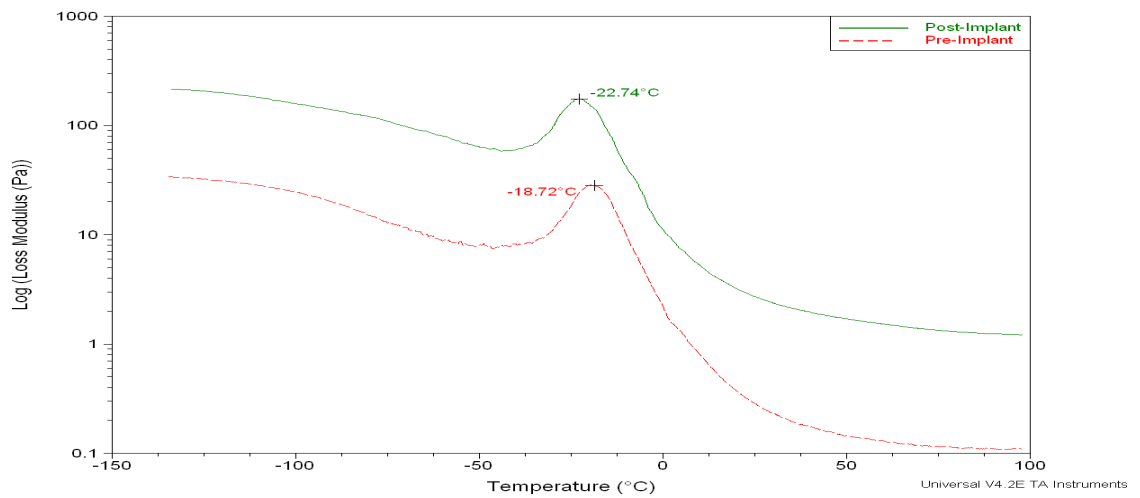


Fig 10.20. DMA result showing the loss modulus from the glassy phase, through the T_g into the rubbery plateau for the pre and post-implantation grafts. The increase in loss modulus after implantation is significant in the glassy phase.

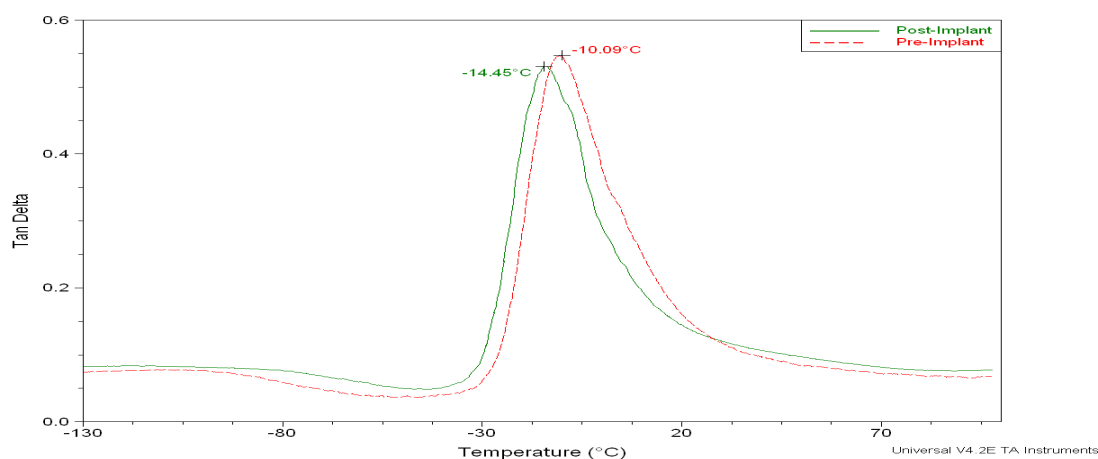


Fig 10.21. $\tan \delta$ against temperature for pre and post-implantation grafts, showing the maximum peak value, corresponding with T_g .

10.6 Discussion

The aim of this animal model was to investigate the biostability, mechanical durability and fatigue-resistance of the graft. It is the same model that has previously shown rapid biodegradation of PCU⁴⁷ (within 10 weeks). In vitro studies have suggested that PCUPOSS would last considerably longer than PCU in the ovine model. However, one concern which existed before the study was that the grafts would occlude in this model before a reasonable period of haemodynamic flow through the prostheses. For a critical vascular prosthesis exposed to continuous haemodynamic stress, industry standards require fatigue testing to a minimum of 20 million cycles. In this case, the graft was subjected to a far greater cycle number. A very conservative estimate of average heart rate for the sheep is 60 beats per minute. For this heart rate, the number of cycles for the 6 grafts which completed the test period range from 45 million to 54 million. This includes the assumption that the one occluded graft occluded on the day of the penultimate duplex showing it to still be patent.

Unlike Aldenhoff's work with PCU in the same model⁴⁷, these grafts were recovered with no visible signs of weakness or degradation. Ultrastructural analysis by SEM confirmed the graft integrity. Compliance analysis of the graft once the capsule was removed, demonstrated the same range of compliance of the pre-implantation graft. However, the fibrous capsule covering each graft

reduced compliance markedly. In fact, the compliance fell to only twice that of PTFE.

The capsule also resulted in a large increase in the burst strength of the graft, which enhances the long term safety profile further. Investigation at the molecular level by bond analysis using FTIR did not show degradation of the vulnerable soft segment; this latter being responsible for the preserved compliance properties of the graft. This correlated with the preceding in-vitro testing³⁷⁶.

This is the first report of endothelialisation of a synthetic vascular bypass graft in an ovine model. Sheep vascular implants with medium term patency have shown no evidence of endothelialisation. The Thoralon® graft, which is a triple lamina poly(ether)urethane was used as an ovine coronary implant and remained patent for up to 426 days³⁸⁷. A thin neointima was observed histologically, similar to that found on PTFE grafts explanted from humans. However, this graft had no transmural endothelialising potential due to a non-porous middle coaxial lamina. Hybrid materials with a biological component have been shown to endothelialise through the graft wall, with Grabenwoger demonstrating endothelial cell presence in the pores created by laser, as well as on the graft surface 3 months after implantation³⁸⁸.

10.7 Conclusion

This is the longest reported in vivo study for any vascular prosthesis in the ovine model. Synthetic grafts have been particularly disappointing in sheep, and these have never endothelialised, making this a stringent model. Incorporation of a POSS nanomolecule into an established polyurethane has conferred biostability to it as demonstrated in this long term stringent durability model incorporating both haemodynamic flow and a biological environment. The fatigue test is well beyond that required for international standard certification for a critical vascular prosthesis. There is evidence of patchy endothelial cell coverage but as this was not a primary outcome measure in this study, this will need to be evaluated with further animal work. The traditional thinking that ovine models only endothelialise grafts from the anastomotic edge is disputed by this report. It may be that other grafts have not been tested in ovine models for long enough to cause significant endothelialisation.

The original graft design included matching of arterial compliance to minimise stenosis and midterm/longterm failure, principally by neointimal hyperplasia (NIH). However, four out of six grafts which were tested till completion of the study showed no evidence of anastomotic narrowing from NIH despite a fibrous capsule which dramatically reduced compliance. This may be partly due to the geometric difference between the end-to-end interpositional model used here compared with the traditional end-to-side anastomosis in clinical use.

The field of nanotechnology reopens opportunities to consider synthetic materials to meet the multiple demands of a successful small caliber vascular bypass graft.

Automated techniques for reproducible industrial manufacture of the graft are currently being developed in order to pursue clinical trials of this prosthesis. Also, to improve patency further, biofunctionalisation³⁸⁹ of the nanocomposite to encourage speedy endothelialisation is being pursued³⁹⁰.

II

Conclusion

At the start of my research I was handed a viscous polymer solution which had shown promising properties in vitro for consideration as a small calibre vascular bypass prosthesis. The department had considerable experience already with the polymer forming its basis – PCU; unfortunately PCU showed worrying bio-stability in vivo within a short time. To combat this problem, the polymer had been modified by covalent attachment of a nano-engineered molecule – POSS, which was composed of dimeric rings of siloxane bonds. My aim was to reproducibly manufacture a small calibre graft which was mechanically robust enough for in vivo studies, in order to then assess the long term biostability and the effect of the biological environment on the mechanical properties.

11.1 Introduction.

As way of introduction, the need for a small calibre synthetic graft was established. The commonplace unavailability of suitable autologous vessels was described, along with the poor unassisted patency of the currently used prostheses. It is clear that the whole avenue of infra-inguinal bypass down to small vessels is severely compromised by the lack of a suitable synthetic prosthesis. By revisiting the history of vascular surgery, it was described how the development of graft materials has been in sporadic bursts, with a long initial paucity of research once vascular bypass was shown to be feasible.

Advances in materials technology and war were associated with the significant advances made. Nevertheless, no better material has been found to date than PTFE, first introduced in 1959 and in common use in the seventies. This is despite a large volume of research into the large number of new materials developed in the modern era. Polyurethane polymer technology looked most promising due to the ability to achieve precise mechanical characteristics by changing chemical composition, but long-term bio-stability of the soft segment was suspect. Polycarbonate-based macroglycol was more stable than polyester and polyether due to overall improved interactions between hard and soft segments within the polyurethane. Further improvement in the shielding effect by the hard segment on the soft segment was postulated by the incorporation of POSS into the hard segment. The intention of this study was to produce and mechanically test a small calibre compliant vascular bypass graft using this nanocomposite polymer.

11.2 Mechanical properties

In order to design a new graft, an appreciation of the mechanical properties required to ensure graft success along with the forces involved in haemodynamic flow needs careful consideration. Most of the literature concerning this is found in biomechanical and engineering journals and relatively inaccessible to the surgeon. It gave valuable insight into ideal graft design and the complex physics could be distilled into easily understood principles. Extrapolation from these concepts needs to be tempered by the realisation that blood is non-Newtonian and arteries are non-rigid pipes with unpredictable branching patterns.

It was derived from Poiseuille's formula that small calibre vessels endured very high vascular resistance. The implication for a potential small calibre graft would be high outflow resistance, promoting relative stasis and the thrombotic state. Furthermore, at the proximal anastomosis, the calibre reduction of the graft would result in high wall shear stress.

High WSS is associated with endothelial injury, which in turn is associated with NIH. Low WSS also contributes to NIH. There is conflicting evidence as to whether peri-anastomotic compliance mismatch between native vessel and graft causes NIH, but it is evident that this mismatch in combination

with anastomotic geometry is responsible for areas of abnormal WSS. With small calibre graft design, it is reasonable to aim for compliance matching, as the consequences of intimal hyperplasia are amplified by graft size.

The flow in small distal vessels is not fully pulsatile due to the influence of vessel viscosity. By dissipation and storage of the pulsatile energy, the effect on flow is to become a more continuous stream, which in turn reduces WSS. A viscoelastic graft would be preferable to a purely elastic one for this reason. The presence of viscosity is inherent within the concept of compliance, which can be considered to be distensibility of the vessel at a given mean haemodynamic pressure. In an artery, distensibility is high at low mean pressures and vice versa, due to the organisation of elastin and collagen fibres.

Porosity is one way in which graft compliance has been manipulated. It may also reduce thrombogenicity by improved blood:graft interface as well as transmural endothelialisation. However high porosity is associated with fibrous ingrowth which reduces compliance in vivo dramatically. High porosity can also result in a reduction in graft burst pressure.

The burst pressure of native vessels far exceeds haemodynamic conditions. The same is true for commercially available prosthetic grafts. However, anastomotic suture lines fail at lower pressures when considering compliant grafts, and additionally, the viscoelastic properties of compliant materials may mean such high burst strengths are not required.

11.3 Thrombogenicity

Although thrombogenicity studies had already been conducted on the nanocomposite polymer by a preceding investigator, it became clear that graft construction could not be separated into mechanical and blood compatibility properties with considerable overlap between the two. Fundamentally, a thrombogenic graft could not allow long term in vivo mechanical testing. The role of compliance matching on the development of intimal hyperplasia is dependent on graft thrombogenicity. Changing graft characteristics such as porosity have simultaneous effects on platelet adhesion and thrombogenicity. Turbulence and excessive WSS causes platelet activation and subsequent thrombosis.

The arterial blood:surface interface is the vascular endothelial cell which

inhibits platelet aggregation through membrane anticoagulants and cytokine release via multiple intracellular signalling pathways. These same mechanisms are attenuated to promote thrombosis to limit the consequences of vascular injury. They are also copied by graft developers to improve surface characteristics. In particular, heparin-bonding is being widely investigated, including clinically; this is particularly feasible with polyurethane which allows the possibility of covalently bonded heparin or heparin-like moieties. Heparin bonding also reduces intimal hyperplasia. More recently, the role of nitric oxide elution for platelet inhibition is being developed.

Rather than mimic the endothelial cell function, many groups have used strategies to encourage endothelialisation of the graft wall. The high flow through small calibre grafts is unlikely to allow significant luminal endothelial cell adherence, and pre-implantation seeding techniques have been examined using compliant grafts and different pulsatile conditions. Transmural angiogenesis and endothelialisation is dependent on the pore size of a graft.

Electronegative and to a lesser extent, hydrophilic graft surfaces are associated with platelet repulsion. Materials with excellent mechanical properties have had to be discounted due to hydrophobicity (silicon) and surface modification with hydrophilic domains such as heparin and polyethylene glycol could be used to convert a hydrophobic surface into an amphiphilic one, provided secure permanent bonding.

In summary, although it has been shown that the nanocomposite has low thrombogenicity, construction of a graft from this polymer needs to take account of the structural components affecting platelet adherence and activation along with the possibility of incorporating strategies to reduce thrombogenicity further. Long term mechanical testing in vivo will not be possible without considering thrombogenicity simultaneously.

11.4 Tissue-engineering

There were several recurring themes which led me to look at tissue-engineered blood vessels. The ideal vascular graft requires multiple characteristics which are difficult to achieve in synthetic prostheses. Several of these criteria appear to be in direct opposition; for example, strength and compliance. Furthermore, the required properties can change depending on the

prevailing haemodynamic conditions, both acutely and in the long term. Synthetic materials have been investigated for over half a century without being able to satisfy these multiple criteria. As native arteries have all of the required properties, it may be easier to artificially reconstruct the artery than develop a synthetic graft which fulfils all the demands.

Generally speaking, a tissue-engineered blood vessel is the combination of viable confluent sheets of cells arranged around a tubular scaffold. Synthetic grafts can act as the scaffold, although if they do not subsequently biodegrade, a hybrid graft rather than a fully tissue-engineered graft results. This former will continue to have many of the perceived disadvantages of a synthetic graft. The advantage of using a synthetic scaffold is that it gives initial mechanical stability, and time for the regenerating tissues to take up haemodynamic stress. Alternative strategies include using collagen sheets as a strong scaffold, or a fibrinous scaffold which stimulates fibroblasts to lay connective tissue down. Smooth muscle cells afford contractility and endothelial cells prevent thrombotic occlusion.

Achieving the appropriate connective tissue matrix and cellular structure along with robust mechanical properties is a huge challenge. Even after endothelial cell seeding mechanical strength required before consideration for implantation requires a month at the very least, excluding it as an option for critical limb ischaemia. As yet, tissue engineering is not a more viable option than a synthetic prosthesis.

Yet at the same time materials science continues to progress rapidly. Nanotechnology is an emerging field which is revolutionising materials science. Although traditional materials technology may not have yielded a graft which fulfils the multiple demands for a successful small calibre vascular graft, nano-engineered molecule attachments may be able to improve the properties of traditional materials.

11.5 Materials

Traditional composite technology is a well established method of improving material properties. Polyurethanes can be considered 'microcomposites' with microphase separation between macroglycol soft

segments imparting elasticity and crystalline hard segments imparting strength. However, polyurethanes have not shown the convincing long term biostability required for a permanent vascular implant. As yet the size-related properties of nanocomposites are not fully predictable. POSS is based on the siloxane bond which is biologically inert, making it suitable for implantation. However, long chains of siloxane have low solubility which makes them weak when used as the soft segment in polyurethanes. The original intention was to improve the biodegradation profile of polyurethanes, and in particular, PCU, by incorporating small cyclical siloxane structures in small quantities in the hard segment. The PCU-POSS polymer used has previously been shown to have low thrombogenicity as well as demonstrating resistance to degradation when exposed to biodegradative environments in vitro. This former property brings the realistic prospect of a small calibre graft that need not rely on endothelialisation in the short, medium or long term. It rebuts the argument that tissue-engineering is the only way to construct such a graft.

The nanocomposite was synthesized in house with a view to manufacturing it into small calibre bypass grafts.

11.6 Graft manufacture

From the previous observations, a compliant porous graft of variable small calibre which could be reproducibly manufactured was sought. A combination of extrusion to ensure a uniform wall and phase inversion to remove solvent from the polymer in a precise manner, thereby coagulating the polymer was used.

A purpose-built bench-top vertical extruder was made. Steel mandrels were driven through a polymer chamber into coagulant solution. Steel mandrel diameter determined graft calibre. The outlet aperture determined wall thickness. The precise alignment of the mandrel in relation to the exit aperture determined the uniformity of the wall thickness. Due to the vertical extrusion process, correction for gravity was unnecessary. Very precise wall uniformity was achieved across the whole graft circumference.

In order for the mandrel to coat itself with polymer within the polymer chamber and drive through into the coagulant without the polymer drifting down

relative to the mandrel, polymer viscosity of 3PaS was required. The maximum usable length of 86mm was achieved by injecting 3.5ml of polymer in the polymer chamber. Storage of the polymer resulted in an increase in viscosity due to the evaporation of the DMAC solvent over time. Using different batches of raw materials had a profound effect on the viscosity. The industrial quality control for the raw materials were accepted, leaving the probability that the chemistry was changing during storage, for example by oxidation, hydration or spontaneous dimerization of the MDI. Therefore, to reduce variability, all of the grafts tested were made from a single batch of polymer made freshly from newly ordered raw materials.

The thin and thick-walled grafts produced using these parameters were of uniform thickness and reproducible as assessed by bespoke image analysis.

Combining the extrusion-phase inversion technique with salt leaching resulted in grafts which mirrored the high compliances of arteries at very low pressures ($15\%/mmHg \times 10^{-2}$). However, the very high porosity was at the expense of strength. In addition, striving for such high compliance was unnecessary, for the compliance of arteries at physiological pressures was much lower ($5\%/mmHg \times 10^{-2}$).

It was discovered that a highly porous structure resulted even without salt-leaching. Using coagulant at $50^{\circ}C$ produced grafts with pores which collapsed after drying the graft. This was prevented by using coagulant at $0^{\circ}C$. This difference was explained by higher porosity in grafts extruded at high temperature. The porosity was not homogenous. The outer surface was non-porous with microscopic ridges; inside this there were small pores; bigger pores near the lumen, and a lumen with few small pores.

Slowing the exchange of solvent for coagulant by reducing the DMAC gradient resulted in an increase in the size of the biggest pores near the lumen, without affecting the other layers. Adding ethanol to the coagulant led to an increase in pore size and pore uniformity at the lumen itself.

The overall effect of the four layer pore design was to ensure the grafts did not need pre-clotting, and would show elastic strain via compression of the vessel wall rather than radial expansion. However, the non-porous outer skin could be associated with fibrous capsule formation, and resultant compliance loss. In addition, low porosity at the lumen is associated with poor spontaneous endothelialisation in animal models. However, unlike in animal models, synthetic

grafts have not been shown to spontaneously endothelialise in humans.

The next step in developing these grafts was to mechanically characterise them.

11.7 Mechanical characterisation

Tensile testing demonstrated the behaviour of the graft material under tensile stress, comparing it with PTFE and using the results to assess reproducibility of mechanical properties of the grafts produced. The testing process was hindered by the small dimensions of the samples and the graft/grip interface; the latter was addressed with bespoke grips.

On considering the testing protocol, it was clear that no single international standard was ideal. ISO 37 for highly elastic materials eliminated the oscillatory movements associated with slow load arm movement, but there was high levels of graft slippage. ISO 7198, which is specific to vascular implants, but not ideal for highly compliant materials resulted in high rates of premature test abortion due to oscillatory tensile movements. A further cause of test failure was test commencement with the sample in tension. This was inevitable with hoop specimen testing, leading to their substitution for small dogbone specimens, using a bespoke small cutter.

The preliminary tensile testing of the nanocomposite cast sheet showed it to be both extremely strong and elastic. The ultimate strength was in the region of 60MPa, compared with 11MPa for commercially available small calibre expanded PTFE graft. POSS incorporation into PCU resulted in a threefold increase in ultimate strength, provided ideal stoichiometry was realised. This ideal chemistry was ensured by meticulous measuring and mixing of the reactants as well as rejecting any dimerised MDI. PTFE showed low elasticity. Although the cast sheets were extremely elastic, with failure occurring at 900 to 1000% strain, at low level (physiological) stresses the elasticity was low. For comparison, PCU alone could be subjected to 600-800% strain before failure.

As expected, the porous grafts were much weaker than the cast sheets, failing at 0.6-1.1 MPa. However, at low level stress, they were highly elastic. The J-shaped curve which protects against aneurysmal dilatation was not evident. The ultimate strength circumferentially was lower than longitudinally.

The stress-relaxation phenomenon was used to demonstrate the viscous component of graft mechanical behaviour under conditions of stress. This visco-elastic behaviour highlighted the importance of assessing graft behaviour exposed to haemodynamic forces rather than stress in single directions, as the results of the latter depend on the rate of stress application. Furthermore, the clinical applicability of the stress/strain results needed to be determined. For these reasons, functional mechanical characterisation was undertaken.

11.8 Functional mechanical characterisation

To achieve the aim of matching human arterial compliance, a clear understanding of normal lower limb artery compliance was required. The compliances previously quoted for artery (including using the same pulsatile flow apparatus used here) were higher than the target compliance for two principle reasons. because they were ex-vivo segments without the restrictive effect of surrounding tissues and neurochemical modulation; the mean pressure used to measure compliance was lower than physiological norms. In vivo measurement using wall tracking ultrasound demonstrated compliance of $3.5\%/mmHg \times 10^{-2}$ at the common femoral artery.

However its compliance within the range of stresses expected in pulsatile haemodynamic flow was low. Porosity was introduced to improve the compliance at low stress levels. Initial attempts using a salt leaching technique in combination with coagulation-phase extrusion resulted in an extremely compliant graft which was too weak to withstand haemodynamic forces. However, on reflection the compliance being sought was higher than that for native artery. The reason for this error was twofold. Firstly the maximum compliance of the lower limb vessels was being considered rather than the normal compliance. So at very low pulse pressures which are not physiologically sustainable, arteries show very high compliance due to the predominance of the role of elastin fibres at low pressures. The second reason for an overestimation of the required compliance is due to the testing of recently explanted arteries rather than in situ investigation. The latter has contribution from inotropes along with the restrictive influence of soft tissue surrounding the vessel. Using wall-tracking ultrasound to measure compliance in native human

common femoral artery, $3.5 \% / \text{mmHg} \times 10^{-2}$ was the result, which tallied with other studies of in-vivo human lower limb arterial compliance. The compliance reduced further distally in smaller arteries.

The salt-leaching technique, when combined with extrusion-phase inversion produced grafts which mirrored the very high compliances of ex-vivo arterial samples tested at low mean pressures ($>15\% / \text{mmHg} \times 10^{-2}$). However, this level of compliance was unnecessary and these grafts burst within the flow circuit at a systolic pressure of only 140mmHg.

The thick-walled nanocomposite grafts manufactured using deionised water at 0°C as coagulant showed a compliance of $5\% / \text{mmHg} \times 10^{-2}$. This compliance was the same for all mean pressures between 25 and 100mmHg, unlike arterial compliance. The thin-walled grafts were more compliant than the thick-walled; this compliance increased with increasing mean pressure which is undesirable due the propensity for aneurysmal dilatation in the long term. This pattern of compliance fitted with the previous tensile testing showing a convex curve as opposed to the desired J-shape. The burst pressures for thin and thick grafts were 220 and 365mmHg respectively.

Modulation of the interaction between hard segment and soft segment was used to try to optimise strain-crystallisation whilst maintaining high burst pressure, thereby improving the compliance properties throughout the range of mean pressures. Increasing the proportion of POSS from 2% to 6% reduced compliance, with no effect on burst pressure. This illustrates that the properties imparted by interactions at the nanoscale level are not improved by increasing the amount of the nano-molecule. Increasing the hard segment proportion similarly reduced compliance. Branching disruption of the hard segment to reduce overall crystallinity did improve the burst pressure to 450 and 560mmHg for thin and thick-walled grafts respectively. It also increased compliance, with the thin-walled grafts demonstrating the desired high compliance at low mean pressure and low compliance at high mean pressure.

All of the nanocomposite polymers used demonstrated pulsatile energy transfer into the graft wall equivalent to that for human arteries; this is important for energy capacitance in the graft wall as well as converting the pulsatile pump energy of the heart into a steady stream of flow at the end organ. Inflation caused elongation (10%) of all nanocomposite grafts due to compliance in the longitudinal direction, meaning subsequent in vivo implantation would require a

10% stretch.

The functional mechanical testing showed that compliant grafts which would in the immediate term be robust enough for in vivo haemodynamic testing. Whether this would translate to longer term stability in the biological environment was addressed in the final experimental chapter. Although the chain-disrupted polymer was found to have the best mechanical properties, only the 2% POSS nanocomposite had been fully chemically characterised so far, including toxicity studies. For this reason, the former was not chosen for animal studies.

11.9 Burst pressure measurement

This small study was inspired by the large number of available standards available for testing materials and specifically critical biomedical implant materials such as cardiovascular devices. The precise standard used was not always important for FDA or CE approval, as long as the exact standard used was stated. The standards did not always prescribe sample preparation. For example a commercial mechanical testing firm prepared dogbone specimens by cutting the samples using scissors, which introduces considerable error, weakness and edge variation compared with a punch-cutter. For some mechanical investigations there were no established testing conditions, although the tests themselves were required for regulatory body approval before clinical use. Burst pressure testing was one such investigation.

Inflation tests of porous grafts was complicated by the leaking of the inflation fluid through the graft wall itself. As graft inflation increases, the pores stretch worsening the problem. Use of a latex lining eliminates this problem, and is essential for porous compliant materials. However, the burst pressure achieved is significantly higher if inflation of the latex lining is undertaken at very high inflation rate. Furthermore, in compliant materials the burst pressure may be lower than the true failure pressure, which is the aneurysmal point for the graft. This is the point at which further inflation does not result in further pressure increase due to aneurysmal ballooning of the graft.

11.10 In vivo model

It was important to show that the graft was strong enough in the dynamic state over a longer term to ensure it would not fatigue easily. In addition, the biostability over PCU suggested in in-vitro testing needed to be confirmed in-vivo. The most stringent test of defatigability would be an ovine model, firstly because of the clear failure of PCU in this model previously, and secondly, because of the poor record of patency of other established and prototype synthetic grafts in this model. However, ovine vascular haemodynamics, blood clotting profile and graft healing is similar to the human, making it an apt model. In particular, in common with humans, the ovine model does not easily endothelialise synthetic grafts. An implantation period which was well in excess of the cycle-testing required from the international standard agencies for a critical vascular prosthesis was achieved with patent grafts. This period was the longest reported implantation of small calibre synthetic grafts in this model. Visual, microscopic, ultrasopic structural analysis, mechanical property analysis and physioco-chemical analysis all confirmed that the implantation in the biological environment, exposed to haemodynamic flow did not cause significant biodegradation. This contrasts markedly with the clear visible degradation of PCU within a few weeks in the ovine model, showing that the incorporation of the POSS nanomolecule afforded impressive resistance to biodegradation.

The patency may have been initially aided by graft compliance but over time a fibrous capsule reduced this property very markedly. This supports the theory that compliance matching is essential to prevent NIH in thrombogenic graft materials, but less important in conduits with a favourable thrombogenicity profile. The low level NIH that was seen may be as a result of the loss of compliance due to the fibrous capsules.

It was altogether a surprise to find some patchy endothelial-like cells which immunostained positive for CD31 and vWF. It may be that unlike humans the ovine model does endothelialise vascular grafts but very slowly, and previous synthetic conduits have occluded before such a time frame has passed. The ovine model was primarily performed to assess biodegradation, and the graft samples were required on explantation for thermal, mechanical and chemical testing. As a result the further investigation of the healing of the

graft including the percentage extent of endothelialisation, the functional capacity of these cells and the timing of laying down of these cells could not be investigated. This is the next step.

11.1 Further Work

As my research progressed, many other exciting avenues opened up, which I would have liked to have pursued, if time and facilities were available. On the mechanical side, the next step would have been to use the detailed biaxial tensile data in a finite element analysis logarithm to see if predictions of graft behaviour could be made from such models.

The final graft used for implantation was necessarily made from the 2% POSS nanocomposite. This was because the cytocompatibility and thrombogenicity studies were performed by my preceding investigators on this particular material. However, during the course of this mechanical investigation, it became clear that the chain-disrupted variant had superior mechanical properties to PCUPOSS. However, this could not be used in animal models without repeating the painstaking work referred to. There just wasn't time. However, this is an exciting avenue to pursue, and may result in an improved next generation nanocomposite graft, by way of its improved mechanical properties.

One graft did occlude, and another showed evidence of stenosis. Possible reasons for this has not been investigated. The fibrous capsule reducing compliance may be partly responsible and a control to implant a vascular graft in the ovine neck without anastomosing it into the vascular tree would start to answer the question of whether it was due to pure inflammatory reaction against the graft material or whether it was due to the constant rubbing of the external wall against the subcutaneous tissues as a result of the pulsation of the compliant graft. Another way to address this question would be to implant the graft as before with another larger graft surrounding it so that the pulsation would be 'hidden' within the outer envelope.

The PhD students following me are developing the graft further mechanically by using the extrusion-phase inversion principle to produce long lengths of graft in association with industrial partners. This will be essential for

the step up to clinical implantation. They are also introducing biofunctionality by adding groups for nitric oxide release and heparin-like moieties. These will add to the patency performance of the graft further.

Simultaneously the nanocomposite is being developed for many other biological implant applications such as microvascular grafts, breast implant capsules, biodegradable scaffolds for bone formation and small bowel.

Reference List

1. Ashley, S., Ridler, B., and Kinsman, R. National Vascular Database Report. The Vascular Surgical Society of Great Britain and Ireland . 2002.
2. Whittemore AD, Kent KC, Donaldson MC, Couch NP, Mannick JA. What is the proper role of polytetrafluoroethylene grafts in infrainguinal reconstruction? *J Vasc Surg* 1989;**10**:299-305.
3. Klinkert P, Post PN, Breslau PJ, van Bockel JH. Saphenous vein versus PTFE for above-knee femoropopliteal bypass. A review of the literature. *Eur J Vasc Endovasc Surg* 2004;**27**:357-62.
4. Veith FJ, Moss CM, Sprayregen S. Preoperative saphenous venography in arterial reconstructive surgery of the lower extremity. *Surgery* 1979;**85**:253-6.
5. Armstrong PA, Bandyk DF, Wilson JS, Shames ML, Johnson BL, Back MR. Optimizing infrainguinal arm vein bypass patency with duplex ultrasound surveillance and endovascular therapy. *J Vasc Surg* 2004;**40**:724-31.
6. Dardik H, Wengerter KR, Qin F, Pangilinan A, Silvestri F, Wolodiger F *et al.* Comparative decades of experience with glutaraldehyde-tanned human umbilical cord vein graft for lower limb revascularization:an analysis of 1275 cases. *J Vasc Surg* 2002;**35**:64-71.
7. Leserche G, Penna C, Bouttier S, Joubert S, Andreassian B. Femorodistal bypass using cryopreserved venous allografts for limb salvage. *Ann Vasc Surg* 1997;**11**:230-6.
8. Pfeiffer RB, Pfeiffer RB Jr, Esses GE, Watts B. In situ femoral to popliteal bypass graft using superficial femoral vein to popliteal vein. *Am Surg* 2004;**70**:617-9.
9. Schulman ML, Badhey MR, Yatco R. Superficial femoral-popliteal veins and reversed saphenous veins as primary femoropopliteal bypass grafts: a randomized comparative study. *J Vasc Surg* 1987;**6**:1-10.
10. Coburn M, Ashworth C, Francis W, Morin C, Broukhim M, Carney WI Jr. Venous stasis complications of the use of the superficial femoral and popliteal veins for lower extremity bypass. *J Vasc Surg* 1994;**19**:759-60.
11. Salacinski HJ, Goldner S, Giudiceandrea A, Hamilton G, Seifalian AM. The mechanical behaviour of vascular grafts: a review. *J Biomater Applic* 2001;**15**:241-78.
12. Devine C, McCollum C, North West Femoro-Popliteal Trial

Participants. Heparin-bonded Dacron or polytetrafluoroethylene for femoropopliteal bypass: five-year results of a prospective randomized multicentre clinical trial. *J Vasc Surg* 2004;**40**:924-31.

13. Ballota E, Renon L, Toffano M, Giau G. Prospective randomized study on bilateral above-knee femoropopliteal revascularization: polytetrafluoroethylene graft versus reversed saphenous vein. *J Vasc Surg* 2003;**38**:1051-5.
14. Sala F, Hassen-Khodja R, Lecis A, Bouillane PJ, Declémy S, Batt M. Long term outcome of femoral above-knee popliteal bypass using autologous saphenous vein versus expanded polytetrafluoroethylene grafts. *Ann Vasc Surg* 2003;**17**:401-7.
15. Ballota E, Renon L, De Rossi A, Barbon B, Terranova O, Da Giau G. Prospective randomized study on reversed saphenous vein infrapopliteal bypass to treat limb-threatening ischaemia: common femoral artery versus superficial femoral or popliteal and tibial arteries as inflow. *J Vasc Surg* 2004;**40**:732-40.
16. Klinkert P, Dijk PJE, Breslau PJ. Polytetrafluoroethylene femorotibial bypass grafting: 5-year patency and limb salvage. *Ann Vasc Surg* 2003;**17**:486-91.
17. Kunlin J. The treatment of arterial obstruction by vein grafting. *Arch Mal Coeur* 1949;**42**:371-5.
18. Blakemore AH, Voorhees AB. The use of tubes constructed from Vinyon "N" cloth in bridging arterial defects - experimental and clinical. *Ann Surg* 1954;**140**:324-34.
19. Hughes CW. Arterial repair during the Korean War. *Ann Surg* 1958;**147**:555-61.
20. Matsumoto H, Hasegawa T, Fuse K, Yamamoto M, Saigusa M. A new vascular prosthesis for a small caliber artery. *Surgery* 1973;**74**:519-23.
21. Raithel D, Groitl H. Small artery reconstruction with a new vascular prosthesis. *World J Surg* 1980;**4**:223-30.
22. Veith FJ, Moss CM, Fell SC, Montefusco C, Rhodes BA, Haimovici H. Comparison of expanded polytetrafluoroethylene and autologous saphenous vein grafts in high risk arterial reconstructions for limb salvage. *Surg Gynecol Obstet* 1978;**147**:749-52.
23. Echave V, Koornick AR, Haimov M, Jacobson JH. Intimal hyperplasia as a complication of the use of the polytetrafluoroethylene graft for femoro-popliteal bypass. *Surgery* 1979;**86**:791-8.
24. Kidson IG, Abbott WM. Low compliance and arterial graft failure. *Circulation* 1978;**58**:I1-4.

25. GReisler HP, Tattersall CW, Henderson SC, Cabusao EA. Polypropylene small-diameter vascular grafts. *J Biomed Mater Res* 1992;**26**:1383-94.
26. Mary C, Marois Y, King MW, Laroche G, Douville Y, Martin L *et al.* Comparison of the in vivo behaviour of polyvinylidene fluoride and polypropylene sutures used in vascular surgery. *ASAIO J* 1998;**44**:199-206.
27. Sottiurai VS. Distal anastomotic intimal hyperplasia: histocytomorphology, pathophysiology, etiology and prevention. *Int J Angiol* 1999;**8**:1-10.
28. Sottiurai VS, Kollros P, Glagov S, Zarins CK, Mathews MB. Morphologic alteration of cultured arterial smooth muscle cells by cyclic stretching. *J Surg Res* 1983;**35**:490-7.
29. Longest PW, Kleinstreuer C. Particle-hemodynamics modeling of the distal end-to-side femoral bypass: effects of graft caliber and graft-end cut. *Medical Engineering and Physics* 2003;**25**:843-58.
30. Perktold K, Leuprecht A, Prosi M, Berk T, Czerny M, Trubel W *et al.* Fluid dynamics, wall mechanics and oxygen transfer in peripheral bypass anastomoses. *Ann Biomed Eng* 2002;**30**:447-60.
31. Habal MB. The biologic basis for the clinical application of the silicones: a correlate to their biocompatibility. *Arch Surg* 1984;**119**:843-8.
32. Kottke-Marchant K, Anderson JM, Miller KM, Marchant RE, Lazarus H. Vascular graft-associated complement activation and leukocyte adhesion in an artificial circulation. *J Biomed Mater Res* 1987;**21**:379-97.
33. Moss AH, Vasilakis C, Holley JL, Foulks CJ, Pillai K, McDowell DE. Use of silicone dual-lumen catheter with a dacron cuff as a long term vascular access for hemodialysis patients. *Am J Kidney Dis* 1990;**16**:211-5.
34. Christenson EM, Dadsetan M, Hiltner A. Biostability and macrophage-mediated foreign body reaction of silicone-modified polyurethanes. *J Biomed Mater Res A* 2005;**74**:141-55.
35. White RA, Klein SR, Shors EC. Preservation of compliance in a small diameter microporous, silicone rubber vascular prosthesis. *J Cardiovasc Surg* 1987;**28**:485-90.
36. Julio CA, de-Queiroz AA, Higa OZ, Marques EF, Maizato MJ. Blood compatibility of tubular polymeric materials studied by biological surface interactions. *Braz J Med Biol Res* 1994;**27**:2565-8.
37. Whalen RL, Cardona RR, Kantrowitz A. A new all silicone rubber small vessel prosthesis. *ASAIO J* 1992;**38**:M207-M212.

38. Puckett MA, DeFriend D, Williams MP, Roobottom CA. A leaking breast prosthesis presenting as an abdominal mass. *Br J Radiol* 2004;**77**:790-1.
39. Garrido L, Pfliederer B, Papisov M, Ackerman JL. In vivo degradation of silicones. *Magn Reson Med* 1993;**29**:839-43.
40. Szycher M. Biostability of polyurethane elastomers: a critical review. *J Biomat Applic* 1988;**3**:297-402.
41. Bedini R, Chistolini P, De Angelis G, Formisano G, Caiazza S. VAD Biomer blood sacs: mechanical tests and ultrastructural observations. *Med Prog Technol* 1993;**19**:83-8.
42. Szycher M, Reed AM, Siciliano AA. In vivo testing of a biostable polyurethane. *J Biomater Appl* 1991;**6**:110-30.
43. Edwards A, Carson RJ, Bowald S, Quist WC. Development of a microporous compliant small bore vascular graft. *J Biomater Appl* 1995;**10**:171-87.
44. Belanger MC, Marois Y, Roy R, Mehri Y, Wagner E, Zhang Z *et al.* Selection of a polyurethane membrane for the manufacture of ventricles for a totally implantable artificial heart: blood compatibility and biocompatibility studies. *Artif Organs* 2000;**24**:879-88.
45. Dempsey DJ, Phaneuf MD, Bide MJ, Szycher M, Quist WC, LoGerfo FW. Synthesis of a novel small diameter polyurethane vascular graft with reactive binding sites. *ASAIO J* 1998;**44**:M506-M510.
46. Wetzels GM, Koole LH. Photoimmobilisation of poly(N-vinylpyrrolidinone) as a means to improve haemocompatibility of polyurethane biomaterials. *Biomaterials* 1999;**20**:1879-87.
47. Aldenhoff YB, van der Veen FH, ter Woost J, Habets J, Poole-Warren LA, Koole LH. Performance of a polyurethane vascular prosthesis carrying a dipyridamole (Persantin) coating on its luminal surface. *J Biomed Mater Res* 2001;**54**:224-33.
48. Fields C, Cassano A, Allen C, Meyer A, Pawlowski KJ, Bowlin GL *et al.* Endothelial cell seeding of a 4-mm I.D. polyurethane vascular graft. *J Biomater Appl* 2002;**17**:45-70.
49. Tang YW, Labow RS, Santerre JP. Enzyme-induced biodegradation of polycarbonate-polyurethanes: dependence on hard-segment chemistry. *J Biomed Mater Res* 2001;**57**:597-611.
50. Kannan RY, Salacinski HJ, De Groot J, Clatworthy I, Bozec L, Horton M *et al.* The antithrombogenic potential of a polyhedral oligomeric silsesquioxane (POSS) nanocomposite. *Biomacromolecules* 2006;**7**:215-23.

51. Campbell CD, Brooks DH, Bahnson HT. Expanded microporous polytetrafluoroethylene (Gore-tex) as a vascular conduit. In Sawyer PN, Kaplitt MJ, eds. *Vascular Grafts*, pp 335-48. New York: Appleton-Century-Crofts, 1978.
52. Sottiurai VS, Yao JST, Batson RC, Sue SL, Jones R, Nakamura YA. Distal anastomotic intimal hyperplasia: histopathologic character and biogenesis. *Ann Vasc Surg* 1989;3:26-33.
53. Chignier E, Eloy R. Adventitial resection of small artery provokes endothelial loss and intimal hyperplasia. *Surg Gynaecol Obstet* 1986;163:327-34.
54. Hasson JE, Megerman J, Abbott WM. Suture technique and para-anastomotic compliance. *J Vasc Surg* 1986;3:591-8.
55. Trubel W, Schima H, Czerny M, Perkold K, Schimek MG, Polterauer P. Experimental comparison of four methods of end-to-side anastomosis with expanded polytetrafluoroethylene. *Br J Surg* 2003;91:159-67.
56. Wu SP, Ringgaard S, Oyre S, Hansen MS, Rasmus S, Pedersen EM. Wall shear rates differ between the normal carotid, femoral and brachial arteries: an in vivo MRI study. *J Magn Reson Imaging* 2004;19:188-93.
57. Fei D-Y, Thomas JD, Rittgers SE. The effect of angle and flow rate upon hemodynamics in distal vascular graft anastomoses: a numerical model study. *J Biomech Eng* 1994;116:331-6.
58. Roeder R, Wolfe J, Lianakis N, Hinson T, Geddes LA, Obermiller J. Compliance, elastic modulus and burst pressure of small intestine submucosa (SIS), small diameter vascular grafts. *J Biomed Mater Res* 1999;47:65-70.
59. Herbert ST, Badylak SF, Geddes LA, Hillberry B, Lantz GC, Kokini K. Elastic modulus of prepared canine jejunum, a new vascular graft material. *Ann Biomed Eng* 1993;21:727-33.
60. Cheng K-S, Tiwari A, Baker CR, Morris R, Hamilton G, Seifalian AM. Impaired carotid and femoral viscoelastic properties and elevated intima-media thickness in peripheral vascular disease. *Atherosclerosis* 2002;164:113-20.
61. Boutouyrie P, Bezie Y, Lacolley P, Challande P, Chamiot-Clerc P, Benetos A *et al.* In vivo/in vitro comparison of rat abdominal aorta wall viscosity. *Arteriosclerosis, Thrombosis, and Vascular Biology* 1997;17:1346-64.
62. Boutouyrie P, Boumaza S, Challande P, Lacolley P, Laurent S. Smooth muscle tone and arterial wall viscosity. *Hypertension* 1998;32:360-4.

63. Armentano R, Megnien JL, Simon A, Bellenfant F, Barra J, Levenson J. Effects of hypertension on viscoelasticity of carotid and femoral arteries in humans. *Hypertension* 1995;**26**:48-54.
64. Walden R, L'Italien GJ, Megerman J, Abbott WM. Matched elastic properties and successful arterial grafting. *Arch Surg* 1980;**115**:1166-9.
65. Rittgers SE, Karayannacos PE, Guy JF, Nerem RM, Shaw GM, Hostetler JR *et al.* Velocity distribution and intimal proliferation in autologous vein grafts in dogs. *Circ Res* 1978;**42**:792-801.
66. Stewart SF, Lyman DJ. Effects of a vascular graft/natural artery compliance mismatch on pulsatile flow. *J Biomech* 1992;**25**:297-310.
67. Ulrich M, Staalsen NH, Jurhuus CB, Christensen TD, Ygaard H, Asenkam JM. In vivo analysis of dynamic tensile stresses at arterial end-to-end anastomoses. Influence of suture line and graft on anastomotic biomechanics. *Eur J Vasc Endovasc Surg* 1999;**18**:515-22.
68. Baguneid MS, Goldner S, Fulford PE, Hamilton G, Walker MG, Seifalian AM. A comparison of para-anastomotic compliance profiles after vascular anastomosis: nonpenetrating clips versus standard sutures. *J Vasc Surg* 2001;**33**:812-20.
69. Piorko D, Knez P, Nelson K, Schmitz-Rixen T. Compliance in anastomoses with and without vein cuff interposition. *Eur J Vasc Endovasc Surg* 2001;**21**:461-6.
70. Sonada H, Urayama S-I, Takamizawa K, Nakayama Y, Uyama C, Yasui H *et al.* Compliant design of artificial graft: compliance determination by new digital X-ray imaging system-based method. *J Biomed Mater Res* 2002;**60**:191-5.
71. Tai NR, Salacinski HJ, Edwards A, Hamilton G, Seifalian AM. Compliance properties of conduits used in vascular reconstruction. *Br J Surg* 2000;**87**:1516-24.
72. Bank AJ, Wang H, Holte JE, Mullen K, Shammass R, Kubo SH. Contribution of collagen, elastin and smooth muscle in vivo human brachial artery wall stress and elastic modulus. *Circulation* 1996;**94**:3263-70.
73. Tiwari A, Salacinski HJ, Seifalian AM, Hamilton G. New prostheses for use in bypass grafts with special emphasis on polyurethanes. *Cardiovascular Surgery* 2002;**10**:191-7.
74. Sonada H, Takamizawa K, Nakayama Y, Yasui H, Matsuda T. Coaxial double-tubular compliant arterial graft prosthesis: time-dependent morphogenesis and compliance changes after implantation. *J Biomed Mater Res* 2003;**65A**:170-81.

75. Rashid ST, Salacinski HJ, Button MJC, Fuller B, Hamilton G, Seifalian AM. Cellular engineering of conduits for coronary and lower limb bypass surgery: role of cell attachment peptides and pre-conditioning in optimising smooth muscle cells (SMC) adherence to compliant poly(carbonate-urea)urethane (Myolink™) scaffolds. *Eur J Vasc Endovasc Surg* 2004;**27**:608-16.
76. Tiwari A, Salacinski HJ, Punshon G, Hamilton G, Seifalian AM. Development of a hybrid cardiovascular graft using a tissue engineering approach. *FASEB J* 2002;**16**:791-6.
77. Salacinski HJ, Odlyha M, Hamilton G, Seifalian AM. Thermo-mechanical analysis of a compliant poly(carbonate-urea)urethane after exposure to hydrolytic, oxidative, peroxidative and biological solutions. *Biomaterials* 2002;**23**:2231-40.
78. Weber R, Stergiopoulos N, Brunner HR, Hayoz D. Contributions of vascular tone and structure to elastic properties of a medium sized artery. *Hypertension* 1996;**27**:816-22.
79. Gurne O, Chenu P, Buche M, Louagie Y, Eucher P, Marchandise B *et al.* Adaptive mechanisms of arterial and venous coronary bypass grafts to an increase in flow demand. *Heart* 1999;**82**:336-42.
80. Hongbird H, Matsuda T. Arterial replacement with compliant hierarchic hybrid vascular graft: biomechanical adaptation and failure. *Tissue Engineering* 2002;**8**:213-24.
81. White R, Goldbegr L, Hirose F, Klein S, Bosco P, Miranda R *et al.* Effect of healing on small internal diameter arterial graft compliance. *Biomater Med Devices Artif Organs* 1983;**11**:21-9.
82. Seifalian AM, Salacinski HJ, Tiwari A, Edwards A, Bowald S, Hamilton G. In vivo biostability of a poly(carbonate-urea)urethane graft. *Biomaterials* 2003;**24**:2549-57.
83. Cheng K-S, Baker CR, Hamilton G, Hoeks AP, Seifalian AM. Arterial elastic properties and cardiovascular risk/event. *Eur J Vasc Endovasc Surg* 2002;**24**:383-97.
84. Hasson JE, Megerman J, Abbott WM. Postsurgical changes in arterial compliance. *Arch Surg* 1984;**119**:788-91.
85. Okuhn SP, Connely DP, Calakos N, Ferrell L, Pan MX, Goldstone J. Does compliance mismatch alone cause neointimal hyperplasia? *J Vasc Surg* 1989;**9**:35-45.
86. Brant AM, Rodgers GJ, Borovetz HS. Measurement in vitro of pulsatile arterial diameter using a helium-neon laser. *J Appl Physiol* 1987;**62**:679-83.
87. Knez P, Nelson K, Hakimi M, Al-Haidary J, Schneider C, Schmitz-Rixen T. Rotational in vitro compliance measurement of diverse

anastomotic configurations: a tool for anastomotic engineering. *J Biomechanics* 2004;**37**:275-80.

88. Peterson LH, Jeneson RE, Parnell J. Mechanical properties of arteries in vivo. *Circ Res* 1960;**8**:622-39.
89. Hansen F, Mangell P, Sonesson B, Lanne T. Diameter and compliance in the human common carotid artery - variations with age and sex. *Ultrasound in Med.and Biol.* 1995;**21**:1-9.
90. Vernhet H, Demaria R, Juan JM, Oliva-Lauraire MC, Quere I, Garipey J *et al.* Validation of a newly developed B-mode image-processing technique versus wall-tracking ultrasound for the study of wall mechanics in small-calibre arteries. *Clin Physiol & Func Im* 2002;**22**:180-6.
91. Long A, Rouet L, Bissery A, Goeau-Brissonniere O, Sapoval M. Aortic compliance in healthy subjects:evaluation of tissue doppler imaging. *Ultrasound in Med.and Biol.* 2004;**30**:753-9.
92. Cheng K-S, Tiwari A, Morris R, Hamilton G, Seifalian AM. The influence of peripheral vascular disease on the carotid and femoral wall mechanics in subjects with abdominal aortic aneurysm. *J Vasc Surg* 2003;**37**:403-9.
93. Lakhani K, Hardiman P, Seifalian AM. Intima-media thickness of elastic and muscular arteries of young women with polycystic ovaries. *Atherosclerosis* 2004;**175**:353-9.
94. Lakhani K, Seifalian AM, Hardiman P. Impaired carotid viscoelastic properties in women with polycystic ovaries. *Circulation* 2002;**106**:81-5.
95. Cheng K-S, Tiwari A, Boutin A, Denton CP, Black CM, Morris R *et al.* Carotid and femoral arterial wall mechanics in scleroderma. *Rheumatology* 2003;**42**:1299-305.
96. Rerkpattanapipat P, Hundley WG, Link KM, Brubaker PH, Hamilton CA, Darty SN *et al.* Relation of aortic distensibility determined by magnetic resonance imaging in patients > or = 60 years of age to systolic heart failure and exercise capacity. *Am J Cardiol* 2002;**90**:1221-5.
97. Cebral JR, Yim PJ, Lohner R, Soto O, Choyke PL. Blood flow modeling in carotid arteries with computational fluid dynamics and MR imaging. *Acad Radiol* 2002;**9**:1286-99.
98. Seifalian AM, Hawkes DJ, Giudiceandrea A. A novel technique of blood flow and compliance measurement using digital subtraction angiography. In Greenhalgh RM, ed. *Vascular Imaging For Surgeons*, pp 51-70. London: W.B. Saunders, 1995.
99. Hirayama H, Nishimura T, Fukuyama Y. An impedance matching

of femoral-popliteal arterial grafts: a theoretical study. *Artificial Organs* 1997;**21**:379-90.

100. Perkold K, Leuprecht A, Prosi M, Berk T, Czerny M, Trubel W *et al.* Fluid dynamics, wall mechanics, and oxygen transfer in peripheral bypass anastomoses. *Ann Biomed Eng* 2002;**30**:447-60.
101. Stewart SF, Lyman DJ. Effects of an artery/vascular graft compliance mismatch on protein transport: a numerical study. *Ann Biomed Eng* 2004;**32**:991-1006.
102. Rachev A, Manoach E, Berry J, Moore Jr JE. A model of stress-induced geometrical remodeling of vessel segments adjacent to stents and artery/graft anastomoses. *J Theor Biol* 2000;**206**:429-43.
103. Shu MC, Hwang NH. Flow phenomena in compliant and non-compliant arteriovenous grafts. *ASAIO Trans* 1988;**34**:519-23.
104. Wu MH, Shi Q, Sauvage LR, Kaplan S, Hayashida N, Patel MD *et al.* The direct effect of graft compliance mismatch per se on development of host arterial intimal hyperplasia at the anastomotic interface. *Ann Vasc Surg* 1993;**7**:156-68.
105. Uchida N, Emoto H, Kambic H, Harasaki H, Chen JF, Hsu SH *et al.* Compliance effect on patency of small diameter vascular grafts. *ASAIO Trans* 1989;**35**:556-8.
106. Norberto JJ, Sidawy AN, Trad KS, Jones Ba, Neville RF, Najjar SF *et al.* The protective effect of vein cuffed anastomoses is not mechanical in origin. *J Vasc Surg* 1995;**21**:558-64.
107. Ballyk PD, Walsh C, Butany J, Ojha M. Compliance mismatch may promote graft-artery intimal hyperplasia by altering suture-line stresses. *J Biomech* 1998;**31**:229-37.
108. Van Tricht I, De Wachter D, Tordoir J, Verdonck P. Hemodynamics in a compliant hydraulic in vitro model of straight versus tapered PTFE arteriovenous graft. *J of Surgical Research* 2004;**116**:297-304.
109. Moore JA, Steinman DA, Prakash S, Johnston KW, Ethier CR. A numerical study of blood flow patterns in anatomically realistic and simplified end-to-side anastomoses. *J Biomech Eng* 1999;**121**:265-72.
110. Treiman GS, Lawrence PF, Bhirangi K, Gazak CE. Effect of outflow level and maximum graft diameter on the velocity parameters of reversed vein bypass grafts. *J Vasc Surg* 1999;**30**:16-25.
111. Abbott WM, Green CJ, Matsumoto T, Wheeler JR, Miller N, Veith FJ. Prosthetic above-knee femoropopliteal bypass grafting: results of a multicentre randomized prospective trial. *J Vasc Surg*

- 1997;**25**:19-28.
112. Wengerter KR, Veith FJ, Gupta SK, Ascer E, Rivers SP. Influence of vein size (diameter) on infrapopliteal reversed vein graft patency. *J Vasc Surg* 1990;**11**:525-31.
 113. Ruygrok PN, Webster MW, Ardill JJ, Chan CC, Mak KH, Meredith IT *et al.* Vessel caliber and restenosis: a prospective clinical and angiographic study of NIR stent deployment in small and large coronary arteries in the same patient. *Catheter Cardiovasc Interv* 2003;**59**:165-71.
 114. Keynton RS, Evancho MM, Sims RL, Rittgers SE. The effect of graft caliber upon wall shear within in vivo distal vascular anastomoses. *J Biomech Eng* 1999;**121**:79-88.
 115. Hofstra L, Bergmans DC, Leunissen KM, Hoeks AP, Kitslaar PJ, Tordoir J. Prosthetic arteriovenous fistulas and venous anastomotic stenosis: influence of a high flow velocity on the development of intimal hyperplasia. *Blood Purif* 1996;**14**:345-9.
 116. Papanicolaou G, Zierler RE, Beach KW, Isaacson RT, Strandness Jr DE. Hemodynamic parameters of failing infrainguinal bypass grafts. *Am J Surg* 1995;**169**:238-44.
 117. Papanicolaou G, Beach KW, Zierler RE, Detmer PR, Strandness Jr DE. Hemodynamics of stenotic infrainguinal vein grafts: theoretical considerations. *Ann Vasc Surg* 1995;**9**:163-71.
 118. Polo JR, Ligerio JM, Diaz-Cartelle J, Garcia-Pajares R, Cervera T, Reparaz L. Randomised comparison of 6-mm straight grafts versus 6- to 8- mm tapered grafts for brachial-axillary dialysis access. *J Vasc Surg* 2004;**40**:319-24.
 119. Wesolowski SA, Fries CC, Karlson KE, De Bakey M, Sawyer PN. Porosity: primary determinant of ultimate fate of synthetic vascular grafts. *Surgery* 1961;**50**:91-6.
 120. Zhang Z, Wang Z, Liu S, Kodama M. Pore size, tissue ingrowth, and endothelialization of small diameter microporous polyurethane vascular prostheses. *Biomaterials* 2003;**25**:177-87.
 121. Fujimoto K, Minato M, Miyamoto S, Kaneko T, Kikuchi H, Sakai K *et al.* Porous polyurethane tubes as vascular graft. *J Appl Biomater* 1993;**4**:347-54.
 122. Salacinski HJ, Tai NR, Punshon G, Giudiceandrea A, Hamilton G, Seifalian AM. Optimal endothelialisation of a new compliant poly(carbonate-urea)urethane vascular graft with effect of physiological shear stress. *Eur J Vasc Endovasc Surg* 2000;**20**:342-52.
 123. Giudiceandrea A, Seifalian AM, Krijgsman B, Hamilton G. Effect of

- prolonged pulsatile shear stress in vitro on endothelial cell seeded PTFE and compliant polyurethane vascular grafts. *Eur J Vasc Endovasc Surg* 1998;**15**:147-54.
124. MacLeod TM, Sarathchandra P, Williams G, Sanders R, Green CJ. The diamond CO₂ laser as a method of improving the vascularisation of a permanent collagen implant. *Burns* 2004;**30**:704-12.
 125. Guidon R, Chakfe N, Maurel S, How T, Batt M, Marois M. Expanded polytetrafluoroethylene arterial prostheses in humans: a histopathological study of 298 surgically excised grafts. *Biomaterials* 1993;**14**:678-93.
 126. Losi P, Lombardi S, Briganti E, Soldani G. Luminal surface microgeometry affects platelet adhesion in small-diameter synthetic grafts. *Biomaterials* 2004;**25**:4447-55.
 127. Eberhart A, Zhang Z, Guidoin R, Laroche G, Guay L, De La Faye D *et al.* A new generation of polyurethane vascular prostheses: rara avis or ignis fatuus ? *J Biomed Mater Res* 1999;**48**:546-58.
 128. Amore R, Pagani C, Youssef MN, Netto CA, Lewgoy HR. Polymerization shrinkage evaluation of three packable composite resins using a gas pycnometer. *Pesqui Odontol Bras* 2003;**17**:273-7.
 129. Hofmann A, Pelletier M, Michot M, Stradner A, Schurtenberger P, Kretzschmar R *et al.* Characterization of the pores in hydrous ferric oxide aggregates formed by freezing and thawing. *J Colloid Interface Sci* 2004;**271**:163-73.
 130. Roeder R, Lantz GC, Geddes LA. Mechanical remodeling of small-intestine submucosa small-diameter vascular grafts - a preliminary report. *Biomed Instrum Technol* 2001;**35**:110-20.
 131. Lamm P, Juchem G, Milz S, Schuffenhauer M, Reichart B. Autologous endothelialized vein allograft: a solution in the search for small caliber grafts in coronary artery bypass graft operations. *Circulation* 2001;**104**:I108-I114.
 132. Chen JH, Laiw RF, Jiang SF, Lee YD. Microporous segmented polyetherurethane vascular graft: Dependency of graft morphology and mechanical properties on compositions and fabrication conditions. *J Biomed Mater Res* 1998;**48**:235-45.
 133. Stick C, Hiedl U, Witzleb E. Venous pressure in the saphenous vein near the ankle during changes in posture and exercise at different ambient temperatures. *Eur J Appl Physiol* 1993;**66**:434-8.
 134. Stooker W, Niessen HW, Baidoshvili A. Perivenous support reduces early changes in human vein grafts: studies in whole blood perfused human vein segments. *J Thorac Cardiovasc Surg* 2001;**121**:290-7.

135. Westerband A, Crouse D, Richter LC, Aguirre ML, Wixon CC, James DC *et al.* Vein adaptation to arterialization in an experimental model. *J Vasc Surg* 2001;**33**:561-9.
136. Jacot JGJ, Abdullah I, Belkin M, Gerhard-Herman M, Gaccione P, Polak JF *et al.* Early adaptation of human lower extremity vein grafts: wall stiffness changes accompany geometric remodeling. *J Vasc Surg* 2004;**39**:547-55.
137. Shah PJ, Gordon I, Fuller J, Seevanayagam S, Rosalion A, Tatoulis J *et al.* Factors affecting saphenous graft patency: clinical and angiographic study in 1402 symptomatic patients operated on between 1977 and 1999. *J Thorac Cardiovasc Surg* 2003;**126**:1972-7.
138. Stooker W, Gok M, Sipkema P, Niessen HWm, Baidoshvili A, Westerhof N *et al.* Pressure-diameter relationship in the human greater saphenous vein. *Ann Thorac Surg* 2003;**76**:1533-8.
139. Davies AH, Magee TR, Baird RN, Sheffield E, Horrocks M. Vein compliance: a pre-operative indicator of vein morphology and of veins at risk of vascular graft stenosis. *Br J Surg* 1992;**79**:1019-21.
140. Chapman BL, Charlesworth D. An in vivo method of measurement of the mechanical properties of vascular prostheses: the mechanical properties of saphenous bypass grafts. *Physics in Medicine and Biology* 1983;**28**:1067-74.
141. Nishibe T, Okuda Y, Kumada T, Tanabe T, Yasuda K. Enhanced graft healing of high-porosity expanded polytetrafluoroethylene grafts by covalent bonding of fibronectin. *Surg Today* 2000;**30**:426-31.
142. Salacinski HJ, Tai NR, Carson RJ, Edwards A, Hamilton G, Seifalian AM. In vitro stability of a novel compliant poly(carbonate-urea)urethane to oxidative and hydrolytic stress. *J Biomed Mater Res* 2002;**59**:207-18.
143. Niklason LE, Gao J, Abbott WM, Hirschi KK, Houser S, Marini R *et al.* Functional arteries grown in vitro. *Science* 1999;**284**:489-93.
144. Teebken OE, Haverich A. Tissue engineering of small diameter vascular grafts. *Eur J Vasc Endovasc Surg* 2002;**23**:475-85.
145. Kakisis JD, Liapis CD, Breuer C, Sumpio BE. Artificial blood vessel: the Holy Grail of peripheral vascular surgery. *J Vasc Surg* 2005;**41**:349-54.
146. Hoerstrup SP, Zund G, Sodian R, Schnell AM, Grunenfelder J, Turina MI. Tissue engineering of small caliber vascular grafts. *Eur J Cardiothor Surg* 2001;**20**:164-9.
147. Greisler HP, Endean ED, Klosak JJ, Ellinger J, Dennis JW, Buttle K *et*

- al.* Polyglactin 910/polydioxanone bicomponent totally resorbable vascular prostheses. *Science* 1988;**7**:697-705.
148. Niklason LE, Abbott WM, Gao J, Klagges B, Hirschi KK, Ulubayram K *et al.* Morphologic and mechanical characteristics of engineered bovine arteries. *J Vasc Surg* 2001;**33**:628-38.
 149. Nakayama Y, Ishibashi-Ueda H, Takamizawa K. In vivo tissue-engineered small-caliber arterial graft prosthesis consisting of autologous tissue (biotube). *Cell Transplant* 2004;**13**:439-49.
 150. Thomas AC, Campbell GR, Campbell JH. Advances in vascular tissue engineering. *Cardiovascular Pathology* 2003;**12**:271-6.
 151. L'Heureux N, Paquet S, Labbe R, Germain L, Auger FA. A completely biological tissue-engineered human blood vessel. *FASEB J* 1998;**12**:47-56.
 152. Tiwari A, Cheng KS, Salacinski HJ, Hamilton G, Seifalian AM. Improving the patency of vascular bypass grafts: the role of suture materials and surgical techniques on reducing anastomotic compliance mismatch. *Eur J Vasc Endovasc Surg* 2003;**25**:287-95.
 153. Kidane AG, Salacinski HJ, Tiwari A, Bruckdorfer KR, Seifalian AM. Anticoagulant and antiplatelet agents: their clinical and device application(s) together with usages to engineer surfaces. *Biomacromolecules* 2003;**5**:798-813.
 154. Fauvel-Lafeve F. Microfibrils from the arterial subendothelium. *In Rev Cytol* 1999;**188**:1-40.
 155. Forstermann U, Mugge A, Alheid U, Bode SM, Frolich JC. Endothelium-derived relaxing factor (EDRF): a defence mechanism against platelet aggregation and vasospasm in human coronary arteries. *Eur Heart J* 1989;**10**:36-43.
 156. Fungaloi P, Waterman P, Nigri G, Stadius-van Eps R, Sluiter W, van Urk H *et al.* Photochemically modulated endothelial cell thrombogenicity via the thrombomodulin-tissue factor pathway. *Photochem photobiol* 2003;**78**:475-80.
 157. Galvez A, Gomez-Ortiz G, Diaz-Ricart M, Escolar G, Gonzalez-Sarmiento R, Zurbano MJ *et al.* Desmopressin (DDAVP) enhances platelet adhesion to the extracellular matrix of cultured human endothelial cells through increased expression of tissue factor. *Thromb Haemost* 1997;**77**:975-80.
 158. Dardik R, Varon D, Tamarin I, Zivelin A, Salomon O, Shenkman B *et al.* Homocysteine and oxidized low density lipoprotein enhanced platelet adhesion to endothelial cells under flow conditions: distinct mechanisms of thrombogenic modulation. *Thromb Haemost* 2000;**83**:338-44.

159. Banfi C, Camera M, Giandomenico G, Toschi V, Arpaia M, Mussoni L *et al.* Vascular thrombogenicity induced by progressive low density lipoprotein oxidation: protection by antioxidants. *Thromb Haemost* 2003;**89**:544-53.
160. Guidon R, Marois Y, Deng X, Chakfe N, Marois M, Roy R *et al.* Can collagen impregnated polyester arterial prostheses be recommended as small diameter blood conduits ? *ASAIO J* 1996;**42**:974-83.
161. Lin W-C, Tseng C-H, Yang M-C. In-vitro hemocompatibility evaluation of a thermoplastic polyurethane membrane with surface-immobilised water-soluble chitosan and heparin. *Macromolecular bioscience* 2005;**5**:1013-21.
162. Iwai Y. Development of a thermal cross-linking heparinization method and its application to small caliber vascular prostheses. *ASAIO J* 1996;**42**:M693-M697.
163. Mohamed MS, Mukherjee M, Kakkar VV. Thrombogenicity of heparin and non-heparin bound arterial prostheses: an in vitro evaluation. *J R Coll Surg Edinb* 1998;**43**:155-7.
164. Bergqvist D, Jensen N, Persson N. Heparinization of polytetrafluoroethylene (ePTFE) grafts. The effect on pseudointimal hyperplasia. *Int Angiol* 1988;**7**:65-70.
165. Luong-Van F, Grondahl L, Chua KN, Leong KW, Nurcombe V, Cool SM. Controlled release of heparin from poly(epsilon-caprolactone) electrospun fibers. *Biomaterials* 2006;**27**:2042-50.
166. Iakovou I, Schmidt T, Bonizzoni E, Ge L, Sangiorgi GM, Stankovic G *et al.* Incidence, predictors and outcome of thrombosis after successful implantation of drug-eluting stents. *JAMA* 2005;**293**:2126-30.
167. Maekawa K, Kawamoto K, Fuke S, Yoshioka R, Saito H, Sato T *et al.* Severe endothelial dysfunction after sirolimus-eluting stent implantation. *Circulation* 2006;**113**:e850-e851.
168. Lee KH, Han JK, Byun Y, Moon HT, Yoon CJ, Kim SJ *et al.* Heparin-coated angiographic catheters: an in vivo comparison of three coating methods with different heparin release profiles. *Cardiovasc Intervent Radiol* 2004;**27**:507-11.
169. Walluscheck KP, Bierkandt S, Brandt M, Cremer J. Infrainguinal ePTFE vascular graft with bioactive surface heparin bonding. First clinical results. *J Cardiovasc Surg (Torino)* 2005;**46**:425-30.
170. Knetsch MLW, Aldenhoff YBJ, Schraven M, Koole LH. Human endothelial cell attachment and proliferation on a novel vascular graft prototype. *J Biomed Mater Res Pt A* 2004;**71A**:615-24.

171. Aldenhoff YBJ, Knetsch MLW, Hanssen JH, Lindhout T, Wielders SJ, Koole LH. Colis and tubes releasing heparin. Studies on a new vascular graft prototype. *Biomaterials* 2004;**25**:3125-33.
172. Lin PH, Chen C, Bush RL, Yao Q, Lumsden AB, Hanson SR. Small caliber heparin coated ePTFE grafts reduce platelet deposition and neointimal hyperplasia in a baboon model. *J Vasc Surg* 2004;**39**:1322-8.
173. Laredo J, Xue L, Husak VA, Ellinger J, Singh G, Zamora PO *et al.* Silyl-heparin bonding improves the patency and in vivo thromboresistance of carbon coated polytetrafluoroethylene vascular grafts. *J Vasc Surg* 2004;**39**:1059-65.
174. Lin PH, Bush RL, Yao Q, Lumsden AB, Chen C. Evaluation of platelet deposition and neointimal hyperplasia of heparin coated small caliber ePTFE grafts in a canine femoral artery bypass model. *J Surg Res* 2004;**118**:45-52.
175. Keuren JF, Wielders SJ, Driessen A, Verhoeven M, Hendriks M, Lindhout T. Covalently-bound heparin makes collagen thromboresistant. *Arterioscler Thromb Vasc Biol* 2004;**24**:613-7.
176. van der Lei B, Bartels HL, Robinson PH, Bakker WW. Reduced thrombogenicity of vascular prostheses by coating with ADP-ase. *Int Angiol* 1992;**11**:268-71.
177. Nylander S, Mattsson C, Lindahl TL. Characterisation of species differences in the platelet ADP and thrombin response. *Thromb Res* 2005;**117**:543-9.
178. Costa AF, Gamermann PW, Picon PX, Mosmann MP, Kettlun AM, Valenzuela MA *et al.* Intravenous apyrase administration reduces arterial thrombosis in a rabbit model of endothelial denudation in vivo. *Blood Coagul Fibrinolysis* 2004;**15**:545-51.
179. Rubin BG, Toursarkissian B, Petrinec D, Yang LY, Eisenberg PR, Abendschein DR. Preincubation of Dacron grafts with recombinant tissue factor pathway inhibitor decreases their thrombogenicity in vivo. *J Vasc Surg* 1996;**24**:865-70.
180. Sun LB, Utoh J, Moriyama S, Tagami H, Okamoto K, Kitamura N. Pretreatment of a Dacron graft with tissue factor pathway inhibitor decreases thrombogenicity and neointimal thickness: a preliminary animal study. *ASAIO J* 2001;**47**:325-8.
181. Kowalewski R, Zimnoch L, Wojtukiewicz MZ, Glowinski S, Glowinski J. Coagulation activators and inhibitors in the neointima of polyester vascular grafts. *Blood Coagul Fibrinolysis* 2003;**14**:433-9.
182. Mureebe L, Turnquist SE, Silver D. Inhibition of intimal hyperplasia by direct thrombin inhibitors in an animal vein

bypass model. *Ann Vasc Surg* 2004;**18**:147-50.

183. Wyers MC, Phaneuf MD, Rzucidlo EM, Contreras MA, LoGerfo FW, Quist WC. In vivo assessment of a novel dacron surface with a covalently bound recombinant hirudin. *Cardiovasc Pathol* 1999;**8**:153-9.
184. Williams RH, Nollert MU. Platelet derived NO slows thrombus growth on a collagen type III surface. *Thromb J* 2004;**2**.
185. Fleser PS, Nuthakki VK, Malinzak LE, Callahan RE, Seymour ML, Reynolds MM *et al*. Nitric oxide-releasing biopolymers inhibit thrombus formation in a sheep model of arteriovenous bridge grafts. *J Vasc Surg* 2004;**40**:803-11.
186. Gudmundsdottir IJ, McRobbie SJ, Robinson SD, Newby DE, Megson IL. Sildenafil potentiates nitric oxide mediated inhibition of human platelet aggregation. *Biochem Biophys Res Commun* 2005;**337**:382-5.
187. Ozuyaman B, Godecke A, Kusters S, Kirchhoff E, E Scharf R, Schrader J. Endothelial nitric oxide synthase plays a minor role in inhibition of arterial thrombus formation. *Thromb Haemost* 2005;**93**:1161-7.
188. Sawyer PN, Pate JW, Weldon CH. Relations of abnormal and injury electropotential differences to intravascular thrombosis. *Am J Physiol* 1953;**175**:108-16.
189. Jucker BA, Harms H, Zehnder AJ. Adhesion of the positively charged bacterium *Stenotrophomonas (Xanthomonas) maltophilia* 70401 to glass and teflon. *J Bacteriol* 1996;**178**:5472-9.
190. Kallmes DF, McGraw JK, Evans AJ, Mathis JM, Hergenrother RW, Jensen ME *et al*. Thrombogenicity of hydrophilic and nonhydrophilic microcatheters and guiding wires. *Am J Neuroradiol* 1997;**18**:1243-51.
191. Lin J-C, Cooper SL. Surface characterization and ex vivo blood compatibility study of plasma-modified small diameter tubing: effect of sulphur dioxide and hexamethyldisiloxane plasmas. *Biomaterials* 1995;**16**:1017-23.
192. van Kampen CL, Gibbons DF. Effect of implant surface chemistry upon arterial thrombosis. *J Biomed Mater Res* 1979;**13**:517-41.
193. Karrer L, Duwe J, Zisch AH, Khabiri E, Cikirikcioglu M, Napoli A *et al*. PPS-PEG surface coating to reduce thrombogenicity of small diameter ePTFE vascular grafts. *Int J Artif Organs* 2005;**28**:993-1002.
194. Bergstrom K, Osterberg E, Hoffman AS, Schuman TP, Kozlowski A, Harris JM. Effects of branching and molecular weight of surface-

- bound poly(ethylene oxide) on protein rejection. *J Biomater Sci Polymer* 1994;**6**:123-32.
195. Roach P, Farrar D, Perry CC. Interpretation of protein adsorption: surface-induced conformational changes. *J Am Chem Soc* 2005;**127**:8168-73.
 196. Freij-Larson C, Nylander T, Jannasch P, Wesslen B. Adsorption behaviour of amphiphilic polymers at hydrophilic surfaces: effects on protein adsorption. *Biomaterials* 1996;**17**:2199-207.
 197. Rubens FD, Mesana T. The inflammatory response to cardiopulmonary bypass: a therapeutic overview. *Perfusion* 2004;**19**:S5-S12.
 198. Ahmed F, Alexandridis P, Shankaran H, Neelamegham S. The ability of poloxamers to inhibit platelet aggregation depends on their physicochemical properties. *Thromb Haemost* 2001;**86**:1532-9.
 199. Grainger DW, Noriji C, Okano T, Kim SW. In vitro and ex vivo platelet interactions with hydrophilic-hydrophobic poly(ethylene oxide)-polystyrene multiblock copolymers. *J Biomed Mater Res* 1989;**23**:979-1005.
 200. Gu YJ, Boonstra PW, Rijnsburger AA, Haan J, van Oeveren W. Cardiopulmonary bypass circuit treated with surface-modifying additives: a clinical evaluation of blood compatibility. *An Thorac Surg* 1998;**65**:1342-7.
 201. Tsai CC, Huo HH, Kulkarni P, Eberhart RC. Biocompatible coatings with high albumin affinity. *ASAIO J* 1990;**36**:M307-M310.
 202. Frautschi JR, Munro MS, Lloyd DR, Eberhart RC. Alkyl derivatized cellulose acetate membranes with enhanced albumin affinity. *Trans Am Soc Artif Intern Organs* 1983;**29**:242-4.
 203. Frautschi JR, Eberhart RC, Hubbell JA. Alkylated cellulosic membranes with enhanced albumin affinity: influence of competing proteins. *J Biomater Sci Polymer* 1995;**7**:563-75.
 204. Tsai CC, Frautschi JR, Eberhart RC. Enhanced albumin affinity of silicone rubber. *ASAIO J* 1988;**34**:559-63.
 205. Dobrin PB, Hodgett D, Canfield T, Mrvicka R. Mechanical determinants of graft kinking. *Ann Vasc Surg* 2001;**15**:343-9.
 206. Zhang Z, Wang Z, Liu S, Kodama M. Pore size, tissue ingrowth and endothelialization of small diameter microporous polyurethane vascular prostheses. *Biomaterials* 2004;**25**:177-87.
 207. Roberts N, Jahangiri M, Xu Q. Progenitor cells in vascular disease. *J Cell Mol Med* 2005;**9**:583-91.

208. Tomizawa Y, Noishiki Y, Okoshi T, Nishida H, Endo M, Koyanagi H. Endogenous basic fibroblast growth factor for endothelialization due to angiogenesis in fabric vascular prostheses. *ASAIO J* 1996;**42**:M698-M702.
209. Hazama K, Miura H, Shimada T, Okuda Y, Murashita T, Nishibe T. Relationship between fibril length and tissue ingrowth in the healing of expanded polytetrafluoroethylene grafts. *Surg Today* 2004;**34**:685-9.
210. Shi Q, Wu MH-D, Sauvage LR. Clinical and experimental demonstration of complete healing of porous Dacron patch grafts used for closure of the arteriotomy after carotid endarterectomy. *Ann Vasc Surg* 1999;**13**:313-7.
211. Rashid ST, Salacinski HJ, Hamilton G, Seifalian AM. The use of animal models in developing the discipline of cardiovascular tissue engineering: a review. *Biomaterials* 2004;**25**:1627-37.
212. Dixit P, Hern-Anderson D, Ranieri J, Schmidt CE. Vascular graft endothelialization: comparative analysis of canine and human endothelial cell migration on natural biomaterials. *J Biomed Mater Res* 2001;**56**:545-55.
213. Alobaid N, Salacinski HJ, Sales KM, Ramesh B, Kannan RY, Hamilton G *et al*. Nanocomposite containing bioactive peptides promote endothelialisation by circulating progenitor cells: an in vitro evaluation. *Eur J Vasc Endovasc Surg* 2006.
214. Li C, Hill A, Imran M. In vitro and in vivo studies of ePTFE vascular grafts treated with P15 peptide. *J Biomater Sci Polymer* 2005;**16**:875-91.
215. Rotmans JI, Heyligers JM, Verhagen HJ, Velema E, Nagtegaal MM, de Kleijn DP *et al*. In vivo cell seeding with anti-CD34 antibodies successfully accelerates endothelialization but stimulates intimal hyperplasia in porcine arteriovenous expanded polytetrafluoroethylene grafts. *Circulation* 2005;**112**:12-8.
216. Randone B, Cavallaro G, Polistena A, Cucina A, Coluccia P, Graziano P *et al*. Dual role of VEGF in pretreated experimental ePTFE arterial grafts. *J Surg Res* 2005;**127**:70-9.
217. Stachelek SJ, Alferiev I, Choi H, Kronsteiner A, Uttayarat P, Gooch KJ *et al*. Cholesterol-derived polyurethane: characterization and endothelial cell adhesion. *J Biomed Mater Res Pt A* 2005;**72A**:200-12.
218. Wang C, Zhang Q, Uchida S, Kodama M. A new vascular prosthesis coated with polyamino-acid urethane copolymer (PAU) to enhance endothelialization. *J Biomed Mater Res* 2002;**62**:315-22.
219. Santhosh Kumar TR, Krishnan LK. Endothelial cell growth factor

- (ECGF) enmeshed with fibrin matrix enhances proliferation of EC in vitro. *Biomaterials* 2001;**22**:2769-76.
220. Jun H-W, West JL. Endothelialization of microporous YIGSR/PEG-modified polyurethane urea. *Tissue Eng* 2005;**11**:1140.
 221. Kidd KR, Patula VB, Williams SK. Accelerated endothelialization of interpositional 1mm vascular grafts. *J Surg Res* 2003;**113**:234-42.
 222. Lehle K, Buttstaedt J, Birnbaum DE. Expression of adhesion molecules and cytokines in vitro by endothelial cells seeded on various polymer surfaces coated with titanium carboxonitride. *J Biomed Mater Res* 2003;**65A**:393-401.
 223. Pollara P, Alessandri G, Bonardelli S, Simonini A, Cabibbo E, Portolani N *et al.* Complete in vitro prosthesis endothelialization induced by artificial extracellular matrix. *J Invest Surg* 1999;**12**:81-8.
 224. Noishiki Y, Ma XH, Yamane Y, Satoh S, Okoshi T, Takahashi K *et al.* Succinylated collagen crosslinked by thermal treatment for coating vascular prostheses. *Artif Organs* 1998;**22**:672-80.
 225. Wissink MJB, Beernink R, Poot AA, Engbers GHM, Beugeling T, van Aken WG *et al.* Improved endothelialization of vascular grafts by local release of growth factors from heparinized collagen matrices. *J Control Rel* 2000;**64**:103-14.
 226. Doi K, Matsuda T. Enhanced vascularization in a microporous polyurethane graft impregnated with basic fibroblast growth factor and heparin. *J Biomed Mater Res* 1997;**34**:361-70.
 227. Dekker A, Reitsma K, Beugeling T, Bantjes A, Feijen J, van Aken WG. Adhesion of endothelial cells and adsorption of serum proteins on gas plasma-treated polytetrafluoroethylene. *Biomaterials* 1991;**12**:130-8.
 228. Mazzucotelli JP, Moczar M, Zede L, Bambang LS, Loisanche D. Human vascular endothelial cells on expanded PTFE precoated with an engineered protein adhesive factor. *Int J Artif Organs* 1994;**17**:112-7.
 229. Bernex F, Mazzucotelli JP, Roudiere JL, Benhaiem-Sigaux N, Leandri J, Loisanche D. In vitro endothelialization of carbon-coated Dacron vascular grafts. *Int J Artif Organs* 1992;**15**:172-80.
 230. Zilla P, Fasol R, Grimm M, Fischlein T, Eberl T, Preiss P *et al.* Growth properties of cultured human endothelial cells on differently coated artificial heart materials. *J Thorac Cardiovasc Surg* 1991;**101**:671-80.
 231. Seeger JM, Klingman N. Improved in vivo endothelialization of prosthetic grafts by surface modification with fibronectin. *J Vasc*

Surg 1988;**8**:476-82.

232. Greenwald SE, Berry CL. Improving vascular grafts: the importance of mechanical and haemodynamic properties. *J Pathol* 2000;**190**:292-9.
233. Sarkar S, Salacinski HJ, Hamilton G, Seifalian AM. The mechanical properties of infrainguinal vascular bypass grafts: their role in influencing patency. *Eur J Vasc Endovasc Surg* 2006;**31**:627-36.
234. Kannan RY, Salacinski HJ, Butler PE, Seifalian AM. Polyhedral oligomeric silsesquioxane nanocomposites: the next generation material for biomedical applications. *Acc Chem Res* 2005;**38**:879-84.
235. Langer R, Vacanti J. Tissue Engineering. *Science* 1993;**260**:920-6.
236. Gentzkow GD, Iwasaki SD, Hershon KS, Mengel M, Prendergast JJ, Ricotta JJ *et al*. Use of dermagraft, a cultured human dermis, to treat diabetic foot ulcers. *Diabetes Care* 1996;**19**:350-4.
237. Brittberg M, Lindahl A, Nilsson A, Ohlsson C, Isaksson O, Peterson L. Treatment of deep cartilage defects in the knee with autologous chondrocyte transplantation. *N Engl J Med* 1994;**331**:889-95.
238. Atala A, Bauer SB, Soker S, Yoo JJ, Retik AB. Tissue-engineered autologous bladders for patients needing cystoplasty. *Lancet* 2006;**367**:1241-6.
239. Takei T, Sakai S, Ono T, Ijima H, Kawakami K. Fabrication of endothelialized tube in collagen gel as starting point for self-developing capillary-like network to construct three-dimensional organs in vitro. *Biotechnol Bioeng* 2006;**95**:1-7.
240. Sekiya S, Shimizu T, Yamato M, Kikuchi A, Okano T. Bioengineered cardiac cell sheet grafts have intrinsic angiogenic potential. *Biochem Biophys Res Commun* 2006;**341**:573-82.
241. Matsumura G, Hibino N, Ikada Y, Kurosawa H, Shin'oka T. Successful application of tissue engineered vascular autografts: clinical experience. *Biomaterials* 2003;**24**:2303-8.
242. Isenberg BC, Williams C, Tranquillo RT. Small-diameter artificial arteries engineered in vitro. *Circ Res* 2006;**98**:25-35.
243. Vara DS, Salacinski HJ, Kannan RY, Bordenave L, Hamilton G, Seifalian AM. Cardiovascular tissue engineering: state of the art. *Pathol Biol (Paris)* 2005;**53**:599-612.
244. Kannan RY, Salacinski HJ, Butler PE, Hamilton G, Seifalian AM. Current status of prosthetic bypass grafts: a review. *J Biomed Mater Res* 2005;**74B**:570-81.

245. Isenburg JC, Simionescu DT, Vyavahare NR. Elastin stabilization in cardiovascular implants: improved resistance to enzymatic degradation by treatment with tannic acid. *Biomaterials* 2004;**25**:3293-302.
246. Zilla P, Deutsch M, Meinhart J. Endothelial cell transplantation. *Semin Vasc Surg* 1999;**12**:52-63.
247. Stitzel JD, Pawlowski KJ, Wnek GE, Simpson DG, Bowlin GL. Arterial smooth muscle cell proliferation on a novel biomimicking, biodegradable vascular graft scaffold. *J Biomater Appl* 2001;**16**:22-33.
248. Yavuz K, Geyik S, Pavcnik D, Uchida BT, Corless CL, Hartley DE *et al.* Comparison of the endothelialization of small intestinal submucosa, dacron and expanded polytetrafluoroethylene suspended in the thoracoabdominal aorta of sheep. *J Vasc Interv Radiol* 2006;**17**:873-82.
249. Nemcova S, Noel AA, Jost CJ, Gloviczki P, Miller VM, Brockbank KG. Evaluation of a xenogeneic acellular collagenmatrix as a small diameter vascular graft in dogs - preliminary observations. *J Invest Surg* 2001;**14**:321-30.
250. Robotin-Johnson MC, Swanson PE, Johnson DC, Schuessler RB, Cox JL. An experimental model of small intestinal submucosa as a growing vascular graft. *J Thorac Cardiovasc Surg* 1998;**116**:805-11.
251. Sandusky GE, Lantz GC, Badylak SF. Healing comparison of small intestine submucosa and ePTFE grafts in the canine carotid artery. *J Surg Res* 1995;**58**:415-20.
252. Jernigan TW, Croce MA, Cagiannos C, Shell DH, Handorf CR, Fabian TC. Small intestinal submucosa for vascular reconstruction in the presence of gastrointestinal contamination. *Ann Surg* 2004;**239**:733-8.
253. Fletcher CD, Kruavit A, Mayou B, McKee PH. Experimental microvascular autogenous vein grafts for arterial defects: II. A histopathologic study of the grafts. *Microsurgery* 1988;**9**:82-6.
254. Clerin, V, Gusic, R, and Gooch, K. Ex-vivo remodelling of excised blood vessels for vascular grafts. (7011623). 2006. US.
Ref Type: Patent
255. Barocas VH, Girton TS, Tranquillo RT. Engineered alignment in media equivalents: magnetic prealignment and mandrel compaction. *J Biomech Eng* 1998;**120**:660-6.
256. Lewus KE, Nauman EA. In vitro characterization of a bone marrow stem cell-seeded collagen gel composite for soft tissue grafts: effects of fiber number and serum concentration. *Tissue Eng*

2005;**11**:1015-22.

257. Thie M, Schlumberger W, Semich R, Rauterberg J, Robenek H. Aortic smooth muscle cells in collagen lattice culture: effects on ultrastructure, proliferation and collagen synthesis. *Eur J Cell Biol* 1991;**55**:295-304.
258. Long JL, Tranquillo RT. Elastic fiber production in cardiovascular tissue-equivalents. *Matrix Biol* 2003;**22**:339-50.
259. Isenberg BC, Williams C, Tranquillo RT. Endothelialization and flow conditioning of fibrin-based media-equivalents. *Ann Biomed Eng* 2006;**34**:971-85.
260. Wise SG, Byrom MJ, Waterhouse A, Bannon PG, Ng MK, Weiss AS. A multilayered synthetic human elastin/polycaprolactone hybrid vascular graft with tailored mechanical properties. *Acta Biomater* 2010.
261. L'Heureux N, Duserre N, Konig G, Victor B, Keire P, Wight T *et al*. Human tissue-engineered blood vessels for adult arterial revascularization. *Nat Med* 2006;**12**:361-5.
262. McKee JA, Banik SSR, Boyer MJ, Hamad NM, Lawson JH, Niklason LE *et al*. Human arteries engineered in vitro. *EMBO Rep* 2003;**4**:633-8.
263. Sarkar S, Sales KM, Hamilton G, Seifalian AM. Addressing thrombogenicity in vascular graft construction. *J Biomed Mater Res B* 2006;**82**:100-8.
264. Bordenave L, Fernandez P, Remy-Zolghadri M, Villars S, Daculsi R, Midy D. In vitro endothelialized ePTFE prostheses: clinical update 20 years after the first realisation. *Clinical Hemorheology and microcirculation* 2005;**33**:227-34.
265. Cozens-Roberts C, Lauffenburger D, Quinn J. Receptor-mediated cell attachment and detachment kinetics. I. Probabilistic model and analysis. *Biophysics J* 1990;**58**:841-56.
266. Vara DS, Punshon G, Sales KM, Hamilton G, Seifalian AM. The effect of shear stress on human endothelial cells seeded on cylindrical viscoelastic conduits: an investigation of gene expression. *Biotechnol Bioeng* 2006;**45**:119-30.
267. Asano Y, Ichioka S, Shibata M, Ando J, Nakatsuka T. Sprouting from arteriovenous shunt vessels with increased blood flow. *Med Biol Eng Comput* 2005;**43**:126-30.
268. Riha GM, Lin PH, Lumsden AB, Yao Q, Chen C. Review: application of stem cells for vascular tissue engineering. *Tissue Eng* 2005;**11**:1535-52.

269. Mcfetridge P, Daniel J, Bodamyali T, Horrocks M, Chaudhuri J. Preparation of porcine carotid arteries for vascular tissue-engineering applications. *J Biomed Mater Res* 2004;**70A**:224-34.
270. Shadwick RE. Mechanical design in arteries. *J Exper Biol* 1999;**202**:3305-13.
271. Gupta BS, Kasyanov VA. Biomechanics of human common carotid artery and design of novel hybrid textile compliant vascular grafts. *J Biomed Mater Res* 1997;**34**:341-9.
272. Weinberg CB, Bell E. A blood vessel model constructed from collagen and cultured vascular cells. *Science* 1986;**231**:397-400.
273. Berglund JD, Nerem RM, Sambanis A. Incorporation of intact elastin scaffolds in tissue-engineered collagen-based vascular grafts. *Tissue Eng* 2004;**10**:1526-35.
274. Leach JB, Wolinsky JB, Stone PJ, Wong JY. Crosslinked alpha-elastin biomaterials: towards a processable elastin-mimetic scaffold. *Acta Biomater* 2005;**1**:155-64.
275. L'Heureux N, Germain L, Labbe R, Auger FA. In vitro construction of a human blood vessel from cultured vascular cells: a morphologic study. *J Vasc Surg* 1993;**17**:499-509.
276. Lepidi S, Abatangelo G, Vindigni V, Deriu GP, Zavan B, Tonello C *et al*. In vivo regeneration of small-diameter (2mm) arteries using a polymer scaffold. *FASEB J* 2006;**20**:103-5.
277. Remuzzi A, Mantero S, Columbo M, Morigi M, Binda E, Camozzi D *et al*. Vascular smooth muscle cells on hyaluronic acid: culture and mechanical characterization of an engineered vascular construct. *Tissue Eng* 2004;**10**:699-710.
278. Simionescu DT, Lu Q, Song Y, Lee JS, Rosenbalm TN, Kelley C *et al*. Biocompatibility and remodeling potential of pure arterial elastin and collagen scaffolds. *Biomaterials* 2006;**27**:702-13.
279. Banz Y, Rieben R. Endothelial cell protection in xenotransplantation: looking after a key player in rejection. *Xenotransplantation* 2006;**13**:19-30.
280. Hsu SH, Tsai IJ, Lin DJ, Chen DC. The effect of dynamic culture conditions on endothelial cell seeding and retention on small diameter polyurethane vascular grafts. *Med Eng Phys* 2005;**27**:267-72.
281. Yeh H-I, Lu S-K, Tian T-Y, Hong R-C, Lee W-H, Tsai C-H. Comparison of endothelial cells grown on different stent materials. *J Biomed Mater Res A* 2006;**76**:835-41.
282. Mano Y, Sawasaki Y, Takahashi K, Goto T. Cultivation of arterial

- endothelial cells from human umbilical cord. *Experientia* 1983;**39**:1144-6.
283. Oedayrajsingh-Varma MJ, van Ham SM, Knippenberg M, Helder MN, Klein-Nulend J, Schouten TE *et al.* Adipose tissue-derived mesenchymal stem cell yield and growth characteristics are affected by the tissue-harvesting procedure. *Cytotherapy* 2006;**8**:166-77.
284. Noer A, Sorensen AL, Boquest AC, Collas P. Stable CpG hypomethylation of adipogenic promoters in freshly isolated, cultured, and differentiated mesenchymal stem cells from adipose tissue. *Mol Biol Cell* 2006;**17**:3543-56.
285. Nakagami H, Morishita R, Maeda K, Kikuchi Y, Ogihara T, Kaneda Y. Adipose tissue-derived stromal cells as a novel option for regenerative cell therapy. *J Atheroscler Thromb* 2006;**13**:77-81.
286. Cho SW, Lim SH, Kim IK, Hong YS, Kim SS, Yoo KJ *et al.* Small-diameter blood vessels engineered with bone marrow-derived cells. *Ann Surg* 2005;**241**:506-15.
287. Shin'oka T, Matsumura G, Hibino N, Naito Y, Watanabe M, Konuma T *et al.* Midterm clinical result of tissue-engineered vascular autografts seeded with autologous bone marrow cells. *J Thorac Cardiovasc Surg* 2005;**129**:1330-8.
288. Walter DH, Rittig K, Bahlmann FH, Kirchmair R, Silver M, Murayama T *et al.* Statin therapy accelerates reendothelialization: a novel effect involving mobilization and incorporation of bone-marrow derived endothelial cells. *Circulation* 2002;**105**:3017-24.
289. Thijssen DH, Vos JB, Verseyden C, van Zonneveld AJ, Smits P, Sweep FC *et al.* Haematopoietic stem cells and endothelial progenitor cells in healthy men: effect of aging and training. *Aging Cell* 2006;**5**:495-503.
290. Fadini GP, Sartore S, Schiavon M, Albiero M, Baesso I, Cabrelle A *et al.* Diabetes impairs progenitor cell mobilisation after hindlimb ischaemia-reperfusion injury in rats. *Diabetologia* 2006;**49**:3075-84.
291. Honold J, Lehmann R, Heeschen C, Walter DH, Assmus B, Sasaki K *et al.* Effects of granulocyte colony stimulating factor on functional activities of endothelial progenitor cells in patients with chronic ischemic heart disease. *Arterioscler Thromb Vasc Biol* 2006;**26**:2238-43.
292. Sreerekha PR, Krishnan LK. Cultivation of endothelial progenitor cells on fibrin matrix and layering on Dacron/polytetrafluoroethylene vascular grafts. *Artif Organs* 2006;**30**:242-9.

293. Lev EI, Aboulfatova K, Harris D, Granada JF, Alviar C, Kleiman NS *et al.* Potential role of activated platelets in homing of human endothelial progenitor cells in subendothelial matrix. *Thromb Haemost* 2006;**96**:498-504.
294. Opitz F, Schenke-Layland K, Richter W, Martin DP, Degenkolbe I, Wahlers T *et al.* Tissue engineering of ovine aortic blood vessel substitutes using applied shear stress and enzymatically derived vascular smooth muscle cells. *Ann Biomed Eng* 2004;**32**:212-22.
295. Ma Z, He W, Yong T, Ramakrishna S. Grafting of gelatin on electrospun poly(caprolactone) nanofibers to improve endothelial cell spreading and proliferation and to control cell orientation. *Tissue Eng* 2005;**11**:1149-58.
296. Iwai S, Sawa Y, Ichikawa H, Taketani S, Uchimura E, Chen G *et al.* Biodegradable polymer with collagen microsp sponge serves as a new bioengineered cardiovascular prosthesis. *J Thorac Cardiovasc Surg* 2004;**128**:472-9.
297. He H, Shirota T, Yasui H, Matsuda T. Canine endothelial progenitor cell-lined hybrid vascular graft with nonthrombogenic potential. *J Thorac Cardiovasc Surg* 2003;**126**:455-64.
298. Shirota T, He H, Yasui H, Matsuda H. Human endothelial progenitor cell-seeded hybrid graft: proliferative and antithrombogenic potentials in vitro and fabrication processing. *Tissue Eng* 2003;**9**:127-36.
299. Cho SW, Lim JE, Chu HS, Hyun HJ, Choi CY, Hwang KC *et al.* Enhancement of in vivo endothelialization of tissue-engineered vascular grafts by granulocyte colony-stimulating factor. *J Biomed Mater Res A* 2006;**76**:252-63.
300. Hsu SH, Sun SH, Chen DC. Improved retention of endothelial cells seeded on polyurethane small-diameter vascular grafts modified by a recombinant RGD-containing protein. *Artif Organs* 2003;**27**:1068-78.
301. Kidane A, Salacinski HJ, Punshon G, Ramesh B, Srai KS. Synthesis and evaluation of slightly hydrophobic RGD derivative(s): use(s) for solvent casting in polymers and bioengineering application(s). *Med Biol Eng Comput* 2003;**41**:1-6.
302. Conklin BS, Wu H, Lin PH, Lumsden AB, Chen C. Basic fibroblast growth factor coating and endothelial cell seeding of a decellularized heparin-coated vascular graft. *Artif Organs* 2004;**28**:668-75.
303. Eriksson AC, Whiss PA. Measurement of adhesion of human platelets in plasma to protein surfaces in microplates. *J Pharmacol Toxicol Methods* 2005;**52**:356-65.

304. Tiwari A, Kidane A, Salacinski HJ, Punshon G, Hamilton G, Siefalian AM. Improving endothelial cell retention for single stage seeding of prosthetic grafts: use of polymer sequences of arginine-glycine-aspartate. *Eur J Vasc Endovasc Surg* 2003;**25**:325-9.
305. Quadrani P, Pasini A, Mattioli-Belmonte M, Zannoni C, Tampieri A, Landi E *et al.* High-resolution 3D scaffold model for engineered tissue fabrication using a rapid prototyping technique. *Med Biol Eng Comput* 2005;**43**:196-9.
306. van Cleynenbreugel T, Schrooten J, Van Oosterwyck H, Vander SJ. Micro-CT-based screening of biomechanical and structural properties of bone tissue engineering scaffolds. *Med Biol Eng Comput* 2006;**44**:517-25.
307. Ashammakhi N, Ndreu A, Piras AM, Nikkola L, Sindelar T, Ylikauppila H *et al.* Biodegradable nanomats produced by electrospinning: expanding multifunctionality and potential for tissue engineering. *J Nanosci.Nanotechnol.* 2007;**7**:862-82.
308. Sinha N, Yeow JT. Carbon nanotubes for biomedical applications. *IEEE Trans Nanobioscience* 2005;**4**:180-95.
309. Magrez A, Kasas S, Salicio V, Pasquier N, Seo JW, Celio M *et al.* Cellular toxicity of carbon-based nanomaterials. *Nano Lett* 2006;**6**:1121-5.
310. Rhodes NP, Bellon JM, Bujan MJ, Soldani G, Hunt JA. Inflammatory response to anovel series of siloxane-crosslinked polyurethane elastomers having controlled biodegradation. *J Mater Sci Mater Med* 2005;**16**:1207-11.
311. Shibayama M, Suetsugu M, Sakurai S, Yamamoto T, Nomura S. Structure characterization of polyurethanes containing poly(dimethylsiloxane). *Macromolecules* 1991;**24**:6254-62.
312. Labow RS, Meek E, Santerre JP. Hydrolytic degradation of poly(carbonate)-urethanes by monocyte-derived macrophages. *Biomaterials* 2001;**22**:3025-33.
313. Agnihotri A, Garrett JT, Runt J, Siedlecki CA. Atomic force microscopy visualization of poly(urethane urea) microphase rearrangements under aqueous environment. *J Biomater Sci Polymer Edn* 2006;**17**:227-38.
314. Shah V. Mechanical properties. In Shah V, ed. *Handbook of plastics testing technology*, pp 10-88. New York: John Wiley & Son, 1998.
315. Flanagan M. Mechanical and rheological testing. In Hunt BJ, James MI, eds. *Polymer Characterisation*, pp 261-96. London: Chapman and Hall, 1993.

316. Lind L, Fors N, Hall J, Marttala K, Stenborg A. A comparison of three different methods to determine arterial compliance in the elderly. *J Hypertens* 2006;**24**:1075-82.
317. Tu R, McIntyre J, Hata C, Lu CL, Wang E, Quijano RC. Dynamic internal compliance of a vascular prosthesis. *ASAIO Trans* 1991;**37**:M470-M472.
318. Pearson TC. Hemorheology in the erythrocytoses. *Mount Sinai J Med* 2001;**68**:182-91.
319. Pfafferoth C, Nash GB, Meiselman HJ. Red blood cell deformation in shear flow. Effects of internal and external phase viscosity and of in vivo aging. *Biophysics J* 1985;**47**:695-704.
320. McDonald DA, Womersley J, Taylor M. The nature of flow of a liquid. In Nichols WW, O'Rourke MF, eds. *McDonald's Blood Flow in Arteries. Theoretical, Experimental and Clinical Principles*, pp 11-48. London: Hodder Arnold, 2005.
321. Levy MN, Zieske H. A closed circulatory system model. *Physiologist* 1967;**10**:419-24.
322. Inoguchi H, Kwon IK, Inoue E, Takamizawa K, Maehara Y, Matsuda T. Mechanical responses of a compliant electrospun poly(L-lactide-co-epsilon-caprolactone) small-diameter vascular graft. *Biomaterials* 2006;**27**:1470-8.
323. Khorasani MT, Shorgashti S. Fabrication of microporous polyurethane by spray phase inversion method as small diameter vascular grafts material. *J Biomed Mater Res A* 2006;**77**:253-60.
324. Doi K, Nakayama Y, Matsuda T. Novel compliant and tissue-permeable microporous polyurethane vascular prosthesis fabricated using an excimer laser ablation technique. *J Biomed Mater Res* 1996;**31**:27-33.
325. Stimpson C, White R, Klein S, Shors F. Patency and durability of small diameter silicone rubber vascular prostheses. *Biomater Artif Cells Artif Organs* 1989;**17**:31-43.
326. Zdrhala RJ. Small caliber vascular grafts. Part II: Polyurethanes revisited. *J Biomater Applic* 1996;**11**:37-61.
327. Moroni L, de Wijn JR, van Blitterswijk CA. 3D fiber-deposited scaffolds for tissue engineering: influence of pores geometry and architecture on dynamic mechanical properties. *Biomaterials* 2006;**27**:974-85.
328. Tsuchida H, Wilson SE, Ishimaru S. Healing mechanisms of high-porosity PTFE grafts: significance of transmural structure. *J Surg Res* 1997;**71**:187-95.

329. George SJ, Izzat MB, Gadsdon P, Johnson JL, Yim AP, Wan S *et al.* Macro-porosity is necessary for the reduction of neointimal and medial thickening by external stenting of porcine saphenous vein bypass grafts. *Atherosclerosis* 2001;**155**:329-36.
330. Rosengren A, Bjursten LM. Pore size in implanted polypropylene filters is critical for tissue organisation. *J Biomed Mater Res A* 2003;**67**:918-26.
331. Kannan RY, Salacinski HJ, Edirisinghe MJ, Hamilton G, Seifalian AM. Polyhedral oligomeric silsesquioxane-polyurethane nanocomposite microvessels for an artificial capillary bed. *Biomaterials* 2006;**27**:4618-26.
332. Charlesworth, D, White, E. T, and Kent, S. (US 2,130,521B). 1985.
Ref Type: Patent
333. Soletti L, Hong Y, Guan J, Stankus JJ, El Kurdi MS, Wagner WR *et al.* A bilayered elastomeric scaffold for tissue engineering of small diameter vascular grafts. *Acta Biomater* 2010;**6**:110-22.
334. Khorasani MT, Shorgashti S. Fabrication of microporous thermoplastic polyurethane for use as small-diameter vascular graft material. I. Phase-inversion method. *J Biomed Mater Res B* 2006;**76B**:41-8.
335. Underwood CJ, Tait WF, Charlesworth D. Design considerations for a small bore vascular prosthesis. *Int J Artif Organs* 1988;**11**:272-6.
336. Bergmeister H, Boeck P, Kasimir MT, Fleck T, Fitzal F, Husinsky W *et al.* Effect of laser perforation on the remodelling of acellular matrix grafts. *J Biomed Mater Res B Appl Biomater* 2005;**74**:495-503.
337. Lumsden AB, Chen C, Coyle KA, Ofenloch JC, Wang JH, Yasuda HK *et al.* Nonporous silicone polymer coating of expanded polytetrafluoroethylene grafts reduces graft neointimal hyperplasia in dog and baboon models. *J Vasc Surg* 1996;**24**:825-33.
338. Rubber, vulcanized or thermoplastic - determination of tensile stress-strain properties. ISO 37:2005(E). 2005.
Ref Type: Generic
339. Cardiovascular implants - Tubular vascular prostheses. ISO 7198. 1998.
Ref Type: Generic
340. Bergel DH. The static elastic properties of the arterial wall. *J Physiol* 1961;**156**:445-57.
341. Tai NR, Giudiceandrea A, Salacinski HJ, Seifalian AM, Hamilton G.

- In vivo femoropopliteal arterial wall compliance in subjects with and without lower limb vascular disease. *J Vasc Surg* 1999;**30**:936-45.
342. Nichols WW, O'Rourke MF. Contours of pressure and flow waves in arteries. *McDonald's blood flow in arteies*, pp 165-91. London: Hodder Arnold, 2005.
343. Lee DK, Tsai HB. Properties of segmented polyurethanes derived from different diisocyanates. *J Appl Polymer Sci* 2000;**75**:167-74.
344. Gao X, Mao LX, Tian M, Zhang LQ, Jin RG. Polycarbonate/polypropylene/fibrillar silicate ternary nanocomposites: morphology and mechanical properties. *J Mat Sci Tech* 2006;**22**:87-92.
345. Shau Y-W, Wang C-L, Shieh J-Y, Hsu T-C. Noninvasive assessment of the viscoelasticity of peripheral arteries. *Ultrasound in Med and Biol* 1999;**25**:1377-88.
346. Visontai Z, Lenard Z, Karlocai K, Kollai M. Assessment of the viscosity of the pulmonary artery wall. *Eur Respir J* 2000;**16**:1134-41.
347. Zhou J, Fung YC. The degree of nonlinearity and anisotropy of blood vessel elasticity. *Proc Natl Acad Sci* 1997;**94**:14255-60.
348. Cinthio M, Ahlgren AR, Bergkvist J, Jansson T, Persson HW, Lindstrom K. Longitudinal movements and resulting shear strain of the arterial wall. *Am J Physiol Heart Circ Physiol* 2006;**291**:H394-402.
349. Khaira HS, Vohra H. True aneurysm in a femoro-popliteal dacron graft - a case report and literature review. *Cardiovascular Surgery* 2002;**10**:644-6.
350. Van Damme H, Deprez M, Creemers E, Limet R. Intrinsic structural failure of polyester (Dacron) vascular grafts. A general review. *Acta Chir Belg* 2005;**105**:249-55.
351. McClurken M, McHaney J, Colone W. Physical properties and test methods for expanded polytetrafluoroethylene (PTFE) grafts. In Kambic H, Kantrowitz A, Sung A, eds. *Vascular graft update. Safety and performance*, pp 82-94. Philadelphia: American Society for Testing of Materials, 1986.
352. Nichols WW, O'Rourke MF. Properties of the arterial wall: theory. In Nichols WW, O'Rourke MF, eds. *McDonald's Blood Flow in Arteries*, pp 49-66. London: Hodder Arnold, 2005.
353. Guidance document for vascular prostheses 510(k) submissions. 2000. U.S. Dept of health and human services; Food and Drug Administration; Centre for devices and radiological health.

354. Yang J, Motlagh D, Webb AR, Ameer GA. Novel biphasic elastomeric scaffold for small diameter blood vessel tissue engineering. *Tissue Engineering* 2005;**11**:1876-86.
355. Xu J, Ge H, Zhou X, Yang D, Guo T, He J *et al.* Tissue-engineered vessel strengthens quickly under physiological deformation: application of a new perfusion bioreactor with machine vision. *J Vasc Res* 2005;**42**:503-8.
356. Thierry B, Merhi Y, Silver J, Tabrizian M. Biodegradable membrane-covered stent from chitosan-based polymers. *J Biomed Mater Res* 2005;**75A**:556-66.
357. Qu L, Jing Z, Wang Y. Sutureless anastomoses of small and medium sized vessels by medical adhesive. *Eur J Vasc Endovasc Surg* 2004;**28**:526-33.
358. Tamura N, Nakamura T, Terai H, Iwakura A, Nomura S, Shimizu Y *et al.* A new acellular vascular prosthesis as a scaffold for host tissue regeneration. *Int J Artif Organs* 2003;**26**:783-92.
359. Harding SI, Afoke A, Brown RA, MacLeod A, Shamlou PA, Dunnill P. Engineering and cell attachment properties of human fibronectin-fibrinogen scaffolds for use in tissue engineered blood vessels. *Bioprocess Biosyst Eng* 2002;**25**:53-9.
360. Harold KL, Pollinger H, Matthews BD, Kercher KW, Sing RF, Heniford BD. Comparison of ultrasonic energy, bipolar thermal energy and large vascular clips for the hemostasis of small-, medium- and large-sized arteries. *Surg Endosc* 2003;**17**:1228-30.
361. Oskoui P, Stadler I, Lanzafame RJ. A preliminary study of laser tissue soldering as arterial wall reinforcement in an acute experimental aneurysm model. *Lasers in Surgery and Medicine* 2003;**32**:346-8.
362. Conklin BS, Richter ER, Kreutziger KL, Zhong DS, Chen C. Development and evaluation of a novel decellularized vascular xenograft. *Medical Engineering and Physics* 2002;**24**:173-83.
363. Higami T, Maruo A, Yamashita T, Shida T, Ogawa K. Histologic and physiological evaluation of skeletonized internal thoracic artery harvesting with an ultrasonic scalpel. *J Thorac Cardiovasc Surg* 2000;**120**:1142-7.
364. Roeder R, Wolfe J, Lianakis N, Hinson T, Geddes LA. Burst pressure of canine carotid arteries. *Australas Phys Eng Sci Med* 2000;**23**:66-7.
365. Birch JF, Mandley DJ, Williams SL, Worrall DR, Trotter PJ, Wilkinson F *et al.* Methylene blue based protein solder for vascular anastomoses: an in vitro burst pressure study. *Lasers in Surgery and Medicine* 2000;**26**:323-9.

366. Wallace DG, Cruise GM, Rhee WM, Schroeder JA, Prior JJ, Ju J *et al.* A tissue sealant based on reactive multifunctional polyethylene glycol. *J Biomed Mater Res (Appl Biomater)* 2001;**58**:545-55.
367. Kobashi T, Matsuda T. Fabrication of compliant hybrid grafts supported with elastomeric meshes. *Cell Transplant* 1999;**8**:477-88.
368. Klein SL, Chen H, Israel-Graff J. A comparison of burst testing of three types of vascular anastomosis. *Microsurgery* 1998;**18**:29-32.
369. Small W4, Heredia NJ, Maitland DJ, Da Silva LB, Matthews DL. Dye-enhanced protein solders and patches in laser-assisted tissue welding. *J Clin Laser Med Surg* 1997;**15**:205-8.
370. Kennedy JS, Stranahan PL, Chandler JG. High-burst-strength, feedback-controlled bipolar vessel sealing. *Surg Endosc* 1997;**12**:876-8.
371. Yashar JJ, Richman MH, Dyckman J, Witoszka M, Burnand RJ, Weyman AK *et al.* Failure of Dacron prostheses caused by a structural defect. *Surgery* 1978;**84**:659-63.
372. Wiggins MJ, Anderson JM, Hiltner A. Biodegradation of polyurethane under fatigue loading. *J Biomed Mater Res A* 2003;**65A**:524-35.
373. Zhao Q, Casas-Bejar J, Urbanski P, Stokes K. Glass wool-H₂O₂/CoCl₂ test system for in vitro evaluation of biodegradative stress cracking in polyurethane elastomers. *J Biomed Mater Res* 1995;**29**:467-75.
374. Labow RS, Meek E. Synthesis of cholesterol esterase by monocyte-derived macrophages: a potential role in the biodegradation of poly(urethane)s. *J Biomat Appl* 1999;**13**:187-205.
375. Christenson EM, Anderson JM, Hiltner A. Oxidative mechanisms of poly(carbonate urethane) and poly(ether urethane) biodegradation: in vivo and in vitro correlations. *J Biomed Mater Res A* 2004;**70A**:245-55.
376. Kannan RY, Salacinski HJ, Odlyha M, Butler PE, Seifalian AM. The degradative resistance of polyhedral oligomeric silsesquioxane nanocore integrated polyurethanes: an in vitro study. *Biomaterials* 2006;**27**:1971-9.
377. Clowes AW, Kirkman TR, Reidy MA. Mechanisms of arterial graft healing. Rapid transmural capillary ingrowth provides a source of intimal endothelium and smooth muscle in porous PTFE prostheses. *Am J Pathol* 1986;**123**:220-30.
378. Meinhart JG, Deutsch M, Fischlein T, Howanietz N, Froschl A, Zilla P. Clinical autologous in vitro endothelialization of 153

- infrainguinal ePTFE grafts. *Ann Thorac Surg* 2001;**71**:S327-S331.
379. Ortenwall P, Wadenvik H, Kutti J, Risberg B. Endothelial cell seeding reduces thrombogenicity of Dacron grafts in humans. *J Vasc Surg* 1990;**11**:403-10.
380. Durante CM, Camboni A, Bianchi S, Macchiarelli G. Short-term patency of 1mm diameter PTFE prosthesis: an angiographic, doppler-flowmetric and morphological experimental study. *Ital J Anat Embryol* 2005;**110**:117-25.
381. Sakai O, Nakayama Y, Nemoto Y, Okamoto Y, Watanabe T, Kanda K *et al.* Development of sutureless vascular connecting system for easy implantation of small-caliber artificial grafts. *J Artif Organs* 2005;**8**:119-24.
382. Kohler TR, Stratton JR, Kirkman TR, Johansen KH, Zierler BK, Clowes AW. Conventional versus high-porosity polytetrafluoroethylene grafts: clinical evaluation. *Surgery* 1992;**112**:901-7.
383. Hansen SB, Nielsen SL, Christensen TD, Gravergaard AE, Baandrup U, Bille S *et al.* Latissimus dorsi cardiomyoplasty: a chronic experimental porcine model. Feasibility study of cardiomyoplasty in Danish Landrace pigs and Gottingen minipigs. *Lab Anim Sci* 1998;**48**:483-9.
384. Mellander S, Fogelstrand P, Enocson K, Johansson BR, Mattsson E. Healing of PTFE grafts in a pig model recruit neointimal cells from different sources and do not endothelialize. *Eur J Vasc Endovasc Surg* 2005;**30**:63-70.
385. Poole-Warren LA, Schindhelm K, Graham AR, Slowiaczek P, Noble KR. Performance of small diameter synthetic vascular prostheses with confluent autologous endothelial cell linings. *J Biomed Mater Res* 1996;**30**:221-9.
386. James NL, Schindhelm K, Slowiaczek P, Milthorpe B, Graham AR, Munro VF *et al.* In vivo patency of endothelial cell-lined expanded polytetrafluoroethylene prostheses in an ovine model. *Artif Organs* 1992;**16**:346-53.
387. Farrar DJ. Development of a prosthetic coronary artery bypass graft. *The Heart Surgery Forum* 2000;**3**:36-40.
388. Grabenwoger M, Fitzal F, Sider J, Cseko C, Bergmeister H, Schima H *et al.* Endothelialization of biosynthetic vascular prostheses after laser perforation. *Ann Thorac Surg* 1998;**66**:S110-S114.
389. de Mel A, Jell G, Stevens MM, Seifalian AM. Biofunctionalization of biomaterials for accelerated in situ endothelialization: a review. *Biomacromolecules* 2008;**9**:2969-79.

390. de Mel A, Punshon G, Ramesh B, Sarkar S, Darbyshire A, Hamilton G *et al.* In situ endothelialization potential of a biofunctionalised nanocomposite biomaterial-based small diameter bypass graft. *Biomed Mater Eng* 2009;**19**:317-31.